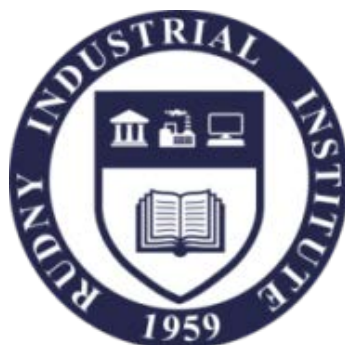


**THE MINISTRY OF EDUCATION AND SCIENCE OF  
THE REPUBLIC OF KAZAKHSTAN**

**RUDNY INDUSTRIAL INSTITUTE**



**A.B. Naizabekov, S.N. Lezhnev, A.S. Arbuz, E.A. Panin**

**THEORETICAL AND TECHNOLOGICAL BASES OF OBTAINING  
SUB-ULTRA-FINE-GRAINED STRUCTURAL METALS AND ALLOYS  
BY THE NEW COMBINED PROCESS  
"SCREW ROLLING – ECA-PRESSING»  
(monograph)**

Rudny  
2019

UDC 669  
LBC 34.3  
Th44

*Reviewers:*

T.A. Koinov - doctor of technical sciences, professor, University of chemical technology and metallurgy, Sofia;

D.V. Kuis - candidate of technical sciences, Belarusian state technological University;

A.Kh. Nurumgaliev – doctor of technical sciences, professor, Karaganda state industrial University.

**A.B. Naizabekov, S.N. Lezhnev, A.S. Arbuz, E.A. Panin**

Th44 Theoretical and technological bases of obtaining sub-ultra-fine-grained structural metals and alloys by the new combined process "screw rolling – ECA-pressing»: monograph/ A.B. Naizabekov, S.N. Lezhnev, A.S. Arbuz et al. – Rudny: RII, 2019. – 172 p.

ISBN 978-601-7994-02-0

This monograph is intended for students, undergraduates and doctoral students in the PhD program, studying in the specialties "Metallurgy", "Mechanical engineering", "Technology of materials processing by pressure", "Nanomaterials and nanotechnology". This monograph discusses the theoretical and technological basis for the production of high-quality sub – ultrafine-grain structure of round billets from various structural (ferrous and non-ferrous) metals and alloys new combined process "screw rolling - ECA-pressing", implementing in the metal of severe plastic deformation.

Recommended for publication by the Scientific Council of the Rudny Industrial Institute.

UDC 669  
LBC 34.3

ISBN 978-601-7994-02-0

© MES RK  
© RII  
© Naizabekov A.B.  
© Lezhnev S.N.  
© Arbuz A.S.  
© Panin E.A.

## TABLE OF CONTENTS

INTRODUCTION .....	6
1 ANALYSIS OF THE MODERN COMBINED ENERGY SAVING TECHNOLOGIES OF OBTAINING OF METALS AND ALLOYS WITH UFG STRUCTURE AND THE DEVELOPMENT OF A NEW COMBINED PROCESS OF "SCREW ROLLING - EQUAL CHANNEL ANGULAR PRESSING» .....	8
1.1 Features of sub-ultrafine-grained (SUFUG) materials .....	8
1.2 Conditions and basic techniques for UFG materials .....	10
1.3 Combined energy-saving SPD processes .....	21
1.4 Theoretical aspects of combination of screw rolling and equal-channel angular pressing (ECA-pressing) .....	26
2 COMPUTER SIMULATION OF THE COMBINED PROCESS " SCREW ROLLING – ECA-PRESSING" TO ANALYZE THE POSSIBILITY OF THIS PROCESS IMPLEMENTING .....	29
3 ANALYSIS OF THE INFLUENCE OF STRESS-STRAIN STATE AND TEMPERATURE ON THE QUALITY OF THE METAL BASED THE SIMULATION OF COMBINED PROCESS " SCREW ROLLING – ECA-PRESSING» .....	37
3.1 Analysis of the deformation scheme of the combined process "screw rolling - pressing» .....	37
3.2 Stress state stud .....	41
3.3 Strain state study .....	44
3.4 Study of models with variable parameters .....	46
3.4.1 Model with increased workpiece heating temperature 1150 °C .....	47
3.4.2 Model with reduced workpiece heating temperature 850 °C .....	50
3.4.3 Model with an increased angle of channels intersection in matrix 160° ....	54
3.4.4 Models with altered friction coefficients of rolls and matrix .....	57
3.5 Study of the influence of the number of passes on the strain state of the workpiece in order to form the UFG-structure .....	57
4 THE STUDY OF THE INFLUENCE OF TEMPERATURE AND STRAIN RATE DURING IMPLEMENTING A NEW PROCESS ON THE MICROSTRUCTURE EVOLUTION ON THE BASIS OF THE CONSTRUCTED MODELS USING SPECIALIZED SOFTWARE .....	61
4.1. Study of the microstructure evolution in the base model .....	61
4.2. Study of the microstructure evolution in models with varying values of workpiece heating temperature .....	62
4.3. Study of the microstructure evolution in models with varying values of strain rates .....	64
4.4. Study of the microstructure evolution after several deformation cycles .....	65

5 DESIGN AND FABRICATION OF TOOLS AND EQUIPMENT FOR THE STAND IMPLEMENTING A COMBINED PROCESS "SCREW ROLLING – ECA-PRESSING". COMMISSIONING STAND WORKS .....	68
5.1 Design of the stand for realization of combined process "screw rolling - pressing» .....	68
5.2 Strength analysis of ECA-matrix for experimental stand .....	72
5.3 Production of the tool, equipment and commissioning stand works realizing the combined process “screw rolling-pressing” .....	78
5.3.1 Production of matrices and assembly of the stand .....	78
5.3.2 Modernization of the engine control system of the mill .....	79
6 THEORETICAL STUDY OF ENERGY-POWER PARAMETERS OF A NEW COMBINED PROCESS WITH THE AIM OF DETERMINING THE OPTIMAL GEOMETRICAL AND TECHNOLOGICAL PARAMETERS ON THE BASIS OF MATHEMATICAL MODELING .....	86
7 EXPERIMENTAL INVESTIGATION OF ENERGY-POWER PARAMETERS OF COMBINED PROCESS "SCREW ROLLING – ECA-PRESSING» .....	91
7.1 Design of the experiment concept .....	91
7.2 Method of measurement of axial force of screw rolling .....	92
7.3 Equipment and materials .....	95
7.4 Design, manufacture and calibration of measuring equipment .....	99
7.5 Experimental study of the maximum axial force of screw rolling.....	102
7.6 The ability of rolling and pressing combination.....	108
8 LABORATORY RESEARCH OF DEFORMATION PROCESS ON SAMPLES OF FERROUS AND NONFERROUS METALS AND ALLOYS AT THE STAND, IMPLEMENTING ENERGY-SAVING COMBINED PROCESS "SCREW ROLLING – ECA-PRESSING» .....	112
9 IMPACT OF THE NEW COMBINED PROCESS "SCREW - ROLLING – ECA-PRESSING" ON THE MICROSTRUCTURE EVOLUTION AND MECHANICAL PROPERTIES OF THE DEFORMED STRUCTURAL MATERIAL .....	119
9.1 Microstructure evolution and mechanical properties changes of AISI-5140 structural steel .....	119
9.2 Microstructure evolution and mechanical properties changes of technical copper M1 .....	123
9.3 Microstructure evolution and mechanical properties changes of complex alloyed stainless heat-resistant steel AISI-321 .....	126
10 QUALITATIVE ANALYSIS THE QUALITY OF THE PRODUCTS WITH ENERGY EFFICIENCY IN VIEW .....	132

11 RECOMMENDATIONS FOR THE IMPLEMENTATION OF A NEW  
COMBINED PROCESS "SCREW ROLLING – ECA-PRESSING" IN  
PRODUCTION ..... 155

CONCLUSION ..... 157

REFERENCES ..... 159

ANNEX ..... 169

## INTRODUCTION

Due to the inevitable long-term growth of energy and raw materials prices, the role of energy-saving technologies for metal production with relatively high quality characteristics, such as mechanical and physical properties of the metal, is increasing. The effect of energy saving is achieved by using innovative methods of metal processing. One of the main directions in the use of energy-saving technologies is the technology of severe plastic deformation (SPD).

Over the past few decades, SPD technologies have attracted great interest for the production of sub-ultra and ultra-fine-grained (SUFG and UFG) materials. For bulk SUFG and UFG materials, in addition to the grain size, the requirements of high isotropy, homogeneity with equiaxed grains, the boundaries of disorientation of which are mainly high-angle. Under these conditions, high strength is achieved with high ductility of the processed material.

Traditional deformation technologies such as drawing and cold rolling are also accompanied by the grinding of the structure. However, basically, the substructure has a cellular character with grains elongated in the direction of drawing or rolling, also containing a high proportion of small-angle boundaries. This fact contributes to the anisotropy of product properties in the absence of a combination of high strength and ductility properties at the same time.

However, the growth of demand is significantly limited by the high cost of production of products from such materials, due to the high energy and labor intensity of their production. The most common and studied method of obtaining SUFG and UFG is equal channel angular pressing (ECAP), but the disadvantage of this and many other known processes is their discreteness, i.e. the impossibility of processing products of relatively long length and the need for a large number of processing cycles. Screw rolling is another method of SPD, which allows you to quickly and continuously obtain the UFG structure, but there are problems with the development of the central zone of the bar, the structure of which is oriented with small grain boundaries, elongated in the direction of rolling, with a quality equiaxed UFG structure of the peripheral part of the bar.

Ensuring the continuity of the ECAP, by combining it with screw rolling, will solve the problem of uneven processing of the rod and dramatically increase the overall performance and energy efficiency, which will be the goal of this work.

At this stage, the goal is achieved by an in-depth analysis of modern energy-saving combined technologies for producing metals and alloys with UFG structure and the development of a new combined process "screw rolling-pressing". For this purpose, the finite element modeling of the combined process, the search for the best technological parameters for combining, the analysis of the stress-strain state and modeling of microstructural changes for different process options.

The scientific novelty of these studies lies in the development of a completely new energy-saving technology of deformation of long products, which ensures the development of intense plastic deformations in the entire volume of the deformable metal, and leads to an increased resource of plasticity of the deformed material due to the formation of a small grain size with a low dislocation density in

it and the formation of high-angle grain boundaries with a significant decrease in the anisotropy of properties in the center and periphery of the bar.

The practical value of the work lies in the fact that the developed combined technology "screw rolling-pressing" will provide a high-quality rod of ferrous and non-ferrous metals alloys with sub-ultra-fine-grained structure and high mechanical properties.

# 1 ANALYSIS OF THE MODERN COMBINED ENERGY SAVING TECHNOLOGIES OF OBTAINING OF METALS AND ALLOYS WITH UFG STRUCTURE AND THE DEVELOPMENT OF A NEW COMBINED PROCESS OF "SCREW ROLLING - EQUAL CHANNEL ANGULAR PRESSING»

## 1.1 Features of sub-ultrafine-grained (SUGF) materials

One of the urgent problems of materials science and engineering is to improve the physical and mechanical properties of products and semi-finished products. Traditional industrial processes are mainly aimed at forming and technological processes. As a rule, metal products then have a coarse-grained structure.

Ultrafine-grained materials are polycrystalline substances (usually metals and alloys) with the size of the constituent crystallites, according to the definition of most researchers, less than 1  $\mu\text{m}$  [1-4]. This structure is a transition from the usual grain structure of most metals and alloys to the nanostructure (NS), the boundary of which is usually designated as 100 nm. Materials having the size of structural units (grains) close to 1  $\mu\text{m}$  are also often referred to as sub-ultrafine-grained (SUGF).

Under the conditions when the size of the structural units of the material is approaching the size of 100 nm, the material more clearly begins to show unusual properties and combinations of properties unattainable in other structural States. Thus, states with grains smaller than one micron and a special state of the boundaries can significantly (2-3 times) increase the strength of technically pure metals and alloys in 1.5-2 times in combination with a sufficiently high plasticity, or even in increasing plasticity. Figure 1.1, according to R.Z. Valiev [5], shows a comparison of the mechanical properties of UFG materials (Cu and Ti) with conventional metals, as well as with metals subjected to cold rolling with different degrees of deformation (Cu and Al graphs) is shown. The figure clearly illustrates an unusual combination of high strength and plasticity characteristic of UFG materials and fundamentally distinguishes them from conventional materials.

The reason for such properties of UFG materials is caused by their unusual structure, characterized not only by the grain size, but also by the special state of grain boundaries having a high-angle character, significant distortion of the crystal lattice in the boundary region and a high density of grain boundary dislocations.

Traditional methods of thermomechanical processing through the use of micro-alloying resources and the development of regulated thermodeformation modes of rolling, drawing, drawing also allow to obtain materials with a high degree of dispersion of the structure up to UFG. When varying the scheme, temperature, degree and rate of deformation, it is possible to obtain dispersed structures with small-angle grain orientations [6-7]. Such structures are characterized by a high level of strength and a sufficient level of plastic characteristics immediately after production.

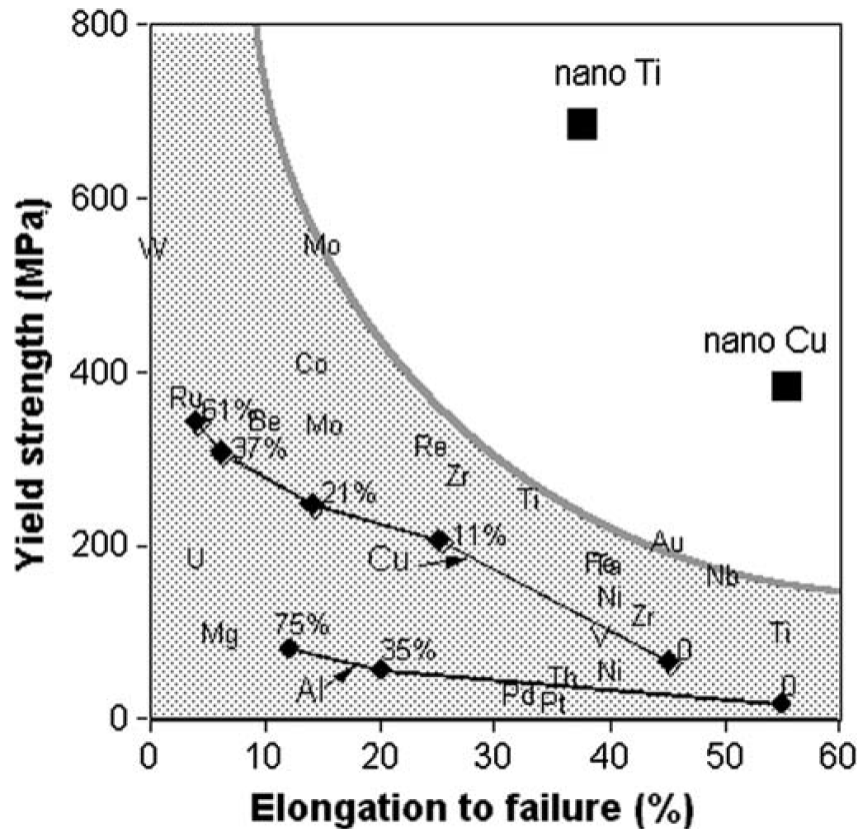


Figure 1.1 - Mechanical properties of ordinary and UFG structural states for different metals

However, structural instability and relatively low life of the material during further processing limited the scope of such materials, which led to the need to develop technologies that can improve the plastic characteristics [6].

Due to the small size of the grains, submicrocrystalline materials contain a large number of grain boundaries in the structure, which play a decisive role in the formation of their physical and mechanical properties. Ideas about non-equilibrium grain boundaries are based on studies of the interaction of lattice dislocations and grain boundaries, which resulted in the introduction of grain boundary dislocations (GBD). They form a special state of grain boundaries, which allows to obtain increased physical and mechanical properties of materials. This effect was studied in detail in the works of Valiev R.Z. [1, 5, 8], Horita Z., [9-10] Langdon T.G. [11], Pashinskaya E.G. [6].

Thus, the nature and state of the intergrain boundaries have a decisive influence on the properties of the material. The main purpose of the work on grinding the structure of metals and alloys is to obtain structures close to those shown in figure 1.2 [1].

Triangles of different sizes and orientations indicate different forces and signs. The difference sub-ultrafine-grained structure from UFG structure depicted in figure 1.2 consists only in size.

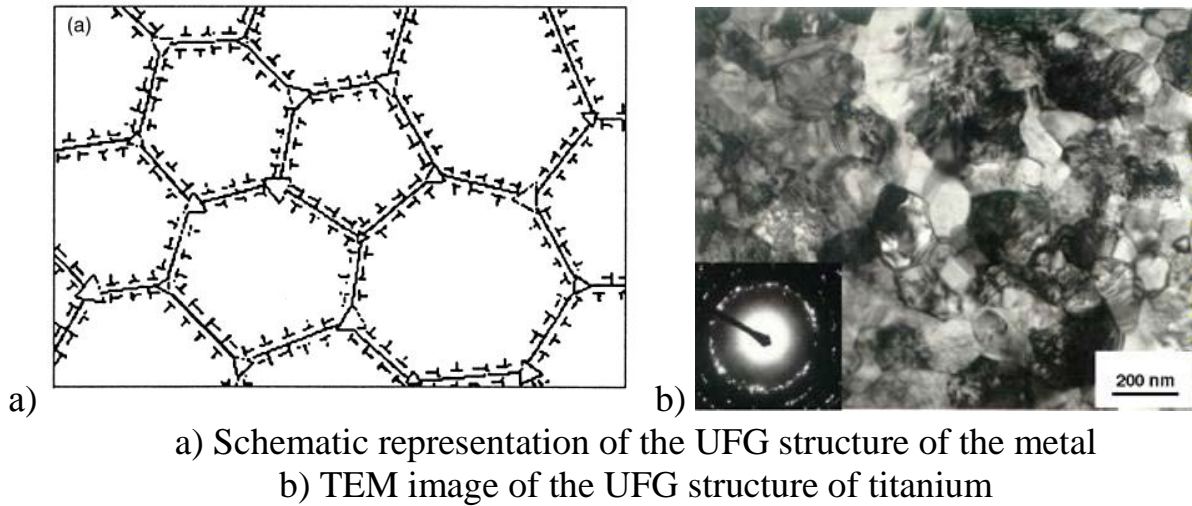


Figure 1.2 - Structure of UFG materials

It is possible to allocate the basic requirements to UFG material:

- 1) grain size less than 1  $\mu\text{m}$ ;
- 2) predominantly high-angle grain boundaries;
- 3) formation of a homogeneous structure throughout the sample volume;
- 4) the samples must not have the damage and mechanical damage that may occur when using traditional methods of pressure treatment.

It is also worth noting that the fundamental difference between the hardening of metals by grinding their grain structure from hardening by increasing the degree of hardening (cold plastic deformation processes) is a higher final ductility of UFG materials. This unique combination of properties is of great practical importance for use in mechanical engineering, since such a detail in the case of peak load will not collapse, leading to an emergency, but only deformed and will be replaced at the next scheduled preventive maintenance. Therefore, obtaining the UFG state is important even for materials with a relatively small degree of hardening.

The importance of these prospects for the use of parts from the UFG and NS materials, such as their lower metal content (including the proportion of alloying elements in metal) and weight for equal mechanical properties, which reduces the metal consumption in the production but also the energy consumption during operation of such components, allowing them to increase the specific power of the machines, having in its design the details of these materials.

The use of UFG materials is relevant for such areas as: aerospace industry, (where weight is critical), medical implants (where size is important), general engineering (where performance properties are important).

## 1.2 Conditions and basic techniques for UFG materials

It is possible to obtain such materials in macro volumes in two fundamentally different ways – by compacting the mass of the already obtained separate particles of the material having the appropriate size, or by severe plastic deformation of the

macro-billets with grinding the size of the structural units of the material to the desired ones.

The first method involves first controlled condensation of crystals from the gas phase, or grinding the material in ball mills to an ultrafine powder, and then compacting it into a finished part. This direction was investigated in the works of S. Koch [12-13], I.V. Alexandrov [14] and others.

The method has a number of disadvantages associated with the residual porosity of finished products, geometric restrictions on the size of the resulting parts and the inevitable impurities of contaminants in the powder. Also, the technological and economic part of the issue is very important, which is expressed in the need to use consistently two complex and very energy-intensive processes on complex equipment.

The described disadvantages are devoid of methods of severe plastic deformation (SPD). Obtaining by this method of equiaxial UFG grains with high-angle boundaries, according to numerous studies [1, 6, 10, 15], possible under the following conditions:

- 1) achieving high degrees of deformation for grain grinding ( $\epsilon > 6-8$ );
- 2) formation of high hydrostatic pressure preventing sample destruction and annihilation of crystal lattice defects (1 GPa and higher);
- 3) deformation at temperatures around 0.4 of the melting point and below, preventing recrystallization;
- 4) providing turbulence and non-monotonicity of deformation, contributing to the formation of high-angle intergranular boundaries.

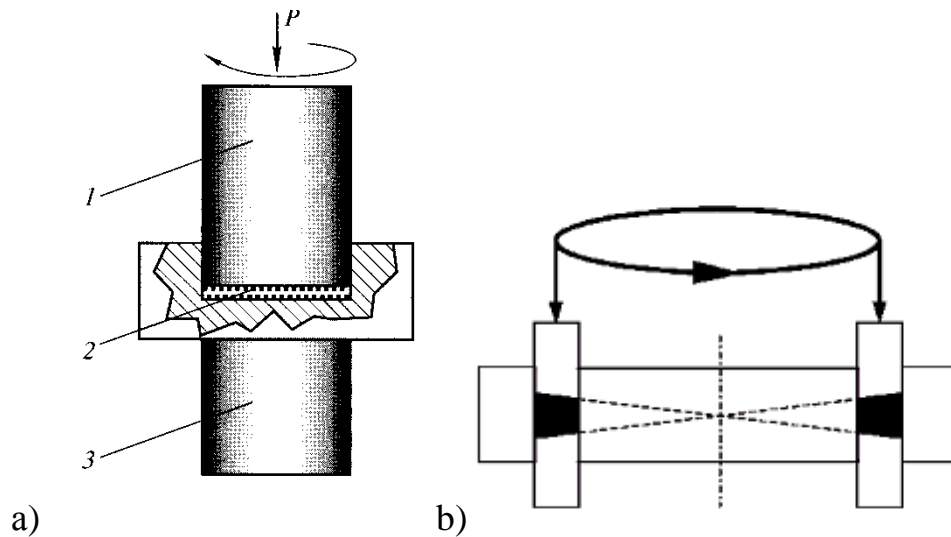
Similar conditions can be obtained by deforming the metal by methods such as high-pressure torsion, equal-channel angular pressing (ECAP), screw extrusion, all-round forging, and some others.

High-pressure torsion (HPT), as the evolution of the Bridgman anvils was one of the first ways of obtaining three-dimensional UFG and nanostructured samples, and later developed in works [1, 6, 17-19].

The samples obtained by high-pressure torsion have the shape of discs. The sample is clamped between the punch and the caliper and compressed at an applied pressure of several GPa. The caliper rotates, and, the forces of surface friction and cause the specimen to deform by shear.

The geometric shape of the sample is such that the bulk of the material is deformed under quasi-hydrostatic compression under the influence of applied pressure and pressure from the outer layers of the sample. As a result, the deformable sample, despite the high degree of deformation, is not destroyed [1].

In this case, the deformation of the sample has a radial inhomogeneity, which can be minimized by a large number of revolutions [1]. By the method of torsion under high pressure, it is also possible to process the workpiece in the form of a ring, according to the scheme proposed by S. Erbel [20]. Process scheme is shown in figure 1.3.



a) – High-pressure torsion scheme of the disk sample  
 b) – High-pressure torsion scheme of the ring sample  
 1 – punch; 2 – billet; 3 – support.

Figure 1.3 – Scheme of realization of severe plastic deformation by high-pressure torsion

This method has the development and improvement aimed at improving the homogeneity of the resulting structure in different ways in the center and on the periphery of the sample, manufacturability and expansion of the types of produced materials.

Thus, in the patent [21] it is proposed to carry out a cyclic change in the specific pressure by 10-20% of the current value with a frequency of 0.1-1.5 of the set speed of rotation of the striker in the high-pressure torsion process. In addition, the task is achieved by the fact that the speed of rotation of the striker during deformation is also cyclically changed. In addition, the task is achieved by the fact that in the process of deformation change the direction of rotation of the striker in increments of 0.1-1.5 turns.

The technical result is achieved by the fact that the cycling of the load during the SPD by torsion leads to a change in the concentration of vacancies in the workpiece material, which in turn affects the rate of "crawling" of the dislocation and thereby on the deformation mechanisms and mechanisms of formation of an ultra-fine-grained structure, ensuring its homogeneity. The cycling of the load at the SPD by torsion is similar to the rotation of the sample during equal-channel angular pressing, which leads to a change of sliding systems during processing and thus provides a more uniform microstructure of the material and, consequently, an increase in physical and mechanical properties, such as tensile strength and microhardness.

Thus, the authors [21], to further increase the uniformity of the microstructure of the sample, focus on providing the condition (4) – non-monotonicity and turbulence of deformation.

The patent [22] describes a method for obtaining products from magnetically soft amorphous alloys by torsion under high pressure with cryogenic temperature (77 K) deformation. According to the authors [22], this approach allows to improve the magnetic (hysteresis) characteristics of amorphous soft magnetic alloys by grinding the structural units of the material to 100 nm or less. Here, for ultra-high grinding, the authors used the condition (3) – to ensure the lowest possible temperatures, while the deformation of materials of this class without destruction, especially at low temperatures, is possible only under high hydrostatic pressure.

Also known are a number of patents aimed at technical improvement of components and parts of the installation itself [23-24]. In addition, there are attempts to introduce torsion elements as intensifying shear deformations in other SPD methods [25-26].

Using the high-pressure torsion method, many researchers in many materials managed to obtain a structure with the smallest grain size (up to 20 nm), study its features and evaluate a number of their mechanical and physical properties [1, 5, 17-19].

However, the prospects of using high-pressure torsion as an industrial method have significant disadvantages, due primarily to the small size of the workpiece and low tool life due to high loads on it. This fact seriously narrows the practical application of this method and actually limits it to the academic environment.

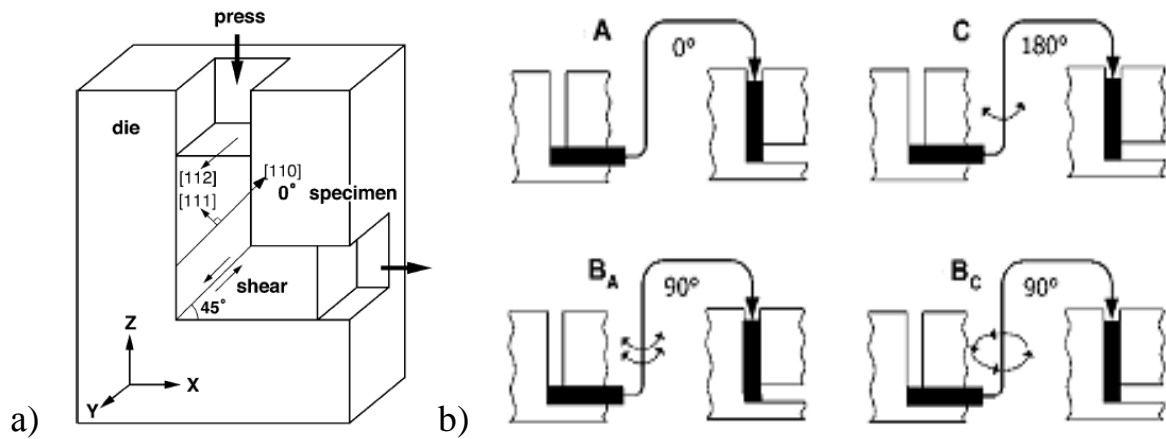
The method of equal-channel angular pressing (ECAP) is devoid of many of the above disadvantages and allows to obtain volumetric prismatic samples with a homogeneous UFG structure at a grain size of 100-200 nm and does not require complex equipment. The method consists in pushing the workpiece through the angular channel of the matrix and implements a simple shear scheme. Various options for implementing ECAP are shown in figure 1.4.

This method was invented and patented by V. Segal in 1973 [27] for crushing the cast structure of ingots. The idea of significant deformation without changing the shape of the workpieces was attractive.

However, the application of ECAP for obtaining of UFG and NS materials began only in 1990s R.Z. Valiev, T.G. Langdon, Z. Horita, V. Segal and others. The most complete anatomy of ECAP and its various variations is generalized and presented in the work of R. Z. Valiev and Langdon T.G. [29], as well as in the works [1-2, 4-6, 10-11, 15-16, 27]

According to many studies (see above) to obtain a uniform UFG structure over the entire volume of the workpiece, it is necessary from four to eight passes with an intermediate edging of the sample, for example, according to the scheme shown in figure 1.4 (b) [1].

This method is most studied and is one of the most frequently mentioned in scientific articles devoted to the study of the properties of various UFG and NS materials. Also, this method has many variations of technical and technological performance presented in patents of different countries. Various versions of ECAP are shown in figure 1.4.



a) – schematic diagram of ECAP; b) – different pressing routes to ensure the desired degree and uniformity of deformation in the sample

Figure 1.4 – Scheme of equal channel angular pressing (ECAP)

The improvements are mainly aimed at increasing the degree of deformation and in one pass, and increasing the uniformity of the structure throughout the volume.

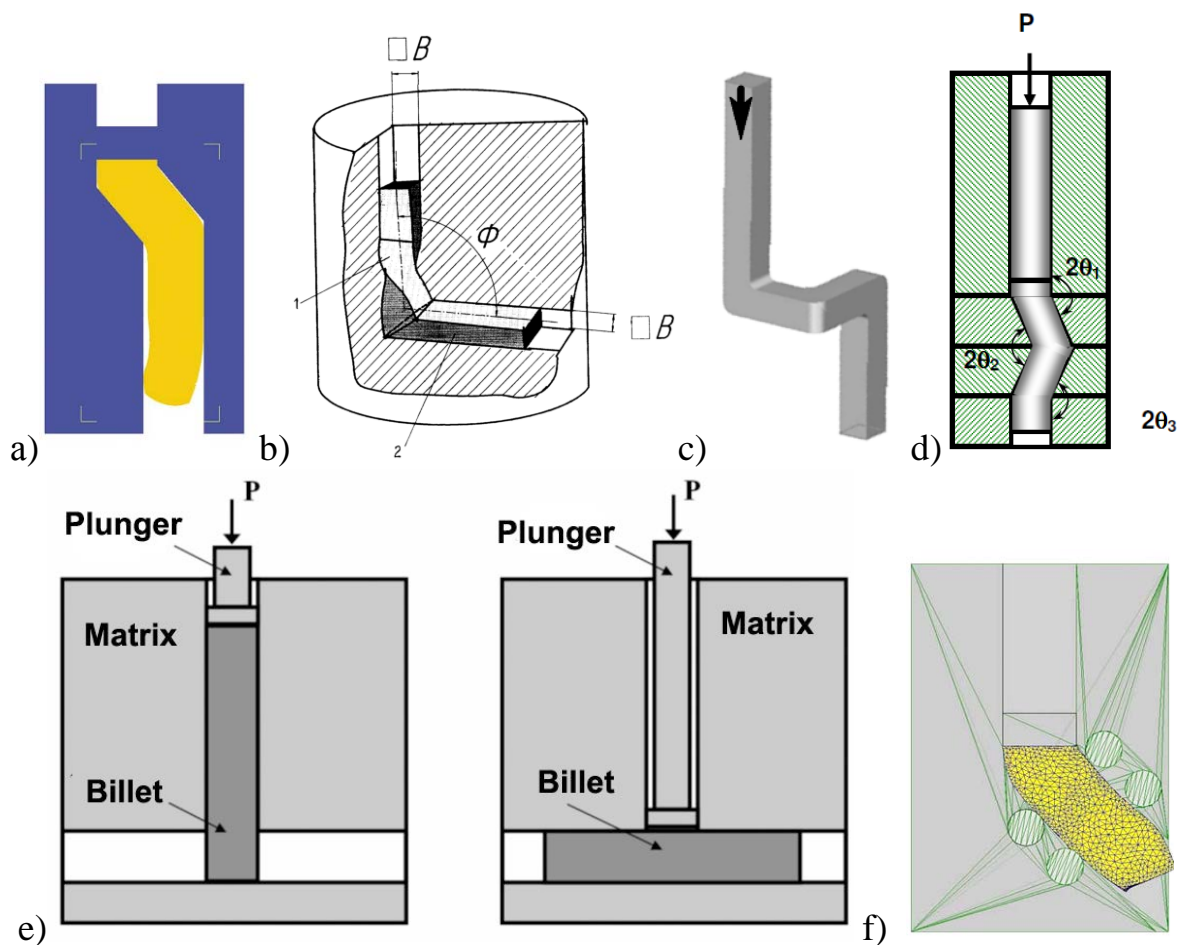
The most attention will be paid to the step ECA matrix (in some sources – ECA matrix with parallel channels) [30-31] (figure 1.5a), which allows to implement two alternating centers of deformation, provided the co-direction of the input and output channels. This scheme is also energy-saving, because it allows to realize a greater degree of deformation in one pass at the same force. Due to the co-direction of the input and output channel and a relatively small pressing force, this type of matrix is most convenient for creating combined processes.

There is a certain tendency to combine torsion deformation with pressing and other metal forming processes, which can be concluded from the review of patent sources and works [1, 5]. It is also stated that torsion deformation slightly reduces the required deformation force.

In the method described in the patent [32] (figure 1.5 b), the combined severe plastic deformation of the billets is carried out in the following sequence: torsion deformation in the screw channel, then the workpiece passes into the matrix section that implements equal-channel angular pressing.

When pressing the workpiece through the screw channel of the matrix, it experiences intense shear deformation mainly in the cross section, which is superimposed on the subsequent ECA-pressing homogeneous intense bulk shear deformation. In the process of a full cycle of pressing in the material of the blanks, the structure is crushed, while the proposed sequence leads to a more isotropic structural state. This is due to the fact that a more uniform and intense shear deformation is imposed on a less homogeneous torsional deformation by the nature of the torsion, which smoothes the resulting heterogeneity after torsion, both structurally and in obtaining more homogeneous properties. The reverse sequence leads to the imposition of a more heterogeneous state on the homogeneous, which is fixed in the workpiece after pressing. While all known methods of pressure

treatment show that the values of these characteristics of the material in different directions of the workpiece are significantly different.



a) ECAP in the step matrix; b) Combined method: torsion and ECAP; c) and d) Equal channel multiangular extrusion; e) Equal-channel angular T-shaped pressing; f) ECAP in a rolled matrix

Figure 1.5 – Different types of equal-channel angular pressing

Close to the described invention is a method [33] combining ECA-pressing and torsion deformation provided by rotating the workpiece in a horizontal channel by means of a gear wheel.

There is also a tendency to create multi-angle equal-channel matrices (Equal channel multiangular extrusion, ECMAE) in order to implement alternating deformations. The most interesting solutions are presented in the European patent [34], [35] (figure 1.5 c), and [5, 37-38] (figure 1.5 d). These methods increase the degree and uniformity of deformation in one pass, but require significantly more effort and are not suitable for all materials and temperature-speed deformation conditions.

Pressing in them is accompanied by a change in the direction of shift in the next zone, including the opposite - in terms of the nature of the structure formation is important, because it means a change in the sign of deformation. In each zone,

the main axes of deformation undergo rotation, and when the material passes through each subsequent zone, the direction of rotation of the axes changes to the opposite. This contributes to the effective fragmentation of the structural components and the formation of isotropy of the structure in each deformation cycle. With each subsequent focus and deformation cycle as a result of the appearance of a large number of directions in which an elementary shift in the micro volumes of the deformable material can occur, a redistribution of the micro-distortions of the crystal lattice between the individual micro-volumes of the plastically deformable material occurs. This also contributes to the intensive crushing process of mosaic blocks and individual crystallites, resulting in a fine structure [5, 39].

In these methods, the intensity of hardening is less than in the traditional monotonic plastic deformation (for example, hydroextrusion), due to some relaxation of microstresses as a result of more intensive crushing of the structure with intermittent alternating deformation process.

The above-described physical features of deformation in multi-angle ECA matrices can also be applied to the description of the processes occurring in the metal during compression in a step matrix.

With all the described advantages of multi-angle ECA-pressing in the formation of a homogeneous UFG and nanostructure, it also has disadvantages associated with a large effort or the need for a large number of passes, or are not suitable for all materials and temperature-speed deformation conditions.

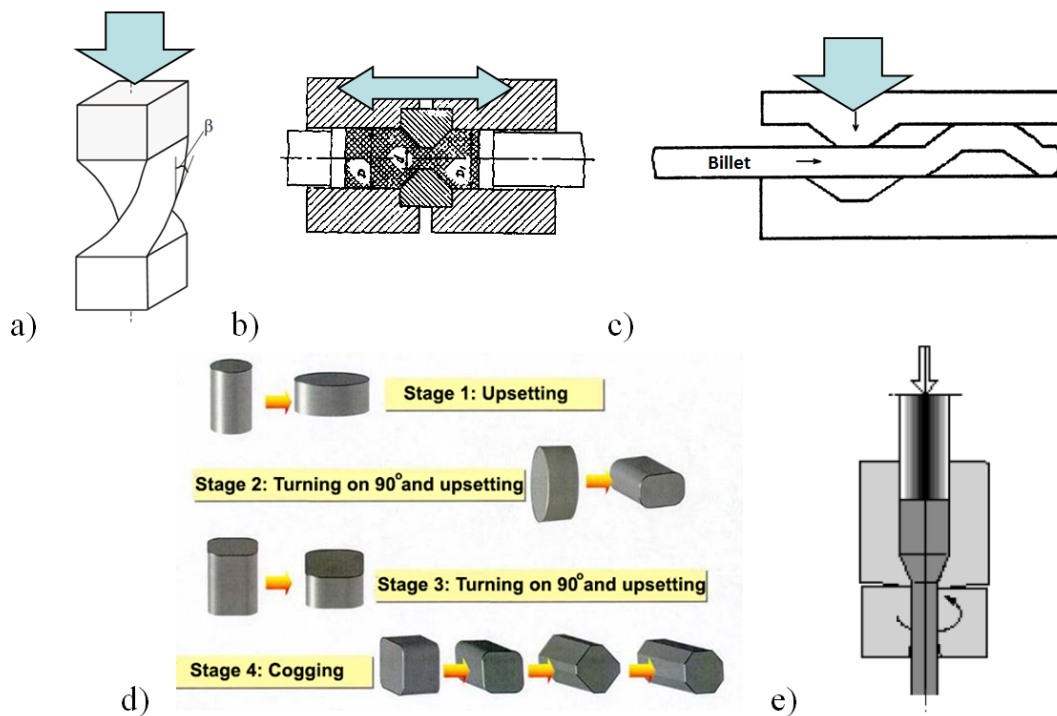
The design of the T-shaped matrix described in [5] (figure 1.5 e) creates too uneven deformation in the volume of the workpiece and requires a large number of cycles to obtain an isotropic structure.

A common disadvantage of the ECAP process is the need for a large deformation force in the processing of massive bodies and low tool life. Elimination of these shortcomings is possible when pressing the blanks in the roller matrix. The roller matrix known from the patent [40] allows to obtain the UFG structure with much less effort, but it requires a greater number of passes. Nevertheless, relatively small efforts allow us to recommend such designs for the creation of combined units.

The described methods and devices are the most effective and popular for obtaining UFG and nanostructures, however, there are other methods that also allow to obtain UFG products by intense plastic deformation. Other methods are shown in figure 1.6.

Screw extrusion is shown in figure 1.6 (a) [41-45]. The essence of the SE is that the prismatic sample is pressed through a matrix with a channel containing two prismatic sections separated by a portion of the screw shape. During processing, the material undergoes intense shear, maintaining the identity of the initial and final cross sections of the sample. The latter circumstance makes it possible to carry out its multiple extrusion in order to accumulate a large deformation that leads to a change in the structure and properties of the material, which makes this process similar to the ECA. The most important distinguishing feature of the SE from other methods of SPD is a powerful vortex flow in the deformation site, which provides

intensive mixing of the deformable material and creates prerequisites for the formation of unusual structures and the formation of new phases. The efficiency of processing by SE is currently shown on the following metals and alloys: secondary aluminum alloys AK9, AK5M2, AV87; titanium alloys VT1-0, VT-6, VT-22, VT3-1; copper-phosphorus alloys, Al-Mg-Sc alloys and others [43].



a) – Screw extrusion; b) – Cyclic extrusion ("hourglass"); C) – Forging in trapezoidal strikers; d) – All-round forging; e) – Pressing with torsion.

Figure 1.6 – Different ways of implementing severe plastic deformation

Another method of deformation of blanks, allowing to implement significant shear deformation is invented by M. Richert (Krakow University, Poland) [46] cyclic extrusion-compression (CEC, "hourglass") shown in figure 1.6 (b).

This method consists in repeated deformation of the metal by extrusion, or pressing, through the narrowed hole of the tooling, the longitudinal section of which has the shape of an hourglass. If you apply the force of extrusion to the deposited part of the workpiece on the other hand, the process will repeat. Such a deformation scheme in a multi-cycle mode allows to obtain a structure in the UFG billets with a diameter of 15 mm and a length of up to 100 mm.

The method was first used for the accumulation of large plastic deformations in pure aluminum at room temperature. Experiments show that the saturation of stresses occurs after 4-5 extrusion cycles. To date, the method has been used only for deformation of a limited number of materials [46-48].

Comprehensive forging (multiaxial forging, 3D forging) can also be used to form UFG and nanostructures in massive samples (figure 1.6 (d)). This method was proposed by G.A. Salishchev with co-authors [49] and improved by Gosh [35]. The process of all-round forging is usually accompanied by dynamic recrystallization.

The scheme of all-round forging is based on the use of multiple repetition of free forging operations: draft-broach with a change of the axis of the applied deforming force. The uniformity of deformation in this technological scheme in comparison with ECA-pressing or torsion is lower. However, this method makes it possible to obtain the UFG state in sufficiently brittle materials, since the processing begins with elevated temperatures and provides small specific loads on the tool. The choice of appropriate temperature-speed deformation conditions allows to obtain very small grains of about 100-500 nm in pure metals and less than 100 nm in alloys. This approach is usually implemented at plastic deformation temperatures in the range (0.3-0.6) of the melting point [1, 49].

Also, to intensify the deformation of the forging process, special forms are used (for example, the strikers shown in figure 1.6 b), after broaching in which it is possible to obtain a more uniform structure in less time than with comprehensive forging [50-52].

Disadvantages of forging processes – their high labor and energy consumption, with a non-uniform distribution of deformation in the volume of the workpiece.

Conventional pressing with torsion (twist extrusion) shown in figure 1.6 (d) also allows to intensify shear deformation and reduce the pressing force, but it is inherent in almost all the shortcomings of ECAP [35, 50].

There are attempts to achieve an intensive and uniform study of the rolling structure, by using a special form of rolls or gauges in them. The hot rolling scheme, the number of passes, the deformation temperature, especially the temperature of its end, determine the flow of austenite decay processes together with the influence of the cooling rate. Traditional forms of rolling, developed and tested over a number of years, optimize the deformation process by the efforts of stands, roll stability, mill performance. Regulation of the temperature of the end of rolling and cooling rate, as well as micro-alloying of steels allow to obtain fine grain with a large number of dislocations in the grain body fixed by impurity atoms [5, 54]. Thus, in Ukraine, E.G. Pashinskaya patented scheme of hot rolling rod with the implementation of intensive shear [55], which allows to obtain an equiaxial structure with a grain size of up to 2 microns [54].

For larger variational profiles it is possible to use a system of gauges "rhombus-square" with a non-diagonal arrangement of the rhombic caliber relative to the longitudinal axis of the rolls in such a way that the two opposite sides of the rhombus are parallel to the axis of the rolls, and the other two sides of the rhombus at an angle to the axis of the rolls. As a result, the billet of square or rectangular cross-section, specified in such a rhombic gauge, receives along with high-altitude compression and transverse shear, which provides intensive plastic study of the structure [56].

There are also some other ways to intensify the variational and even sheet rolling, but none of these methods is not able to provide a structure in the metal close in quality to the structure obtained by the ECAP.

The only exception is the type of cross-screw rolling (Cross-rolling or less Helical rolling, even less Screw rolling), allocated by its authors in a separate

method called "Radial-shear rolling" (RSR) and patented [57]. Contrast to conventional helical rolling, are used, for example, when the piercing of the pipes, is that there is a rolling of the solid rod in the three-roll scheme, with higher values of angles of flow. The scheme of the process and its features are shown in figure 1.7.

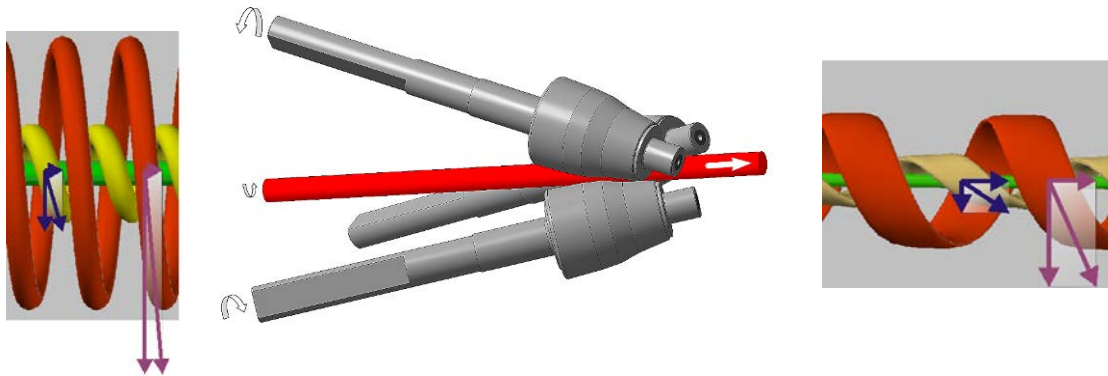


Figure 1.7 – Scheme of cross-screw rolling and features of the metal flow in axial, intermediate and peripheral zones of the workpiece

The deformation zone is formed by three drive rolls, deployed at an angle to the axis of the workpiece and at an angle to each other. Unlike traditional pipe mills of screw rolling in RSR mills, conditions are created not for loosening of the central zone, but on the contrary, for compaction and intensive deformation processing of metal in the entire volume of rolled products [58].

In screw rolling, a stress state scheme close to all-round compression with large shear deformations is implemented in the deformation center. The most intense shear deformations are localized in the zone of intersection of metal sliding lines – the ring zone of the cross-section characteristic of the three-roll scheme. In other words, in the deformation center conditions are created that satisfy the listed at the beginning of the subsection and are optimal for the formation of the UFG structure.

The main feature of screw rolling is the non-monotonicity and turbulence of deformation, as well as differences in the plastic flow and study of the structure of different zones of the workpiece, due to the trajectory-speed features of the process shown in figure 1.7 [57].

In the method of screw rolling [57-58], compression is carried out with a slowdown in the movement of the metal, reducing the length of the screw trajectories in the outer layer of the workpiece, while accelerating the movement of the metal, increasing the length of the trajectories in the inner layer of the workpiece, with the thickness of the outer layer in the rolled workpiece is 0.3...0.7 of its radius, and the ratio of linear compression deformations along the screw trajectories on the surface of the workpiece and stretching along its axis is -0.1...-0.5 [57].

In the outer layer, each small trajectory-oriented element undergoes compression deformation along the radius of the workpiece, compression

deformation in the direction of expiration (along the helical path) and, accordingly, tensile deformation across the helical path. It is important that there is a constant gradient of velocities and flow directions along the radius, which adds additional shear elements to the overall complex picture of the stress-strain state. Elements of the structural structure of the metal subjected to an expanding flow with bilateral sediment (along the trajectory and along the radius) take the form of isotropic isolated particles of high dispersion.

The speed of the particles in the axial fiber and its length as well as in the longitudinal rolling increases in proportion to the coefficient of extraction. The cross section of the central current tubes is reduced. Study of the metal structure acts on the type of longitudinal rolling in calibers with multilateral compression or compression. The structural elements of the structure are extracted and refined with the formation of characteristic structural banding.

In general, in terms of the volume of the workpiece, the helicoidal flow of the metal with the inhibition of the surface layers and the acceleration of the central ones creates the effect of a volumetric macrodrive, which also contributes to the deepening of the metal structure study [59].

Screw rolling with the above features is possible rolling a wide range of materials up to complex alloyed hard-to-formable special alloys of ferrous and non-ferrous metals [61-62]. In the work [63] by combining long-range rolling with rolling on the mill described in the patent [58] it was possible to obtain a homogeneous globular ultra-fine-grained structure with an average grain size of 150 nm from titanium of technical purity at a grain size of 50 nm to 500 nm.

The improvement of the same method allowed the same authors [61] to obtain long rods with a diameter of 8 mm of titanium UFG with an average grain size of 90 nm, while grains from 30 nm to 300 nm were recorded, and the proportion of grains with a size of less than 100 nm was 64 %.

Also known work [64-65] in which thermomechanical processing using screw rolling were obtained UFG structure on titanium W-6 and steels 45 and U10A.

After reviewing the basic methods of obtaining UFG materials with non-equilibrium high-angle grain boundaries, we can conclude that the most complete all the conditions for obtaining the desired structure, satisfies the high-pressure torsion method. However, it is the least suitable for any practical application, since it allows processing samples of only small sizes (disks of the order of 10 mm in diameter and 0.5 mm thick), which is not enough even for laboratory studies. The method is very energy intensive and is not suitable for modernization.

Equal-channel angular pressing in its various forms is the most compromise way to obtain bulk products with high-quality homogeneous UFG structure, but also has its basic limitations associated with the inability to produce long products, the need to perform a large number of deformation cycles, strong tool wear, insufficient manufacturability, and, still high, for industrial production energy consumption, which significantly reduces the productivity of the process and its commercial appeal. In the existing form, the industrial implementation of ECAP is

suitable at best only for small-scale subsidized production of small products with properties that can not be obtained in other ways (medical implants, etc.).

Comprehensive forging and forging in the special strikers realizing SPD to some extent allows to bypass restrictions on the sizes of the made products, but at the price of high power inputs in comparison with ECAP, and besides, production of UFG of products forging is a little suitable for creation of high-performance, cost-effective production. Production of forging is a getting of massive piece of UFG products that cannot be obtain in other ways.

Different types of rolling with a shift, or do not provide a sufficient level of isotropy of the structure, or the resulting structure does not fully meet the requirements set out at the beginning of the subsection, as a rule, is not provided throughout the special state of the grain boundaries, shown in figure 1.1. In particular – screw rolling, forming UFG structure on the periphery – does not provide sufficient elaboration of the axial zone of the workpiece.

Having critically studied the materials on the above methods of obtaining UFG products, it can be concluded that in the current state none of the known methods, due to high energy costs, is ready for economically justified wide industrial application. The problem can be solved only by ensuring the continuity of the process. The solution to this problem seems to lie in the area of combining processes.

### 1.3 Combined energy-saving SPD processes

It is possible to radically reduce energy consumption by building a combined process that allows to obtain long blanks in a continuous way.

As a basis for the creation of combined SPD methods, a special place is occupied by the method of continuous pressing Conform, as the most studied in scientific works and already having some industrial application, and it is especially promising in non-ferrous metallurgy [66-69]. The scheme of the combined process of ECAP-Conform is shown in figure 1.8.

The deforming force is formed by the active friction forces acting on the working surface of the rotor. In this case, the working channel of pressing is formed by the rotor and the working surfaces of the clamping and stop.

Using this method allows you to remove the restriction on the length of the pressed workpiece. However, to obtain a uniform UFG structure requires several cycles of pressing, and therefore, there are new problems associated with compliance with the temperature regime for a long workpiece.

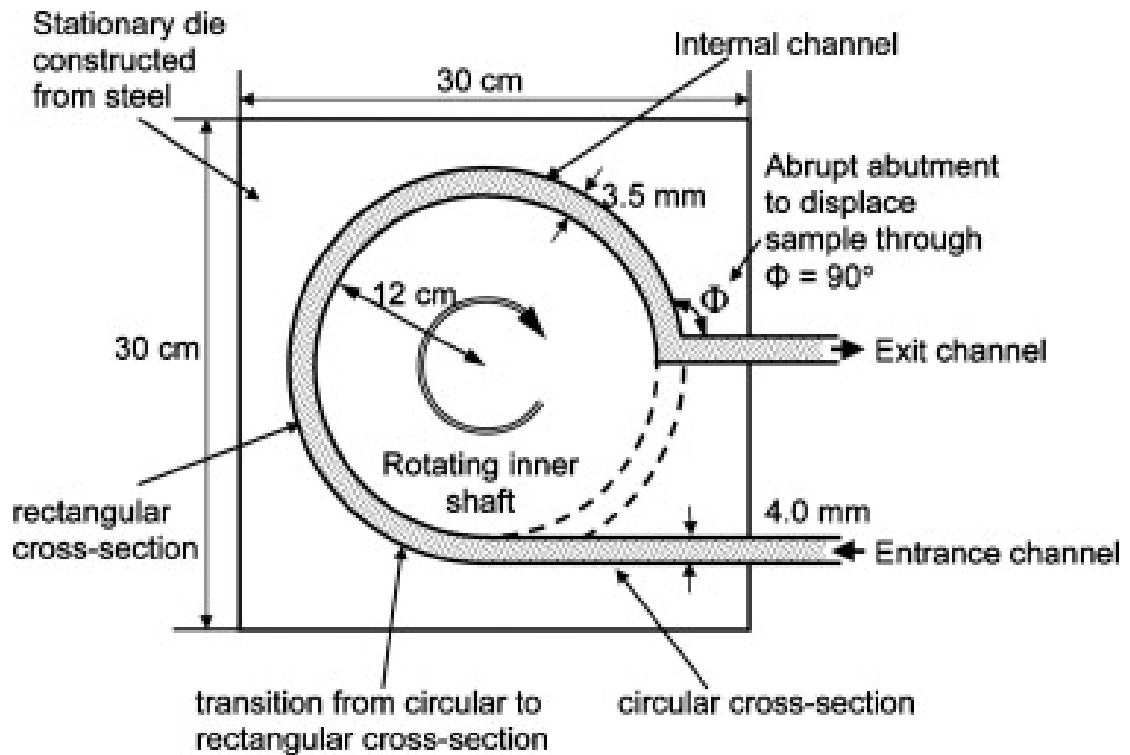
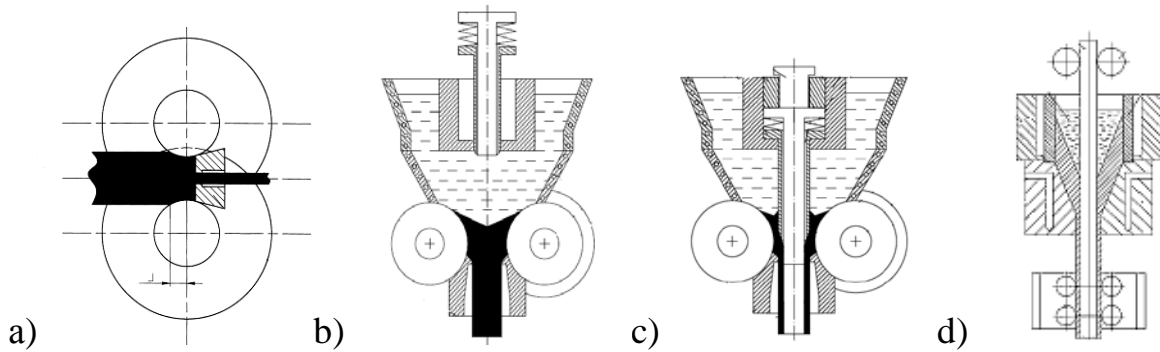


Figure 1.8 - Scheme of continuous pressing process "ECAP-Conform»

The successful application of the combined process "rcup-Conform" to obtain the UFG structure in the metal was made by G. Raab [66]. And since the autumn of 2014 at the enterprise "COMTES FHT" (Pilsen, Czech Republic) the combined stand Conform-ECAP created on the basis of the serial machine "CONFORM 315i" is put into trial and commercial operation [70]. The plant receives UFG titanium for medical implants. This is a real area of application of UFG materials, as, for example, says the us patent [71] obtained in 2002.

Similar devices are described in articles and patents by scientists of the Siberian Federal University under the guidance of prof. S. Sidelnikov [72-75]. A number of developed and patented by them combined processes based on Conform are known such as "rolling-pressing" [76-77], "casting-rolling-pressing" of solid [77] and hollow profiles [78]. Also from the patent of O. Lekhov [79] and the work [80] the combined process of "casting and rolling of a bimetallic rod" is known. The general essence of the methods is that the melt is poured directly into the rolls-crystallizers, crystallized in the form of a rectangular workpiece, which is deformed by means of the same rolls, and then extruded through the gauge hole of the matrix. An illustration of these methods is shown in figure 1.9.

For the first time such a method of manufacturing press products patented in England under the name "Castex". According to this method, leading in this direction firms Babcock Wire Equipment and Holton Machinery LTD are manufactured and replicated line of continuous casting and pressing of non-ferrous metals on the basis of Conform stands [75].

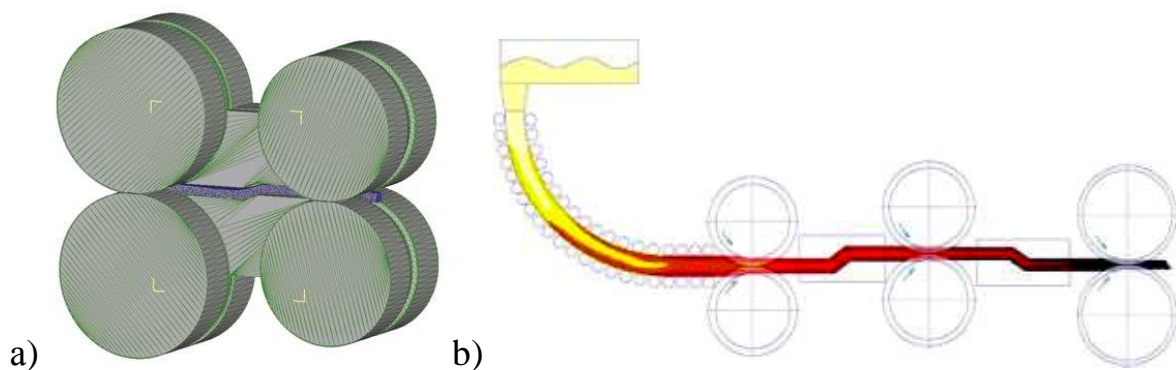


a) "rolling-pressing"; b) "casting-rolling-pressing" solid billet; c) "casting-rolling-pressing" of hollow billet; d) "casting-rolling-pressing" of bimetallic billet

Figure 1.9 – Combined methods

Almost all of these methods (except for ECAP-Conform), despite their advantages and innovative potential are not aimed at obtaining the UFG structure and the use of all of them is limited only to non-ferrous metals.

For the purposeful formation of UFG structure of a wide range of materials, a continuous combined method of "rolling-pressing" using a stepped ECA matrix was invented [81]. The same authors [82] have the idea of a combined process "casting-rolling-ECAP". Both methods are shown in figure 1.10.

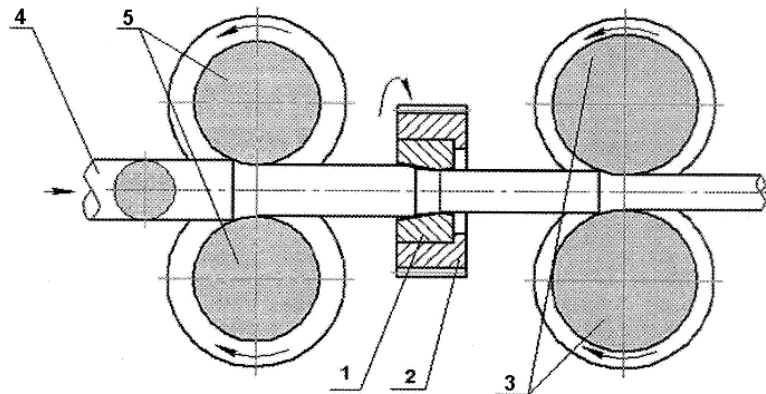


a) «rolling-ECAP»; b) «casting-rolling-ECAP»

Figure 1.10 – Combined processes with continuous ECAP

Theoretical study and justification of the first process was carried out in [82-83], experimental study of rolling-pressing of aluminum in [84]. After three cycles of continuous pressing it was possible to achieve grinding of grain from 180 microns to 3.5 microns. The method is aimed at energy-saving obtaining of UFG structure, however, it does not allow to develop the required level of deformation in one pass, and the shape of the resulting product is limited to a rectangular cross section.

Increase the intensity and non-monotonicity of deformation can be included in the scheme of combining torsion elements, as a device claimed in the patent [86] and shown in figure 1.11.



1 – matrix; 2 – gear wheel; 3 – calibrating rolls; 4 – billet; 5 – feed rolls

Figure 1.11 – Combined “rolling-torsion-rolling” process

The workpiece 4 by means of the feed rolls 5 enters the horizontal channel of the matrix 1. By means of the gear wheel 2, the workpiece is deformed by torsion in the hearth located between the feed rolls and the torsion node. The degree of deformation depends on the speed of rotation of the gear and the speed of rotation of the feed rolls 5 and calibrating rolls 3. The presence of comb-shaped protrusions in the conical part of the horizontal channel eliminates the possibility of turning the workpiece inside the matrix. Next, the workpiece falls on the calibrating rolls 3 for the final finishing of the shape and size to the desired. In addition, when processing the calibration rolls, the surface layers of the workpiece are strengthened (deformation by rolling) and the surface roughness is reduced. By changing the speed of rotation of the calibration rolls, the back pressure force required to achieve higher degrees of deformation can be changed smoothly without stopping the processing. Torsion deformation and rolling according to the present invention provide an severe plastic deformation in the workpiece material, which leads to an improvement in the mechanical properties and quality of the processed blanks.

However, to create a uniform UFG structure of such deformation may not be enough, therefore, methods have been developed for various combinations of screw rolling and shape rolling with the implementation of intensive twisting of the workpiece in the intercellular interval [87-89]. Thus, by having a place of intense deformation at screw rolling added warp torsion and a small compression in the bars of the crate.

In the patent [87] a way to "screw rolling - shape rolling", allowing according to the authors, to obtain more uniform fine structure due to the twisting of deformed workpiece after the helical rolling in front of the caliber of shape stand.

The proposed method was developed and tested in "VNIIMETMASH" on a pilot plant consisting of a series of induction furnace, a screw rolling stand, two longitudinal rolling stands and scissors. The method is as follows. The heated billet

is fed to the screw rolling stand, captured by the working rolls and crimped to the required size. Then the front end of the roll is captured by the rolls of the longitudinal rolling stand and torsion deformation occurs in the intercellular interval.

Then, to stabilize the process and more accurate control of extracellular shear deformations, the method was improved by the authors and declared in the patent [88]. The improvement was that the extra-roll deformation of the billet by twisting is produced in the screw rolling stand, stopping the rotation of the billet at the output of the rolls by roller wiring, and then the rod is captured by the rolls of the varietal stand. This method is shown in figure 1.12.

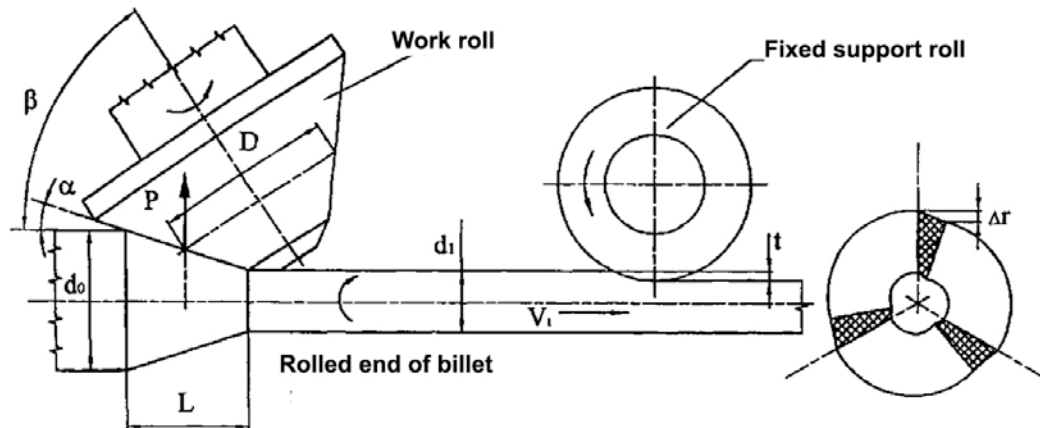


Figure 1.12 – Combined process "screw rolling-longitudinal rolling»

There is also a variant of the reverse combination of longitudinal and screw rolling, declared in the patent [89]. The method is shown in figure 1.13.

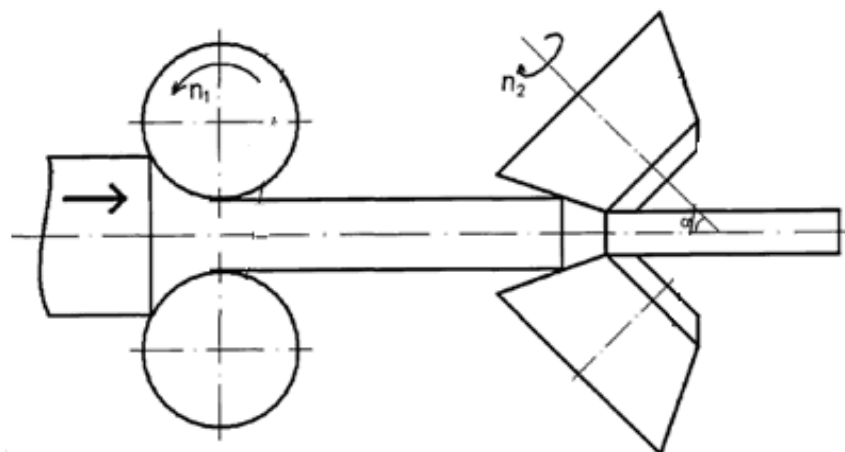


Figure 1.13 – Combined process "longitudinal rolling – helical rolling»

The magnitude of the force of the support depends on the mechanical properties of the material and the degree of shear deformation and is selected empirically. The backstop force, according to the authors of the invention, can be achieved up to 10 GPA [89].

As the previous one, this method includes extra-roll deformation of the workpiece by twisting in the interval between adjacent stands of screw and longitudinal rolling. Deformation, accompanied by a change in the physical and mechanical properties of the metal and the formation of a fine-grained structure, is provided by the fact that the processing is started by longitudinal rolling, after which the cross-screw rolling is carried out with circular compression and rotation of the workpiece, acting on the workpiece compressive stress due to the force of the support, achieved due to the difference in the metal flow rates during longitudinal and helical rolling.

Finishing the review of combined methods, we will mention other methods that are not included in the detailed review. There are known combined methods of "pressing-drawing", equal-channel angular broaching, continuous pressing by the method of Extrolling, Linex, and some others [1, 5, 74-76], which are either too highly specialized or do not provide the formation of the structure of the desired quality.

From all considered methods, the most attention was drawn to the methods of "rolling-ECAP" and "longitudinal rolling-screw rolling". But the first method, producing a uniform study of the structure due to the step ECAP, however, does not provide a sufficient degree of deformation in one pass, which forces the use of a multi-flight scheme with high energy consumption, and the second method, developing a sufficient deformation for the UFG formation, suggests some anisotropy of the properties of the axial and peripheral zones of the rod.

In general, the most promising seems to be the use in the combined process of screw rolling with additional deformation, leveling properties on the cross section of the bar and the ability to achieve a sub-ultra-fine-grained structure for fewer passes, which will be the main factor in energy saving and approximation, thus, to industrial implementation.

#### 1.4 Theoretical aspects of combination of screw rolling and equal-channel angular pressing (ECA-pressing)

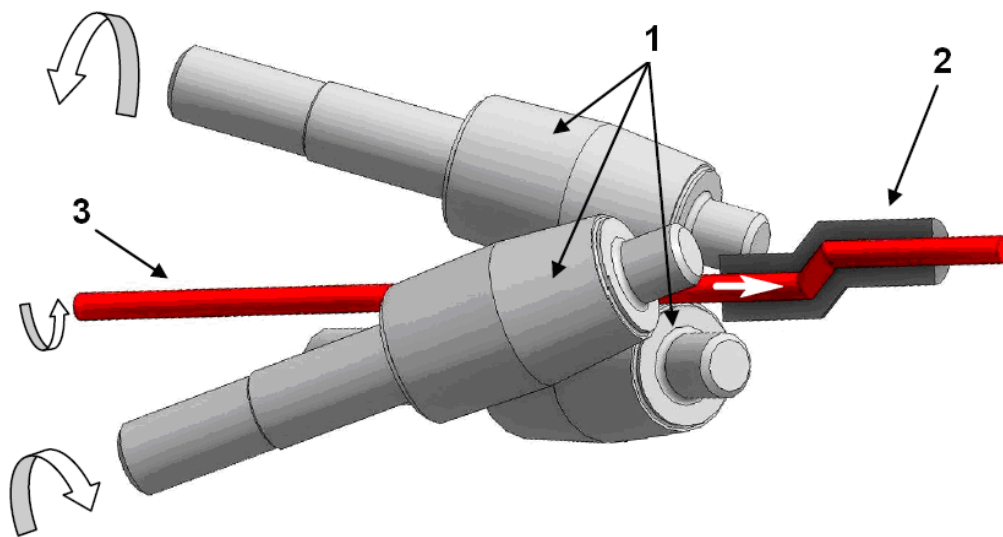
Cross-screw rolling can produce sections with good surface quality and significantly less effort than in longitudinal rolling or extrusion. Due to the peculiarities of the metal flow and the stress-strain state during screw rolling, the greatest deformation, and, consequently, the study of the structure is obtained by the outer zones of the rolled bar. Thus, laminated in a similar way the rod has severely crushed microstructure in the outer areas and more coarse-grained Central part.

The combination of the process of cross-screw rolling and subsequent pressing in the equal-channel angular matrix allows to realize the scheme of the stress-strain state with intensive shear of the surface layers of the metal during screw rolling in the first deformation zone and the combination of intense shear deformation of the angular pressing with torsion in the second deformation zone. In this case, the unprocessed in the first center of the deformation of the central part of

the workpiece, will receive an intensive study under another scheme in the second center – in a step ECA matrix. This creates good conditions for the formation of ultra-fine-grained structure throughout the volume of the round billet. In addition, it is of some interest to study the parameters of angular pressing with torsion. In fact, it turns out the process of continuous pressing with elements of torsion of the workpiece inside the matrix, it will increase the level of accumulated deformation in the volume of the workpiece and will contribute to the development of the central zone. In the same way as in the method [32], a more uniform and intense shear deformation is applied to a less homogeneous torsional deformation by the nature of the torsion, which smoothes the resulting heterogeneity after torsion.

Thus, this method, of all the described methods, is one of the most energy-efficient. Here, in contrast to the "rolling-pressing", the rolling cage serves not only to push the bar into the matrix, but mainly performs a preliminary intensive deformation of the workpiece to a state close to the UFG, and the ECA matrix mainly aligns the structure along the cross section of the workpiece. This allows to achieve in one pass large degrees of deformation, which is the main factor of energy saving.

The device and process are shown in figure 1.14. Three-roll cage of cross-screw rolling, characterized in that three rotating in one direction conical roll (1) are located in the frame according to the vertices of an equilateral triangle, and their axes are at an angle to each other and to the axis of rolling, the output is combined with the matrix for pressing. Matrix (2) has three channels of the same cross section, two of which (input and output) are parallel to each other, and the middle channel is at an angle to the input and output channels.



1 – conical rolls; 2 – stepped ECA matrix; 3 – billet.

Figure 1.14 – Scheme of the combined process "screw rolling-ECA pressing»

The combination of the process of cross-screw rolling and subsequent pressing in the angular equal-channel matrix allows to realize the scheme of the stress-strain state with intensive shear of the surface layers of the metal during

screw rolling in the first deformation zone and the combination of intense shear deformation of the angular pressing with torsion in the second deformation zone. In this case, the untreated and elongated in the first center of deformation of the central part of the workpiece, will receive an intensive study according to another scheme in the second center – in a stepped ECA matrix. This creates good conditions for the formation of ultra-fine-grained structure throughout the volume of the round billet.

The implementation and bringing to industrial use of this process will allow to obtain a high-quality round bar by continuous pressing. The transition to different profiles will be carried out by replacing the matrix and changing the distance between the rolls, which is faster and easier to replace the calibrated rolls. Features of the rolling stand allow you to smoothly adjust the compression before pressing, which creates additional flexibility in the management of the process.

## 2 COMPUTER SIMULATION OF THE COMBINED PROCESS "SCREW ROLLING – ECA-PRESSING" TO ANALYZE THE POSSIBILITY OF THIS PROCESS IMPLEMENTING

At the present stage of development of science and technology has already become obvious that for deep analysis of technological process of conventional calculations is not enough. With further implementation in practice (whether conventional laboratory experiment or full-scale deployment) is necessary to ensure smooth operation of mechanisms, the absence of hardware failures, as well as to minimize the possibility of rejection of manufactured products. For this purpose it is necessary along with the classical methods of calculation to use new and innovative technologies. In particular, in the development and research of processes of processing of materials by pressure one current technique is computer simulation. This method of study of metal forming processes is very important, and several factors contribute to this.

First, the modeling allows the researcher to look "inside" the process, to estimate stress and strain, to predict the occurrence of defects. Second, it allows to identify the optimal parameters of the tool and workpiece for better conditions of process. And third, modern software modeling systems allow to simulate almost any process, avoiding expensive experiments. Therefore, the modeling of various deformation processes in metal forming is an important task.

Currently, when the computer industry offers a wide range of modeling tools, any qualified engineer or technologist should be able not only to simulate complex processes, but also to simulate them with the help of modern technologies, which are implemented in the form of graphical environments and visual modeling packages.

The simulation of metal forming processes is based on the fact that the metal flows in the direction of least resistance. The force of deformation is determined depending on the billet size, shape, friction and material properties. Furthermore, using simulation it is possible to determine such important parameters of the workpiece, as the accumulated strain, stress, temperature, grain direction, the possibility of destruction of the workpiece, tool wear.

One of the most popular products in this category is Deform – a specialized software package designed to simulate the processes of metal forming, heat treatment, developed by the American company SFTC.

Deform allows you to simulate almost all processes used in the processing of metals by pressure (forging, stamping, rolling, pressing, etc.), as well as heat treatment operations (hardening and aging, tempering, etc.) and machining (milling, drilling, etc.).

However, despite all the advantages inherent in this program, it also has disadvantages, which are a consequence of the use of the engine 8 years ago. For example, one of the rigid constraints is the maximum number of finite elements in a single body of 500,000. For large parts such as rolling rolls, ingots, slabs this number of elements is not enough to obtain accurate results. Therefore, at this stage of work, for the computer simulation of the combined process "screw rolling –

pressing" in order to analyze the possibility of implementing this process, it was decided to use the software package Simufact Forming made in Germany (Simufact Engineering GmbH).

Thanks to the proprietary MESHER engine, this software product is completely free of software limitations. When using it, the total number of finite elements in one body is unlimited, and the minimum side of the finite element can reach 1  $\mu\text{m}$ . In addition, Simufact Forming has the ability to simulate discrete modeling, i.e. at the very beginning when creating a model file, you can specify the type of deformation process, and the program will guide the user through the simplest and shortest way to create a model. This method of construction is most relevant for "heavy" models, with a fairly complex movement of the working tool. It was decided to follow this path, since the task of rotational motion in this program is quite a time-consuming task.

In our case, the simulated process is a combination of screw rolling and subsequent equal-channel step pressing in the matrix. The main deforming component in the process is a screw mill consisting of three rolls, which not only rolls the workpiece to a smaller diameter, but also pushes it through the channels of the equal-channel step matrix. Therefore, for this process, the type of deformation model "tube rolling" was chosen, which allows you to set the rotational motion of several tools, the axes of rotation of which lie in different planes.

For the construction of geometric models of the workpiece and the tool was used the software package "KOMPAS", which was created three-dimensional model that was exported to a compatible STL format. As a result, after importing geometry files into Simufact Forming, the following model was obtained (figure 2.1).

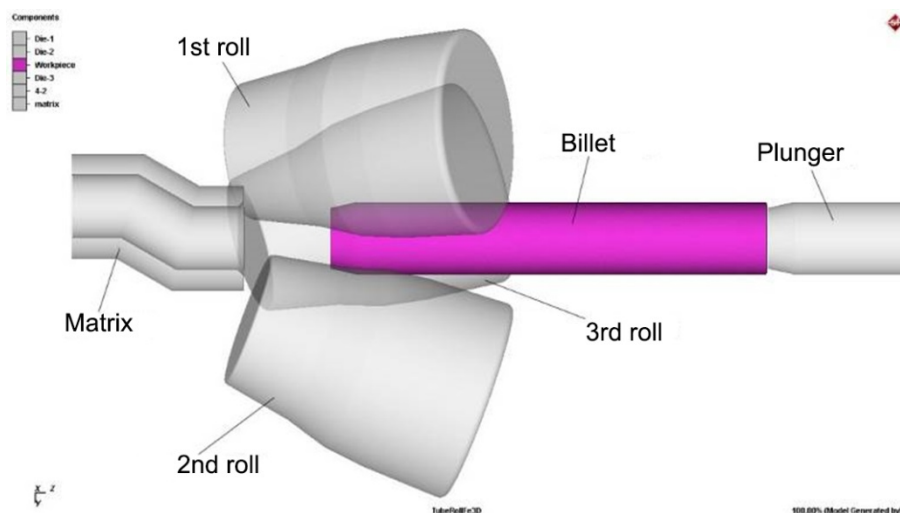


Figure 2.1 – Initial model

The original workpiece was a rod with a diameter of 25 mm and length 150 mm., This diameter value was selected as the most typical possible range of helical mill (mill allows to roll billets with a diameter of from 15 to 30 mm). The selection of the maximum diameter is undesirable, since in this case will require a substantial effort of deformation. Smaller diameter is also undesirable because in multi-pass

deformation (2-3 passage) there is a significant reduction of diameter and in this case has a chance of going beyond the range.

As a model material was selected steel 15. Roll dimensions and their structural location consistent with the design of the laboratory rolling mill 10-30. The roll rotation speed was 100 rpm. After rolling into the matrix enters the workpiece with a diameter of 20 mm. To avoid jamming of the workpiece at the entrance to the matrix was done with a small excess of the diameter of the channel matrix. In result equal-channel step matrix had channel diameter of 21 mm with the length of each stage of the channel is 20 mm.

When determining the value of the angle of intersection of channels in the matrix it was revealed that in the work [90] was found the optimal value of this parameter for the process of longitudinal rolling and pressing of the billet of rectangular cross section, which is equal to 140 degrees. However, in the implementation of helical rolling on the round billets are produced much smaller area of contact with the rollers, which in turn, significantly reduces the magnitude of the active forces of friction arising. It was therefore decided to reduce the angle of intersection in the matrix up to 150°.

The temperature of the billet was accepted by 1000° C as the average value of the recommended temperature interval of hot working steel 15 [91], all the tools in the model had a temperature of 20° C.

From work [92] is known that the axial force at the helical rolling is a highly time-varying value, changing its value within wide limits. Therefore, it was decided that this combined process to facilitate the capture, rolling and subsequent pressing will be used textured rolls with a notch. As a consequence, the coefficient of friction on contact of the workpiece with rolls was taken equal to 0.8, as recommended by the software for tool with a rough surface. The coefficient of friction on contact of the workpiece with the matrix was taken equal to 0,3, corresponding the faceted surface.

Another important factor, influencing all parameters of this combined process, is the distance of matrix from the deformation zone of the rolls. In work [93] was revealed that for a more stable process of rolling-pressing it is necessary that this parameter was minimal. In this case, the distance matrix from the deformation zone of the rolls was set at 15 mm, as the minimal value allowed by design of the mill. Closer to put a matrix is impossible, since it rests on the slanted edges of the rolls.

After calculation was got the next result (figure 2.2).

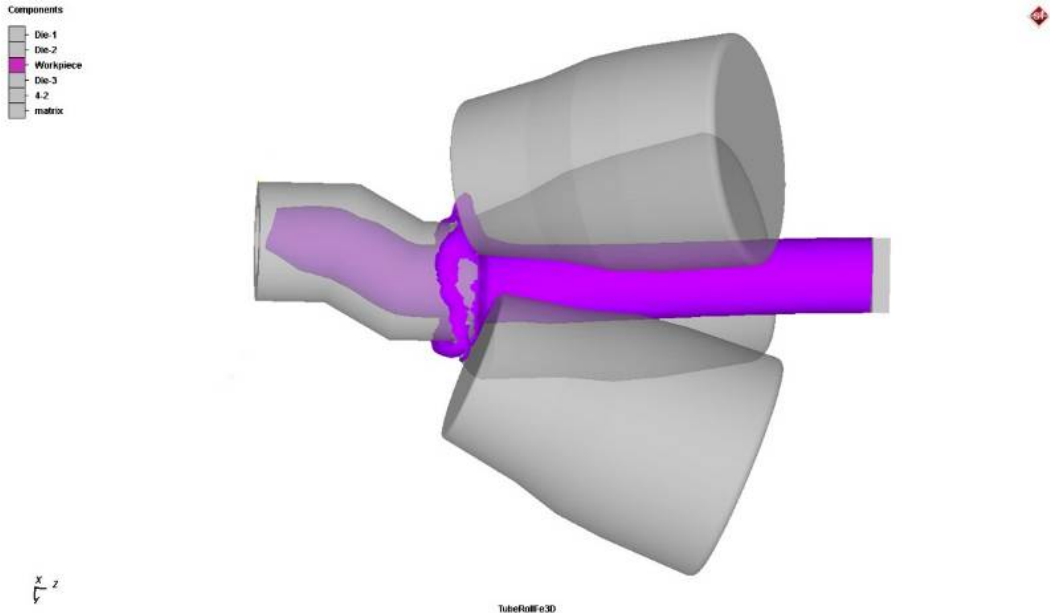


Figure 2.2 – Final model

The resulting model should be regarded as unsuccessful because the front end of the workpiece is not left from the matrix, and the resulting burr has made a further deformation is impossible. Analyzing the occurring forces in the rolls and in the matrix, it was concluded that rolling force generated by the rolls is not enough to overcome the force of back pressure in the matrix. As to increase the magnitude of the coefficient of friction in the rolls unwise due to the use of its maximum possible real value [94], it was decided to reduce the friction coefficient in the matrix – its value was reduced to 0.1. In result was obtained the next result (figure 2.3).

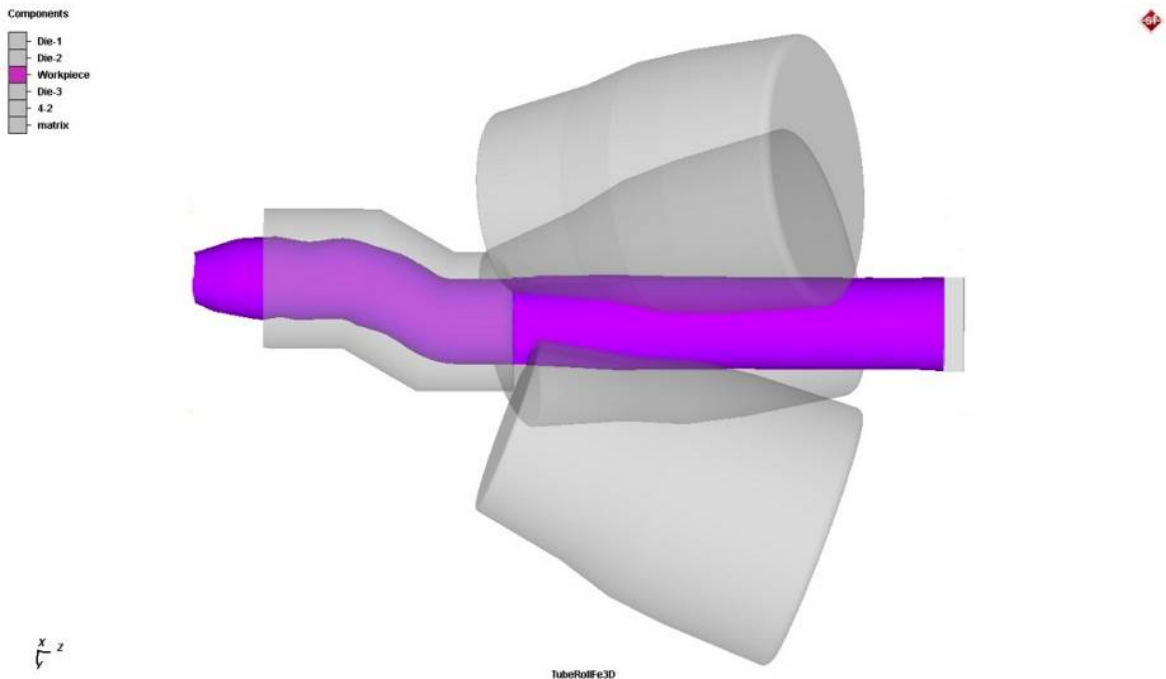


Figure 2.3 – Model with reduced coefficient of friction in the matrix

This model was good because the front end of the workpiece is left from the matrix, and at the input side matrix the burr is not formed.

Conducted computer modeling of the combined process "helical rolling – pressing" had the objective - the feasibility of this process. For this purpose it is necessary to study the influence of various factors on the implementation process. As has been identified above, for the normal deformation is necessary to ensure the greatest possible value of the coefficient of friction in the rolls, and the minimum possible value in the matrix. It was further decided to hold a variation of the two most important process parameters: the distance of matrix from the deformation zone of the rolls and the angle of intersection of channels in the matrix. To do this, additional models were built with the following options:

- model with distance of matrix from the deformation zone of the rolls of 40 mm and 27.5 mm;
- model with the angle of intersection of channels in the matrix  $135^\circ$  and  $142.5^\circ$ .

All other parameters remained unchanged.

In result of calculation of these models the following results were obtained:

A) model with the distance of matrix from the deformation zone of the rolls of 40 mm (figure 2.4)

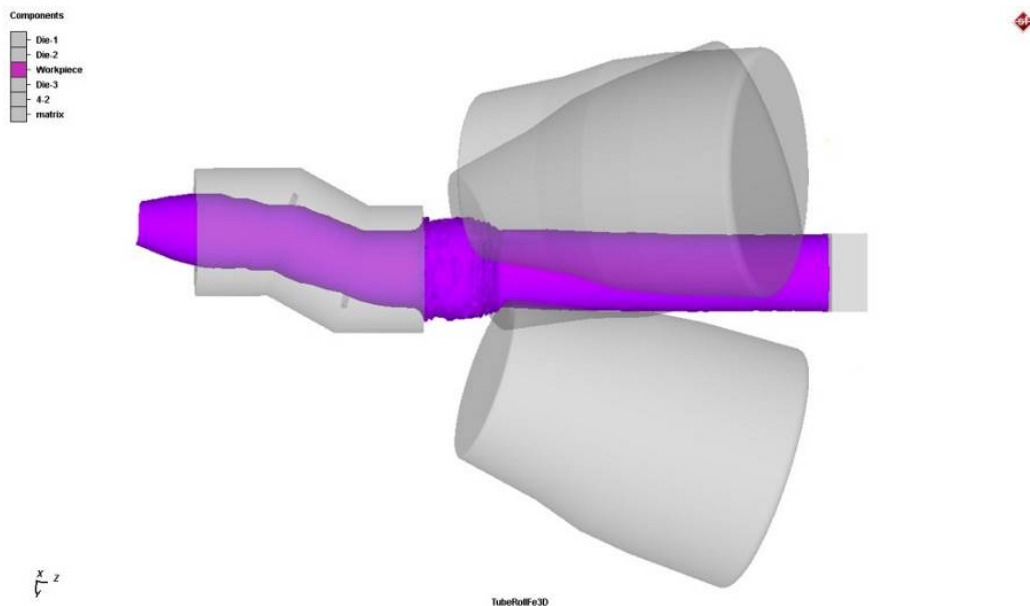


Figure 2.4 – Model with the distance of matrix from the deformation zone of the rolls of 40 mm

This model should be considered as unsuccessful, despite the fact that the front end of the workpiece out from the die. In this case, because of the large distance between zones of deformation in the rolls and the matrix, at the input of matrix was formed barrel influx. This phenomenon occurs when at the input matrix is the observance of inequality (2.1):

$$\sigma = \frac{P}{F} < \sigma_s, \quad (2.1)$$

where  $\sigma$  - current stress in the cross section of the workpiece;  
 $P$  - deformation force;  
 $F$  - cross-sectional area;  
 $\sigma_s$  - deformation resistance of the material.

i.e. the stress in the cross section of the billet in the entrance area in the matrix exceeds the deformation resistance. This phenomenon is discussed in detail in work [93]. Thus, the conclusion was made about the necessary reduction in the value of this parameter.

B) model with the distance of matrix from the deformation zone of the rolls of 27,5 mm (figure 2.5)

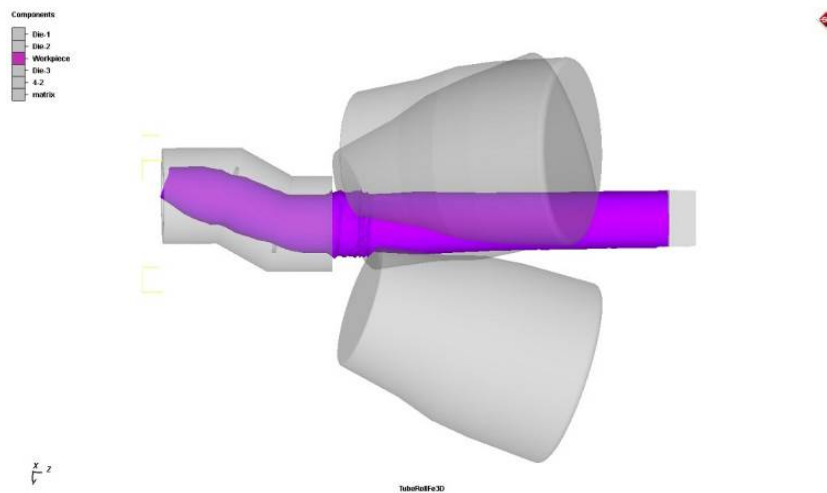


Figure 2.5 – Model with the distance of matrix from the deformation zone of the rolls of 27,5 mm

This model also was unsuccessful. In this case, the distance between zones of deformation in the rolls and the matrix was still large, at the entrance to the matrix again formed barrel influx, albeit in a much smaller size. Based on data from the last two models we can conclude that for better flow of combined process "helical rolling – pressing" need to set the matrix at the minimum possible distance from the deformation zone of the rolls.

C) model with the angle of intersection of channels in the matrix 135° (figure 2.6)

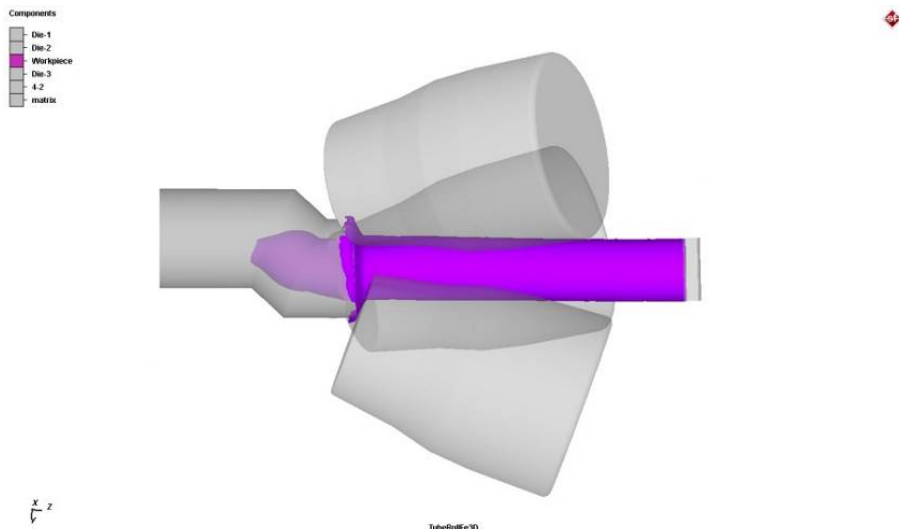


Figure 2.6 – Model with the angle of intersection of channels in the matrix  $135^\circ$

The model with the lower value of the angle of intersection of the channels was unsuccessful. Due to the decrease in the value of an angle of intersection in the matrix drastically increased the force of back pressure, resulting in the input into the matrix has occurred the broadening of the workpiece. Similar data were obtained in work [95] with the combined process "rolling-pressing".

D) model with the angle of intersection of channels in the matrix  $142,5^\circ$  (figure 2.7)

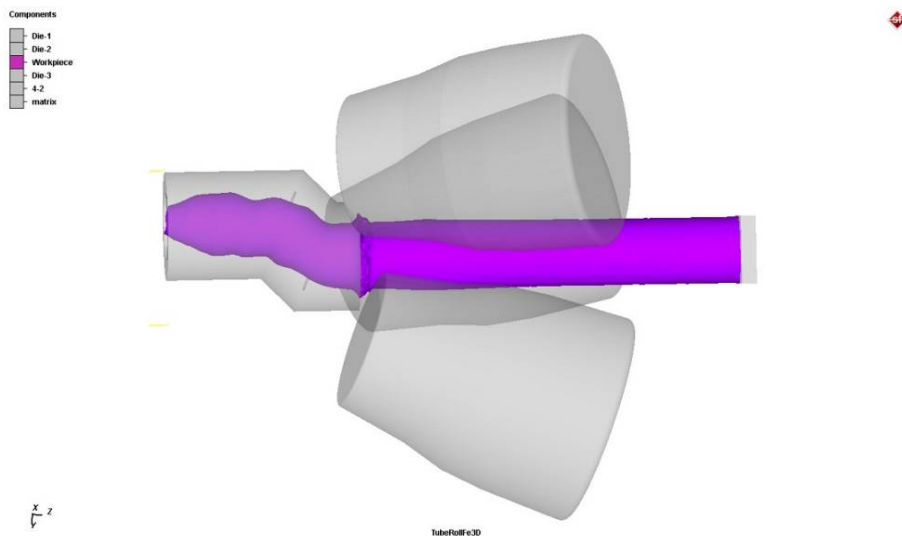


Figure 2.7 – Model with the angle of intersection of channels in the matrix  $142,5^\circ$

Model with an intermediate value of the angle of intersection of channels can be called successful, because, despite the influx of formation at the matrix input, the process continued. With movement of workpiece into the matrix, the surface layers were subjected to compaction, which ultimately led to the formation of a small influx with the burr. This model can be considered suitable only if you are a single deformation of the workpiece. When implementing a continuous deformation, when after rolling the billet to rolls will be supplied the next material, which will be pushed through the matrix predetermined earlier, this model will

fail, so the best model is the model presented in figure 2.3, which will ensure the continuity of the proposed process.

In result of computer simulation of the combined process "helical rolling – pressing" in the software package Simufact.Forming were obtained several models of this process. To analyze the possibility of implementation of this process was carried out the varying of key parameters that have a significant impact on the implementation process. In result were obtained the following optimal values:

- coefficient of friction in the rolls is not less than 0,8;
- coefficient of friction in the matrix is not more than 0.1;
- angle of intersection of channels in the matrix – not less than  $150^\circ$ ;
- distance of matrix from the deformation zone of the rolls is not more than 15 mm.

### 3 ANALYSIS OF THE INFLUENCE OF STRESS-STRAIN STATE AND TEMPERATURE ON THE QUALITY OF THE METAL BASED THE SIMULATION OF COMBINED PROCESS «SCREW ROLLING – ECA-PRESSING»

#### 3.1 Analysis of the deformation scheme of the combined process "screw rolling - pressing»

In the study of any pressure treatment process, the key position before laboratory or industrial testing is the study of the stress-strain state (SSS). This will allow to identify the distribution of stresses and strains in the process, as well as to determine their critical values, which, in turn, will make it possible to check the working tool for strength.

To determine the stress and strain values, it is necessary to find the values of the components of the corresponding tensors, which are very difficult to visualize for a three-dimensional metal flow. Therefore, when considering the SSS parameters, simple strain and stress intensity indicators, or so-called equivalent strain and equivalent stress, are usually used, which include strain and stress components in the following form:

$$\varepsilon_{EQV} = \frac{\sqrt{2}}{3} \sqrt{(\varepsilon_1 - \varepsilon_2)^2 + (\varepsilon_2 - \varepsilon_3)^2 + (\varepsilon_3 - \varepsilon_1)^2}, \quad (3.1)$$

$$\sigma_{EQV} = \frac{1}{\sqrt{2}} \sqrt{(\sigma_1 - \sigma_2)^2 + (\sigma_2 - \sigma_3)^2 + (\sigma_3 - \sigma_1)^2}, \quad (3.2)$$

where  $\varepsilon_1, \varepsilon_2, \varepsilon_3$  - main strains,  
 $\sigma_1, \sigma_2, \sigma_3$  - main stresses.

However, for the considered combined process "screw rolling-pressing" these two parameters are not enough because of the rather complex plastic flow of the metal during deformation. To understand this, refer to the diagram shown in figure 3.1.

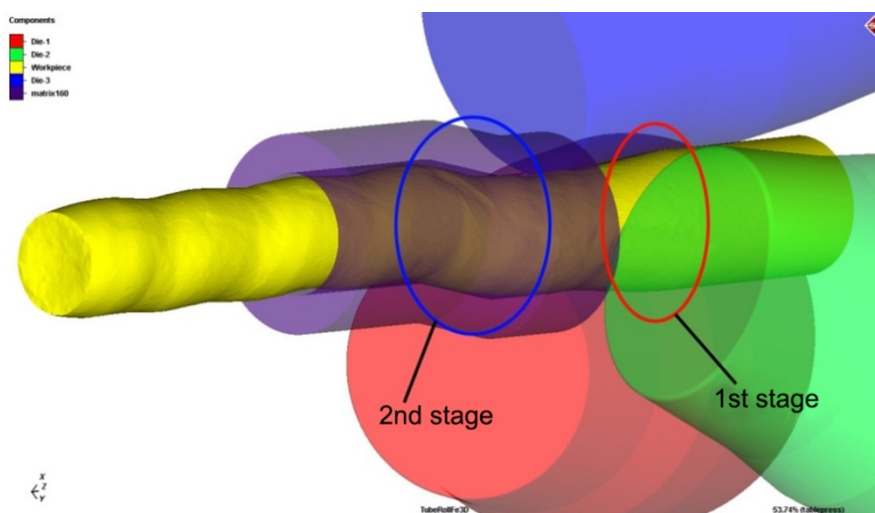


Figure 3.1 – Deformation stages in the combined process "screw rolling-pressing»

Conditionally, the process of rod deformation in this process can be divided into 2 stages: screw rolling in rolls and equal-channel step pressing in the matrix. At the same time, each of these stages of deformation is a complex process.

At the first stage, two different schemes of stress-strain state, shown in figure 3.2, arise during screw rolling in the deformation zone. In longitudinal direction the workpiece is compressed in two directions and stretching in one direction, which corresponds to the course of rolling. In fact, this scheme of forces occurs during the drawing. In the transverse direction, in addition to compression, twisting of the workpiece is also realized, which occurs under the action of torque from the rolls. As a result, after passing the deformation zone in the rolls, the workpiece is reduced in diameter, lengthened and twisted around its axis at a certain angle. The value of the twisting angle will depend on the amount of torque, the workpiece material and its geometric parameters.

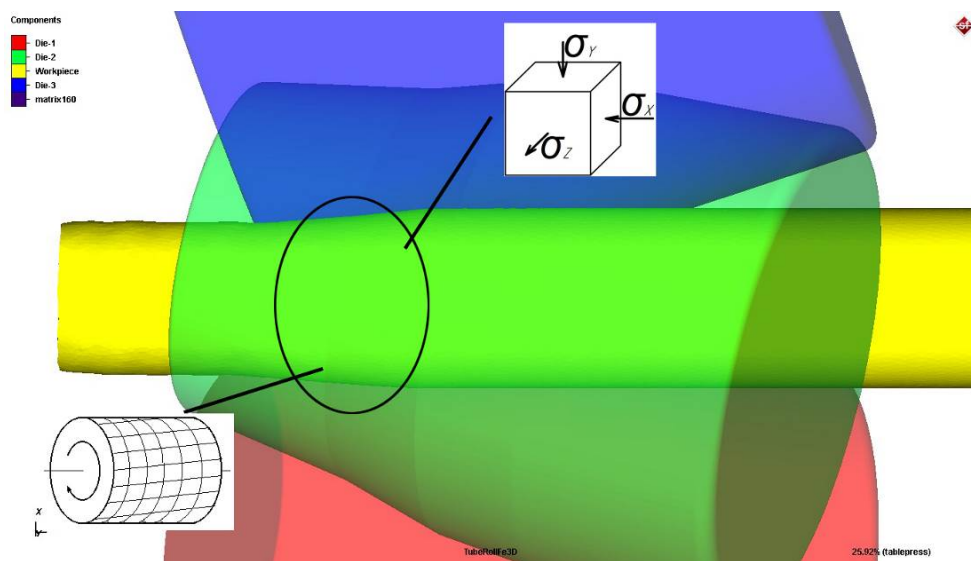


Figure 3.2 – First stage of deformation

It should also be noted that the twisting of the workpiece in the transverse direction is very heterogeneous. All cross-section of the rod during screw rolling can be divided into 3 zones: central, neutral and surface [57]. These zones, the features of the metal flow in them and the formation of the microstructure are shown in figure 3.3.

In the surface area, each small trajectory-oriented element is subjected to compression deformation along the radius of the workpiece, compression deformation in the direction of movement (along the helical path) and tensile deformation across the helical path. The thickness of the surface area in the rolled billet is 0.3...0.7 of its radius (from the surface of the workpiece).

In the central zone, each small trajectory-oriented element is subjected to compression deformation along the radius of the workpiece, stretching deformation in the direction of movement (along the trajectory) and, accordingly, compression deformation across the trajectory. Study of the metal structure acts on the type of longitudinal rolling in calibers with multilateral compression or compression. The

structural elements of the buildings stretch and refine with the formation of structural banding. The thickness of the central zone in the rolled billet is 0.25...0,6 of the radius (from the centre of the workpiece).

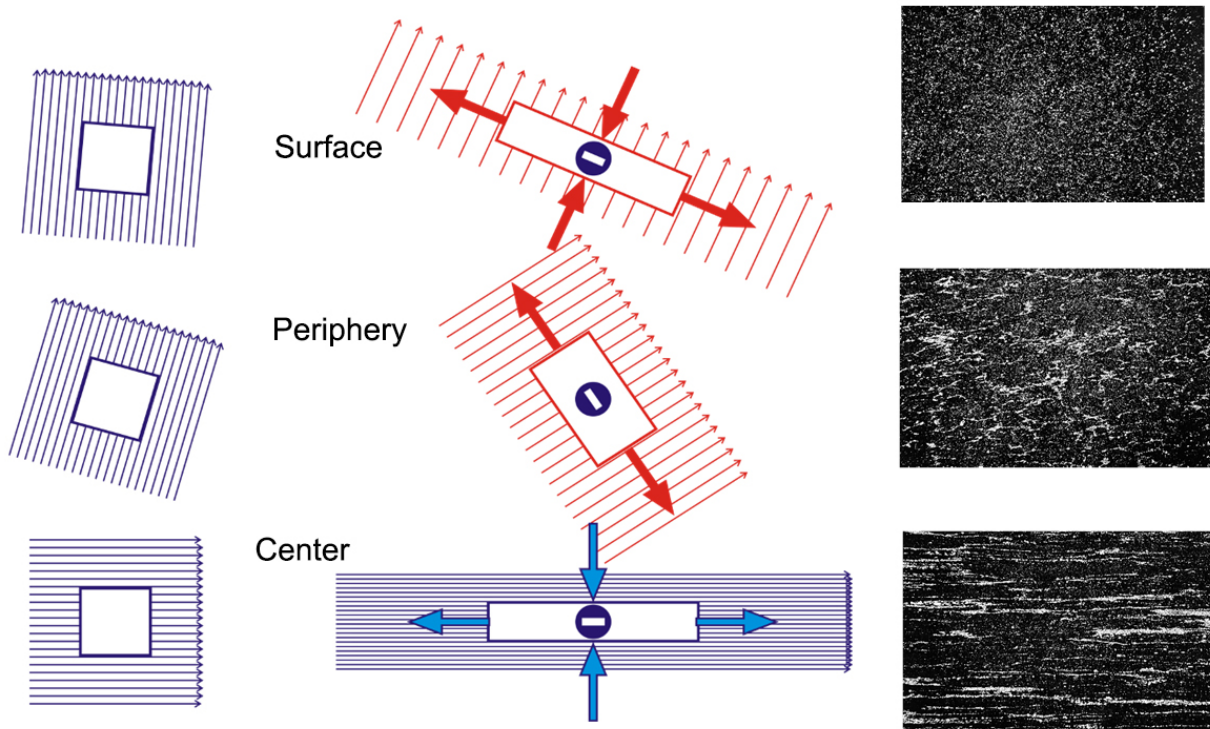


Figure 3.3 – Trajectory-velocity conditions of metal flow and formation of microstructure during screw rolling

In the neutral zone trajectory-velocity deformation conditions are intermediate. Here, there is no linear deformation along the trajectory of elementary volumes, the absolute speed of movement remains constant. Trajectory-oriented elementary volumes of metal are exposed to only two linear deformations opposite in sign: compression along the radius of the workpiece and stretching perpendicular to the trajectory. Study of the structure in the neutral zone is the type of longitudinal rolling of the sheet without broadening. The thickness of the neutral zone in the rolled billet is 0.05...0.1 of its radius. Thus, the twisting angle increases from zero to maximum in the direction from the central zone to the surface.

At the second stage of deformation, the workpiece is subjected to equal-channel step pressing in the matrix (figure 3.4). Two types of deformation also occur here. The first type is a simple shift that occurs in the longitudinal direction of the workpiece when it passes through the channels of the matrix. Moreover, in contrast to the angular pressing, in this case, a alternating simple shift is realized, since the workpiece changes its direction twice. In the transverse direction there is a second type of deformation – twisting the workpiece. But this time the direction of twisting is the opposite. This is because the workpiece in the matrix experiences translational-rotational motion transmitted to it from the rolls. When the workpiece is in contact with the walls of the fixed matrix there is a back pressure force, which is directed in the opposite direction to the original rotation.

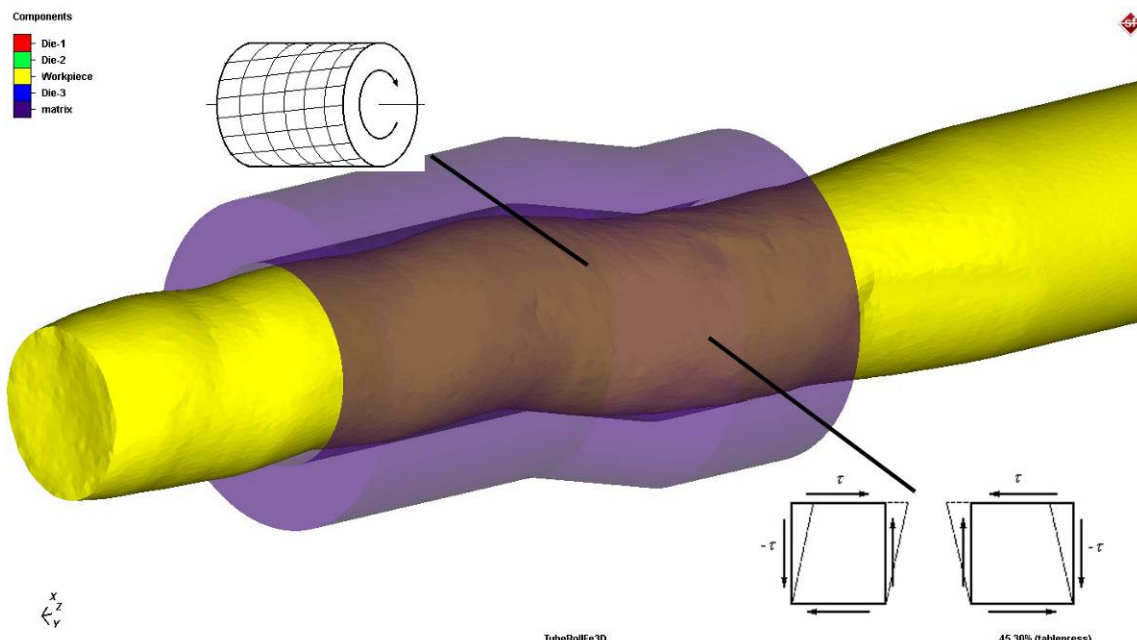


Figure 3.4 – Second stage of deformation

Thus, the implementation of the considered combined process "screw rolling - pressing" in the workpiece consistently occur 5 different types of deformation, which makes this process quite complex. Therefore, as noted above, for the SSS parameters it is necessary to study not only the equivalent deformation and equivalent stress, but also the parameters that allow to estimate the proportion of tensile and compressive stresses in the deformation site. These are the main stresses  $\sigma_1$  and  $\sigma_3$ . Their values are found by the following formulas:

$$\sigma_1 = \frac{\sigma_x + \sigma_y}{2} + \sqrt{\left(\frac{\sigma_x - \sigma_y}{2}\right)^2 + \tau_{xy}^2}, \quad (3.3)$$

$$\sigma_3 = \frac{\sigma_x + \sigma_y}{2} - \sqrt{\left(\frac{\sigma_x - \sigma_y}{2}\right)^2 + \tau_{xy}^2}. \quad (3.4)$$

The component  $\sigma_2$  is not usually considered because it is the arithmetic mean of  $\sigma_1$  and  $\sigma_3$ .

Also in the study of SSS is very useful to study the temperature conditions of the process, since the change in temperature of the deformable metal significantly affects the energy parameters of deformation.

In result of computer simulation of the combined process "helical rolling - pressing" in the software package Simufact Forming was obtained a successful model of this process with the following optimum values:

- coefficient of friction in the rolls – 0,8;
- coefficient of friction in the matrix - 0,1;
- the angle of intersection of channels in the matrix – 150°;

- the distance between matrix and deformation zone of the rolls - 15 mm.

The initial workpiece was a rod with a diameter of 25 mm and a length of 150 mm. Steel 15 was selected as material. Roll dimensions and their structural location consistent with the design of the laboratory rolling mill 10-30. The roll rotation speed was 100 rpm. Equal channel step matrix had channel diameter of 21 mm. Temperature of the billet was accepted by 1000° C, all tools in the model had a temperature of 20° C.

In figure 3.5 a,b showed the temperature distribution of the workpiece. In the contact zone of the workpiece with the rolls the temperature is reduced to 950-970° C. In the zone of junction of the channels of the matrix temperature is lowered to 850° C. In further temperature drop across the section is leveled due to heat transfer from the central layer to surface.

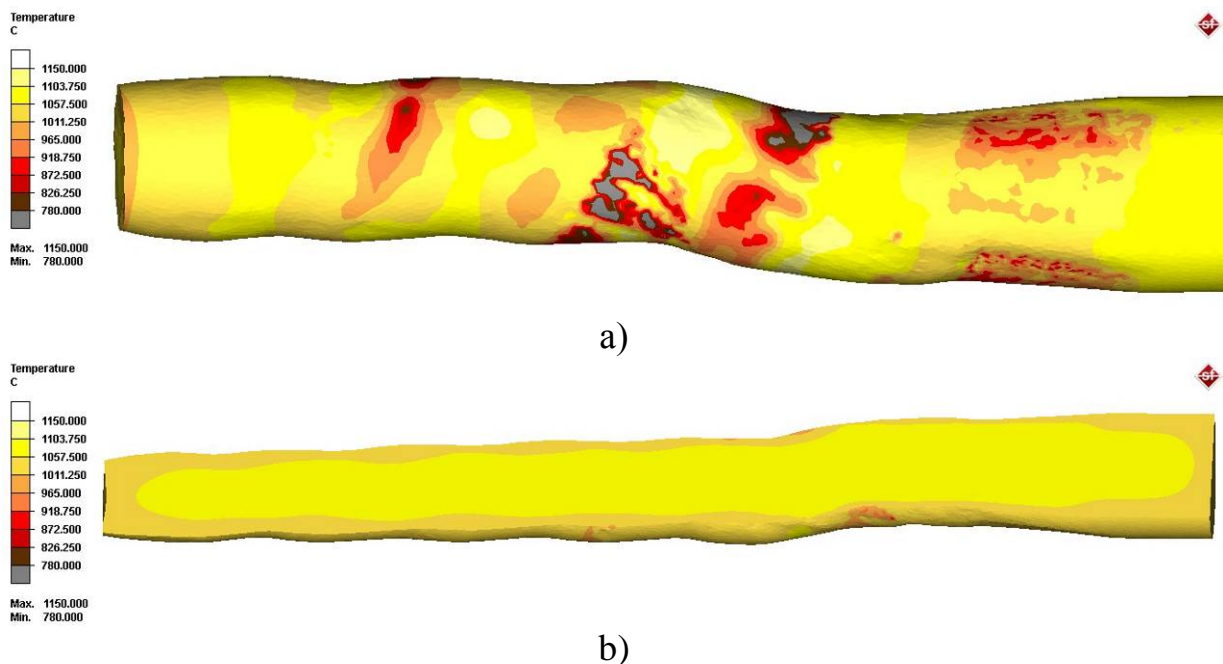


Figure 3.5 – Temperature distribution

### 3.2 Stress state study

In the study of the stress state, the following results were obtained, presented in figures 3.6-3.8.

When considering the component  $\sigma_1$ , the compressive stresses take minimum values, while the tensile stresses become maximum. This allows us to estimate the maximum level of tensile stresses occurring in the workpiece, the growth of which can lead to the formation of defects. In the first stage (figure 3.6 a), when screw rolling, the tensile stresses reach 230 MPa, which are directed along the tangent line to the workpiece. In the area of direct contact of the workpiece with the rollers are formed of normal confining stress, reaches a value of -400 MPa. This distribution of stresses can be considered favorable, since the level of compressive stresses in absolute value exceeds almost 2 times the level of the maximum possible tensile stresses. As a result, the action of tensile stresses is suppressed.

At the second stage (figure 3.6 b), the workpiece is simultaneously rolled in rolls and deformed in the matrix. Thus, the formation of two of the deformation zone. In conventional longitudinal rolling, with the occurrence of backwater there is a decrease in tensile stresses [95], in this process there is the opposite picture. This is explained by the kinematics of the screw rolling process, where local zones of different stresses occur in the deformation zone – normal compressive stresses act in the zones of metal contact with the rolls; tensile stresses act in the contact-free zones.

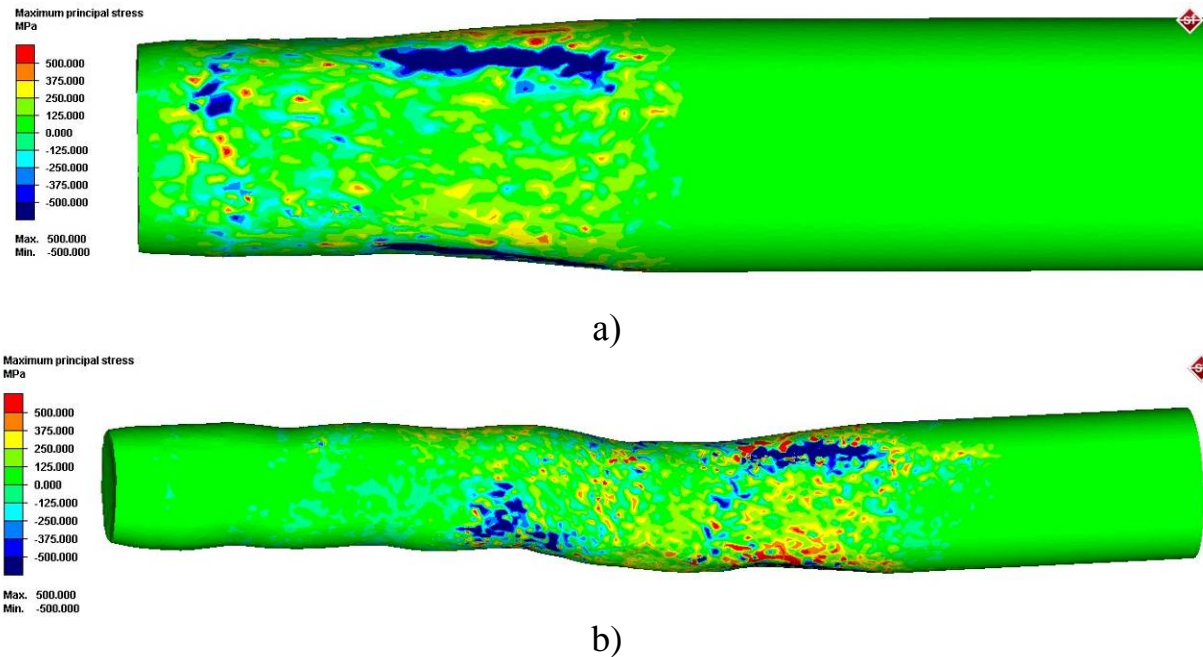


Figure 3.6 – Main (maximum tensile) stress  $\sigma_1$  in the base model

When the back pressure from the matrix increases the angle of twisting, which leads to an increase in tensile stresses. In the rolling zone, the tensile stress value increases to 400 MPa, i.e. there is an increase of 74%. Compressive stresses also vary, their value is -450 MPa (+12.5%). In the zone of the junction of the channels, the tensile stress is 280 MPa; the compressive stress reaches -340 MPa. As in the first stage, here the stress distribution can also be considered favorable, because the level of compressive stresses in absolute value exceeds the level of the maximum possible tensile stresses.

When considering the component  $\sigma_3$ , the compressive stresses assume maximum values, while the tensile stresses become minimal. This allows us to estimate the maximum level of compressive stresses occurring in the workpiece, the growth of which leads to the closure of internal defects in the metal structure and is generally favorable for the deformation process. At the first stage (figure 3.7 a) the value of the main tensile stress is much lower, it reaches 110 MPa. In the zone of direct contact of the workpiece with the rolls are formed normal compressive stresses reaching values -450 MPa.

At the second stage (figure 3.7 b) in the rolling zone, as in the case of the component  $\sigma_1$ , there is an increase in tensile stresses to a value of 200 MPa. This is a consequence of the action of backpressure on the part of the matrix, resulting in

an increase in the angle of twisting the workpiece, which leads to an increase in tensile stresses. Despite this, the value of compressive stresses also changes to the level of -480 MPa, which exceeds the level of tensile stresses by 2.4 times. In the area of the junction of the channels, the tensile stress is 80 MPa; the value of compressive stresses reaches -450 MPa, exceeding the level of tensile stresses 5.6 times. Thus, as in the consideration of the component  $\sigma_1$ , it was found that this deformation scheme provides the repayment of the resulting tensile stresses by a significant level of compressive stresses, which is a favorable factor for the formation of a sub-ultra-fine-grained structure by methods of severe plastic deformation.

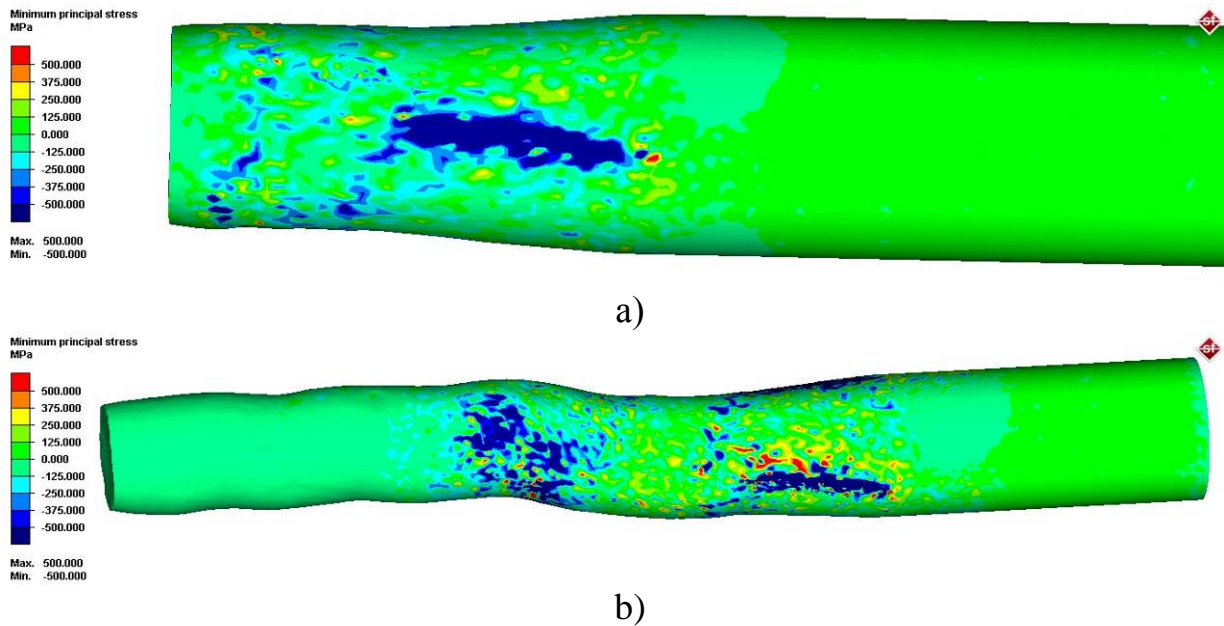


Figure 3.7 – Main (maximum compressive) stress  $\sigma_3$  in the base model

As it was revealed in the work [83], the main factors influencing the change of the stress state during pressing in the equal-channel step matrix are the joint angle and the length of the inclined channel. Therefore, when considering the deformation zone in the matrix, the length of the compressive stress zone covering the entire inclined channel is clearly visible.

When considering the equivalent stress it should understand that this option does not show, what stress operates at a specific point - tensile or compressive. As a radical expression, its value is always positive. It shows the intensity of the action of the stress, i.e., is there at this point stress or not. Its value characterizes the average value of all stresses acting at a given point.

At the first stage, during helical rolling (figure 3.8 a) stress covers the entire deformation zone of the rolls. In zones of contact of metal with rolls its value reaches 150 MPa, in zones free of contact, the value of this parameter reaches 120 MPa.

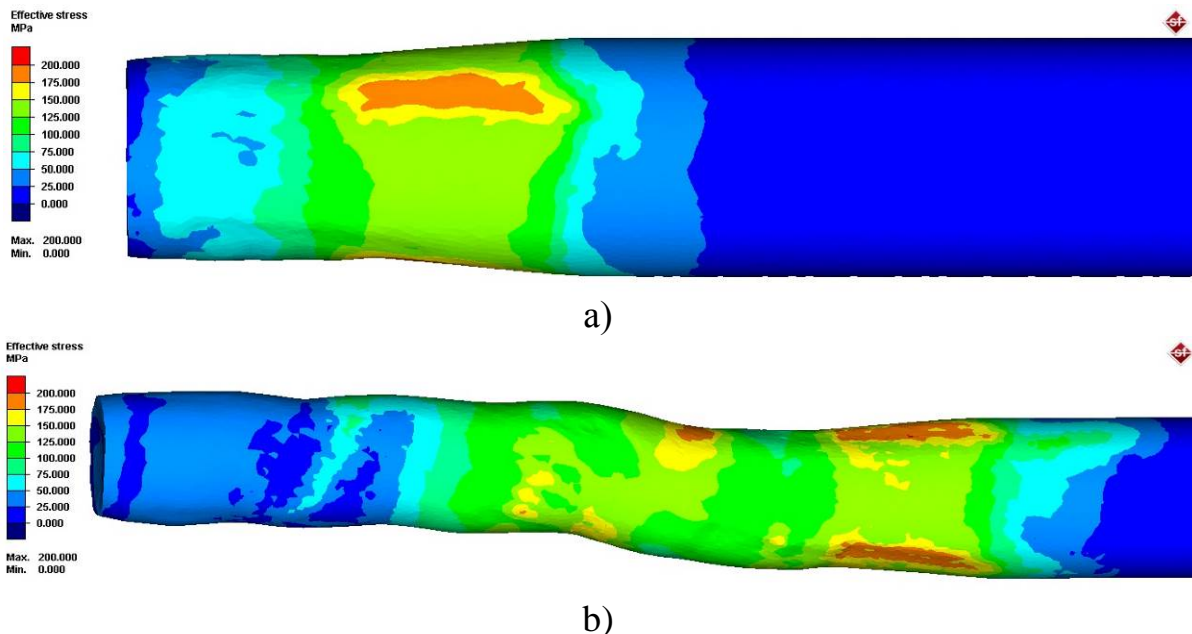


Figure 3.8 – Equivalent stress in base model

In the second stage, during pressing (figure 3.8 b) stress covers a vast area, connecting two of the deformation. In longitudinal rolling with the support of such a merger does not occur, because there is no twisting of the blank, causing the growth of shear stresses. Due to the action of backpressure, stress within the deformation zone of the rolls is increased to 190 MPa in the contact zones of the metal with the rolls. Free from contact zones, the value of this parameter is in the limit of 140 MPa. In the zone of junction of the channels of the matrix the magnitude of equivalent stresses up to 160 MPa.

There is also clearly tracks the forces of backpressure. Behind the zones of contact of metal with rolls arise extent of physical deformation area that is a consequence of two concurrent factors – backpressure from the side of the matrix and twisting of the workpiece.

### 3.3 Strain state study

As noted above, to study the strain state use the indicator of intensity of deformation – equivalent strain, which includes major components of deformation. This option allows to monitor the degree of accumulated strain, which is cumulative.

When studying the strain state is necessary not only to ensure a high level of equivalent strain, required for the formation of UFG structure, but a uniform distribution of this parameter over the cross section of the workpiece.

During helical rolling (figure 3.9 a) deformation develops in the deformation zone of the rolls in the following form: its value reaches 1.2 in the surface layers; in central layers this parameter value is at 0.7 (figure 3.9 b), i.e. the difference of the values of the equivalent strain reaches 72%.

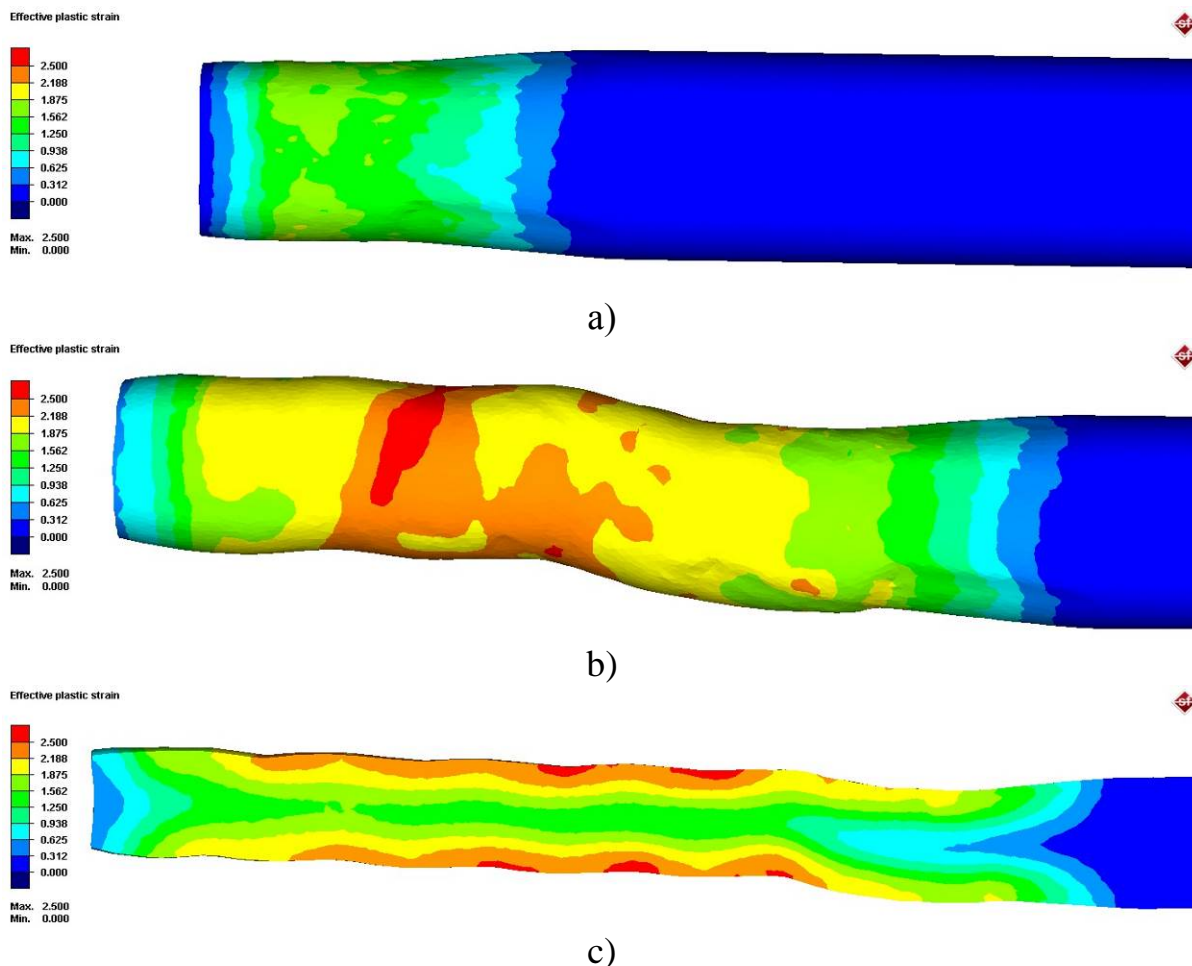


Figure 3.9 – Equivalent strain in base model

During pressing there is a significant increase of this parameter due to the implementation of shear deformation during the movement of billet through the channels of the matrix. The value of equivalent strain is 2.3 in the surface layers, in central layers the value of this parameter is at the level of 1.4, i.e. the difference of the values of the equivalent strain reaches 64%. Thus, the difference of values of this parameter after passing through the channels of the matrix decreased by 8%.

As a comparison of the equivalent strain values in the surface and central layers of the workpiece, the distribution of this parameter over the cross section is quite uneven. In addition, the directions of the metal flow in the surface and central layers are also very different – in surface layers the turbulent nature of the flow prevails, and in the central layers is laminar nature (figure 3.3). All this leads to the formation of a characteristic structure of screw rolling with an equiaxed fine-grained surface and an elongated, striped structure of the central part.

Thus, it is important not only to achieve a uniform distribution of the equivalent deformation across the bar section, but mainly – changes in the nature (direction) of the deformation in the central part of the bar. This will break the oriented striped structure of the central part of the bar and align the anisotropy of its properties formed after the screw rolling over the cross section.

It can be concluded that the difference in equivalent strain in the central zone to the entrance to the matrix and after the matrix, equal to 0.7, the difference is the portion of deformation corresponding to simple shear in the matrix. That is, the

center of the workpiece when passing the channel matrix gains equivalent strain of 0.7 in the direction perpendicular to the direction of deformation of the previous stage and also perpendicular to the orientation of the structure of the central part. Several cycles of such deformation should contribute to the transformation oriented streaky structures in a more equiaxed, thus reducing the anisotropy of properties on the section of the rod.

### 3.4 Study of models with variable parameters

The above model of the combined process "screw rolling - pressing" has the boundary values of geometric and technological parameters, the values of which were found in the second chapter of this work. Next, the task was to find out how each of these parameters affects the stress-strain state of the process. For this purpose, several more models were built, which differed from the basic model by the changed value of only one parameter. The need for "real" variation was also taken into account, only those parameters that we could change on the operating laboratory mill were changed.

At the previous stage, the following optimal values were obtained:

- coefficient of friction in the rolls is not less than 0,8;
- coefficient of friction in the matrix is not more than 0.1;
- angle of intersection of channels in the matrix – not less than 150°;
- distance of matrix from the deformation zone of the rolls is not more than 15 mm.

Changing the value of the distance of the matrix from the deformation center in the rolls is very problematic, because the current design of the matrix in the model is close to the minimum possible distance to the rolls. To bring the matrix even closer to the rolls, it is necessary to use rolls with a different shape and diameter, which in the conditions of the existing laboratory mill is irrational, because it will have to significantly change the bearing structure of the mill, which can adversely affect its strength. It was therefore decided to carry out the variation of the values of both coefficients of friction and the size of the angle of intersection of channels in the matrix.

It was also decided to vary the heating temperature of the workpiece in both directions, since for a given steel 15 the initial value of the heating temperature (1000 °C) is the average value in the recommended forging temperature range (780 °C÷1150 °C). For this purpose, 2 more models with billet heating temperatures were built.

As a result, models with the following modified parameters were built:

- 1) with billet heating temperature 1150 °C;
- 2) with billet heating temperature 850 °C;
- 3) with the angle of intersection of channels in the matrix 160°;
- 4) with the friction coefficient in the rolls 0,9;
- 5) with the friction coefficient in the matrix 0,05.

### 3.4.1 Model with increased workpiece heating temperature 1150 °C

Figure 3.10 shows the temperature distribution on the surface and in the longitudinal section of the workpiece. Since the initial heating temperature was increased by 150 °C, and the rolling speed remained unchanged, the cooling of the workpiece is much lower than in the base model. In the zone of contact of the workpiece with rolls, the temperature is reduced to 1020-1050 °C. In the zone of junction of the channels of the matrix the temperature goes down to 980-1000 °C. Further the temperature wedge in the cross section flattens out.

In the study of the main components of the stress (both tensile and compressive), it was found that in the model with an increased heating temperature of the workpiece there is a decrease in the values at both stages. This is due to the fact that the workpiece has a higher temperature and, as a consequence, higher plasticity, which allows it to deform at lower energy costs.

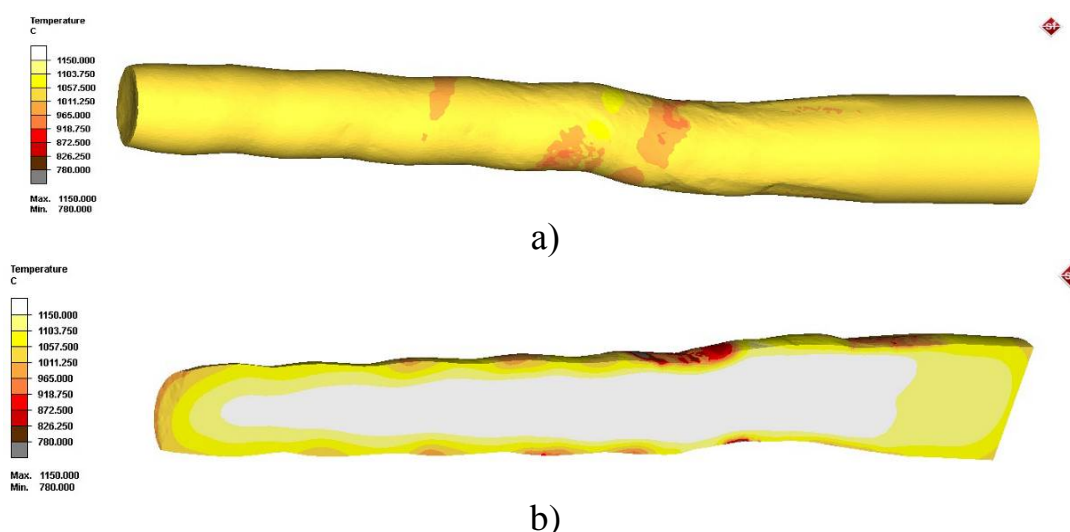


Figure 3.10 – Temperature distribution in a model with increased workpiece heating temperature 1150 °C

At the first stage (figure 3.11 a), the value of the main tensile stress  $\sigma_1$ , reaches 150 MPa in the contact-free zones, which decreased by 35% compared to the base model. In the contact zone of the workpiece with rolls the compressive stresses are formed reaching a value of -300 MPa, which is 25% lower than the base model. At the second stage (figure 3.11 (b)) in the rolling zone, the tensile stress value is 270 MPa, which is lower than the value of the base model by 32 %. Compressive stresses also vary, their value is -350 MPa, there is also a decrease in the value of the parameter in comparison with the base model by 22 %. In the zone of junction of the channels, the magnitude of the tensile stress is 200 MPa, the value of the parameter has decreased by 28 %; the magnitude of compressive stress reaches -300 MPa, the value decreased by 12 %.

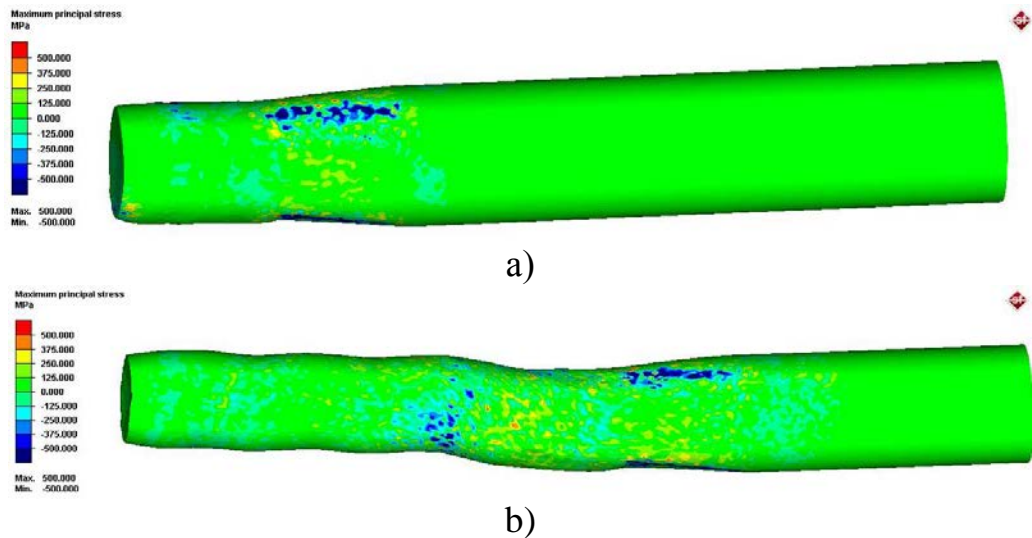


Figure 3.11 – Main tensile stress  $\sigma_1$  in a model with increased workpiece heating temperature 1150 °C

When considering the main compressive component  $\sigma_3$  at the first stage (figure 3.12 a), the value of the main tensile stress on the contact-free zones reaches 70 MPa, which is lower than the value of this parameter in the base model by 36 %. In the contact zone of the workpiece with the rolls are formed compressive stresses reaching values -350 MPa, it is lower than the value in the base model by 22 %. At the second stage (figure 3.12 b) in the rolling zone, the tensile stress value reaches 180 MPa, which is lower than the base value by 10 %. Compressive stresses also vary, their value is -400 MPa, this value has decreased by 17 % compared to the base. In the zone of junction of channels, the tensile stress is 50 MPa, which is lower than the base value by 38 %; the compressive stress reaches -360 MPa, which is lower than the base value by 20 %.

As in the case of the basic model, here the stress distribution can be considered favorable, since the level of compressive stresses in absolute value exceeds the level of the maximum possible tensile stresses.

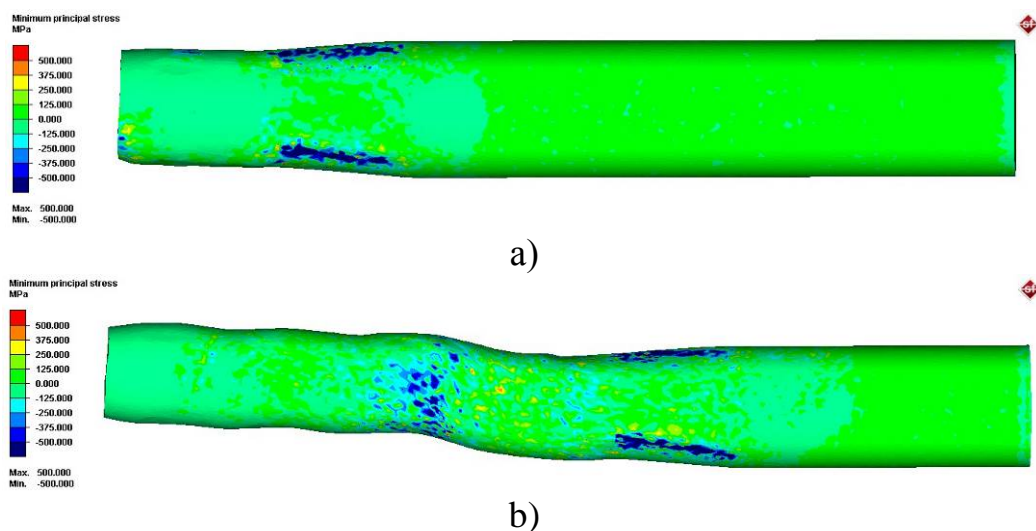


Figure 3.12 – Main compressive stress  $\sigma_3$  in a model with increased workpiece heating temperature 1150 °C

Since the equivalent stress is determined from the values of the main stresses, in the model with an increased heating temperature of the workpiece, the value of this parameter will be lower than in the base model, since the values of the main stresses decreased due to an increase in the temperature of the workpiece, which led to an increase in the level of plasticity of the material.

In the first stage (figure 3.13 a) in the areas of contact of the metal with the rolls, its equivalent stress reaches 105 MPa, the value is reduced by 30 % compared to the base. In contact-free zones, the value of this parameter is within the limit of 80 MPa, which is 33% lower than the base value.

At the second stage (figure 3.13 b) due to the action of the backpressure, the stress value in the deformation zone of the rolls is 130 MPa in the areas of metal contact with the rolls, this is lower than the base value by 32 %. In contact-free zones, the value of this parameter remains within the 95 MPa limit, which is also 32% lower. In the zone of junction of the channels of the matrix, the magnitude of the equivalent stress exceeds 120 MPa, the value decreased by 25% compared to the baseline.

Behind the zones of metal contact with the rolls, there are also coniferous lengths of the physical zone of deformation, but their length is significantly lower due to the general decrease in stress.

In the study of the deformed state in the model with an increased heating temperature of the workpiece, a general increase in the level of equivalent deformation was noted.

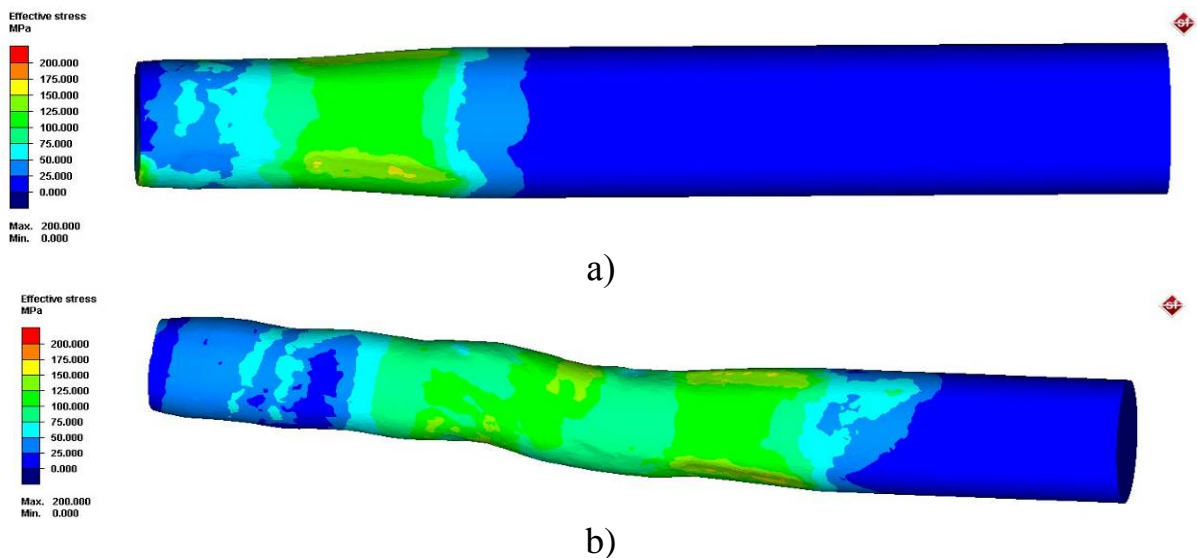


Figure 3.13 – Equivalent stress in a model with increased workpiece heating temperature 1150 °C

In the first stage (figure 3.14 a), the equivalent strain value reaches 1.5 in the surface layers, which is 25% higher than the base value, in the central layers the value of this parameter is within the limit of 0.95, which is 36% higher than the value in the base model (figure 3.9 c). In the second stage (figure 3.14 b), the value of this parameter reaches 2.5 in the surface layers, which is 14 % higher than the

base value, in the central layers the value of this parameter is within 1.7, this is higher by 21 % compared to the base model.

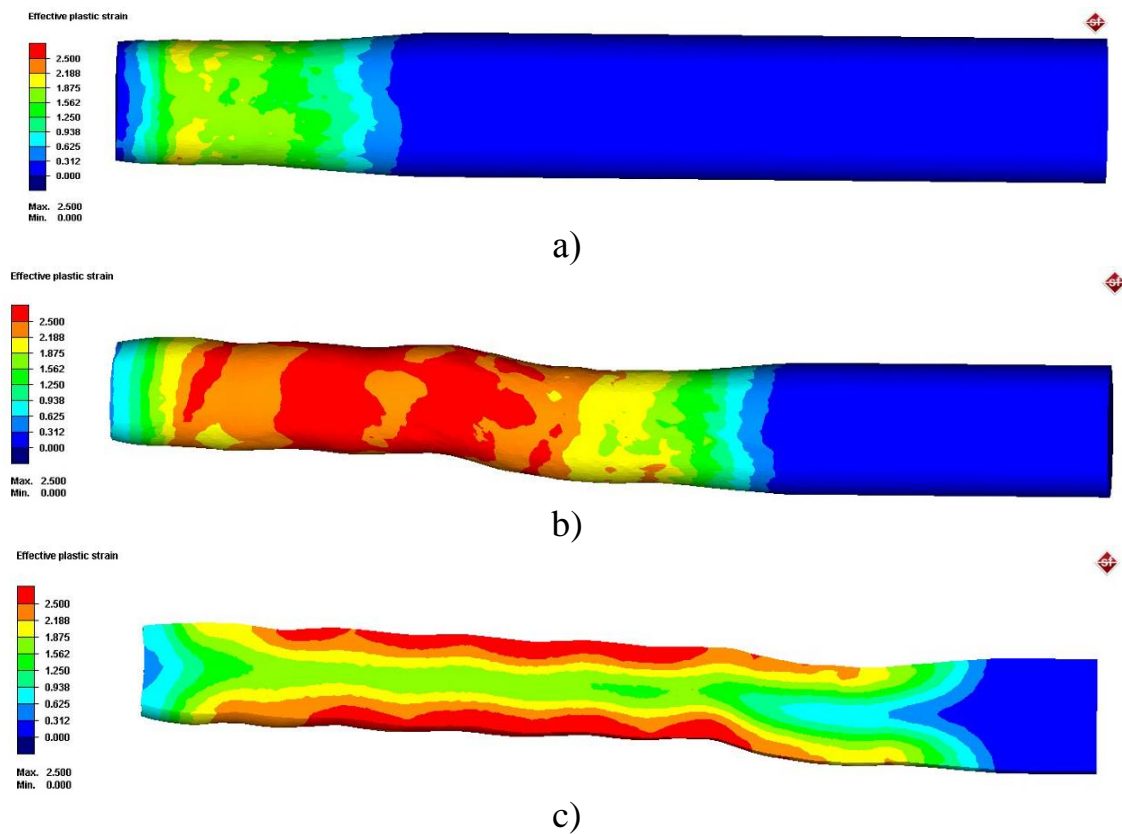


Figure 3.14 – Equivalent strain in a model with increased workpiece heating temperature 1150 °C

The increase in the overall level of deformation is a consequence of the use of a workpiece with an increased heating temperature. Under this condition, the actual resistance of the material is much lower. Despite the fact that the shear deformation does not change, because the geometric parameters of the process remain unchanged, the overall level of deformation is increased by reducing the resistance of the workpiece to twisting.

The increased level of equivalent deformation is undoubtedly positive, contributing to a deeper study of the original structure of the material. On the other hand, the increase in the heating temperature of the workpiece intensifies the process of static recrystallization, which provokes a significant increase in grain, thus nullifying the impact of deformation.

### 3.4.2 Model with reduced workpiece heating temperature 850 °C

The temperature distribution on the surface and in the longitudinal section of the workpiece at a reduced temperature is shown in figure 3.15. In the contact zone of the workpiece with the rolling rolls, the temperature decreases to 800-810° C. In the channel intersection zone of the matrix, the temperature drops to 780 °C. Peculiarity of this model is that in the future the temperature wedge along the

section is aligned much less. As well as the central layers of the workpiece cool down less intensively. This is due to the fact that the temperature of the rolls and the matrix in all the models considered remained unchanged. In the implementation of heat transfer from the workpiece to the tool in this model is more intense cooling.

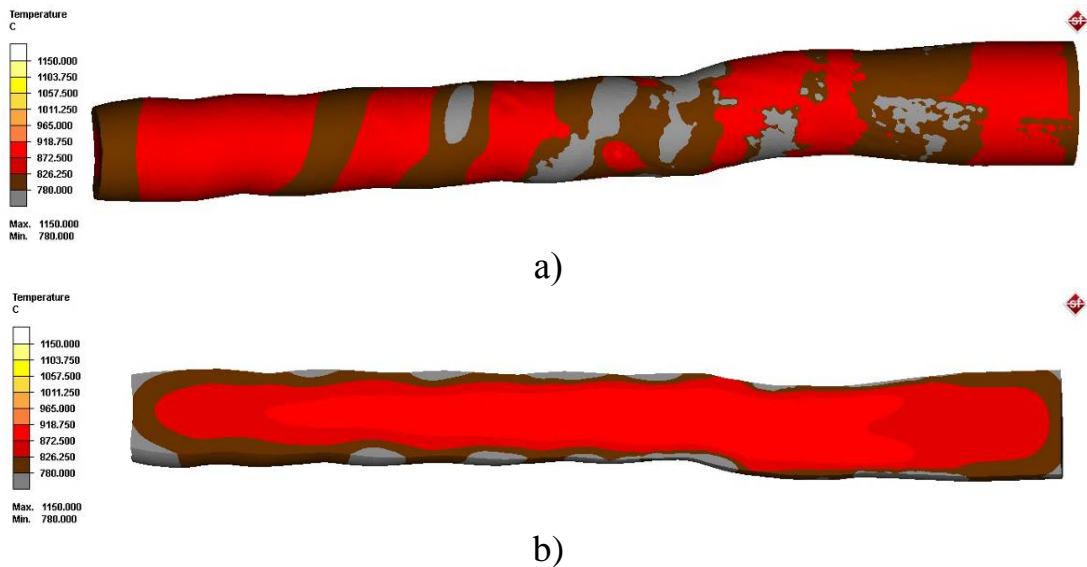


Figure 3.15 – Temperature distribution in a model with reduced workpiece heating temperature 850 °C

In the study of the main stress components (both tensile  $\sigma_1$  and compressive  $\sigma_3$ ) it was found that in the model with a reduced heating temperature of the workpiece there is an increase in the values at both stages. This is due to the fact that the workpiece, having a lower temperature and a lower level of plasticity, requires much more energy for shaping.

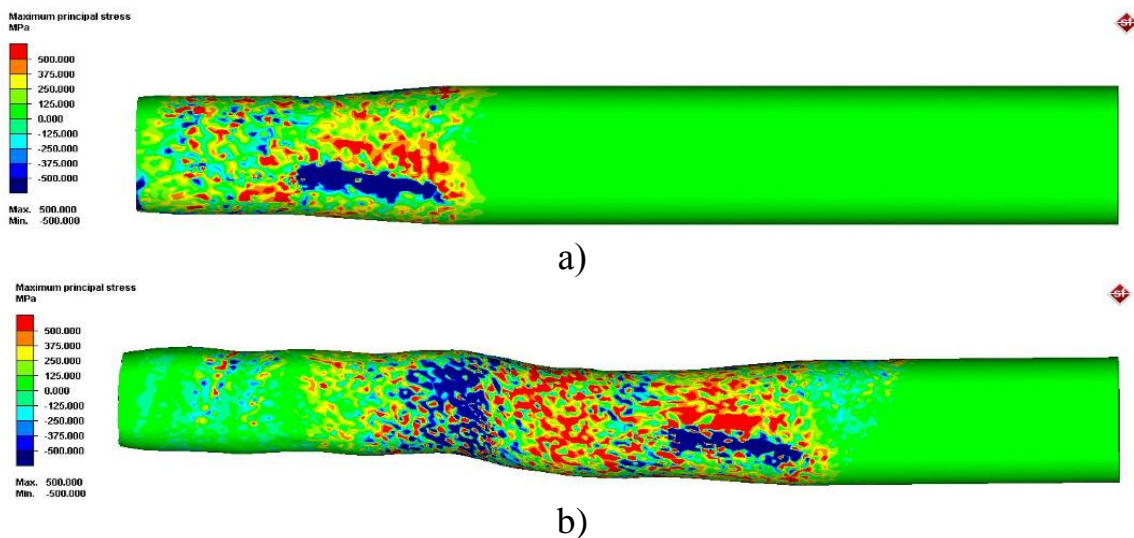


Figure 3.16 – Main tensile stress  $\sigma_1$  in a model with reduced workpiece heating temperature 850 °C

In the first stage (figure 3.16 a), when considering the component  $\sigma_1$ , the tensile stress on the contact-free zones reaches 340 MPa, which is 48% higher than the base value. In the contact zone of the workpiece with the rolls are formed compressive stresses reaching a value of -480 MPa, which is higher than the base value by 20 %.

At the second stage (figure 3.16 b) in the rolling zone, the tensile stress value increases to 450 MPa, which is 12% higher than the value in the base model. Compressive stresses also change, their value is -490 MPa, which is higher than the value in the base model by 9 %. In the area of the channel intersection, the tensile stress is 380 MPa, which is higher by 35 % than in the base model; the compressive stress reaches -400 MPa, which is 18% higher in comparison with the base model.

When considering the component  $\sigma_3$  in the first stage (figure 3.17 a), the tensile stress value on the contact-free zones reaches 140 MPa, which is higher than the same value of the base model by 27 %. In the contact zone of the workpiece with the rolls are formed compressive stresses reaching values -470 MPa, which is higher than the same value of the base model by 4 %. At the second stage (figure 3.17 b) in the rolling zone, the tensile stress value increases to 280 MPa, which is higher than the base value by 40 %. Compressive stresses also vary, their value is -500 MPa, which is higher than the base value by 4 %. In the zone of junction of channels, the tensile stress is 130 MPa, which is higher than the base value by 62 %; the compressive stress reaches -460 MPa, which is higher than the base value by 2 %.

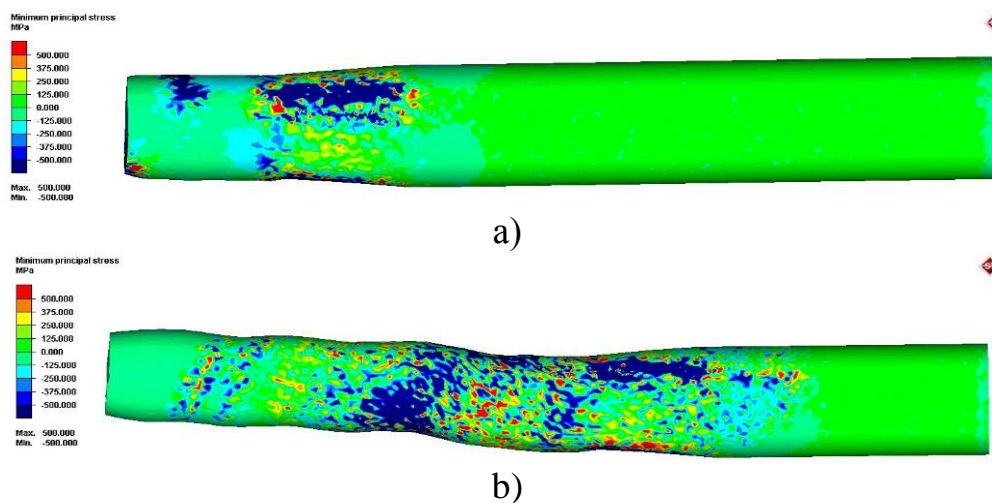


Figure 3.17 – Main compressive stress  $\sigma_3$  in a model with reduced workpiece heating temperature 850 °C

Despite the fact that in this model the growth of tensile stresses was noted, which is undesirable in nature, in general, the stress distribution can be considered favorable, since the level of compressive stresses in absolute value exceeds the level of the maximum possible tensile stresses.

In the study of the equivalent stress, it was noted that in the model with a reduced heating temperature of the workpiece, the value of this parameter is higher than in the base model, since the values of the main stresses increased due to a

decrease in the temperature of the workpiece, which led to a decrease in the level of plasticity of the material.

In the first stage (figure 3.18 a), in the zones of metal contact with the rolls, the equivalent stress reaches 170 MPa, which is higher than the base value by 13 %, in the contact-free zones, the value of this parameter is in the limit of 140 MPa, which is higher than the base value by 17%.

At the second stage (figure 3.18 b), due to the action of the backwater, the stress value in the deformation zone of the rolls increases to 220 MPa in the areas of metal contact with the rolls, which is 16% higher than the base value. In contact-free zones, the value of this parameter is 160 MPa, which exceeds the base value by 14 %. In the zone of junction of the channels of the matrix, the magnitude of the equivalent stress reaches 180 MPa, which is above the base value by 13 %.

In the study of the strain state in a model with a reduced heating temperature of the workpiece, a decrease in the level of equivalent deformation was observed.

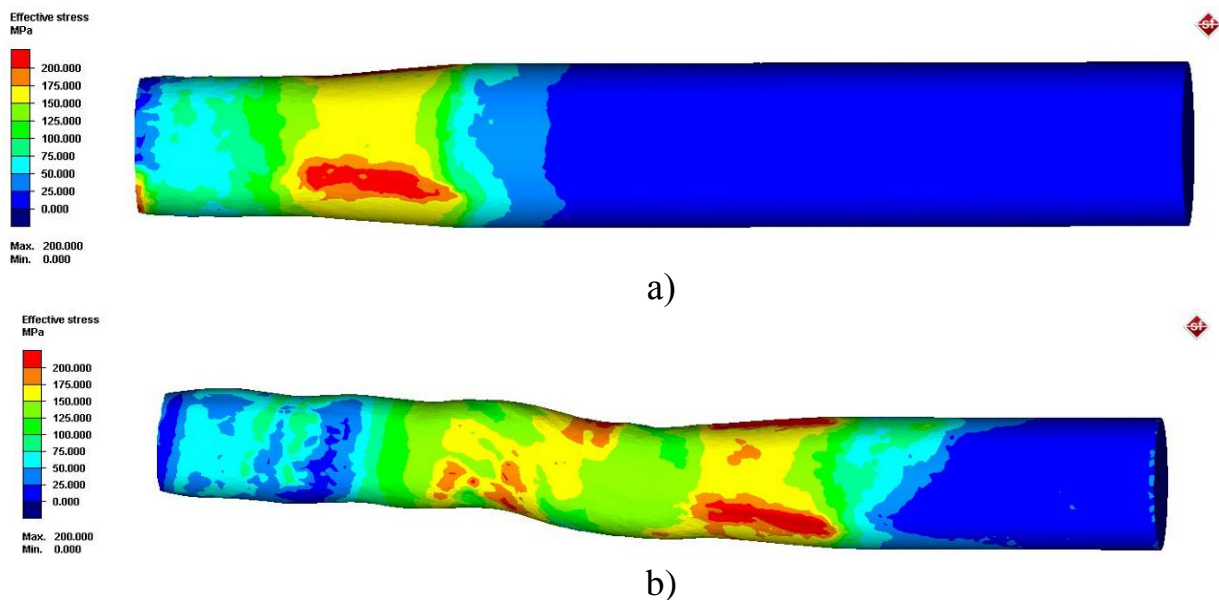


Figure 3.18 – Equivalent stress in a model with a reduced heating temperature of the workpiece 850 °C

In the first stage (figure 3.19 a), the equivalent strain value reaches 0.9 in the surface layers, which is 25% lower than the level of the base model, in the central layers, the value of this parameter is in the limit of 0.5, which is lower than the level of the base model by 29 % . In the second stage (figure 3.19 b), the value of this parameter reaches 1.8 in the surface layers, which is lower by 18 % in comparison with the value of the base model, in the central layers the value of this parameter is in the limit of 1.2, which is lower by 14 % than in the base model.

The use of a workpiece with a reduced heating temperature leads to a decrease in the overall level of deformation. In this model, the overall level of deformation is reduced by increasing the resistance of the workpiece to twisting.

Reduction of the equivalent strain level in the model with a reduced heating temperature of the workpiece is undesirable. However, lowering the heating temperature significantly reduces the intensity of the static recrystallization process,

which slows the growth of grain. As shown by many studies in this area [1-2, 4-6, 9-11, 15], reducing the deformation temperature in all cases is more advantageous for the formation of a fine-grained structure.

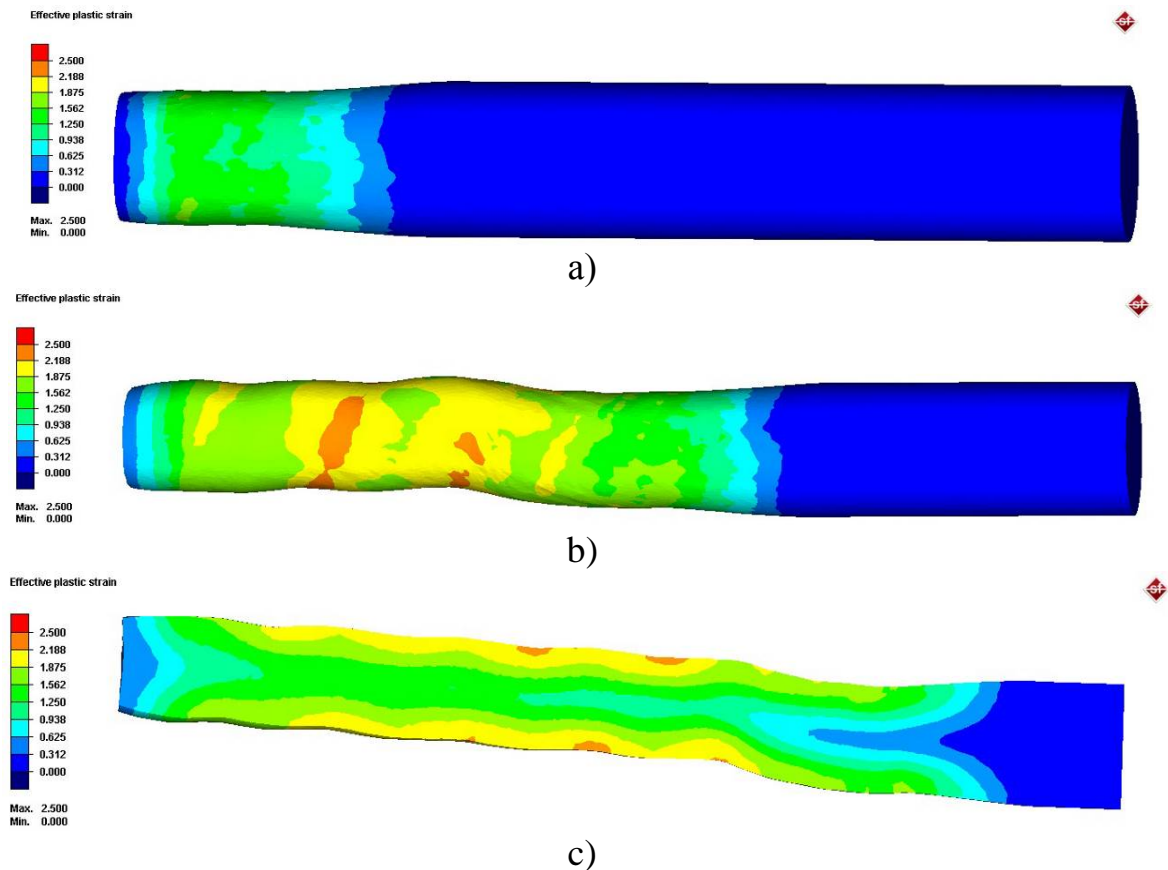


Figure 3.19 – Equivalent strain in a model with a reduced heating temperature of the workpiece 850 °C

### 3.4.3 Model with an increased angle of channels intersection in matrix 160°

This model, in contrast to the two previously considered, has a modified geometric parameter - the angle of the junction of channels in the matrix. In the study of this model, it was found that the SSS parameters, when compared with the base model, change only in the compression zone, i.e. in the deformation zone of the matrix. At the same time, all the studied parameters in the hearth of the rolling rolls are practically unchanged (the difference in values when compared was 1.5-2%, which can be attributed to calculation errors). Therefore, it was decided to study this model, considering only the 2nd stage of deformation.

As noted above, the stress parameters in the rolling zone are almost unchanged. In the intersection zone of the matrix channels there is a significant reduction of both tensile and compressive stresses. This is due to the fact that with increasing the angle of the junction of channels in the matrix, the level of back pressure force that occurs when the workpiece moves in the matrix is significantly reduced. As a result, both the level of shear deformation and the intensity of twisting of the workpiece are reduced. In the channel intersection zone (figure

3.20), the tensile stress is 210 MPa, which is lower than the value of the base model by 25 %; the value of compressive stresses reaches -280 MPa, which is lower than the same value of the base model by 18 %.

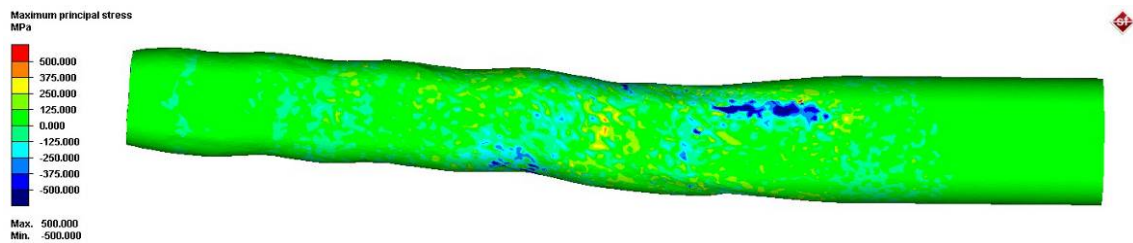


Figure 3.20 – Main tensile stress  $\sigma_1$  in a model with an increased angle of channels intersection in matrix  $160^\circ$

Similar to the component  $\sigma_1$ , when considering the maximum compressive stress  $\sigma_3$  (figure 3.21), a decrease in this parameter is noted, which shows the obvious effect of increasing the angle of the junction of the channels. The tensile stress is 30 MPa, which is 63% lower than the base level; the compressive stress reaches -400 MPa, which is 11% lower than the base model.

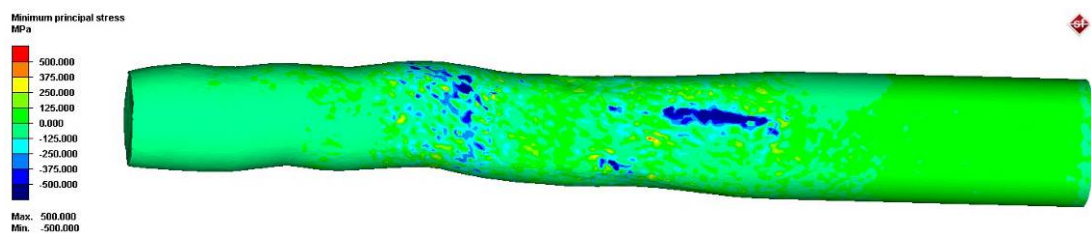


Figure 3.21 – Main compressive stress  $\sigma_3$  in a model with an increased angle of channels intersection in matrix  $160^\circ$

In general, the distribution of the main stresses in the model with an increased angle of the channel joint in the matrix is favorable, since it was found that this deformation scheme provides the repayment of the resulting tensile stresses by the prevailing level of compressive stresses, which is a favorable condition for deformation.

When considering the equivalent stress (figure 3.22), a decrease in this parameter was revealed by reducing the action of the backwater. The stress value in the deformation zone of the rolls was 130 MPa in the areas of metal contact with the rolls, which is lower than the base level by 32 %. In contact-free zones, the value of this parameter is within the 90 MPa limit, which is 36% below the baseline. In the zone of junction of the channels of the matrix, the magnitude of the equivalent stress is 110 MPa, which is lower than the baseline by 31 %.

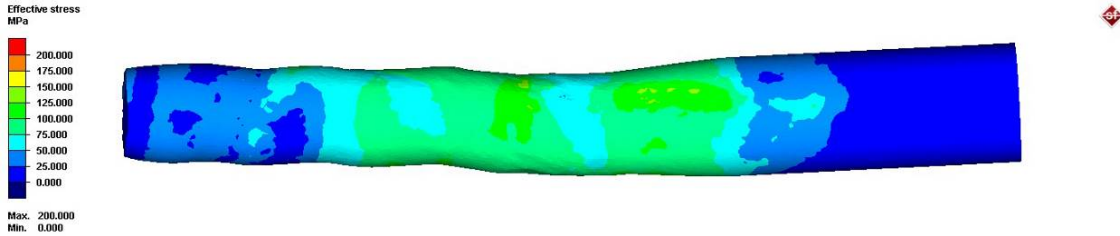


Figure 3.22 – Equivalent stress in a model with an increased angle of channels intersection in matrix  $160^\circ$

Behind the zones of metal contact with the rolls there are also coniferous lengths of the physical center of deformation, but their length is very small and does not have a distinct shape due to the general decrease in stress.

In the study of equivalent strain, it was found that the change in the angle of the junction of the channels has a significant impact on the value of this parameter (figure 3.23). The value of equivalent strain reaches 1.8 in the surface layers, which is lower than the value of the base model by 22 %, in the central layers the value of this parameter is at the level of 1.0, which is lower than the value of the base model by 40 %.

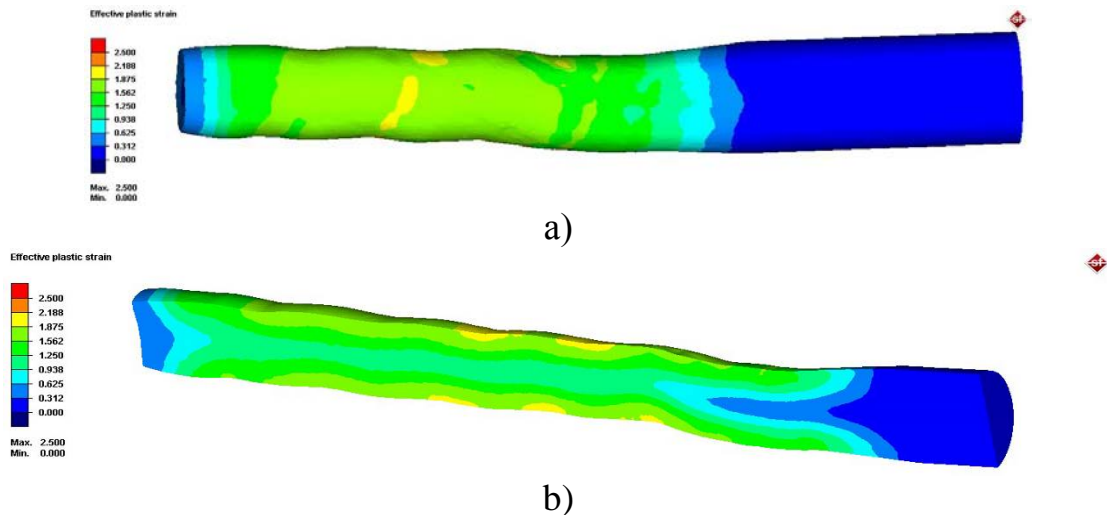


Figure 3.22 – Equivalent strain in a model with an increased angle of channels intersection in matrix  $160^\circ$

Since the change in the value of the junction angle of the channels mainly affects the change in the SSS parameters in the matrix, the increase in the value of the junction angle is impractical. Despite the fact that this leads to a decrease in energy consumption for deformation, an increase in the angle of the junction of the channels has a negative impact on the growth of equivalent deformation. Especially critical in this case is the reduction in the proportion of simple shear deformation, which should contribute to the transformation of the oriented banded structure of the central part of the bar into a more equiaxed, thus reducing the anisotropy of the properties throughout the cross section. Ultimately, this will lead to the need for more deformation cycles to achieve a given level of structure design.

#### 3.4.4 Models with altered friction coefficients of rolls and matrix

The study of these two models revealed the following patterns:

1) the change of stress state parameters occurs only in the deformation zone where the friction coefficient changes directly;

2) comparative analysis of the stress state showed that the difference in the parameters is minimal (less than 1%). Despite the fact that the results of studies of the dependence of the coefficient of friction on the SSS parameters of various deformation processes [96, 97] are known, in which a significant effect of this parameter is noted – in this case, the minimum effect of changing the coefficient of friction in comparison with the base model was obtained. This is due to the very small optimal range of variation of this parameter, both in rolls and in the matrix.

3) the change of parameters of the deformed state does not occur in any of the centers of deformation, which is also a consequence of the small range of variation of this parameter.

As a result, it was decided not to consider these models.

#### 3.5 Study of the influence of the number of passes on the strain state of the workpiece in order to form the UFG-structure

As noted earlier, the comparison of equivalent strain values in the surface and central layers of the workpiece in the base model and in models with variable parameters showed that the distribution of this parameter over the cross section is quite uneven. The difference between the surface and central zones can be as high as 60-70 %. This is a very negative factor, because in this case there is a significant anisotropy of the properties of the material over the cross section of the bar. This problem can be solved if the workpiece is subjected to several successive deformation cycles. This will not only significantly increase the overall level of accumulated deformation, but also align its value across the cross section of the workpiece, thus achieving the transformation of the oriented striped structure of the central part of the bar in a more equiaxed.

For multi-pass deformation, the basic model was chosen for the following reasons. Despite the fact that in the analysis of models with variable parameters it was found that the increase in the heating temperature of the workpiece causes an increase in the overall level of deformation, this causes an intensification of the process of static recrystallization, which is an extremely undesirable factor for the formation of the UFG structure. In the works devoted to the production of UFG and nanostructured materials by the SPD methods, the use of lower deformation temperatures led to better results in all cases [4-6, 15]. The use of a model with a reduced heating temperature of the workpiece is also irrational, because in this case, the level of tensile stresses in the workpiece increases significantly, which when the tensile strength value is reached will lead to the destruction of the material.

The decrease in the value of the angle of intersection of channels in the matrix also causes the negative effect of reducing the level of strain that will ultimately require much larger number of cycles of deformation to obtain the desired level of maturity structure. Therefore, the choice of the channel junction angle of  $150^\circ$  is the most weighted.

Deformation was carried out in 3 passes:

- first pass: the workpiece with a diameter of 25 mm was rolled to a diameter of 20 mm and passed through a matrix with a channel diameter of 21 mm;
- second pass: billet with a diameter of 20 mm were rolled to a diameter of 17 mm and passed through a die with a channel diameter of 18 mm;
- third pass: the blank with a diameter of 17 mm was rolled to a diameter of 14 mm and passed through a matrix with a channel diameter of 15 mm.

The simulation results are shown in figures 3.24-3.26 below.

After the first pass, the equivalent strain reaches 2.3 in the surface layers and 1.4 in the central layers. Thus, the difference of equivalent strain values reaches 64 % (figure 3.24).

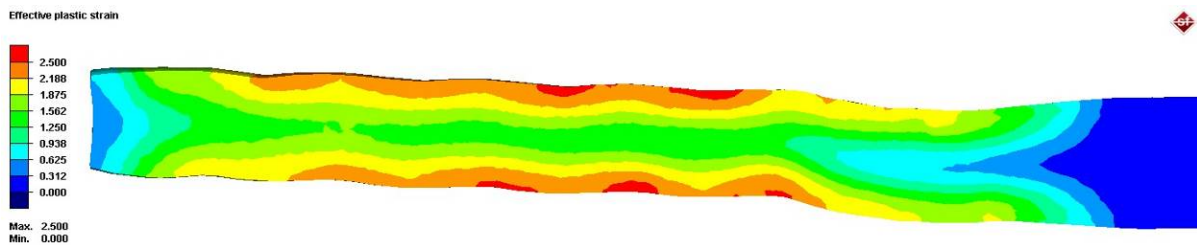


Figure 3.24 – Equivalent strain after the first pass

At the second deformation cycle, the accumulation of equivalent deformation in the entire volume of the workpiece continues. Screw rolling contributes to the intensive elaboration of the surface layer, and the compression occurring behind it in the matrix due to shear deformation evens the difference in deformation values between the surface and central layers. After the second pass, the equivalent strain reaches 5 in the surface layers and 3.2 in the central layers. Thus, the difference of equivalent strain values reaches 56 % (figure 3.25). At the same time at both ends of the workpiece there are typical screw rolling tightening, which is a consequence of a higher rate of deformation in the surface layers.

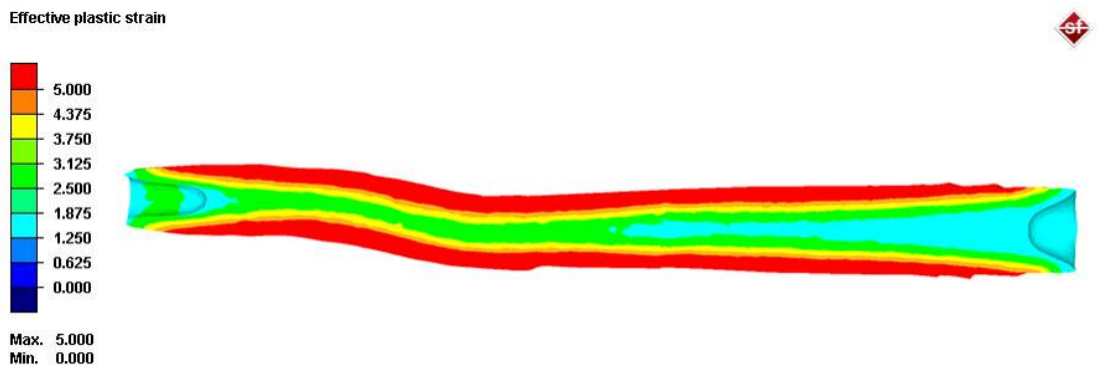


Figure 3.25 – Equivalent strain after the second pass

In the third deformation cycle, the character of accumulation of equivalent deformation is similar to the previous two passes. After screw rolling, the thickness of the worked surface layer continues to increase. Subsequent pressing in the matrix after the passage of two joints of the channels causes the accumulation of deformation throughout the cross section. After the third pass, the equivalent strain reaches 7.5 in the surface layers and 5.4 in the central layers. Thus, the difference of equivalent strain values reaches 39 % (figure 3.26).

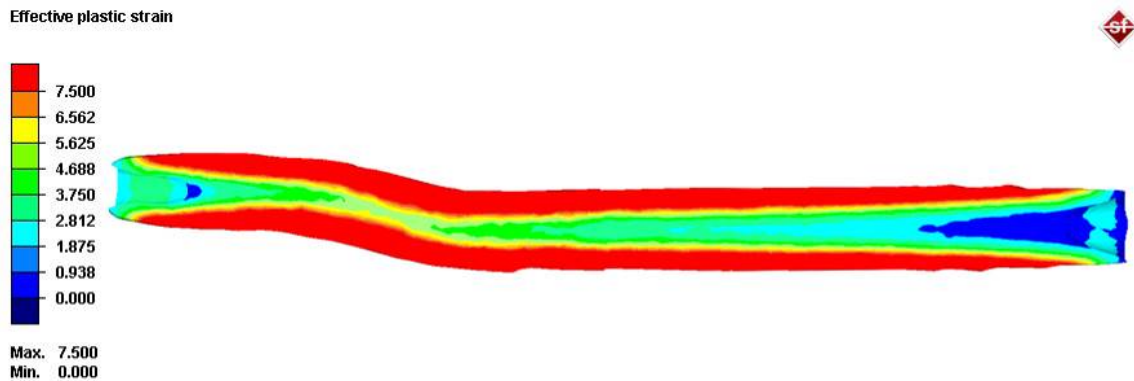


Figure 3.26 – Equivalent strain after the third pass

Thus, it was found that the multi-pass deformation in the combined process "screw rolling – ECA-pressing" contributes not only to the overall increase in the level of equivalent strain, but also the alignment of its value across the cross section of the workpiece between the surface and central layers. Ultimately, this will allow to predict the production of high quality bars with soveltamisalasta structure and uniform distribution of mechanical properties over the cross section of the workpiece.

Summarizing all the above, it is safe to say that this combined process "screw rolling – ECA-pressing" is an effective way of obtaining high-quality blanks of circular cross section. This conclusion allows us to make the value of compressive stresses in both centers of deformation, which exceeds the value of tensile stresses. The distribution of equivalent deformation also indicates an effective working out of the metal, especially in the surface layers.

However, a negative factor is the distribution of equivalent strain on the cross section of the workpiece. Uneven elaboration inevitably leads to anisotropy of the mechanical properties of the cross section of the bar.

In order to reduce the difference in the deformation of the central and surface layers, it is necessary to carry out several deformation cycles. In particular, in order to obtain a difference of strain values between the surface and central layers of less than 50%, it is necessary to carry out at least three passes of deformation.

This deformation scheme contributes to a significant grinding of the original grain due to the increase in the level of equivalent deformation, as well as the alignment of its value across the cross section of the workpiece between the surface and the central layers.

It should also be noted that not all parameters of the process, which can be varied in real conditions, equally affect the SSS parameters. For example, an increase in the heating temperature of the workpiece has a positive effect on the indicators of the deformed state, causing an increase in the overall level of deformation. The decrease in temperature leads to an increase in the resistance of the deformable material to twisting, which slows down the growth of the deformation level. In addition, both compressive and tensile stresses increase at low temperature, which is not a favorable condition. The decrease in the value of the angle of intersection of channels in the matrix also causes the negative effect of reducing the level of strain that will ultimately require a greater number of cycles of deformation to obtain the desired level of maturity structure.

## 4 THE STUDY OF THE INFLUENCE OF TEMPERATURE AND STRAIN RATE DURING IMPLEMENTING A NEW PROCESS ON THE MICROSTRUCTURE EVOLUTION ON THE BASIS OF THE CONSTRUCTED MODELS USING SPECIALIZED SOFTWARE

### 4.1. Study of the microstructure evolution in the base model

To study the microstructure evolution, a specialized microstructure database of the Matilda program was used. This program is a tool for modeling physical and chemical processes occurring in the deformable body and is a modular add-on to the program Simufact. Matilda uses the data of stress-strain state, strain rate and temperature from the finished calculated model in Simufact Forming, complements them with the data of physical and chemical properties and their behavior for a given material and its structure from its own database, then, according to The Yada algorithm [98], calculates the parameters of static and dynamic recrystallization processes that affect the grain size change. The grain size is also calculated for each node of the finite element model and is displayed at the end of the simulation in any form convenient for visualization.

Thus, the basic model was imported property data AISI-1015 steel corresponding to steel 15, of specialized software Matilda. When modeling the microstructure, the program uses the assumption that the workpiece prior to deformation has a uniform structure with the same grain size at any point. The average grain diameter of 30  $\mu\text{m}$  was accepted as the initial size, which corresponds to the 7th point [99].

After calculating the model, the results of the evolution of the microstructure were obtained, which were considered separately on the surface and in the longitudinal section of the workpiece. During screw rolling, the surface layers of the workpiece are subjected to intense deformation, which contributes to a significant grinding of grain from 30 microns to 20 microns, which corresponds to the 8th point (figure 4.1). After passing through the channels of the matrix due to the implementation of shear deformation, the grain is further crushed to 14 microns, which corresponds to the 9th point.

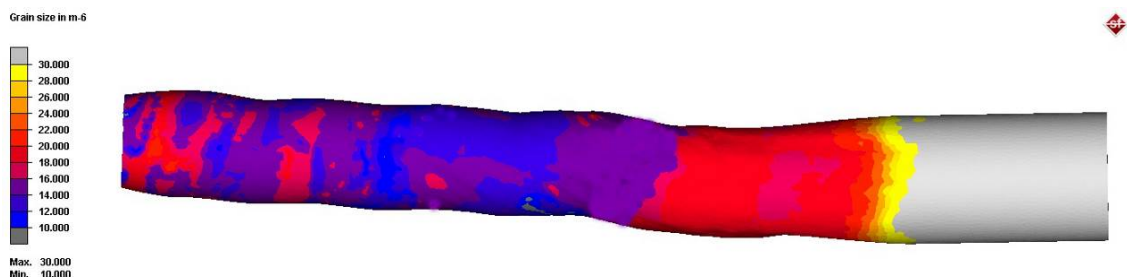


Figure 4.1 – Changing the grain size on the workpiece surface

The central layers of the workpiece during the screw rolling are processed less intensively – here the grain size varies from 30 microns to 28 microns (figure 4.2). The most interesting is the area of the workpiece after the passage of the matrix channels. Here is the grinding of grain throughout the section of the

workpiece, in the central zone of the grain size varies from 28 microns to 22 microns. Thus, after one deformation cycle, the difference in grain size values is 57%, which once again confirms the fact that in the implementation of this combined process, the workpiece is worked out unevenly across the section and several deformation cycles are necessary to align the properties across the section. It should also be noted that the results of modeling the microstructure correlate well enough with the results of the study of equivalent deformation, the nature of the distribution of which in the cross section is largely similar to the picture of the evolution of the microstructure.

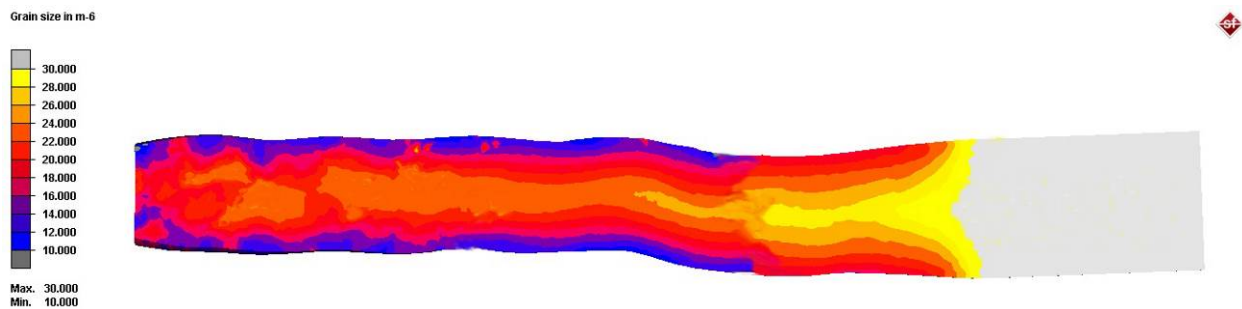


Figure 4.2 – Grain size change in the longitudinal section of the workpiece

After considering the basic model, the task was to identify how the change in the main technological parameters, namely, the change in the heating temperature of the workpiece and the deformation rate, affects the grain size. These parameters were chosen because they are the most flexible in terms of changing values. The temperature is easy enough to vary when heating the workpiece in the oven. The speed of deformation in this combined process is determined by the speed of rolling on the screw mill, the value of which is also easy to change with the frequency converter installed.

#### 4.2. Study of the microstructure evolution in models with varying values of workpiece heating temperature

In studying the effect of temperature on the microstructure evolution were used previously constructed models – with heating temperatures of the workpiece 1150 °C and 850 °C. As shown by the study of these models, the effect of temperature on the grain size change is very significant. A decrease in the heating temperature causes an intensification of the grinding of the initial grain, while an increase in the heating temperature slows down this process. This is clearly seen in the histogram shown in figure 4.3. This is due to the fact that when the heating temperature of the metal increases, the process of static recrystallization is significantly accelerated in it, which is undesirable because it leads to the emergence and growth of new grains. When the temperature decreases, this type of recrystallization slows down significantly, and the grain is crushed under the

influence of dynamic recrystallization, which takes place directly during the deformation process.

In the analysis of the spread of values, it was found that in the model with a heating temperature of the workpiece 1150 °C during screw rolling, the difference in grain size between the central and surface zones is 17%; after pressing in the matrix, this difference is 32%. The increase in the spread is due to the fact that, despite the increased value of the heating temperature of the workpiece, when it comes into contact with the working tool, the surface layers cool more intensively than the central ones. Therefore, when deforming in the matrix, where the contact with the tool has a higher duration than in screw rolling, there is an intensive grinding of grain in the surface area.

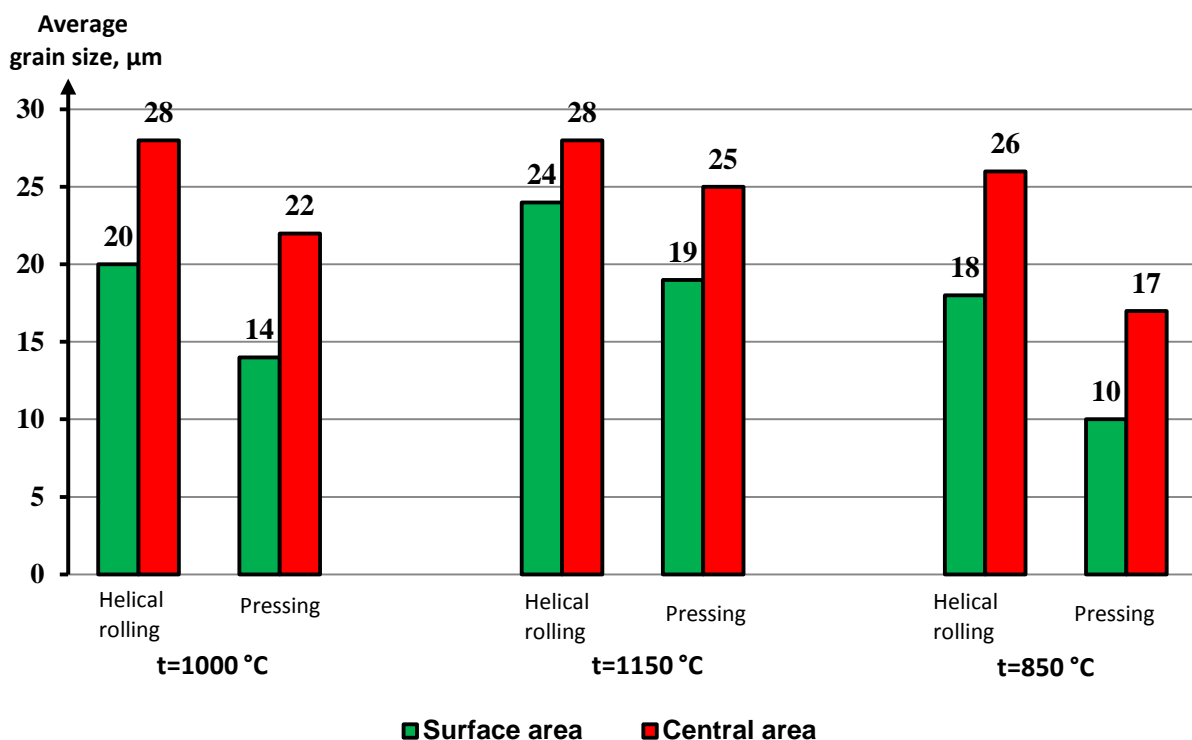


Figure 4.3 – Change in grain size at varying heating temperature of the workpiece

In the model with a preform heating temperature of 850 °C during screw rolling, the difference in grain size between the central and surface zones is 44 %; after pressing in the matrix, this difference reaches 70 %. Here it is necessary to note not only an increase in the spread between the central and surface zones, but also a decrease in the overall level of grain size compared to the base model. Both of these factors are the result of lowering the heating temperature of the workpiece, which leads to a decrease in the impact of static recrystallization.

It should be noted here that, despite the increased level of dispersion of values, the model with a reduced heating temperature is optimal in terms of more intensive grinding of grain. This is especially evident when comparing the grain size values in the central part, which is worked much worse than the surface area. As has already been proved in the study of the deformed state, to align the values of

the accumulated deformation it is necessary to carry out several passes of deformation. In this case, it will also reduce the spread of grain size values. Therefore, for subsequent multi-pass deformation, it was decided to use a preform heating temperature equal to 850 °C.

#### 4.3. Study of the microstructure evolution in models with varying values of strain rates

When studying the influence of the deformation rate on the microstructure evolution, it was necessary to build additional models with different rolling speeds and compare them with the basic model, where the speed of rotation of the rolls is 100 rpm.

Since the screw mill is equipped with a roll speed control system using a frequency converter, it was decided to study the grain size change at extreme values of rolling speed. In particular, the minimum technologically possible speed of rotation of the rolls is 10 rpm; the maximum possible speed of rotation of the rolls is 300 rpm. This choice was made due to the fact that in many works [1,4,9,15,29] in the study of ECAP it was proved that the change in the rate of deformation in a relatively small range (3-5 times) practically does not affect the change in grain size.

The results of the microstructure simulation shown in figure 4.4 confirmed the results of the above studies. When the deformation rate varies from 10 to 300 rpm, the microstructure of the workpiece practically does not change. A small change in the average grain diameter (1-2 microns) occurs only in the surface area at a reduced rolling speed. This is directly due to the fact that when the deformation rate decreases, the workpiece has a longer contact with the tool, as a result, the surface layers cool down more strongly.

Here it should be noted that the variation of the deformation rate will be impractical solution. Increasing the speed of rotation of the rolls leads to an increase in dynamic loads on the bed of the rolling stand, which is a negative factor. Excessive reduction in the rate of deformation is also undesirable, since it leads to a significant cooling of the workpiece and the possible growth of grain in the central parts of large billets due to static recrystallization.

Despite the fact that in the study of the ECAP process [1,15,29] it was found that a decrease in the deformation temperature is a favorable condition for the formation of a fine-grained structure, in the implementation of this combined process, a situation may arise when the workpiece cools down so that the forces generated by the rolling mill will not be enough to push the workpiece through the channels of the matrix. Therefore, for the subsequent multi-pass deformation, it was decided to use the deformation rate from the base model equal to 100 rpm.

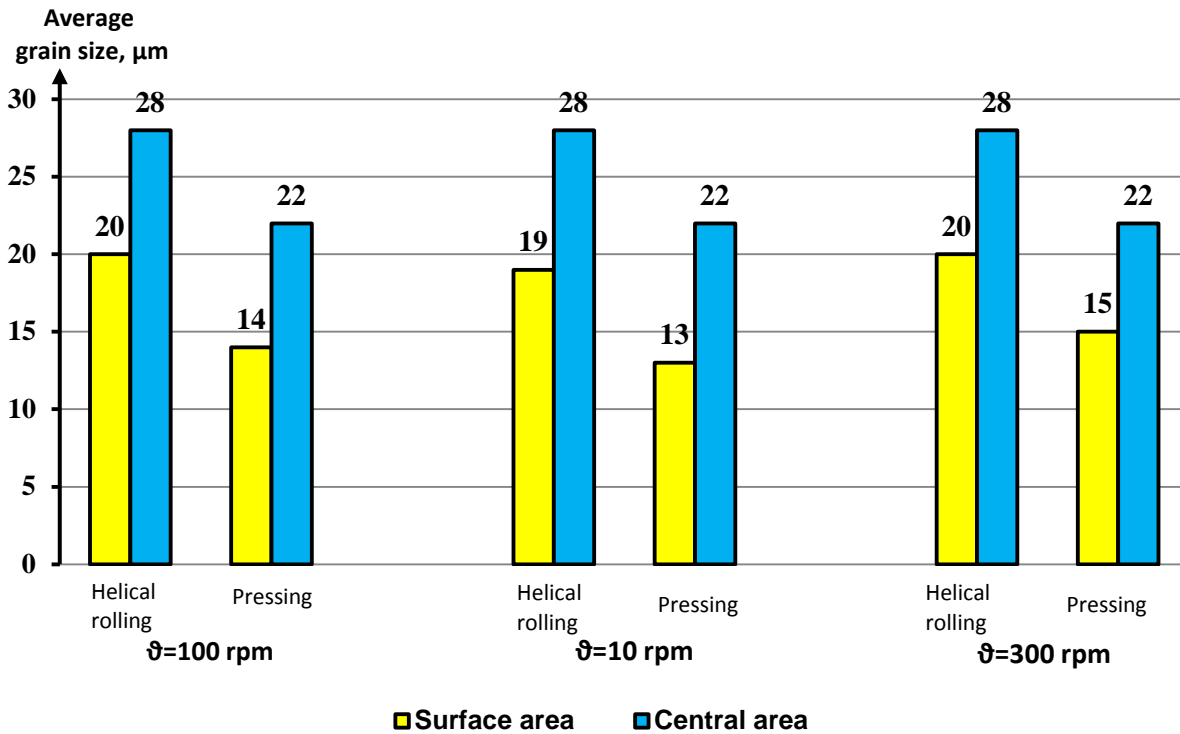


Figure 4.4 – Change of grain size with variation of strain rate

#### 4.4. Study of the microstructure evolution after several deformation cycles

The initial model for multi-pass deformation was a model with a reduced heating temperature of 850 °C, which was determined as the most optimal. Deformation in the 2nd and 3rd pass was carried out under conditions similar to multi-pass deformation in the study of the deformed state:

- second pass: billet with a diameter of 20 mm were rolled to a diameter of 17 mm and passed through a die with a channel diameter of 18 mm;
- third pass: the blank with a diameter of 17 mm was rolled to a diameter of 14 mm and passed through a matrix with a channel diameter of 15 mm.

As a result, the following data were obtained (Fig. 4.5). In the first pass after screw rolling, the difference in the average grain diameter between the central and surface area was 8 µm; after pressing in the matrix, the difference reached 7 µm.

During the second pass, the grinding of grain during screw rolling is not as intense as in the first pass. This is due to the fact that the compression in this passage was 3 mm, which is less than in the first passage (5 mm). Here, the average grain diameter in the surface zone was 8 µm, in the central zone – 13 µm, i.e. the difference was 5 µm. During subsequent pressing in the matrix, the average grain diameter decreased to 6 µm in the surface area and 10 µm in the central zone. The difference between the values decreased to 4 µm.

During the third pass after screw rolling, the average grain diameter in the surface area was 5 µm, in the central zone – 9 µm, i.e. the difference was 4 µm. During pressing in the matrix, the average grain diameter decreased to 3 µm in the surface zone and 6 µm in the central zone. Thus, the difference was only 3 µm.

As a result of the study of the multi-pass deformation model, it was found that with an increase in the number of passes, there is not only a general decrease in the average grain diameter, but also a gradual alignment of this parameter between the central and surface zone.

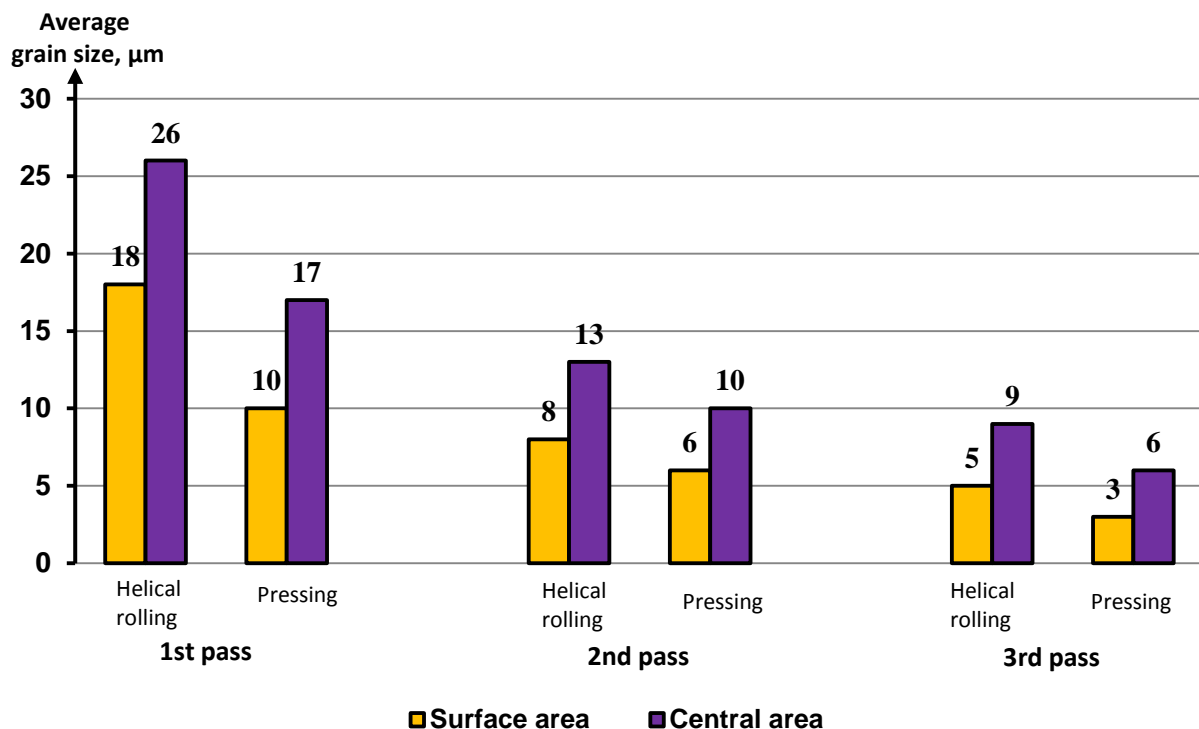


Figure 4.5 – Grain size change in multi-pass deformation

As a result of studying the evolution of the microstructure in the combined process "screw rolling – ECA-pressing" it was found that this combined method of deformation can significantly grind the original grain size. Variation of the main technological parameters showed that the influence of the heating temperature of the workpiece plays a significant role in the degree of grain grinding. While the rate of deformation, within the permissible installation design limits, does not have a significant effect on the process of changing the microstructure.

Due to the screw rolling grain grinding occurs mainly in the surface layers of the workpiece. Subsequent pressing in the matrix leads to a change in grain size already throughout the section of the workpiece. But, despite this, the difference in the average grain diameter between the central and surface area remains. In order to reduce the observed dispersion of values and alignment of grain size across the section, it is necessary to subject the workpiece to several deformation cycles. Thus, after the third pass, the difference between the average grain size between the central and surface areas is only 3 microns, which is much less than that after the first pass (7 microns). This allows us to talk about a fairly uniform study of the structure of the cross section of the workpiece.

It should be noted that the receipt of such results by the method of ECAP requires 4-6 cycles of pressing, at the time, as the results presented were obtained as a result of all three passes, despite the fact that the time of each passage to the

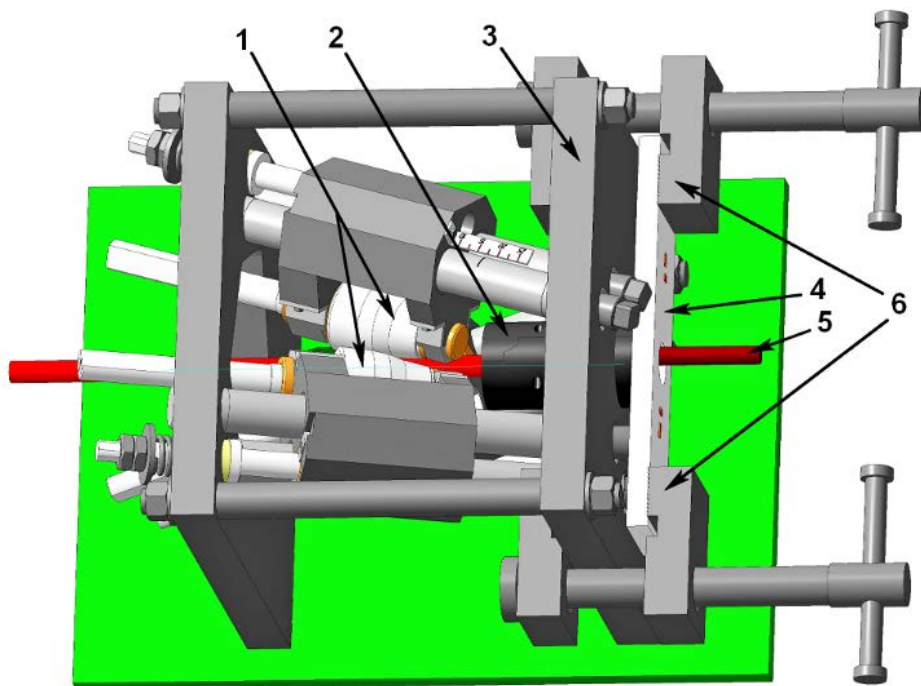
original rods with 250 mm length is 5-8 seconds. Performance, at the same time, (according to the performance of mill-bases a combined installation) will be up to 100 kg/h high quality round steel bar without restrictions of length sub-ultrafine-grained structure. This is significantly higher than the main competing processes and makes it possible to talk about the greater efficiency of the proposed process.

## 5 DESIGN AND FABRICATION OF TOOLS AND EQUIPMENT FOR THE STAND IMPLEMENTING A COMBINED PROCESS "SCREW ROLLING – ECA-PRESSING". COMMISSIONING STAND WORKS

### 5.1 Design of the stand for realization of combined process "screw rolling - pressing»

According to certain and stated in the previous chapters, the optimal parameters favorable for the formation of ultra-fine-grained structure, on the basis of the screw rolling mill RSR it was decided to design a plant for the implementation of the combined process.

The stand should provide screw rolling and subsequent continuous pressing of bars with diameters of 17-20 mm through a matrix with an angle of junction of channels of 150°. The matrix should be fixed in front of the mill at a distance of not more than 27.5 mm from the front edge of the rolls. The requirement to limit the size of the matrix to an external diameter of 70 mm was added to the above requirements. In addition, the design should be sufficient for pressing the total stiffness to provide a quick and simple assembly and disassembly for rapid extraction of the butt-end and replace the current matrix with a matrix with a different channel diameter for the next pass. A sketch of the installation project for the implementation of the combined process "screw rolling-pressing" on the basis of the RSR mill is shown in figure 5.1.



1 – rolls; 2 – matrix; 3 – front frame; 4 – thrust plate; 5 – processed rod; 6 – holding clamps (or staples)

Figure 5.1 – Sketch of the installation project for the implementation of the combined process "screw rolling – ECA-pressing" on the basis of RSR mill

These are rather strict requirements. To match them, you must select the appropriate installation design. As can be seen from figure 5.1 – to ensure the requirement of speed of assembly and disassembly operations when changing the diameter of the rolled rod, the matrix (2) is freely inserted into the hole in the plate of the front frame of the mill, pressed against the rolls (1) and locked by the thrust plate (4), which is freely inserted into the holding clamps or brackets (6) fixed to the front frame of the mill (3).

In practice, it was decided to use the massive brackets remaining after the experiment to measure the maximum axial force of the screw rolling, which will be described in Chapter 7. Due to the inability to change the distance between the planes of the brackets (as opposed to clamps), for maximum pressing of the matrix (2) to the rolls (1) at different rolling diameters, between the matrix (2) and the thrust plate (4) can be used metal pads. For industrial implementation of the installation it is preferable to use clamps.

To exclude the rotation of the matrix under the action of the torque of the rolled rod, a small flat should be provided on the matrix, into which the plate is inserted fixed by two bolts on the front frame. When disassembling, one bolt is unscrewed and the plate is rotated releasing the matrix.

Thus, the overall design of the plant will have to provide a simple and quick replacement of the matrices in the mill.

Now we need to design the matrix itself. Requirements to the equal-channel angular matrix for combined installation are as follows:

- the bore diameter of 17-20 mm;
- channel junction angle 150°;
- external diameter not more than 70 mm;
- speed and simplicity of assembly and disassembly operations.

The analysis of structures of equal-channel angular matrices with a round channel, carried out on the materials [1-2, 4-6, 26-31] described in the first Chapter, as well as in the source [100], allows us to conclude that the most common design of ECA matrices is the simplest design – two symmetrical halves of the matrix with a bolted connection divided along the axis of the channel [100]. This design has significant disadvantages associated with the rigidity of the matrix, which is very often insufficient, the halves are extracted and Burr is formed. At the same time, in addition to the deterioration of the quality of the pressed workpiece, the pressing force increases, which can exceed the calculated and lead to matrix failure. Such cases occur regularly. In addition, the matrix of the described design, due to the large number of stressed bolt connections, requires a lot of time for disassembly to extract the press residue, which contradicts the requirement of the matrix replacement speed. It is impossible to make a matrix with a monolithic construction because of the curvature of the internal channel and the need for its disassembly to extract the press residue, so the matrix should consist of several mating parts. A typical construction of such matrices is shown in figure 5.2 [100, p. 338].

Also, protruding bolt connections are difficult to fit into the 70 mm outer diameter, which is limited by the design. To solve this problem, you can use bolts

with a hidden head under the hex key, which are screwed into the thread, cut in the other half of the matrix.

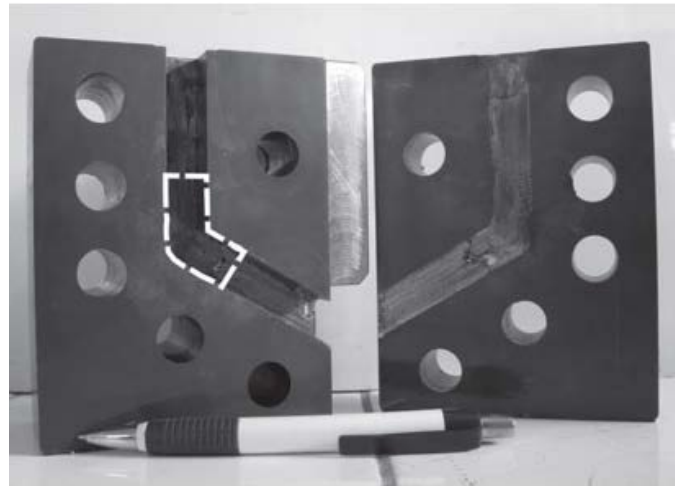


Figure 5.2 – Typical matrix design for ECAP

However, the use of such a move is risky because of the ease of damage to the thread on the bolts and in the matrix in case of emergency situations. A damaged bolt in a conventional design can be knocked out with a sledgehammer after cutting the nut, and in the case of threads in the matrix itself – a dangerous drilling operation is required. All these drawbacks make us look for less standard ways of constructing a compromise matrix construction.

To increase the reliability and rigidity of the structure, while ensuring the speed and simplicity of assembly and disassembly operations, it is only possible to abandon the use of a bolt connection as such.

Examples of structures of matrices without bolts are known, for example, symmetrical matrix halves having a small taper of the outer face are added together and placed in a massive container. The hole for the matrix in the container also has a conical shape and is precisely matched in size with the matrix. The matrix halves are held in the container by friction forces. Such a design would be very good for reasons of modularity of the design, allowing the matrix to be installed in a container with different channel diameters (a range of 17-20 mm is required). It was decided to stop on two diameters of matrices in 17 mm and 18,5 mm because they allow to carry out 2 passes of the combined process and at the same time provide the least loadings.

However, despite all the advantages of the above design, its use for our purposes is seriously limited by the permissible dimensions of the matrix. The design of this type of sufficient rigidity will take obviously more space than required, so the option with the container will not work.

Thus, the rationale for rejection of bolted connections because of their complexity, unreliability and more work on the assembly portable operation, and from the outside of the cage because of dimensional restrictions, it postulates the search for other solutions of the connection parts ECA-matrix.

One of the possible ways of connecting without bolt connection is on the principle of the dovetail. This compound is common in precision instrument-and machine-tool, forging and stamping production, as well as in optical and astronomical technology. This type of tongue and groove connection provides linear movement for highly loaded precision components of precision mechanisms. This indicates a very high stiffness of the compound [101-102].

The use of a dovetail connection for symmetrical ECA-matrix halves, such as those shown in figure 5.2, will result in uneven loading due to the asymmetry of the matrix channel. This problem can be solved by dividing the matrix into two unequal halves and on the other axis – as shown in figure 5.3.

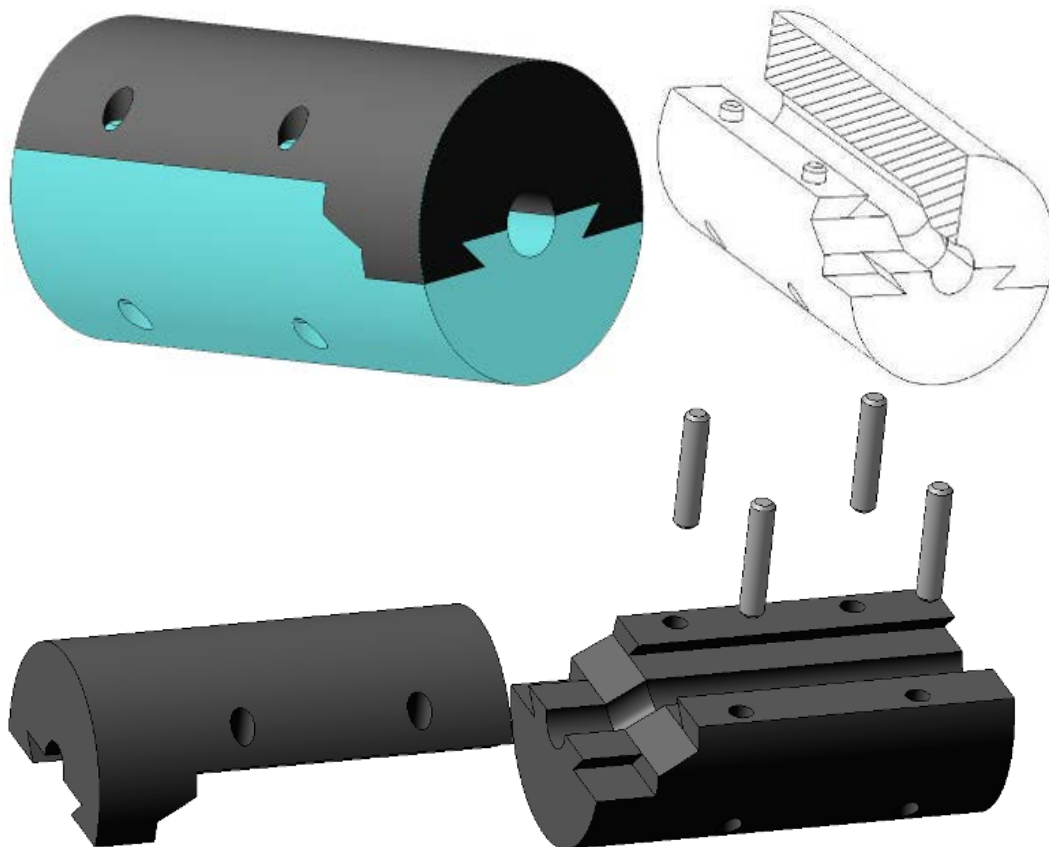


Figure 5.3 – Proposed construction of ECA-matrix

This design will provide the maximum rigidity of the matrix structure with a minimum metal content, since all metal parts are uniformly involved in the engagement. To prevent the shift of the matrix halves, 4 pins with a diameter of 8 mm are provided. However, for their fixation of the matrix parts in the assembled state, due to their special shape, there should be enough friction forces. Also, this design is extremely simple in assembly and disassembly operations, fits well into the overall dimensions and the concept of combined stand.

To ensure the possibility of processing in several passes and taking into account the results of modeling, it was decided to make 2 matrices with channel diameters of 18.5 mm and 17 mm. Angle of the junction of the channels was 150°. However, to check the reliability of the selected scheme, a strength analysis of the structure should be carried out.

## 5.2 Strength analysis of ECA-matrix for experimental stand

To verify the suitability of the selected design, it was decided to conduct a strength analysis. For analysis we selected the model with the diameter of the inner canal 18.5 mm, since when you work with it the highest expected load, and if this model will be suitable, then a model with a smaller bore diameter 17 mm, would also be suitable as a result of smaller loads.

In the system of the automated designing KOMPAS-3D, was created three-dimensional assembly model of the design matrix in two parts and four standard pins with a diameter of 8 mm and a length of 45 mm. Then, the resulting three-dimensional structure was imported into a specialized design library "APM FEM: Strength analysis", development of scientific-technical center "APM". Employees of STC APM created unique algorithms for solving linear and nonlinear problems of dynamics, strength, stability, etc., based on the finite element method and the latest methods of numerical modeling [103].

The application uses the finite element method already discussed in Chapter 3 as the basis for the calculation. To solve the problem of strength calculation of the proposed design is required to first set the desired areas of the model expected load, select the material, and then determine the parameters of the finite element grid and calculation parameters.

Since during the experiment to measure the maximum axial force of the screw rolling described in Chapter 2, the maximum force of 50 kN was recorded, it was decided to use 50 kN as the pressing force. It was also assumed that the pressure on the walls of the channel of the ECA matrix will also be the same value. Each of the six faces of the channel was loaded with a force of 50 kN, and a large face is fixed, because it should rest against the thrust plate during the experiment, while the second (smaller) half of the matrix, due to the bursting pressure of the metal in the middle, inclined channel, can move the opposite side of the bar movement. The model loading scheme is shown in figure 5.4.

After determining the loads, we determine the material for the matrix parts. For the manufacture of the matrix is most suitable steel grade 5HV2S. This steel is used for the manufacture of dies of complex shape, working with high shock loads, knives for cold cutting of metal, thread rolling dies, punches and crimping dies during cold work. Assign to the parts of the matrix steel of this brand from the inner library of materials KOMPAS-3D. The chemical composition of steel 5HV2S, as well as its mechanical properties after heat treatment by quenching at 880°C in oil followed by a two-hour release at 200°C in air are given in Annex B in tables B1-B2.

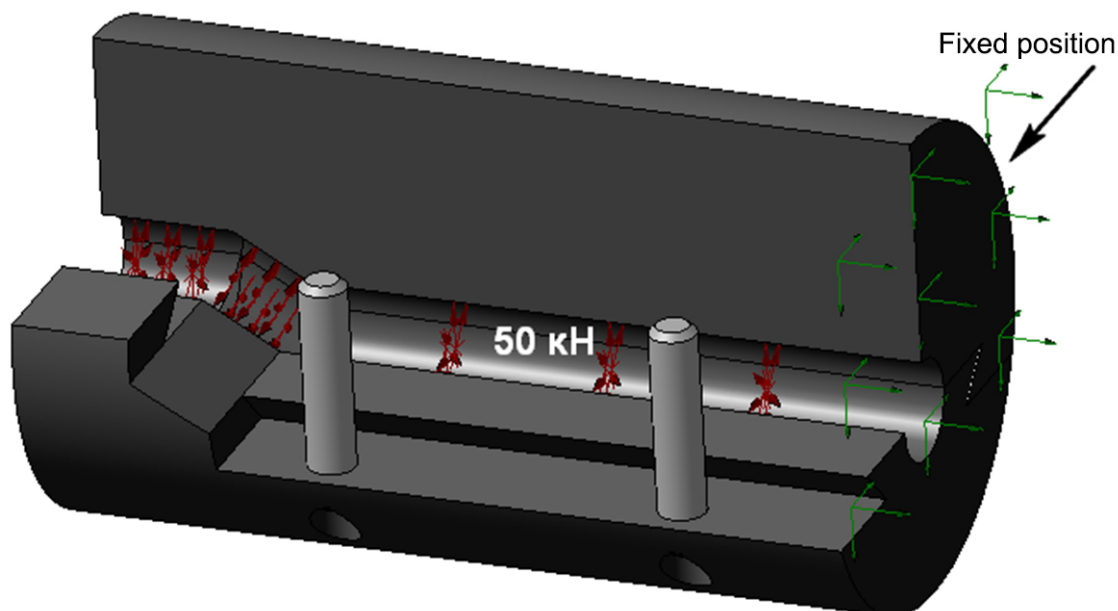


Figure 5.4 – Loading scheme of the ECA-matrix model

Now, the assembled model must be broken down into finite elements (FE). Four-node tetrahedra were used as finite elements to construct the grid. The maximum length of the FE is 1 mm, as recommended for sufficient calculation accuracy in many applications using FEM (including in DEFORM-3D).

Here it is worth noting one feature of the finite element method and mesh construction for FE for calculation. The fact is that very often, different parts of the model require different calculation details. For example, for an anvil, high-loaded flanges of complex shape and small size, for adequate calculation require the approximation of a large number of finite elements of smaller size than the main massive part of it. Of course, you can make a detailed approximation of the entire model the same FE, based on the smallest. With this approach, for example, for the currently calculated matrix, the number of FE will reach several hundred million. Such a task is difficult even for computing clusters. For comparison, the number of FE in the combined process model in DEFORM-3D was about 100 000. In addition, we do not get a real increase in the accuracy of the calculation, because in the massive homogeneous parts of the parts, the stress field is distributed according to simple laws. Increased detail in such places does not lead to a change in the picture of the stress-strain state. Clarification of the calculation is necessary only in places of complex shape (especially contact), or the concentration of loads. This position of optimization of calculation is repeatedly checked by calculations and is widely used in the software packages realizing FEM.

In APM FEM, which is included in CAD KOMPAS-3D, to adjust the granularity of the partitioning model in the finite element grid, there are 2 options. The maximum ratio of the thickening of the mesh on the surface – the ratio determines how the following item can be made (where necessary) less. Thus, when moving to smaller parts of the structure, the generator of the FE-grid gets the right to create a finite element  $k$  times smaller than the previous FE. If the value is 1 – we get the so-called "non-adaptive" (uniform) breakdown. In this case, the elements of the design with fewer than the specified maximum length dimensions

will be "swallowed" or to become coarser as. Setting a value greater than 1 generates an "adaptive" breakdown. In this case, the FE-grid will reflect the geometry of the "weak point" as accurately as possible. The reverse side of the accuracy will be the increase in the total number of FE and the calculation time [103-104].

The second parameter is the dilution factor in the volume – the degree of increase (decrease) of the tetrahedron side when generating a grid deep into the volume of the solid model. The closer to 1, the more similar become the layers of the FE. At values greater than 1, the internal FE are larger than those at the surface. This leads to a decrease in the total number of FE, without reducing the accuracy of the calculation. Range of variation: 0.7...5 [103, APM section].

For an adequate and sufficiently accurate approximation, the thickening coefficient on the surface was chosen 1,2. The volume dilution factor was also 1.2, with the base value of the finite element length of 1 mm. the Model was broken down into finite elements using algorithms based on the Delone tetrahedrization method. Have been used 1 048 750 finite element 232 at 466 knots. The generated grid (with cross section) is shown in figure 5.5. The results of the static calculation are shown in figures 5.6-5.9. In figure 5.6, the model movements are shown on a scale of 1000:1, the curvature of the input channel and the connection of parts is noticeable.

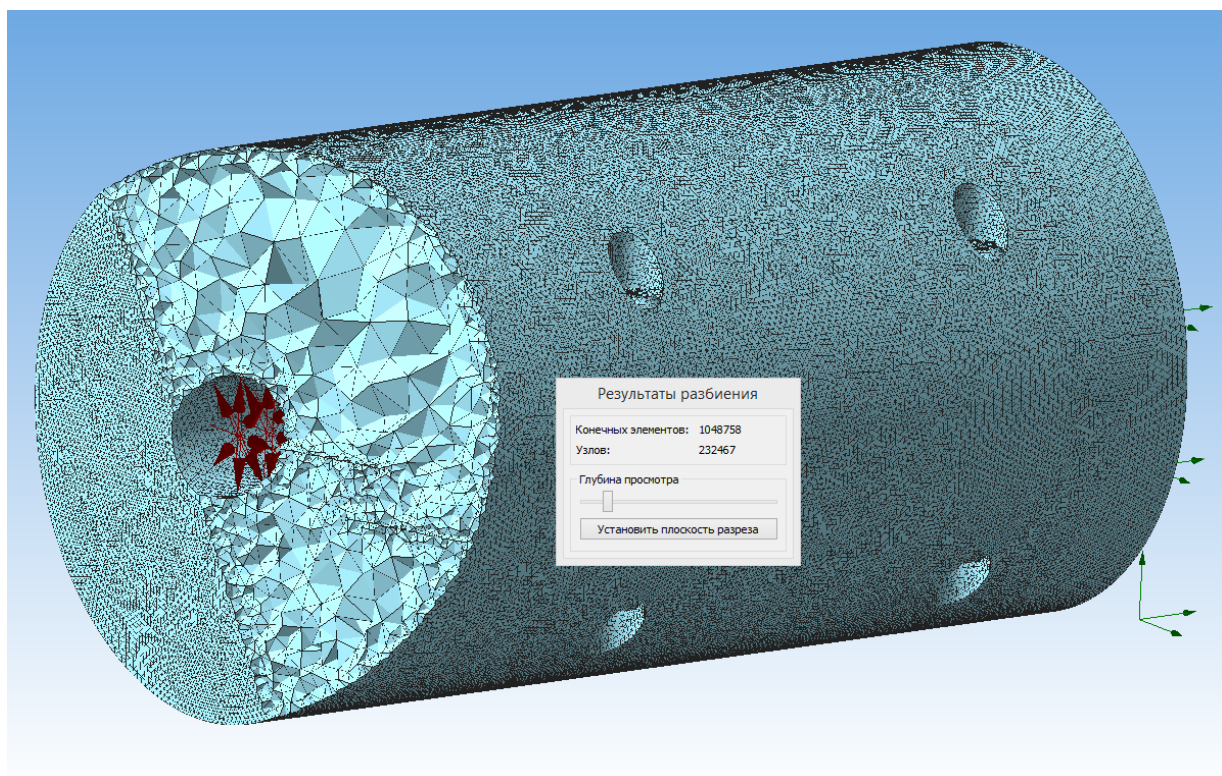


Figure 5.5 – Results of finite element mesh generation for matrix model strength calculation

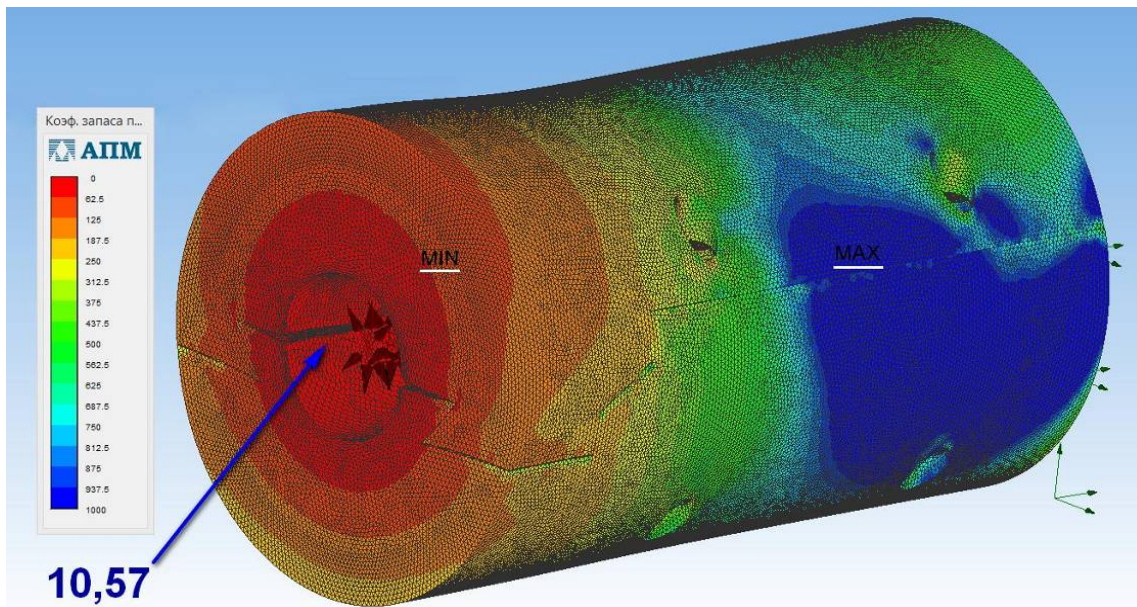
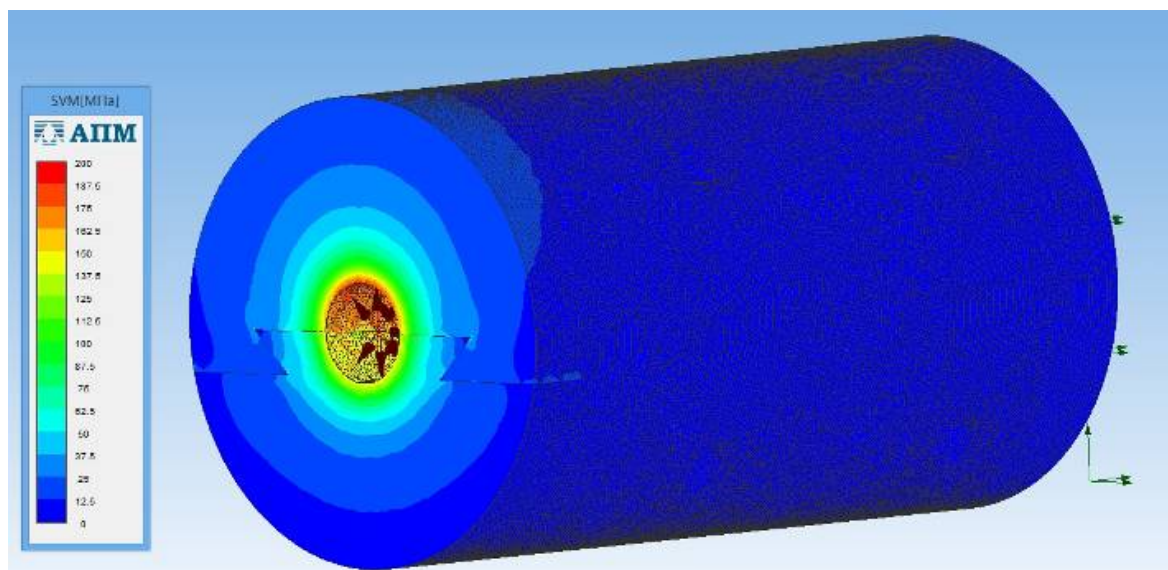


Figure 5.6 – Result of stress calculation (displacement scale 1000:1)

For a more detailed analysis, consider the stress distribution. The stresses are concentrated around the inclined channel and the entrance to the matrix. At the same time, the value at the most stressed areas does not exceed 200 MPa, which is a safe value when the yield strength is 1810 MPa. The places of connection of the matrix halves are also weakly loaded, which indicates the correctness of the chosen structure of the connection by the type of dovetail. The stress distribution in the cross section and on the surface is shown in figure 5.7. Arrows show the applied loads.



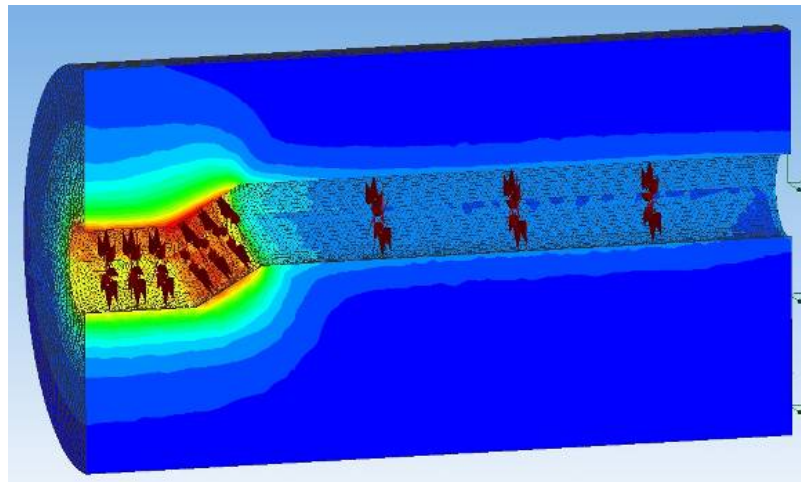


Figure 5.7 – Result of the stress calculation, MPa

Since the stresses do not exceed the yield strength, the matrix will not deform plastically even in the most loaded places. Therefore, we consider the results of the calculation of linear displacements of structural elements under the action of elastic deformation. The total linear movement of structural elements is shown in figure 5.8.

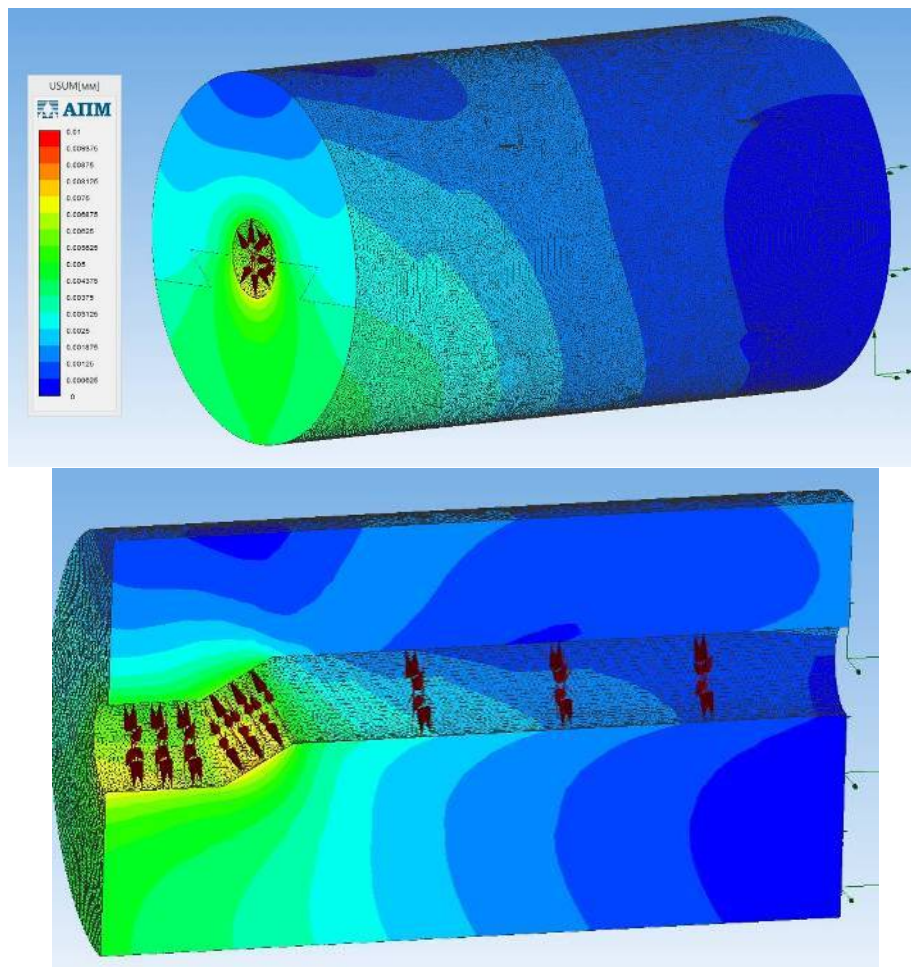


Figure 5.8 – Total linear displacement of structural elements, mm

The study of elastic deformation shows its greatest value in the lower (most) part of the matrix at the input and inclined channels. The maximum value of linear displacement reaches 0.008 mm, which is negligible and allows us to talk about the increased rigidity of the proposed design and its suitability for pressing coming out of the screw rod mill during the combined process.

Now let's assess the safety margin of the structure. The evaluation was conducted with respect to the value of the yield point, because although plastic deformation does not lead to the destruction of the structure, but in the case of the matrix for pressing it is unacceptable to any extent and leads to an emergency. The distribution of the factor of safety over the yield strength is shown in figure 5.9.

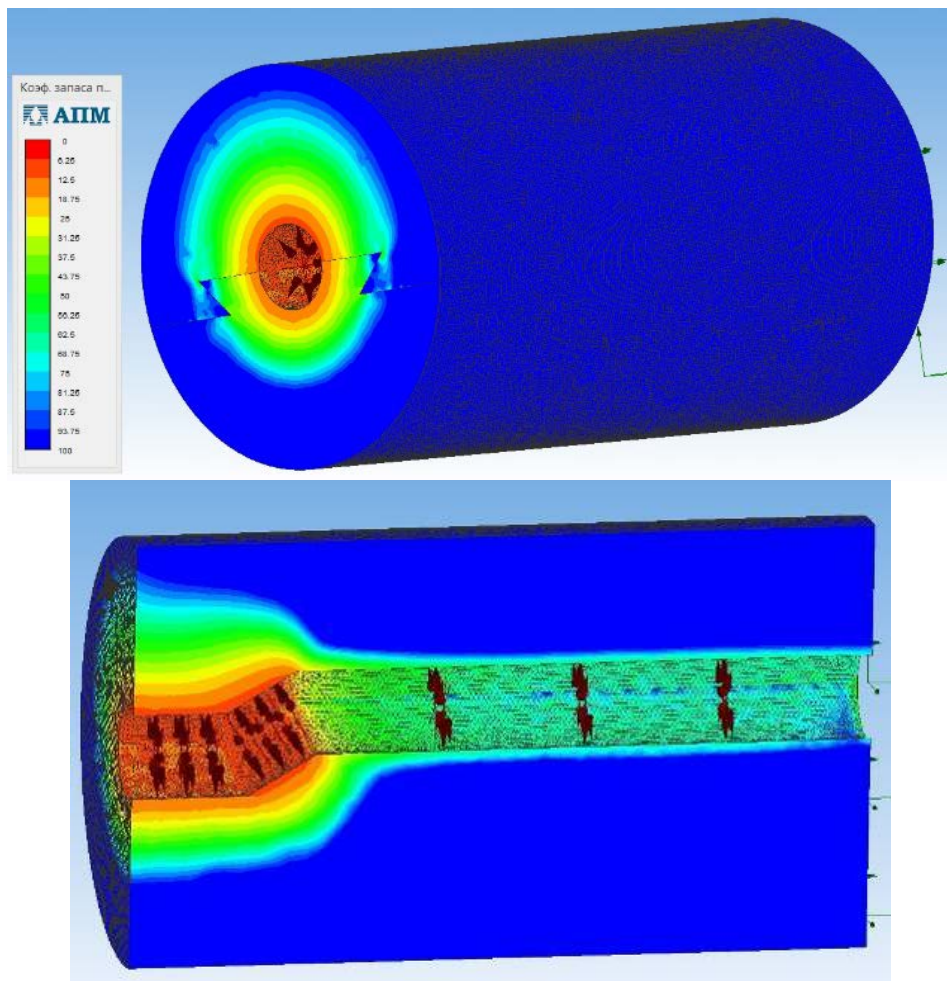


Figure 5.9 – Factor of safety for yield strength

Features of distribution of factor of safety repeat those in pictures of distribution of stresses that is natural. The minimum value of the factor of safety was 10, with the total level of safety of the most stressed areas in 40-60. At the same time, the margin of safety in metallurgical equipment is usually 5, and in special critical structures and structures that pose a danger to the life of personnel – 10. The calculated safety margin is more than enough for the combined installation for the experiment. It can be concluded that the strength analysis fully confirmed and justified the correctness, feasibility and safety of the chosen matrix design. The

simulation results were produced working drawings of two matrices with the diameter of the channel 17 and 18.5 mm. Drawings are given in Annex A.

### 5.3 Production of the tool, equipment and commissioning stand works realizing the combined process “screw rolling-pressing”

#### 5.3.1 Production of matrices and assembly of the stand

According to the obtained drawings, 2 matrices with inner channel diameters of 18.5 mm and 17 mm were made. For each matrix, two round billets with a diameter of 70 mm and a length of 100 mm were ordered from 5HV2S steel, the properties of which are given in tables 5.1-5.2 [91]. Machining of matrix blanks was performed on metal-cutting machines. The main manufacturing operations were carried out on planer, milling and drilling machines, and a grinding machine was used. The final finishing of the channels of the matrices was carried out manually by a drill with a cone and ball grinding stone. Then the channels of the matrix have been manually polished.

Table 5.1 – Chemical composition of steel 5HV2S

C	Si	Mn	Ni	Cr	Mo	W	V	Cu
0.45 - 0.55	0.8 - 1.1	0.15 - 0.45	till 0.35	0.9 - 1.2	till 0.3	1.8 - 2.3	till 0.3	till 0.3

Table 5.2 – Mechanical properties of steel 5HV2S after heat treatment

Yield stress, MPa	Ultimate stress, MPa	Elongation, %	Contraction, %	Impact strength, kJ /cm <sup>2</sup>
1960	1810	6	13	15

The final heat treatment of the manufactured matrices after machining was quenching and tempering. Heating of the matrices assembled for quenching was carried out in electric furnaces to a temperature of 880 °C. For a uniform temperature distribution over the entire volume of the tool, an aging of 45 minutes was carried out at the quenching temperature, after which quenching in oil was carried out. The vacation was held at a temperature of 200 °C, the holding time during the vacation was 120 minutes (2 hours) [105].

These measures guarantee high hardness and wear resistance of the matrix channels, and the strength of the structure as a whole. One of the manufactured matrices with a channel diameter of 18.5 mm is shown in figure 5.10.

To fix the matrix to the mill were used massive brackets thickness of 40 mm cut from the slab, and the matrix was locked thrust plate thickness of 14 mm and a width of 100 mm. In the center of the plate was drilled hole with a diameter of 22 mm to exit the bar. The plate was also made of steel grade 5HV2S and underwent the same heat treatment as the parts of the matrix, with the difference that to avoid residual curvature of the plate due to thermal stresses, it was fastened between two

massive metal bars and the heating time, for uniform temperature distribution was increased to 70 minutes.

The front frame of the RSR mill was removed and processed on a lathe in order to expand the output hole of the bar from 40 mm to  $70^{+0.5}$  mm. Then the mill design was assembled, the roll adjustment system was recalibrated, and the matrix and the brackets and holding plate necessary for locking the matrix were mounted on the front frame. The distance of edge of the rolls from the front frame when adjusting to different rolling diameters is different. Therefore, the design was configured to work with a matrix with the smallest diameter of the channel, providing the closest position of the rolls to the front frame. For accurate fixation of other matrices, a trial adjustment of the mill rolls to work with each of the three of them was carried out and the thickness of the pads between the matrix and the plate was determined, which turned out to be equal to 3 mm and 6 mm, respectively, for matrices with a channel diameter of 17 mm and 18.5 mm. Ring-shaped pads were held by friction forces and the matrix stop pressed from the inside by the rolls.



Figure 5.10 – Fabricated matrix with a channel diameter of 18.5 mm

### 5.3.2 Modernization of the engine control system of the mill

Initially, the engines of RSR mill were run individually by circuit breakers. The engines were set to the factory parameters of 100 rpm and did not provide for the possibility of regulating the speed of rotation or smooth start-up, or measurements. It is also important to note that the factory control system does not provide a reverse mode, which is critically necessary for experiments on the measurement of power parameters and debugging of the combined process, since

the testing and testing of modes will periodically arise situations of jamming the bar in the rolls or matrix (for example, in case of exceeding the maximum allowable compression) which is most optimally solved by reversing the rolls, avoiding the analysis of the mill.

Currently, the existing technical solution of the control system is considered outdated and all modern industrial and especially laboratory mills are equipped with a motor control system based on the use of frequency converters in conjunction with built-in or external programmable controllers.

World practice shows that frequency converters make it possible to: smooth start without starting currents and shocks and stop the motor, as well as the reversibility of its direction of rotation; full electrical protection of the motor from overcurrent, phase breakage and leakage to the ground, overheating; smooth control of the speed of the motor shaft from almost zero to the value of the permissible motor in previously unregulated technological processes; the formation of closed systems with the ability to accurately maintain the established technological parameters; simultaneous control of several electric motors from one frequency converter; reduction of power consumption due to optimal control of the electric motor depending on the load; increase the durability of the electric drive and equipment.

So, drawing a conclusion from the above, we can conclude on the feasibility of using as an electric drive win-tov rolling mills individual drive using frequency-controlled asynchronous squirrel-cage motors, which allows in addition to flexible regulation of the technological parameters of the rolling process, the removal and recording of torque data on the motor shaft to solve the problem of energy saving.

To modernize the control system, a series of frequency converters of the VFD-E series was selected (figure 5.11) created by Delta Electronics (China) on the basis of a new, innovative VFD-E platform developed by Delta using all-encompassing computer simulation technologies.



Figure 5.11 – DELTA frequency converters

The drives of the VFD-E Delta Electronics series are characterized by an optimal modular design with a programmable graphic display, improved thermal design, completely isolating the main cooling system from the electronics, the presence of an integrated radio frequency filter and a choke in the DC link. VFD-E series actuators are well adapted to severe environmental conditions and comply with the European electromagnetic compatibility standard EM61800-3.

The design of the drive provides for flange mounting in a special opening of the cabinet, when the hot elements of the drive are generally taken out of its limits. The "hot" part of the drive is located behind the first flange, so it is possible to carry it out of the cabinet and complete isolation from the cold [106].

It is worth noting, the coating composition, which provides dust and moisture protection boards and contacts. Delta drives of VFD-E series have small overall dimensions and significantly smaller drives of competitors in almost all cases.

Converters of this series is one of the simplest and most inexpensive in the line, implementing a simple scalar control of the engine V/F. However, VFD-E allows the implementation of sensorless vector control with the function of auto-tuning to the engine parameters, characteristic of the most expensive and advanced "flagship" series [106].

This system allows for speed control in the range of 10-200 rpm, which is sufficient for experimental studies on the mill.

To simplify the control and management of the mill, removal and recording of engine parameters, the use of frequency converters allows you to design a SCADA-system of almost any complexity.

The simplest SCADA system (figure 5.12) for the rolling process is a tool for monitoring the energy-power parameters of the process in real time. The use of this system will significantly reduce the time of determining the values of energy-power parameters. Also, there is the possibility of collecting and archiving of data and their subsequent analysis.

Rolling power is determined by the product of the power consumed by the electric motor on the efficiency of the installation, which is usually equal to 0.83—0.92:

$$N = N_{ENG} \cdot \eta \quad . \quad (5.1)$$

The power consumed by the electric motor is determined by the frequency converter and transmitted to the controller where the rolling power is calculated. The resulting rolling power is displayed on the operator panel.



Figure 5.12 – Block diagram of a SCADA system

The rolling moment can be determined based on the rolling power and the number of rotations per minute:

$$M = \frac{N}{\omega} = \frac{60N}{2\pi n}, \quad (5.2)$$

where  $N$  – rolling power,  
 $\omega$  - angular velocity (rad/s),  
 $n$  – number of rotations per minute (rpm).

When adjusting the speed of the motor using a frequency converter, the value of the speed of rotation of the rolls will deviate from the nominal. The calculation of the speed values will be made depending on the specified frequency of the converter:

$$\omega = 2\pi f, \quad (5.3)$$

where  $f$  – frequency specified by the converter.

The use of additional equipment in the rolling process, and in particular in the control system of electric drives, will allow to obtain not only the calculated data of power parameters, but also to remove their actual values. The introduction of a speed sensor will allow to obtain the actual value of the speed and the actual torque of the engine. In this case, the speed value determined by the sensor is transmitted to the controller, then this value is processed taking into account the gear ratio of the entire installation and the real speed of rotation of the rolls is calculated.

SCADA-system also allows you to build graphs of changes in the parameters of interest, which greatly increases the visibility and simplifies the control of the process. The window displaying graphs of process parameters changes is shown in figure 5.13.

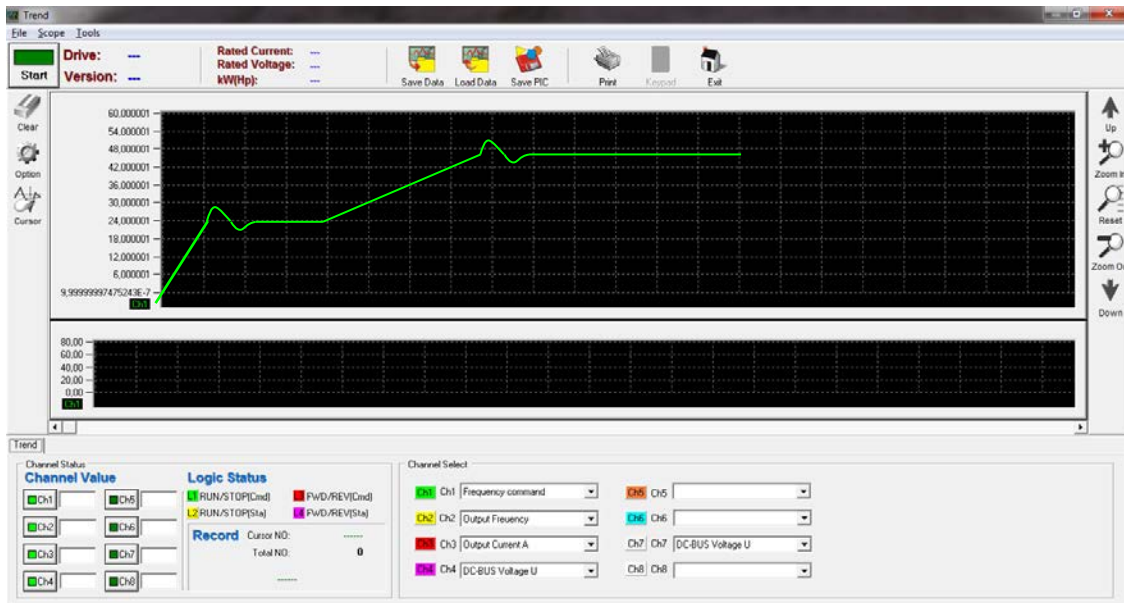


Figure 5.13 – Window displaying graphs of parameters changes

The SCADA system can be adapted for automated process control. The values of the main parameters obtained from the measuring sensors are processed by the system. Next, the system selects the optimal values of the speed or torque parameters (vector control) of the electric motors, and adjusts the speed of rotation of the rolls or torque. This will optimize the energy consumption of the process and improve product quality.

Thus, the requirements were formulated and the characteristics of the new mill control cabinet were derived, providing flexible modern control of the combined process, tracking process parameters in real time, in the most visual form.

The cabinet set includes:

1) frequency converter vector type VFD-E with built-in PLC power 7.5 kW – 3 PCs. output frequency of the Converter - 0.1-600 Hz, starting torque – 150 % at 3.0 Hz, rated current – 18 A, overload capacity – 150 % of the rated current for 1 min, transmission frequency – three zones, with a range of 0.1-400 Hz, acceleration/deceleration time 0.1-600 C., operating temperature -10°C...+50°C (without condensate and frost).

2) DOP-B03S211 operator panel with 4.1” screen diagonal. Touch panel, high resolution. Supports RS-232/485/422 interfaces, USB Hub port allowing to connect various peripherals (USB flash drive, printer, mouse and keyboard) to the panel, USB Client port for fast program loading.

- 3) power supply with 1-phase voltage. Input voltage range - 85-264 VAC, output voltage - 24 VDC, output current – 1A, power – 24W.
- 4) the electromagnetic contactor 7,5 kW – 2 PCs. Rated current is 18A.
- 5) Intermediate relays included in the control circuits. Mounting type – DIN rail, coil voltage – 220V AC, load – 5A AC 250V/DC 28V, led power indicator.
- 6) Switches, control buttons, forming the control Board.

The control cabinet with the specified parameters, including operator panel programming and connection architecture was ordered, manufactured and installed on the mill. The mounted cabinet is shown in figure 5.14.

Motor control from the operator panel is provided as a separate and group. The operator panel shows in real time the speed of rotation of the rolls set by the operator, the real speed of rotation of the rolls and the calculated torque on the shaft of each engine. The speed can be set both from the operator panel in touch mode and by rotating the analog controller on the cabinet. The control system provides for the reverse mode, which is critically necessary for the experiments, and is not available in the factory control system.

After assembly and adjustment, the combined unit was started and a trial rolling of several bars with a diameter of 17 mm was carried out. Experimental unit at the time of the experiment and the under-rolled press residue is shown in figure 5.15.



Figure 5.14 – RSP mill control cabinet



Figure 5.15 – Stand of the combined process "screw rolling-pressing" at the time of commissioning and under-rolled billet

An important advantage of the new system is also the implementation of the missing function of the reverse of the engines and switching group and individual control, which is very important when testing and testing the limit modes of rolling and combining the process. In addition, the new system due to the implementation of smooth start and some other improvements significantly increases energy efficiency.

## 6 THEORETICAL STUDY OF ENERGY-POWER PARAMETERS OF A NEW COMBINED PROCESS WITH THE AIM OF DETERMINING THE OPTIMAL GEOMETRICAL AND TECHNOLOGICAL PARAMETERS ON THE BASIS OF MATHEMATICAL MODELING

Power parameters of processes are the basic input data for the design of technological machines and equipment. The theoretical justification of the combined processes should include finding the conditions of combination, ensuring the balance of power parameters. Theoretical solutions are known for the implementation of different variants of the combined process "rolling-pressing" from the works [82-83, 90].

Since the workpiece will be pushed through the matrix due to the action of the active friction forces created by the rolls, in order for the process of "screw rolling-pressing" to be feasible, it is necessary, the sum of the projections of forces created by the rolls in the deformation center on the X axis (we denote  $P_{ROLL}$ ), there was more pressing force  $P_{PRESS}$ , necessary to push the workpiece through all the channels of the matrix and more backing force, created by the matrix in the implementation of the process "screw rolling-pressing" [90]. This is schematically shown in figure 6.1. In the future, to indicate the axial force of the screw rolling, we will use  $P$  instead of  $P_{ROLL}$ .

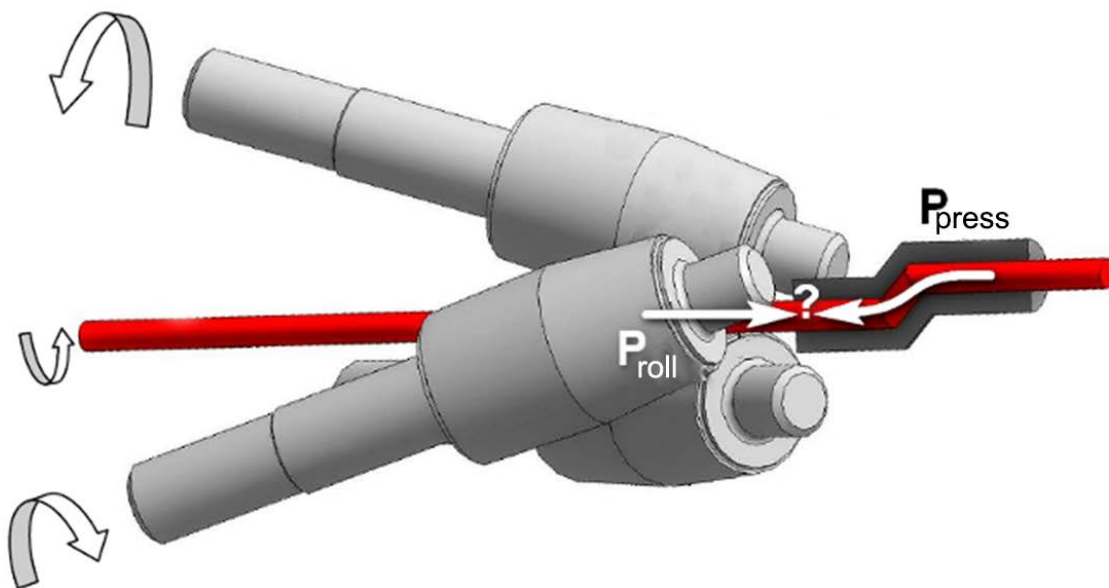


Figure 6.1 – Scheme of the combined process "screw rolling-pressing»

To determine these parameters, it was decided to conduct a theoretical study by computer simulation by the finite element method (FEM). This method has been described in more detail in Chapter 2. Based on the geometry of the most successful model of the previous research cycle, a number of new models with matrices with a diameter of 17 mm and 18.5 mm and roll speeds of 50 rpm, 100 rpm (nominal) and 150 rpm for each diameter were created. The initial blank was a rod with a diameter of 23 mm and a length of 150 mm for models with a matrix channel diameter of 18.5 mm and a rod with a diameter of 21.5 mm at a length of

150 mm for models with a matrix channel diameter of 17 mm. These values of the workpiece diameters were selected as providing the maximum compression of the workpiece before entering the matrix.

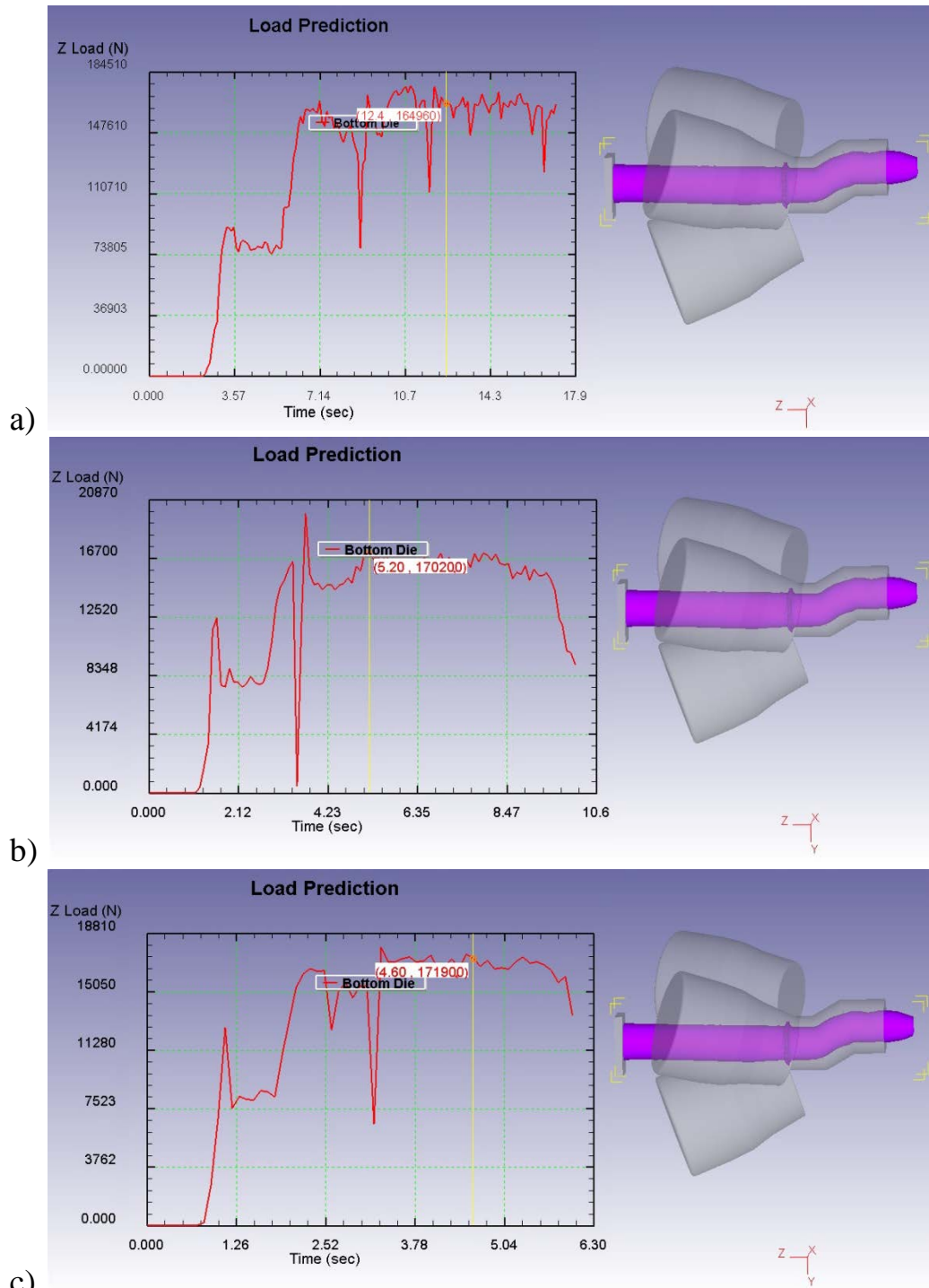
Thus, a total of 6 models were made. The models differed only in the parameters listed above. The other parameters were the same. Steel 15 was chosen as the material of the model. The size of the rolls and their structural location in conformity with the design of the laboratory RSR rolling mill. To avoid jamming of the workpiece at the inlet to the matrix, a small reduction in the diameter of the workpiece at the inlet to the matrix by 0.5 mm – 16.5 mm for the matrix with a channel diameter of 17 mm and 18 mm for the matrix with a channel diameter of 18.5 mm, respectively.

The angle of the junction of the channel matrices corresponds to a particular previously the optimum value is 150 degrees. The temperature of the workpiece was taken 1000 °C, as the average value of the recommended temperature range of hot treatment of steel 15 [105], all the tools in the model had a temperature of 20° C. Number of finite elements in the workpiece was 100 000.

From the work [107-109] it is known that the axial force during screw rolling is an extremely unsteady value that changes its value within a wide range. Therefore, it was assumed that in this combined process, textured rolls with a notch will be used to facilitate capture, rolling and subsequent pressing. As a result, the coefficient of friction at the contact of the workpiece with the rolls was taken to be 0.8, as recommended by the program for a tool with a rough surface. The coefficient of friction at the contact of the workpiece with the matrix was taken to be 0.3, as corresponding to the polished surface.

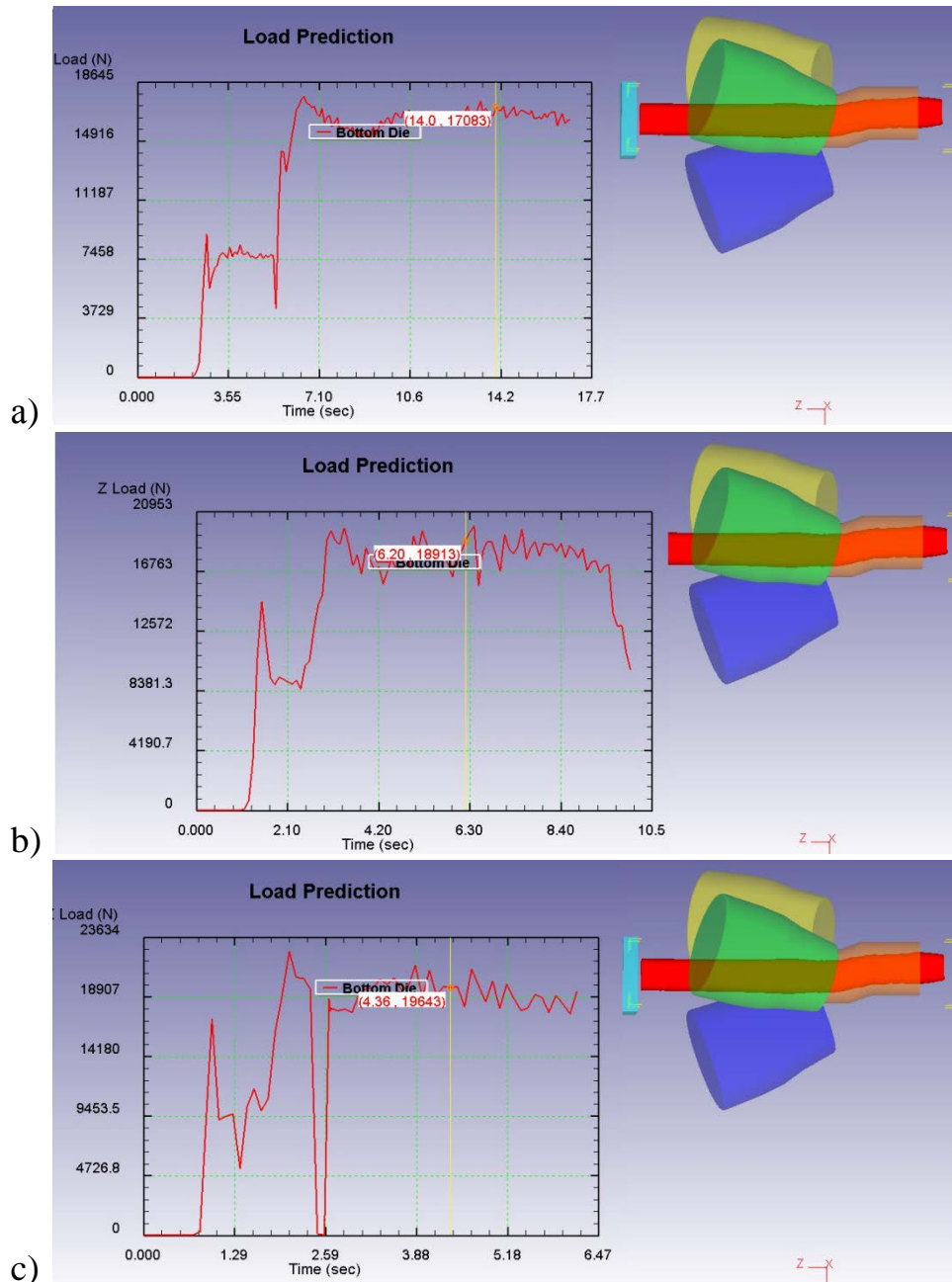
According to the simulation results, for each model were plotted axial force (z - axis on the model) on the matrix, numerically equal to the pressing force of the  $P_{PRESS}$ . All models were successful and the blank came out of the matrix. At the same time, on the workpiece with a diameter of 18.5 mm, a small Burr was formed before entering the matrix. This defect should not be considered critical, since its formation within small limits was predicted by detailed models describing the forming of the workpiece under different conditions and given in Chapter 2.

The models themselves are shown in figures 6.2-6.3 when the simulation is stopped with graphs of the axial force along the Z axis. All graphs have a characteristic step form, where the first stage corresponds to the passage of the workpiece in the first channel of the matrix, followed by an increase in the effort of 2 times the established process.



a) rolling speed 50 rpm; b) rolling speed 100 rpm; c) rolling speed 150 rpm  
 Figure 6.2 – Models with a 17 mm channel diameter matrix

It is also worth noting that all of the graphs except graph 6.2 (a) have an unstable distribution of effort. This is due to the modeling error caused by the discrepancy between the specified strain rate (per modeling step) and the size of the finite elements in the contact zone of the workpiece and the tool. In order to avoid contact loss, it is necessary that in one step of the modeling the workpiece passes a distance equal to no more than  $\frac{1}{2}$  of the length of the face of the finite element, which when changing the deformation rate and the constant number of finite elements can not be fully realized.



a) rolling speed 50 rpm; b) rolling speed 100 rpm; c) rolling speed 150 rpm  
 Figure 6.3 – Models with a 18,5 mm channel diameter matrix

If we trace the dependence of the force on the rolling speed, it becomes noticeable a small (0.5-1%) increase in the force with the speed. A summary graph of modeling efforts is shown in figure 6.4. In general, an increase in the strain rate leads to an increase in the resistance of metals to deformation, which is explained by a sharp increase in the rate of movement of dislocations, causing, in turn, an increase in the resistance of the crystal lattice to this movement.

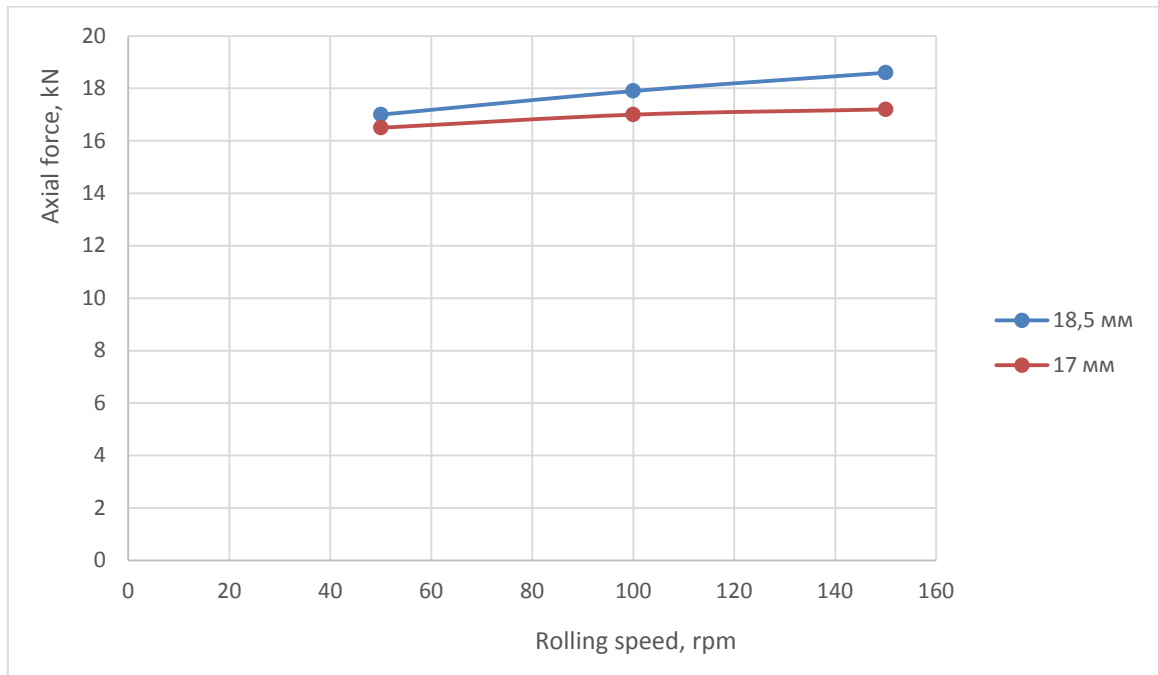


Figure 6.4 – Consolidated graph of efforts on modeling

The nature of the deformation force curves shown in figure 6.4 allows us to draw the following conclusions:

- as the workpiece diameter increases, the total force value increases. This is due to the fact that as the diameter increases, the cross-sectional area of the workpiece increases, which leads to an increase in the effort required to push the workpiece through the inclined channel of the matrix;

- with an increase in the rate of deformation, the deformation force increases, but with an increase in the diameter of the workpiece, the intensity of the increase in the force increases, which is a consequence of the two dependencies of the deformation force on the speed and on the diameter of the workpiece described above.

In terms of the known instability of helical rolling process and the adopted modeling assumptions used to derive the optimal steady-state modes of the combined process requires experimental study of axial force reserve real rolling and its comparison with stress at ECA-pressing in the matrix with desired characteristics.

## 7 EXPERIMENTAL INVESTIGATION OF ENERGY-POWER PARAMETERS OF COMBINED PROCESS "SCREW ROLLING – ECA-PRESSING»

### 7.1 Design of the experiment concept

As can be seen from the previous paragraph, the task of developing a combination of rolling and pressing is localized around finding the conditions of the predominance of the active forces of the friction arising on the contact surface of metal with the rotating rollers over the forces of friction and resistance force of deformation occurring during the pressing in the matrix, like the one used in the already mentioned works [82-83, 90]. Following the logic of work [90], it is necessary to find the axial projection of the rolling force and the pressing force and the support in the matrix at different stages of the process and combine their schedules to find the optimum. Measure the maximum axial force, which, in fact, is a reserve of friction forces on the rolls, with screw rolling, it is possible to place the force sensor on the way out of the rolls of the bar, where the matrix is shown in figure 6.1.

Here it should be noted three key features of the process "screw rolling-pressing»:

- 1) In terms of pressing we have no theoretical description of the new process ECA-pressing with torsion, characterized by increased complexity;
- 2) Theoretical apparatus describing the screw rolling is very complex and ambiguous;
- 3) it is known that the process of screw rolling in three-roll stands is unstable and has high dynamic loads [107-109].

These reasons are extremely complicated theoretical description of the process like [82], and the last argument in general calls into question the feasibility of a purely theoretical solution, because the solution found may be inoperable or unstable in practice. You require a more unique solution that allows you to build a stable working combined installation for comprehensive studies of the process.

On the basis of these considerations, the most rational way to develop a combined process seems to be a combination of computer modeling by finite element method with experimental measurement of the axial component of the screw rolling force, and the identification of its distribution boundaries.

The finite element method (FEM) [104] is successfully used to solve complex problems of plastic metal processing, where the exact theoretical solution is difficult and well suited for such a case. Modeling of the ECA-pressing was carried out many times by different authors in different countries, which allows to build a part of the model containing deformation in the ECA matrix with a sufficient degree of reliability, based on the known experience summarized in paragraph 5.2.

Modeling of screw rolling is less studied and more ambiguous [110], that is why it was decided to verify the resulting axial force by real measurements and to identify the boundaries in which it is possible to build a stable process. It is

important to know not only the features of the formation and flow of the metal, as in many such cases, namely the exact power parameters. It should be noted that direct measurements of the maximum axial force for the case of screw rolling of a continuous profile were not carried out. Known only to measure the axial forces on the mandrel when the firmware of the workpiece in a tube similar to [107]. In fact, the measured parameter will correspond to the reserve of friction forces on the rolls. A sufficient value of the reserve of the real axial force will allow the use of matrices with large angles, providing a better study of the structure of the metal.

It can be concluded that the key factor for the construction of the combined process will be the maximum axial force developed by the rolls of the screw mill. From its value will depend on the parameters and configuration of the ECA matrix in the design of the combined stand.

The objectives of this chapter will be the experimental measurement of the axial force arising from the three-roll screw rolling of a continuous profile, the study of its distribution and the construction of an adequate finite element model of screw rolling for use in the construction and improvement of the combined process model in the next chapter. Experimental measurements will give an unambiguous answer to the question about the possibility of building a combined process. In case of a positive answer, the axial force reserve of the screw rolling will be known, which should be used in the design of the combined stand.

The goals are achieved by solving the following tasks: setting the experiment, design and manufacture of measuring equipment, conducting the experiment and processing its results, construction and verification of the finite element model of screw rolling.

## 7.2 Method of measurement of axial force of screw rolling

Rolling force, the axial projection of which is required to find proportional to the contact area of the metal with the rolls. The contact area depends geometrically on the diameter of the  $D_v$  rolls, the initial diameter of the bar  $D_0$  and the final diameter of the bar  $D_1$ . Instead of the last value in practice often use the concept of relative compression  $\varepsilon$ , expressed in terms of the ratio  $1-D_1/D_0$ , %.

To obtain the required data on the maximum axial force, it was decided to conduct an experiment on two different screw rolling mills with different diameters of rolls  $D_v$ , in several series of 4 experiments each. Each mill used two influencing factors – the ratio of the roll diameter ( $D_v$ ) to the workpiece diameter ( $D_0$ ), and the relative compression diameter  $\varepsilon$ , %, respectively, using different values of the combination of factors for each series. This formulation will allow the accumulation of statistical material to estimate the maximum axial force throughout the mill range. In addition, the use as a factor of the relative index ( $D_v / D_0$ ) makes it possible to combine with the data of such an experiment on the second mill and will further expand the database of experimental data due to experiments on other mills with the same type of calibration and adjustment of rolls.

Half of the experiment was conducted at the MISIS RSP mill (Russia). This mill was chosen as the main one for the implementation of the combined process, as it is specially designed to form the required structure of the bar after rolling [64-65]. Initial profiles with diameters of 16 mm, 20 mm and 25 mm were chosen for the experiment on this mill as the most typical for the mill assortment. The ratio of the diameter of the rolls (71 mm) to the diameter of the workpiece ( $D_v / D_0$ ), as well as the initial ( $D_0$ ) and final dimensions ( $D_1$ ) bars on a series of experiments on this mill are shown in table 7.1.

Table 7.1 – Values of the factor for a series of experiments for the mill RSR 10-30

Series of experiments	$D_v / D_0$	$D_0$ , mm	$D_1$ , mm	$\varepsilon$ , %	Amount of experience
I	2,8	25	23,5	6 %	4
Ia	2,8	25	21	16 %	4
II	3,6	20	18,8	6 %	4
IIa	3,6	20	16,8	16 %	4
III	4,4	16	15	6 %	4
IIIa	4,4	16	13,6	16 %	4

For the second part of the experiment, an experimental pilot industrial universal screw rolling mill in a three-roll configuration was selected, created in 2013 with the support of the Regional Materials Science and Technology Centre for the industrial rolling laboratory Material & Metallurgical Research Ltd. (MMV), Ostrava (Czech Republic). The mill is designed with emphasis on physical modeling of seamless pipe production. However, on the mill, with minimal design changes can be carried out to measure the maximum axial force of the screw rolling solid profile. To do this, instead of the barrel mandrel, the rod is put on a massive metal stop.

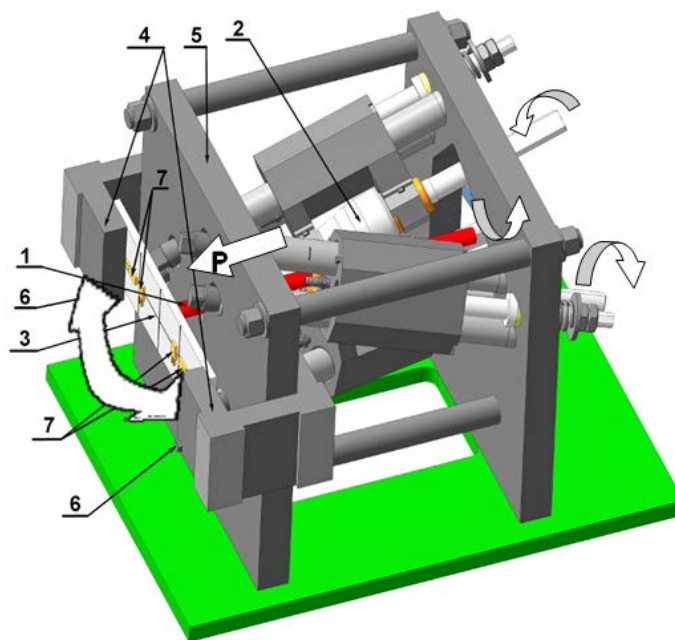
For the experiment, the initial profiles with diameters of 68 mm and 55 mm were chosen as the most typical for the mill assortment. The ratio of the diameter of the rolls (240 mm) to the diameter of the workpiece ( $D_v / D_0$ ), as well as the initial ( $D_0$ ) and final dimensions ( $D_1$ ) bars on a series of experiments on this mill are shown in table 2.2. The difference between the values of the factors of the first and second experiments is dictated by the technical features of the preparation of the experiment and the technological capabilities of the mills.

Relative compression ( $\varepsilon$ , %) for Ia and IIa cases is limited to 10% in diameter for fear of possible injury to the rolls and mill structure under greater load. Blanks for the experiment were round hot-rolled rods GOST 2590-88 300 mm long, with diameters, according to tables 7.1 and 7.2. St3 steel and its Czech analogue S355, as one of the most widespread structural materials in the world, was chosen as the material of billets. The heating temperature of the bars was determined at 1000 °C, and expressed the average value of the hot working temperature for this class of steels [105].

Table 7.2 – Factor values for series of experiments for MMV mill

Series of experiments	$D\sqrt{D_0}$	$D_0$ , mm	$D_I$ , mm	$\varepsilon$ , %	Amount of experience
I	3,5	68	64	5 %	4
Ia	3,5	68	61	10 %	4
II	4,3	55	52	5 %	4
IIa	4,3	55	49	10 %	4

The scheme of the experiment to measure the maximum axial force on the mill RSR 10-30 is shown in figure 7.1.



1 – rod; 2 – rolls; 3 – measuring plate; 4 – brackets; 5 – frame; 6 – mounting bolts; 7 – strain gauges; P – axial force.

Figure 7.1 – Scheme of measurements of the maximum axial force

The method of the experiment is as follows. Rods for experiments, 300 mm long, with diameters, according to table 7.1, in batches of 2 pieces, are planted in a preheated to 1000 °C tubular furnace with an exposure of 16-30 minutes, depending on the cross section and the location of the blanks. Then, the bars are fed in turn into the rolls of the mill. During the rolling process, the rod (1), moving forward, rests against the measuring plate (3) with fixed edges and under the action of the axial force (P) elastically bends it. The deformation of the plate is perceived by the tensor resistors (7) glued to it and recorded by the strain station in the form of a force graph. The peak load value is entered in the results table. Thus, for the study of axial forces rolling in the general case of a planned total of 40 experiments.

### 7.3 Equipment and materials

As a basis for the development of a combined process "screw rolling-pressing" was chosen screw rolling mill RSR [61]. The first part of the experiment was carried out on the same mill.

The mill is designed for the production of bars of small sections of almost all metals and alloys. The diameters of the initial blanks and the resulting rolled products are set continuously. The mill produces bars in the range of diameters  $10\div 25$  mm from the blanks  $15\div 30$  mm, with tolerances on the size within 1% and the curvature of the bars is not more than 1 mm/m. the general view of the mill is shown in figure 7.2.

The mill was developed at the Department of technology and equipment of pipe production of the National research technological University "MISIS", Moscow. In total, since 1992 more than 30 mills of various modifications have been produced.

The operation of this mill proved the possibility of faultless deformation of a wide range of steels and alloys, including low-plastic and hard-to-deform steels.

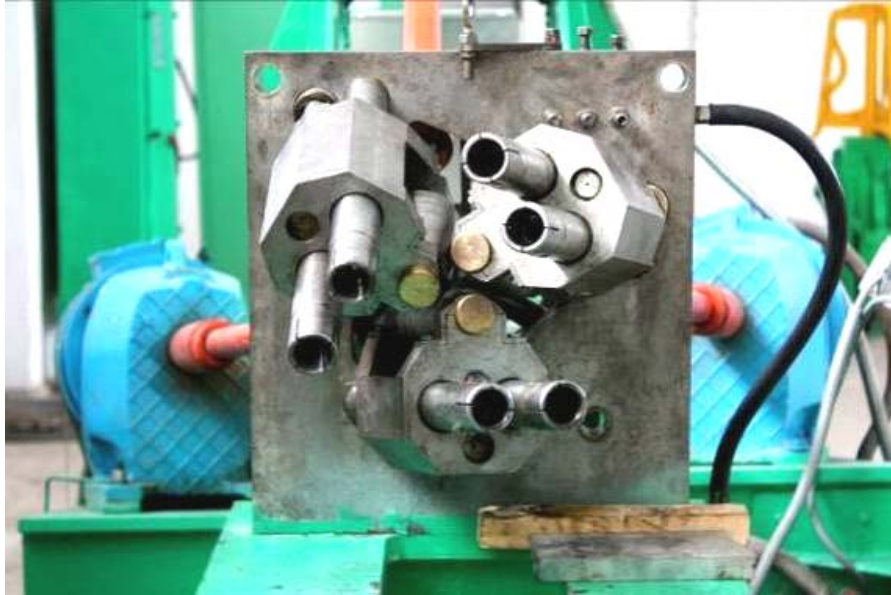
The advantages of the mill should include the fact that the input parameters are not subject to stringent requirements. Even in the case of unintentional deviations of the rolling temperature, the diameter of the initial billet and other input parameters, the high rigidity of the rolling stand allows to maintain a stable narrow tolerances on the size of the bars.

To the greatest extent the efficiency of the mill is manifested in the need for rapid production of small batches of high-precision rolled ferrous and non-ferrous metals.

The mini screw rolling mill consists of a monolithic welded frame mounted on I-beams. The working cage and three gear motors are located on the common frame, the gear motors rotate the working rolls by means of spindles.



a)

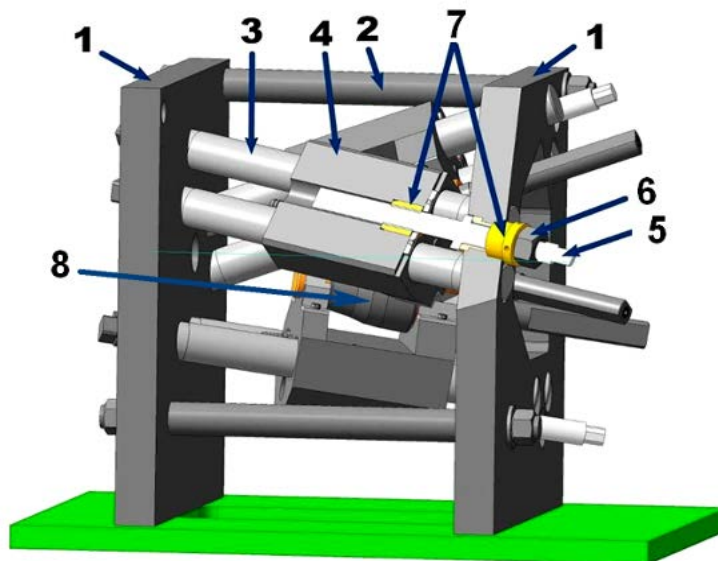


b)  
a) general view of the mill; b) front view with the removed front frame;

Figure 7.2 – RSR mill

The main feature of this mill is the design of the working stand, which provides high rigidity of the structure and completely unloaded from the rolling force of the non-pressing mechanisms for adjusting the position of the rolls. The cage is a closed-type frame consisting of two vertical steel plates connected by ties. Between the plates are rigidly fixed cylindrical guides at a certain angle to the axis of the rolling. Since the guides are parallel to the rolls, in fact, this angle is formed from the rolling angle ( $\approx 20^\circ$ ) and the feed angle ( $\approx 6^\circ$ ).

Rolls slidably mounted cassette, which is placed on the bearing supports of the rolls. To the bearing supports through special rubber tubes supplied grease (grease) from a syringe with a manual drive, mounted on the frame of the mill. The roll adjustment system in the section is shown in figure 7.3.



1 – frame; 2 – tie; 3 – guide; 4 – cassette; 5 – adjusting screw; 6 – lock nut; 7 – threaded bushings; 8 – roll.

Figure 7.3 – Regulatory system of the rolls of the RSR mill

The feed of blanks to the rolls is carried out through the inlet pipe, which provides a more accurate supply of blanks to the working area of the rolls. At the exit of the cage, a replaceable outlet pipe is installed, the inner diameter of which must correspond to the diameter of the manufactured rod. The diameter of the pipe is selected by a size not exceeding 5 mm of the diameter of the rolling. Taking into account the characteristics of the stand of such replaceable nozzles, there should be four with internal diameters not exceeding 5 mm of the rolling diameter [58].

For further measurements was chosen for the experimental-industrial piercing universal rolling mill, industrial rolling laboratory MATERIAL & METALLURGICAL RESEARCH Ltd. (MMV), Ostrava (Czech Republic). The mill is made of four large sections, providing the transformation of the mill into two-and three-roll configuration. Pressure mechanisms and roll adjustment control – hydraulic with electro-mechanical control. The angle of flow and angle of rolling of the rolls change within  $\pm 15^\circ$ . The mill is characterized by high basic automation and the presence of force sensors on all rolls and mandrel. Mill motors are controlled by frequency converters and controller with output of basic information on a large LCD touch screen. The mill is shown in figure 7.4.



Figure 7.4 – Experimental-industrial mill MMV

Also during the experiment the following equipment was used: tubular furnace Nabertherm R120/1000/13; strain station ZET-017-T8; force sensor with strain gauges TKFO1-2-200; laptop to control the strain station and record the signal.

Zet 017-T8 strain station manufactured by JSC "ETMS" is designed to measure power and other parameters through several channels with a time resolution of up to 20 kHz [111].

Connection of the load station to the computer is carried out via USB 2.0, Ethernet or Wi-Fi. Built-in load cell allows you to connect load cells without the

use of intermediate amplifiers. The sensors can be powered by alternating or direct current, or by battery.

The strain station provides: connection of strain gauges on the bridge, half-bridge and quarter-bridge circuits; connection of strain gauges on 6-wire, 4-wire and 2-wire circuits; power supply of the strain gauge can be carried out by constant or alternating voltage; calibration of the measuring channel is made individually or by a group of channels; conversion of signals from the strain gauge on the calibration tables; registration of all measuring channels on the built-in drive; display of the converted signals of the input channels depending on the time (mode loop oscilloscope); parametric display of Lissajous shape signals; spectral analysis of input signals; generation of signals of different shapes, amplitudes and frequencies.

As a sensitive elements of the measuring system of the force transducer used strain gages TKFO1-2-200, on the basis of constantan deposited on the phenolic substrate. Characteristics of this type of strain gages are given in table 7.3 [112]. The appearance of the strain gauges is shown in figure 7.5.

Table 7.3 – Characteristics of strain gauges TKFO1-2-200

Characteristic	Value
Substrate material	phenol
The material of the metal foil grid	constantan
The spread of resistance in the group, no more	$\pm 0,1$ Ohm
Sensitivity	2,0 ... 2,2
Tolerance	1 %
Maximum relative strain	2 (20 000 mil <sup>-1</sup> ), 5, 10 +-1000 mil
The minimum number of cycles of failure-free operation	107 cycles
Operating temperature range	-40 ... +90 °C
Insulation resistance, not less	1000 MOhm
Nominal resistance	200 Ohm
Base length	2 mm
Length without pins	6,2 mm
Width	3,4 mm
Thermocompensation	$5 \cdot 10^{-6} \text{ } ^\circ\text{C}^{-1}$ (ceramic-based composite material), $8,3 \cdot 10^{-6} \text{ } ^\circ\text{C}^{-1}$ (titanium), $12 \cdot 10^{-6} \text{ } ^\circ\text{C}^{-1}$ (steel), $16 \cdot 10^{-6} \text{ } ^\circ\text{C}^{-1}$ (stainless steel and copper-based alloys), $23 \cdot 10^{-6} \text{ } ^\circ\text{C}^{-1}$ (aluminum), $5 \cdot 10^{-6} \text{ } ^\circ\text{C}^{-1}$ (some types of plastic).

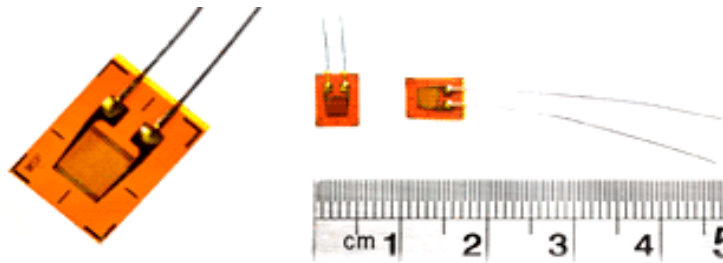


Figure 7.5 – Strain gauge TKFO1-2-200

#### 7.4 Design, manufacture and calibration of measuring equipment

Given the specificity of mill construction, not designed for firmware of the workpiece, and therefore obscure, in contrast to the known works, the application for measuring axial force ready-made solutions (serial load cells), it was decided to fabricate the force sensor for this case alone.

Structurally, the most convenient for use with this type of mill design scheme load cell beam type. This scheme also provides the greatest linearity of measurements, less dependence on the point of application of force [112], greater protection of strain gauges, both from temperature and mechanical damage, simplicity and ease of implementation. Sensors of this type are widely used in electronic scales: platform, conveyor, in dispensers, etc.

The plate of the force sensor with strain gauges is attached to the front (output) frame of the working stand of the mill with two clamps. Rolled rod with force  $P$  acts on the plate, bending it to a certain radius.

Strain gauges, glued to the plate is deformed along with it, changing the amount of electrical resistance. This change is recorded by the strain station, and, according to the results of the previous calibration of the sensor, is automatically converted into a graph of changes in the axial force.

The edges of the plate, realizing the beam scheme, are based on thick-walled brackets, which are connected to the front frame of the rolling mill by mounting bolts. The bolt is necessary for fixing and holding the bracket on the front frame and ensuring the free position of the sensor plate, which lies on the edges of the bolts. The latter is important because it eliminates the pinching of the free ends when bending the plate, thus accurately implementing the beam deformation scheme, as well as reproducing the conditions identical to the calibration. In addition, free standing sensor plates eliminates the operation of subtraction of the level of pre-tension, as when using load cells in stand pillows, what makes the measurement more accurate and convenient. Since there is a significant torque on the rod during screw rolling, therefore, to exclude the rotation of the plate under its action and its subsequent slip out of the brackets, the connection is insured by rings from the wire.

Material load cell was selected 5HV2S steel after quenching, as able to perceive significant elastic deformation. The dimensions of the plate were calculated with the condition of achieving deformation in the places of the sticker

of the strain gauges equal to the maximum permissible deformation of the selected strain gauges (2 %) at a force of 100 kN, which is more than 2.5 times higher than the expected peak force. The scheme of the sticker of joining the strain gauges on the load cell is shown below, in figure 7.6.

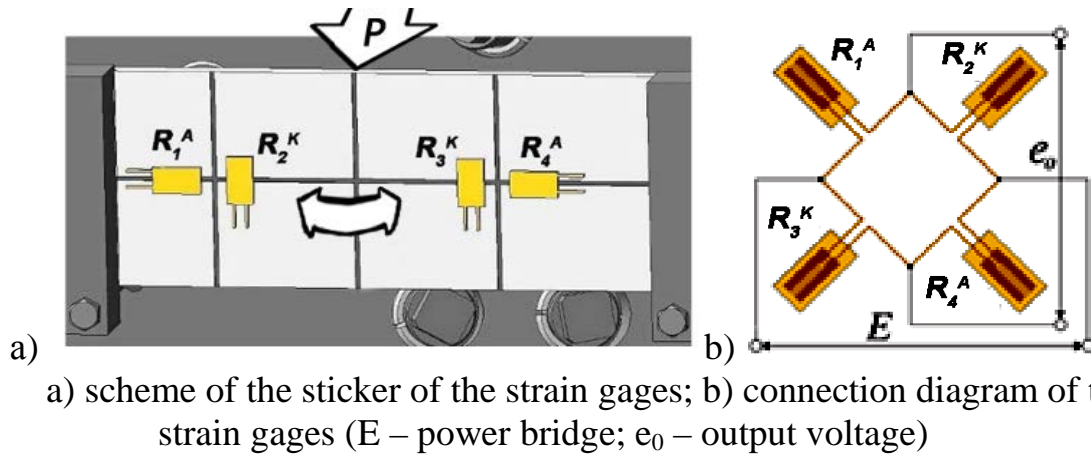


Figure 7.6 – Diagram of the label and connection of strain gauges on the load cell

The strain gauges TKFO1-2-200 are one-component quick-setting special adhesive Z70 (HBM, Germany), halfway between the center of the plate and places reliance. Measuring (active) strain gauges ( $R^A$ ) are glued along the plate, compensation ( $R^K$ ) – across, thus perceiving only temperature disturbances. When connected to the bridge circuit, the measuring ( $R^A$ ) and compensation ( $R^K$ ) elements alternate. This connection provides an increase in the sensitivity of the circuit, while protecting it from temperature interference [32-33]. The circuit is powered by a DC 5V from the strain station. The signal is recorded at a sampling rate of 1 kHz.

The strain gauge, in the form of a measuring plate, as a tool, was calibrated on a hydraulic torsional-breaking machine MI-40KU in compression testing mode, by a technique that minimizes the effect of hysteresis. The use of torsional-stretching machine allows to develop significant efforts (35-40 kN), with accurate and reliable fixation of their values. The change in the stress-strain state of the plate under load causes deformation and linear change in the resistance of the strain gauges glued to it. The essence of calibration is to build the dependence of the binding voltage in the circuit and the force applied to the plate. The relationship must be linear.

To carry out the calibration, the plate was loaded in series with a step of 5 kN in the range from zero to 35 kN. The corresponding voltage values were recorded in the circuit under load and after its removal. In order to reduce hysteresis and improve accuracy, 3 passes were made in the specified range – up, down, up, or 42 measurements. Immediately after manufacturing, the measuring plate was subjected to several test loadings to verify the operation of the measuring and recording systems and working out various situations. After that, calibration was carried out according to the scheme described above. In both cases, the graphs "force-displacement" were obtained ("displacement" corresponds to the value of the stroke

of the upper striker, that is, the deflection of the plate in the center). The graphs are shown in figure 7.7.

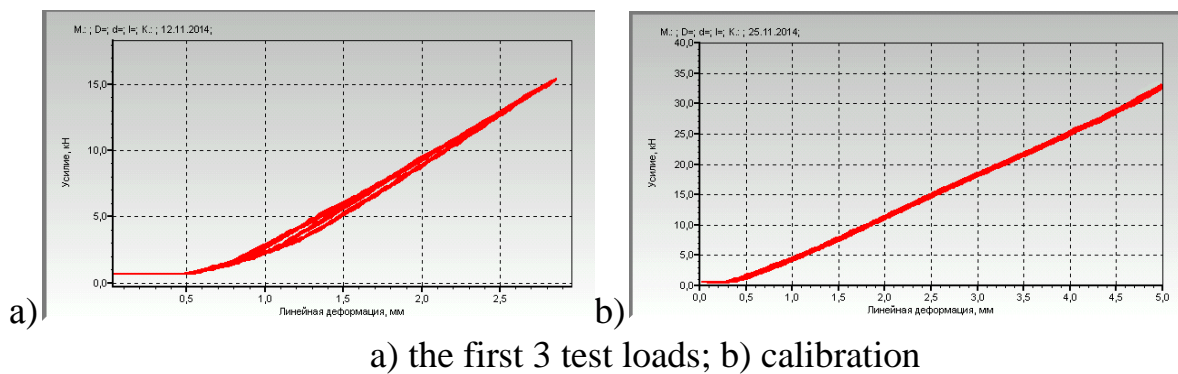


Figure 7.7 Graphics loading at the calibration

The first graph shows the phenomenon of hysteresis, the effect of which, after several loading cycles, is significantly reduced, making almost a linear chart during calibration.

Thus, we can talk about increasing the accuracy of the tool and the correctness of its calibration procedure. A small horizontal straight section at the beginning of the graphs corresponds to the idling of the upper striker.

The data obtained in the course of calibration tests were statistically processed, and a linear regression equation was obtained, which relates the applied force ( $P_i$ , N) to the voltage ( $U_i$ , mV) in the scheme. The equation has the form:  $P_i = U_i - 3631,2 + 10122$ . Determination coefficient  $R^2 = 0.99998$ ; standard measurement error related to the value of the working range of the instrument (50 kN) according to the results of 42 tests was less than 0.2%. The calibration graph is shown in figure 7.8.

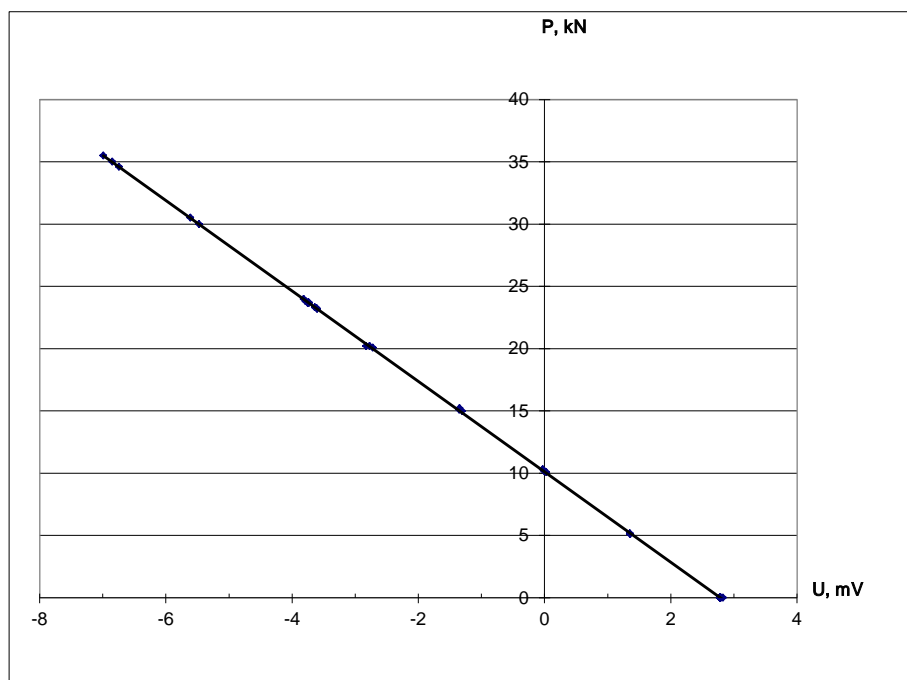


Figure 7.8 - Plot of the calibration

The data obtained were recorded in the program of registration and processing of measurements of the Zet-017-T8 strain station to provide the possibility of recording the signal in the form of a force graph. After the experiment, several random control loads were made, which confirmed the accuracy and stability of the load cell.

### 7.5 Experimental study of the maximum axial force of screw rolling

According to the adopted plan, an experiment was conducted on the RSR and MMV mills. All experiments were conducted normally. At the moment of the beginning of the rolls sliding, the mill engines synchronously stopped so that it was possible to remove the rod from the stand without disturbing the mill settings. A general view of the experimental facilities and the bars extracted after measurement is shown in figures 7.9 and 7.10.

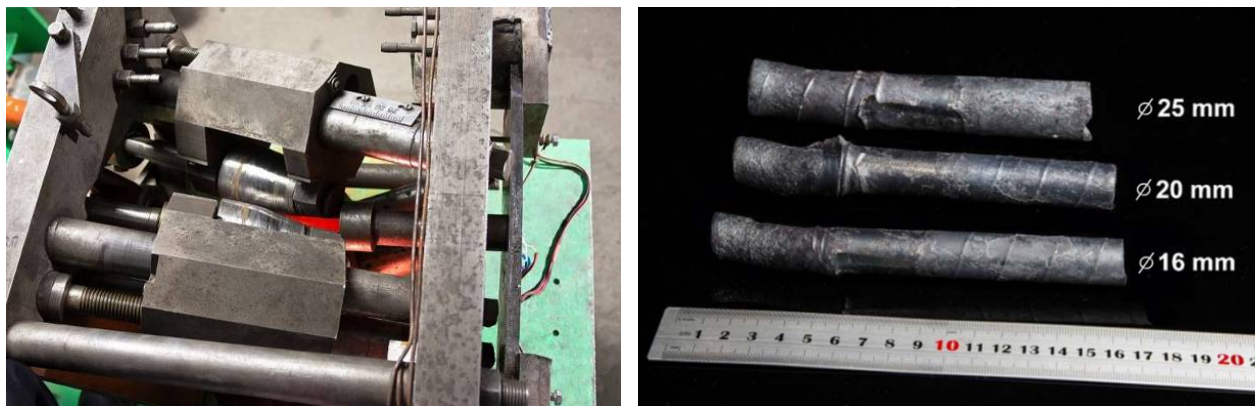


Figure 7.9 – Experiment on the RSP mill



Figure 7.10 – Experiment on the MMV mill

In figure 7.9, the bending of the measuring plate under the action of the axial force is clearly visible. In these figures on the right on the bar are visible prints rolls, characterizing the deformation.

The force graphs recorded by the strain station are generally similar and have the same characteristic areas. As an illustration of this, figure 7.11 shows the graphs of experiments II-3 and II-4 recorded by the strain station, as having the most characteristic graphs.

In the first section there is a sharp (during the order of 0.15 s), the increase in effort with some slowdown closer to the peak. At this stage, the plate is bent under the action of the axial movement of the bar and a small deformation of the front end of the bar. The shape of this section of the graph is approaching the parabola. Then there is a bend of the bar, accompanied by a drop in force by a third and a smooth alignment of the fall of the force associated, apparently with the beginning of the sliding rolls. At the same time, it is important to note that at the last stage, the rod rests not only on the plate, but also on part of the front frame, since, as a rule, at this stage it is strongly curved.

The moment of engine stop is clearly visible on the charts in the form of a short-term negative surge to the right of the peak. As shown by experiments, the time of a stop of engines, nor on the quality (shape and position of characteristic curve plots the effort) or quantitative (measured values) the pattern of change efforts almost no effect.





Figure 7.11 – Graphs of the experiments II-3 (a) and II-4 (b)

The results of each series of experiments were tested for gross errors by Student's t- criterion, then statistical characteristics were calculated for each series: arithmetic mean ( $P_{AM}$ ), maximum ( $P_{MAX}$ ) and minimum ( $P_{MIN}$ ) values, standard deviation ( $P_{SD}$ ). These characteristics are calculated according to the known statistical formulas [113] and are shown in tables 7.4-7.5. The values of the forces for all experiments are shown graphically in figure 7.12.

Table 7.4 – Statistical characteristics of experiments on the RSR mill

Statistical indicator	Series of experiments: $(D_v/D_0) / \varepsilon, \%$					
	2,8 / 16 %	2,8 / 6 %	3,6 / 16 %	3,6 / 6 %	4,4 / 16 %	4,4 / 6 %
$P_{AD}, N$	44,4	44,9	39,7	43,7	20,6	21,5
$P_{MAX}, N$	47,4	48,0	42,0	46,6	23,2	26,4
$P_{MIN}, N$	41,4	42,8	36,3	38,0	17,9	18,7
$P_{SD}, N$	2,5	2,3	2,4	3,9	2,5	3,4

Table 7.5 – Statistical characteristics of experiments on the MMV mil

Statistical indicator	Series of experiments: $(D_v/D_0) / \varepsilon, \%$			
	3,5 / 10 %	3,5 / 5 %	4,3 / 10 %	4,3 / 5 %
$P_{AD}, N$	96,0	68,2	77,6	50,8
$P_{MAX}, N$	101,5	74,7	88,9	53,0
$P_{MIN}, N$	83,6	59,2	66,2	45,5
$P_{SD}, N$	8,4	6,8	10,1	3,6

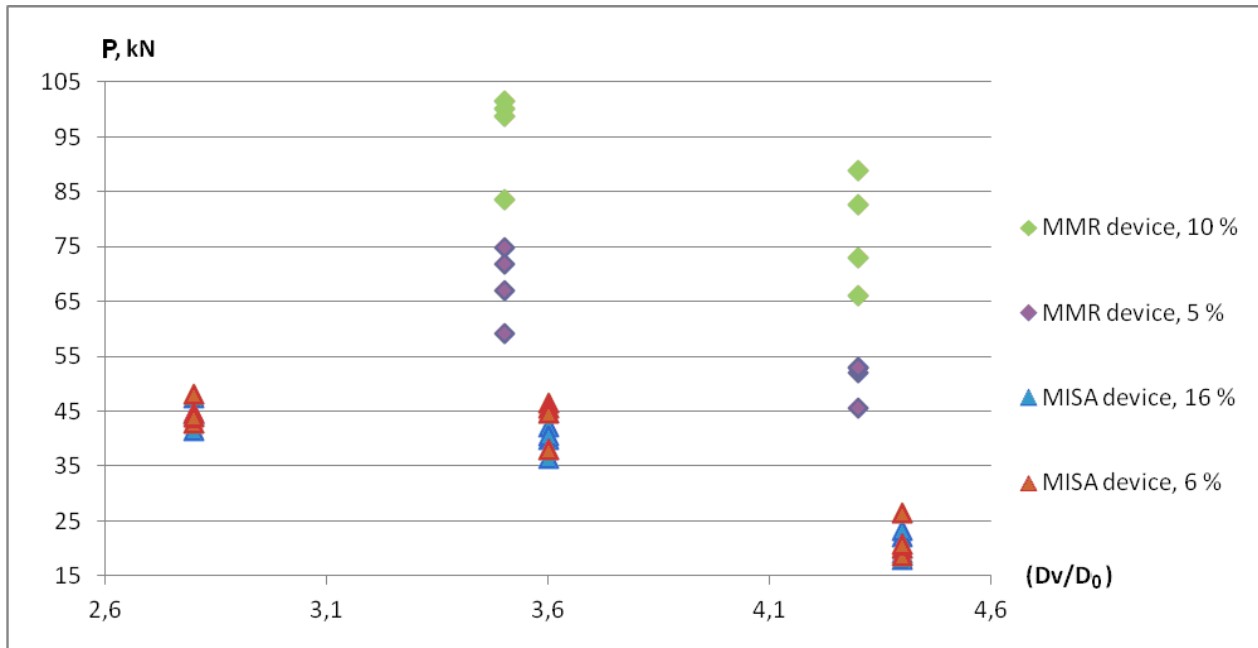


Figure 7.12 – Maximum axial force values

The obtained data of the maximum axial force for 40 experiments served to calculate the multiple regression equation. 3 factors were chosen to calculate the regression:  $X_1$  ( $\varepsilon$ , %);  $X_2$  ( $D_v/D_0$ );  $X_3$  ( $D_v$ , mm).

The parameters of the regression equation are calculated by the least squares method, solving a system of normal equations. Having solved, we obtain the following values of regression coefficients:  $a_0 = 68,786$ ;  $a_1 = 0,626$ ;  $a_2 = -16,271$ ;  $a_3 = 0,263$ . The regression equation looks like:

$$Y = 0,63X_1 - 16,27X_2 + 0,26X_3 + 68,79 \quad (7.1)$$

Then the coefficients of the equation are checked for significance and the elimination of insignificant coefficients. Check the average error of the parameter. The significance of the parameter is checked by comparing its value with the average error – the confidence coefficient  $t$  is determined. The obtained confidence factor  $t$  is compared with the Student's table criterion in absolute value.

To do this, first calculate the variance of the experiment by the formula:

$$S_{y\_calc}^2 = \frac{\sum_{i=1}^n (Y_{CALC} - Y_{AV})^2}{N} \quad (7.2)$$

where  $n$  – number of observations;

$Y_{CALC}$  – calculated value  $Y$ ;

$Y_{AV}$  – average value  $Y$ ;

$N$  – number of factors.

$$S_{y\_calc}^2 = \frac{\sum_{i=1}^{40} (Y_{CALC} - 50,74)^2}{3} = 5696,3.$$

RMS error:

$$S_{y_{CALC}} = \sqrt{S_{y_{CALC}}^2}. \quad (7.3)$$

$$S_{y_{CALC}} = \sqrt{5696} = 75,5.$$

Obtained the trust factor  $t$  compare with the table criterion  $t_{TABLE}=2,0244$  in absolute value. Regression coefficients must satisfy the condition:

$$t = \frac{a_i}{S_{y_{CALC}}} < t_{TABLE}. \quad (7.4)$$

Validation of the model adequacy is based on comparison of the calculated dispersion of the experiment with the residual dispersion. The dispersion of the experiment is found above. The residual dispersion is found by the formula:

$$S_{y_{RES}}^2 = \frac{\sum_{i=1}^n (Y_i - Y_{CALC})^2}{n - N - 1}, \quad (7.5)$$

$$S_{y_{RES}}^2 = \frac{4124}{40 - 3 - 1} = 114,6.$$

Checking for significance (prediction quality) is carried out according to Fisher's F-criterion by the formula:

$$F = S_{y_{CALC}}^2 / S_{y_{RES}}^2 < F_{(v_1; v_2; 10\%)}^{TABLE}, \quad (7.6)$$

where  $v_1 = N$ ;

$v_2 = n - N - 1$ ;

$N$  – number of influencing factors included in the equation,

$$F = 5696,3 / 114,6 = 49,72 > 2,8387_{(3; 36; 5\%)}^{TABLE}.$$

The regression was tested for adequacy. Now we will assess the quality of prediction of the regression obtained through the coefficient of determination. To do this, we find the final variance of the experiment:

$$S_y^2 = \frac{\sum_{i=1}^n (Y_i - Y_{AV})^2}{n - 1}, \quad (7.7)$$

$$S_y^2 = \frac{\sum_{i=1}^{40} (Y_i - 50,74)^2}{40 - 1} = 543,9.$$

The coefficient of determination:

$$R^2 = 1 - \frac{S_{y_{ocm}}^2}{S_y^2}. \quad (7.8)$$

$$R^2 = 1 - \frac{114,6}{543,9} = 0,79.$$

The obtained coefficient of determination indicates a good prediction quality of the model sufficient for its practical application. We construct the equation in decoded, final form, using natural notation of factors:

$$P = 0,63\varepsilon - 16,27(D_v/D_0) + 0,26D_v + 68,79. \quad (7.9)$$

Thus, the equation of dependence of the maximum axial force on the parameters of the mill and its settings is obtained. This equation can be used quite effectively in the general case. However, since it has already been decided to build an installation for a combined process on the basis of the RSR mill, it is more rational to use not the General equation, but the data of measurements of the optimal mode for combining obtained directly on this mill to clarify the parameters of combining. In addition, the boundaries of the distribution of the maximum axial force values are very important. Optimal for combining the rolling mode should provide maximum compression, providing a better preliminary study of the structure of the bar, so for further work, select the measurement data of the maximum axial force on the mill RSR at maximum compression  $\varepsilon = 16\%$ . The distribution graph of the measured values is shown in figure 7.13.

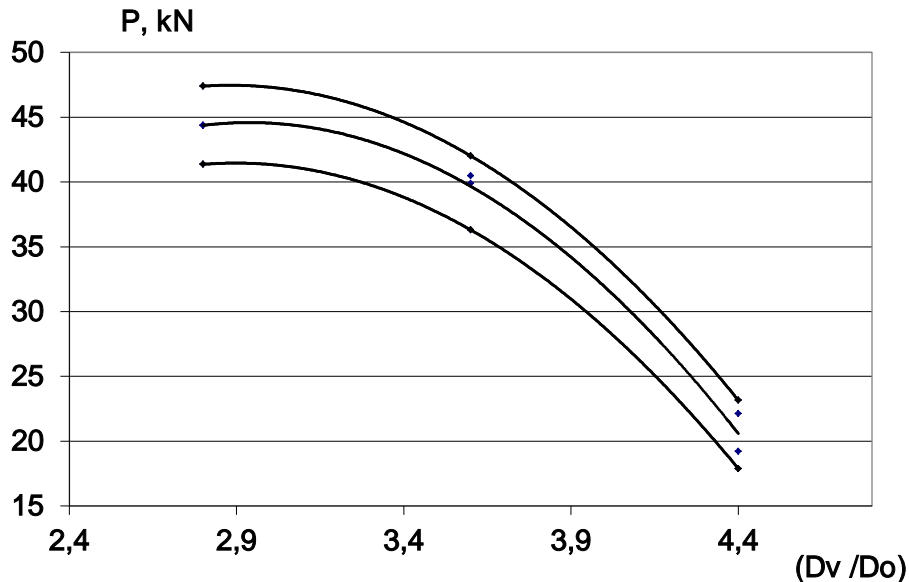


Figure 7.13 – Values of the maximum axial force for rolling the rod with compression  $\varepsilon = 16\%$  on the RSR mill

According to 12 measurements, a quadratic equation was obtained:

$$P = -11,22(D_v/D_0)^2 + 65,94(D_v/D_0) - 52,27. \quad (7.10)$$

This equation characterizes the dependence of the maximum axial force at cross-screw rolling on the ratio of the diameter of the rolls to the diameter of the workpiece at a constant compression  $\varepsilon = 16\%$  (shown by dotted line). The coefficient of determination was  $R^2 = 0,96$ , which indicates an excellent connection in the equation. The range of measured values was 5-6 kN with a slight expansion as the bars of larger diameter were used. This should probably be attributed to the increasing role of the following factors – the features of the internal and contact friction of the workpiece, its rheology, especially the calibration of the deforming tool.

The obtained equation guarantees the practical obtaining of the maximum axial force by the rod, not less than the calculated one and is suitable for the design of combined stand "screw rolling – ECA-pressing" on the basis of the RSR mill.

Further design of the combined process will be carried out by computer simulation by finite element method with correction of power parameters according to the obtained experimental values.

The results of the study, as containing information about the reserve of the axial force (friction forces) of the cross-screw rolling can also be used to optimize the process of flashing solid blanks into the sleeve.

## 7.6 The ability of rolling and pressing combination

The measured values of the axial force (up to 48 kN) indicate the principal possibility of a combined rolling-pressing process at large values of the junction angles of the channels of the ECA-matrix ( $140^\circ$ - $150^\circ$ ). This conclusion can be

made by comparing the measured values with the data of the ECA-pressing force of bars of similar sizes obtained in the works on the theoretical basis of the combined process "rolling-pressing" [82], as well as in the work [114], describing the process of ECA-pressing with torsion and the device for its implementation. From different sources [6, 53, 114] it is known that the introduction of the torsion element reduces the total pressing force. In particular, in the mentioned work [114], the influence of torsion on the power parameters of ECA-pressing is analyzed, the authors prove the reduction of force up to 3-5 times.

Based on these considerations, it seems reasonable to preliminary analysis of the parameters of the combination by comparing the experimentally obtained graph of the force at the screw rolling and the graphs of the pressing force of the ECA without taking into account the friction forces. The increase in force due to the activation of friction forces should be approximately equivalent to the reduction of force due to torsion.

The ECA-pressing force was determined by computer simulation by the finite element method (FEM). More details about this method and its features will be discussed in the next chapter. ECA-pressing is a well-studied process for which computer modeling has been repeatedly carried out, so the adequacy of the results and the feasibility of this method is not in doubt. To determine the ECA-pressing force in the DEFORM-3D software package, 6 models were built, the main parameters of which were agreed with the parameters of the screw rolling used in the experiment to measure the axial force. Model parameters are shown in table 7.6.

The remaining parameters were taken the same for all models and also consistent with the parameters of the screw rolling used in the experiment to measure the axial force. Material – steel AISI-1015 (a close analogue of the steel 3 used in the experiment); temperature 1000 ° C, the pressing speed corresponds to the axial rolling speed for each bar size. Several models with pressing force graphs are shown in figure 7.14.

Table 7.6 – Parameters of ECAP modeling

№	$(D_v / D_0) /$ diameter of workpiece $d$ , mm	Channel junction angle, $\Phi$ , deg
1	4,4 / 15	150°
2	3,6 / 20	150°
3	2,8 / 25	150°
4	4,4 / 15	135°
5	3,6 / 20	135°
6	2,8 / 25	135°

Obtained by modeling the data was presented in charts the efforts of ECA-pressing  $P_{PRESS}$  in matrices with different angles of intersection of the channels  $\Phi$ , superimposed on the previously obtained experimental graph of axial forces rolling  $P_{ROLL}$ . The graphs are shown in figure 4.15.

The curves in figure show that the most preferred for the construction of the combined process appears to be using as the base not the small diameters gauge

screw mill ( $(D_v/ D_0) = 4,4$ ;  $d = 15$  mm), as previously assumed, and average in the field  $(D_v/ D_0) = 3,6-3,8$ , which corresponds to the diameter of the molded rod from 17-19 mm. At the same time, the angle of the junction of the channels of the ECA matrix must be greater than  $135^\circ$ .

According to preliminary data, a stable combined process with parameters  $d = 18$  mm,  $\Phi = 150^\circ$  is expected. Since the graph of the ECA- pressing force was built with large assumptions, it gives only general information that determines the area of search for the optimal solution. Now we need to build a number of the most refined computer models of the combined process in this area and choose among them the best as a prototype for the manufacture of an experimental setup.

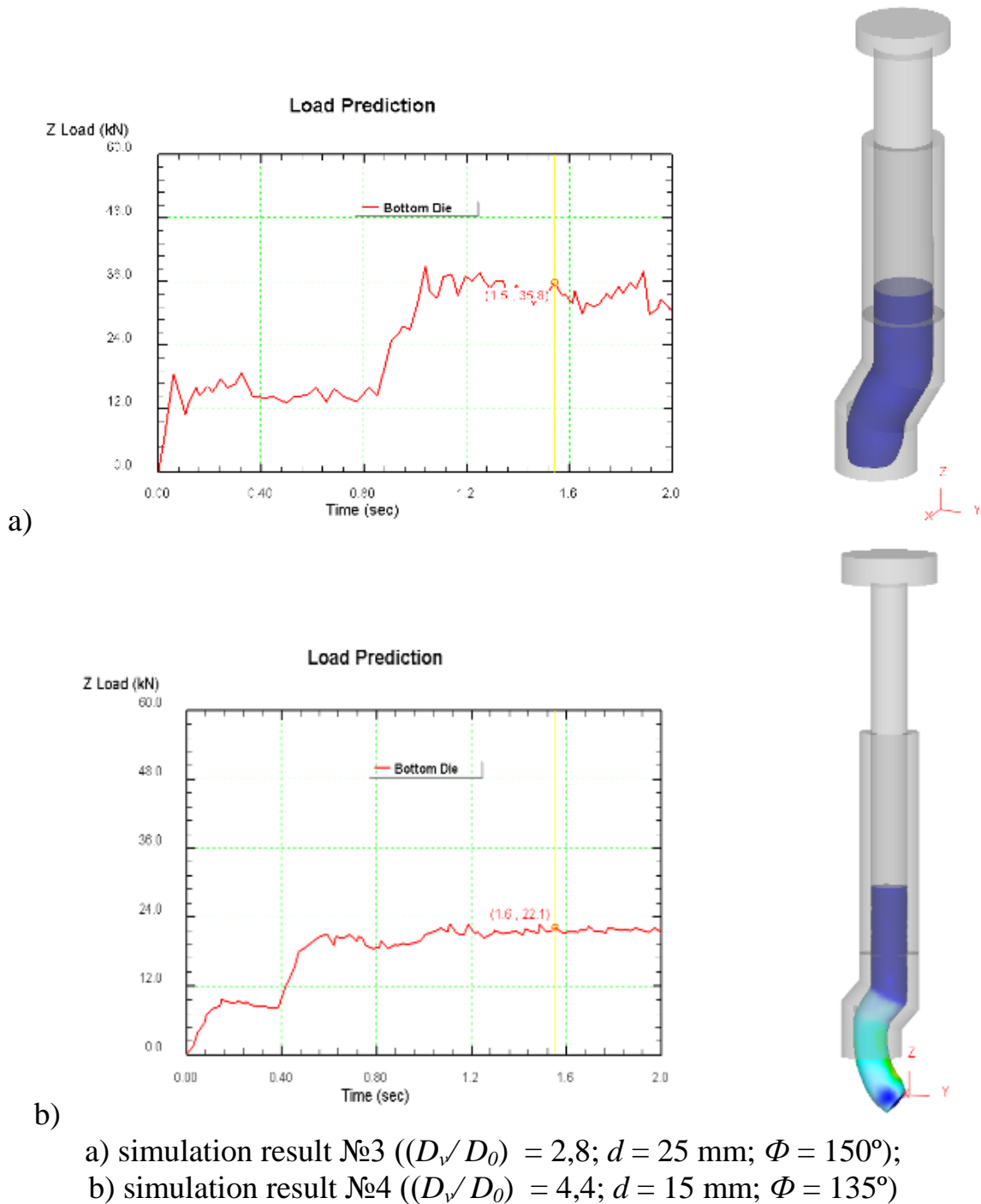


Figure 7.14 – Screenshots of the simulation results of ECA-pressing

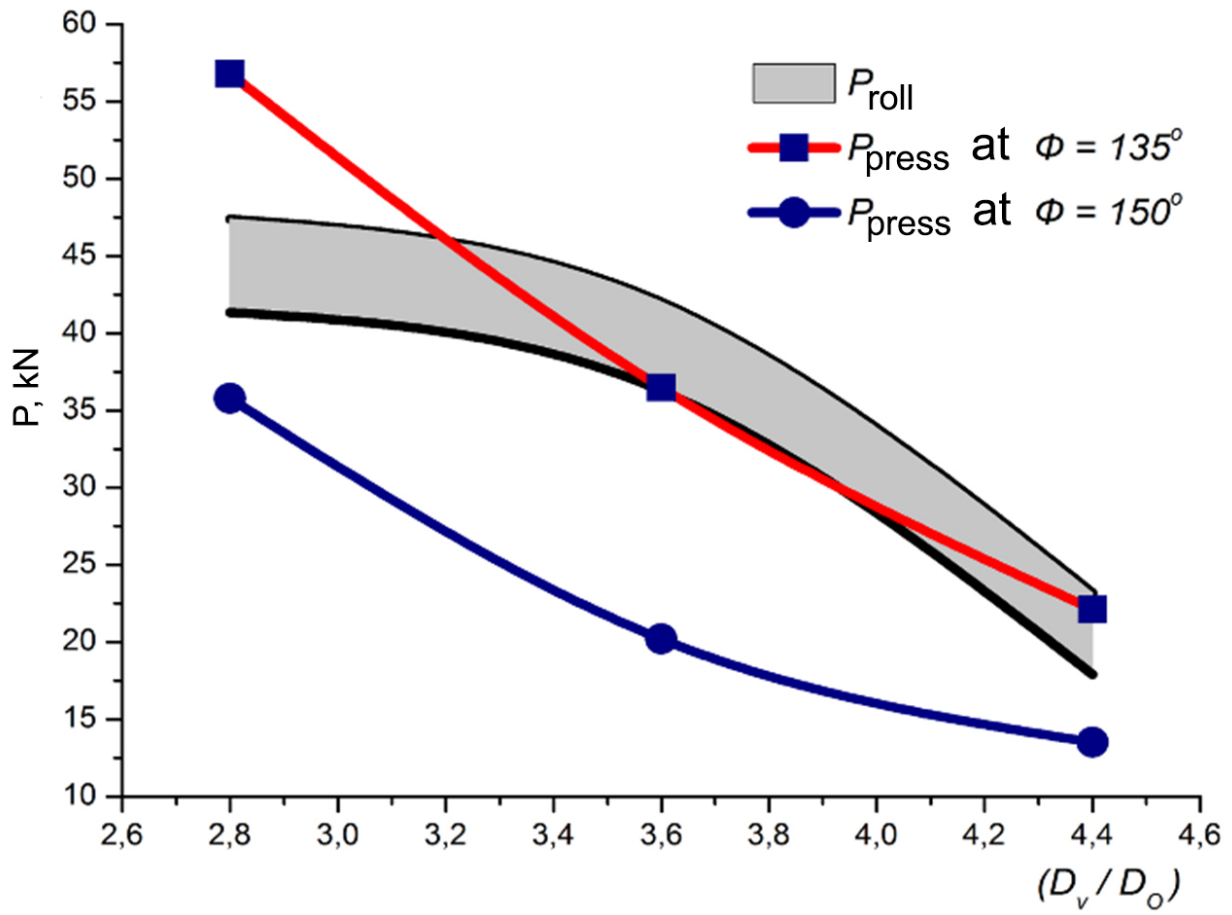


Figure 7.15 – Comparative graph of screw rolling and ECA-pressing forces

## 8. LABORATORY RESEARCH OF DEFORMATION PROCESS ON SAMPLES OF FERROUS AND NONFERROUS METALS AND ALLOYS AT THE STAND, IMPLEMENTING ENERGY-SAVING COMBINED PROCESS "SCREW ROLLING – ECA-PRESSING»

The aim of this experiment is to test the combined stand "screw rolling-pressing" by deformation of different materials in order to develop a technology that provides ultra-fine-grained structure in the samples and determine the most suitable materials for this.

Laboratory experiments on deformation of samples at the installation implementing energy-saving combined process "screw rolling-pressing" it was decided to carry out in 3 series on three different materials – technical copper grade M1, alloy structural steel AISI-5140 and complex alloyed stainless heat-resistant steel AISI-321.

This choice is due to the fact that in this way covers the area of the most used structural and functional materials, using the most typical properties of the brand.

In the experiment, the deformation was carried out according to the same scheme for all three materials. The only difference was the temperature, approximately corresponding to the lower limit of the hot deformation temperature for the material, or slightly below it.

From each material were cut 4 bars with a diameter of 30 mm and a length of 300 mm. After heating to the selected temperature, the bars were rolled on a screw mill to a diameter of 22 mm. At the next stage, the ECA matrix was mounted on the mill and the rod was deformed in a combined way to a diameter of 20 mm. At the same time, to ensure the necessary for entering the workpiece into the gap of matrix, the mill was adjusted for rolling a bar with a diameter of 0.5-1 mm less than the diameter of the input channel of the matrix. So all 4 blanks were rolled, at the same time, the subsequent blank pushed out the previous one from the matrix. Then, the matrix was disassembled, the press residue was extracted, which was aligned in the rolls of the mill with another pass without compression, heated in the furnace to the initial temperature and processed on the combined installation with a rear, untreated end. Then the blanks were heated again, the matrix installed on the mill was replaced with a matrix with a smaller diameter of the channel (18.5 mm and then 17 mm) and in the same way the bars were processed to the diameter of the channel of this matrix. After each pass for metallographic analysis the templates cut out in the longitudinal section of the bar.

For the first series of experiments on the combined stand, 30 mm diameter bars of AISI-5140 steel were used. Steel of this brand was chosen for the experiment due to the content of impurities that contribute to the fragmentation of the structure, especially chromium, which reduces the effect of aging after SPD. At the same time, the steel of this brand has a relatively low deformation resistance compared to many high-alloy steels. AISI-5140 is widely used in mechanical engineering and for the manufacture of tools. The chemical composition of steel is presented in table 8.1 [91].

Table 8.1 – Chemical composition of steel AISI-5140

C	Cr	Mn	Ni	S	P	Si	Cu
0,36 - 0,44	0,8 - 1,1	0,5 - 0,8	till 0,3	till 0,035	till 0,035	0,17 - 0,37	till 0,3

Chromium is an element that increases the hardenability of steel, increases wear resistance and prevents grain growth at elevated temperatures. Specific weight of steel 7820 kg/m<sup>3</sup>; material hardness: HB 10<sup>-1</sup> = 217 MPa; critical point temperature: A<sub>c1</sub> = 743°C, A<sub>c3</sub>(A<sub>cm</sub>) = 815°C, A<sub>r3</sub>(A<sub>rcm</sub>) = 730°C, A<sub>r1</sub> = 693°C; forging temperature: 1250°C - 800°C. Mechanical properties of the steel temperatures are shown in table 8.2. The physical properties are given in table 8.3.

Table 8.2 – Mechanical properties of steel AISI-5140 at elevated temperatures

Temperature, °C	Yield stress, MPa	Tensile stress, MPa	Elongatio n, %	Contraction, %	Impact strength, kJ / m <sup>2</sup>
Quenching at 830 °C in oil. Tempering at 550 °C					
200	700	880	15	42	118
300	680	870	17	58	
400	610	690	18	68	98
500	430	490	21	80	78
Sample with diameter 10 mm, length 50 mm, forged and annealed. The rate of deformation 5 mm/min, strain rate 0.002 1/s					
700	140	175	33	78	
800	54	98	59	98	
900	41	69	65	100	
1000	24	43	68	100	
1100	11	26	68	100	
1200	11	24	70	100	

The main features of the studied steel grade are: a sufficiently high endurance limit; good machinability of sharp and weldability; resistance to warping and decarburization when exposed to high temperatures. Products made of steel AISI-5140 are deformed by forging in the temperature range 800÷1250 ° C. Made from steel plungers, spindles, axles, shafts, rings, gear shafts, crankshafts, Cam shafts, bolts, axles, rods, bushings, foam crowns, bezels and other parts as required. Steel AISI-5140 is widely used for the manufacture of taps, drills, files. These are tools that work at low speed, and the heating temperature is not more than 200 ° C.

Table 8.3 – Physical properties of steel AISI-5140

T, (°C)	E, $10^{-5}$ (MPa)	$\alpha$ , $10^6$ (1/Deg)	L, (W/(m·deg))	$\rho$ , (kg/m <sup>3</sup> )	C, (J/(kg·deg))	R, $10^9$ (Ohm·m)
20	2.14	-	-	7820	-	210
100	2.11	11.9	46	7800	466	285
200	2.06	12.5	42.7	7770	508	346
300	2.03	13.2	42.3	7740	529	425
400	1.85	13.8	38.5	7700	563	528
500	1.76	14.1	35.6	7670	592	642
600	1.64	14.4	31.9	7630	622	780
700	1.43	14.6	28.8	7590	634	936
800	1.32	-	26	7610	664	1100
900	-	-	26.7	7560	-	1140
1000	-	-	28	7510	-	1170
1100	-	-	28.8	7470	-	120
1200	-	-	-	7430	-	1230

The evolution of the microstructure of this steel under the influence of screw rolling at the SVP-08 mill was studied in [115-116]. The study showed the formation of an equiaxed sub-structure-fine-grained microstructure at the periphery of the rod, with an elongated, oriented microstructure of the rod center, therefore, this material is well suited for conducting an experiment on a combined installation in order to obtain a homogeneous SUFG and UFG structure.

For the experiment of steel 40X bars were prepared with a diameter of 30 mm and a length of 300 mm (4 pieces). The rods were heated to 800 ° C in a tubular furnace Nabertherm R120/1000/13 with an exposure time of 30 minutes, according to the recommendations [105] – 1 minute per 1 mm diameter. Then, the samples were rolled for 2 passes on the screw rolling mill SVP-08 to a diameter of 22 mm. At the next stage, the mill was mounted on the ECA matrix and the rod was deformed in a combined way to a diameter of 20 mm. At the same time, in order to provide the necessary for the entry of the workpiece into the matrix of the gap, the mill was adjusted to the rolling rod diameter of 0.5-1 mm less than the diameter of the input channel of the matrix. So all 4 blanks were rolled, at the same time, the subsequent blank pushed out the previous one from the matrix. Then, the matrix was disassembled, the press residue was extracted, which was leveled in the rolls of the mill with another pass without compression, heated in the furnace to the initial temperature of 800 ° C and processed at the combined installation by the rear, untreated end. Then the blanks were heated again, the matrix installed on the mill was replaced with a matrix with a smaller diameter of the channel and in the same way the bars were processed to a diameter of 17 mm. After each pass, samples were cut from the longitudinal section of the bar for metallographic analysis. Strips of steel AISI-5140 were etched in a solution of ferric chloride.

The next experiment was decided to be carried out on a non-ferrous metal. Copper is one of the most common non-ferrous metals. It has high anti-corrosion properties under normal atmospheric conditions, as well as in fresh and sea water and other aggressive environments. In the presence of atmospheric oxygen on the surface of the copper product, a patina film is formed, which protects the metal from corrosion.

Copper is easily processed by pressure and brazing. Having low casting properties, copper is hard to cut and poorly welded. In practice, copper is used in the form of bars, sheets, wire, tires and pipes.

Due to the high thermal conductivity, copper is used for the production of current conductors and electrical products, refrigeration units, elements of heat pipelines, heating and gas supply systems, as well as CCM crystallizers. Since copper is resistant to the influence of aggressive chemicals, rolled from it is used in the oil, gas and chemical industries and for the manufacture of cryogenic products. Copper products have a very long service life, and throughout this period, the products retain their appearance, strength and physical integrity. The chemical composition of M1 grade copper is shown in table 8.4.

Table 8.4 – Chemical composition of M1 copper alloy

Fe	Ni	S	As	Pb	Zn	O	Sb	Bi	Sn	-
0.005	0.002	0.004	0.002	0.005	0.004	0.05	0.002	0.001	0.002	Cu+Ag min 99.9

A great influence on the properties of copper have impurities, which are divided into three groups according to the method of influence:

1) Impurities forming solid solutions with copper – nickel, antimony, aluminum, zinc, iron, tin, etc. Reduce the electrical and thermal conductivity of copper. In this regard, copper with a limited content of arsenic and antimony (0.002 As and 0.002 Sb) is used as current conductors. Antimony also reduces the ability of the alloy to hot plastic deformation.

2) Impurities that are practically insoluble in copper – bismuth, lead, etc. Practically do not affect the electrical conductivity of copper, but worsen its processing pressure.

3) Impurities forming brittle chemical compounds (sulfur, oxygen). Oxygen significantly reduces the strength of copper and reduces electrical conductivity. Sulfur improves the machinability of copper by cutting.

The mechanical properties of this copper grade are given in table 8.5. Physical properties are given in table 8.6.

Table 8.5 - Mechanical properties of M1 copper alloy at a temperature 20°C

Assortment	Tensile stress, MPa	Elongation, %	HB10 <sup>-1</sup> , MPa
Alloy steel cold-rolled soft, GOST 1173-2006	200-260	42	55
Alloy steel cold-rolled hard, GOST 1173-2006	290	6	95

Table 8.6 – Physical properties of M1 copper alloy

T, (°C)	E, $10^{-5}$ (MPa)	a, $10^6$ (1/Deg)	L, (W/(m·deg))	r, (kg/m <sup>3</sup> )	C, (J/(kg·deg))	R, $10^9$ (Ohm·m)
20	1.28	-	387	8940	390	17.8
100	1.32	16.7	-	-	-	

For the laboratory experiment, bars with a diameter of 30 mm and a length of 300 mm made of M1 copper were used. Earlier, a study [117] on the influence of screw rolling on the structure and properties of copper, M1 grade, was conducted outside this project. Studies have shown a significant reduction of the microstructure of the surface layer of copper during compression of 35-20 mm on the SVP-08 mill on the basis of which the combined installation is built.

The deformation temperature of the bars was 500 ° C. The procedure of the experiment is fully repeating the procedure described above. The heated copper rods were deformed on the screw rolling mill SVP-08 to a diameter of 22 mm, then the ECA matrix with a diameter of 20 mm was installed on the mill and, in 3 passes, successively changing the matrix, the rod was deformed in a combined way to a diameter of 17 mm. Thus, a combined deformation scheme "screw rolling-pressing" was carried out.

After each pass, samples were cut out and sections were made for metallographic studies in the longitudinal section, the most informative for the studied type of processes.

The slots were prepared on the tegraforce grinding and polishing machine. To identify the microstructure, the polished surfaces of the samples were degreased with toluene and etched with rubbing for 10-20 seconds with cotton wool with a solution of the following content: 75% saturated solution  $K_2Cr_2MnO_4$ , 10%  $HNO_3$ , 10% HCL, 5%  $H_2SO_4$ . To increase the contrast, additional etching was carried out by immersion of the strip for 2-4 seconds in a solution of 10% HCL; 90% saturated  $Cu_2(SO_4)_3$ .

For the following experiment were selected from complexly alloyed stainless austenitic steel AISI-321. After standard heat treatment, consisting of quenching from 1050 °C with cooling in water, the steel has a structure of the solution. Steel AISI-321 does not undergo any transformations when heated under hot plastic deformation. The main alloying elements of steel are chromium, Nickel and titanium. The chemical composition of steel is presented in table 8.7 [91].

Table 8.7 – Chemical composition of steel AISI-321

C	Si	Mn	Ni	S	P	Cr	Cu	Ti
till 0.08	till 0.8	till 2	9-11	till 0.02	till 0.035	17-19	till 0.3	0,5-0.7

Chromium, the content of which in steel is 17-19%, is the main element that provides the ability of the metal to passivation, which is directly sacred with high corrosion-resistant properties.

Nickel expands  $\gamma$  – region and with a sufficient amount (8..12 %), allowing to obtain an austenitic structure at room temperature.

Titanium restrains grain growth during heating, increasing resistance to grain boundary corrosion. With large deformations, dispersed carbides occur in this steel, which prevent the movement of dislocations, and also contribute to their duplication.

Austenitic steels are characterized by high corrosion resistance in most corrosive environments, including sulfuric and a number of other acids. They are well rolled in hot and cold conditions, welded without embrittlement of the zones. The effect of nickel on corrosion resistance in steel of this class is manifested in the fact that it has an increased resistance to the action of acids, reports this property of steel. In the presence of 0.1% carbon steel has at  $>900^{\circ}\text{C}$  fully austenitic structure, which is associated with a strong austenite-forming effect of carbon. The ratio of chromium and Nickel concentrations has a specific effect on the stability of austenite when the treatment temperature is cooled on the solid solution ( $1050\text{--}1100^{\circ}\text{C}$ ).

The specific weight of steel  $7900\text{ kg/m}^3$ ; Temperature of forging: the beginning of  $1220^{\circ}\text{C}$ , the end of  $900^{\circ}\text{C}$ . Material hardness:  $\text{HB } 10^{-1} = 179\text{ MPa}$ . Since the steel is heat resistant, the physical and mechanical properties should also be considered at normal and elevated temperatures. Physical properties of steel AISI-321 at elevated temperatures are given in table 8.8. Mechanical properties at elevated temperatures are given in table 8.9.

Table 8.8 – Physical properties of steel AISI-321 at elevated temperatures

T, ( $^{\circ}\text{C}$ )	E, $10^{-5}$ (MPa)	a, $10^6$ (1/deg)	l, (BТ/(m·deg))	r, ( $\text{kg/m}^3$ )
20	1.96	-	-	7900
100	-	16.1	16	-
200	-	-	18	-
300	-	17.4	19	-
400	-	-	-	-
500	-	18.2	-	-

Table 8.9 - Mechanical properties of AISI-321 steel at elevated temperatures

Temperature, $^{\circ}\text{C}$	Yield stress, MPa	Tensile stress, MPa	Elongation, %	Contraction, %	Impact strength, $\text{kJ/m}^2$
20	275	610	41	63	245
300	200	450	31	65	-
400	175	440	31	65	313
500	175	440	29	65	363
600	175	390	25	61	353
700	160	270	26	59	333

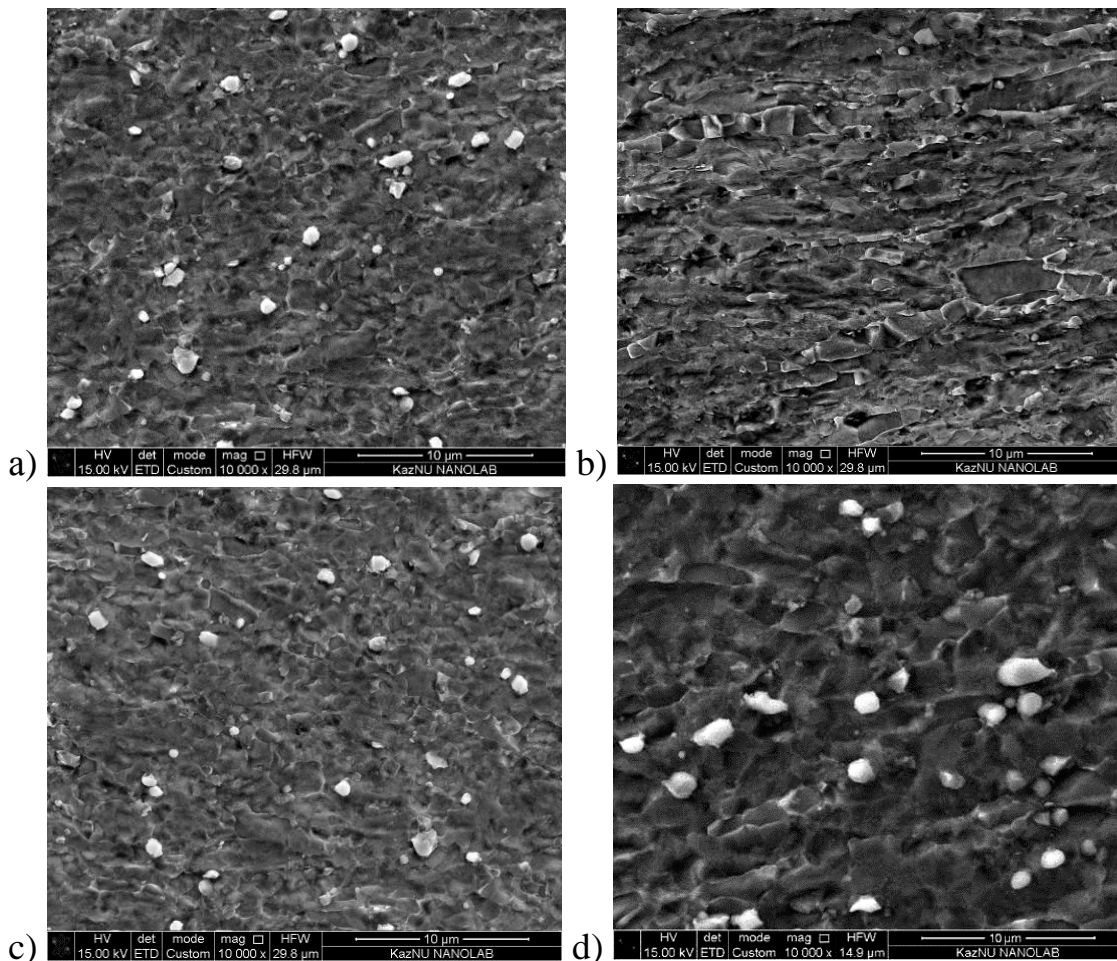
With this steel, a preliminary study [116] was conducted to study the effect of screw rolling on its structure. This study revealed the formation of an equiaxial UFG structure with a grain size of 500-800 nm at the periphery of the rod. Thus, steel AISI-321 more than other considered in this work, suitable for the production of UFG materials. A special role in this choice is played by the fact that the steel of this brand is used for the manufacture of critical parts, working in difficult conditions of many high-tech industries – from chemical technology to nuclear power. It is here that the appearance of a material with high properties can be most in demand and create a demand sufficient to start profitable production and sales of UFG products.

Deformation temperature, according to sources [105, 118] was assigned 800°C. The method of deformation was similar to the methods by which the samples were deformed in paragraphs 1.2 and 1.3. Bars with a diameter of 30 mm and a length of 300 mm were heated in a tubular furnace to 800 ° C. The method of deformation was similar to the methods by which the samples were deformed in paragraphs 1.2 and 1.3. Bars with a diameter of 30 mm and a length of 300 mm were heated in a tubular furnace to 800 ° C, while the exposure was slightly greater than 1 min per 1 mm diameter due to the lower thermal conductivity of stainless steel, then rolled to a diameter of 22 mm on the SVP "14-40" mill, after which they were deformed by the combined technology "screw rolling-pressing" for 3 passes to a diameter of 17 mm. After each pass, samples were selected for the analysis of the microstructure and to determine the mechanical properties.

# 9 IMPACT OF THE NEW COMBINED PROCESS "SCREW - ROLLING – ECA-PRESSING" ON THE MICROSTRUCTURE EVOLUTION AND MECHANICAL PROPERTIES OF THE DEFORMED STRUCTURAL MATERIAL

## 9.1 Microstructure evolution and mechanical properties changes of AISI-5140 structural steel

After each pass, samples were cut from the longitudinal section of the bar for metallographic analysis. Strips of steel AISI-5140 were etched in a solution of ferric chloride. The sections were examined using a scanning electron microscope Quanta 200i 3D. Photos of typical types of microstructure in the center and on the periphery of the rod after screw rolling, and after the third pass are shown in figure 9.1.



a, b – periphery and center of the rod after screw rolling up to 19 mm;  
b, d – periphery and center of the rod after three passes on the combined stand  
"screw rolling – ECA-pressing»

Figure 9.1 – Microstructure of steel AISI-5140 (x 10, 000)

The initial structure in the normalized state of supply has a typical for this type of steel coarse-grained ferrite-pearlite structure with a grain size of 40-60 microns and a microhardness of 150-160 HV.

Figures 9.2 (a) and 9.2 (b) show the structure of the peripheral and central zones of the rod after screw rolling from a diameter of 30 mm to 19 mm. Sample for the study was cut from an under-rolled rod with a diameter of 19 mm before entering the matrix. The microstructure of the peripheral region has a predominantly equiaxed subalternity nature with grain size about 1  $\mu\text{m}$ . In the central zone, structural banding in the form of elongated grains in the rolling direction with dimensions of  $5\div 10 \times 0,9\div 1,5 \mu\text{m}$  and a chain of chromium carbide crystals (white phase) is visible. The chromium carbide type  $\text{M}_3\text{C}$  were identified by energy dispersive analysis (EDX) of the elements of the structure by using the analyser Oxford instruments. The map of distribution of elements of chemical composition, obtained by means of EDX-analyzer, on the characteristic surface of the section, including the main phases is shown in figure 9.2. Linear EDX analysis in the form of graphs of the content of elements superimposed on the image of the microstructure is shown in figure 9.3. The graph clearly shows a sharp and synchronous increase in the level of chromium and carbon at the intersection of the measurement line with the boundary of the white phase crystals. The size of individual particles of chromium carbide is less than 200 nm.

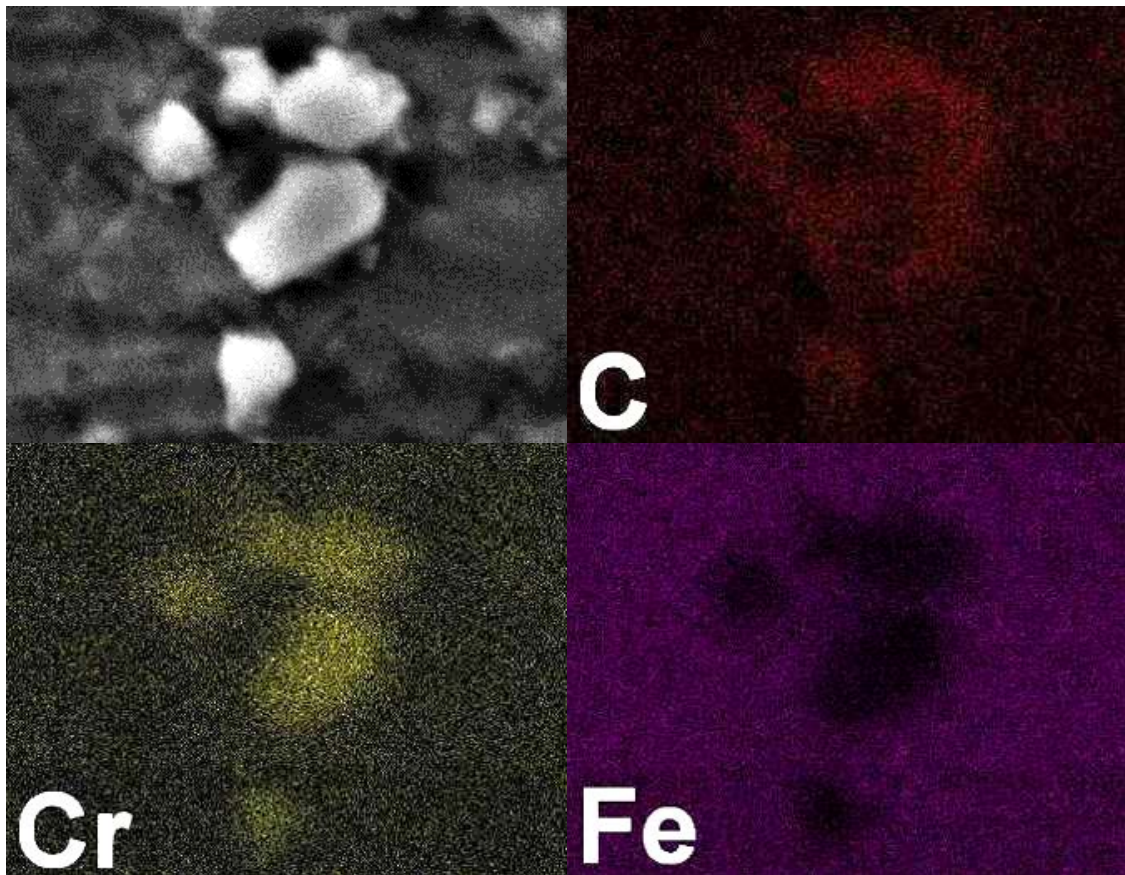


Figure 9.2 – EDX-analysis of the chemical composition on the strip surface

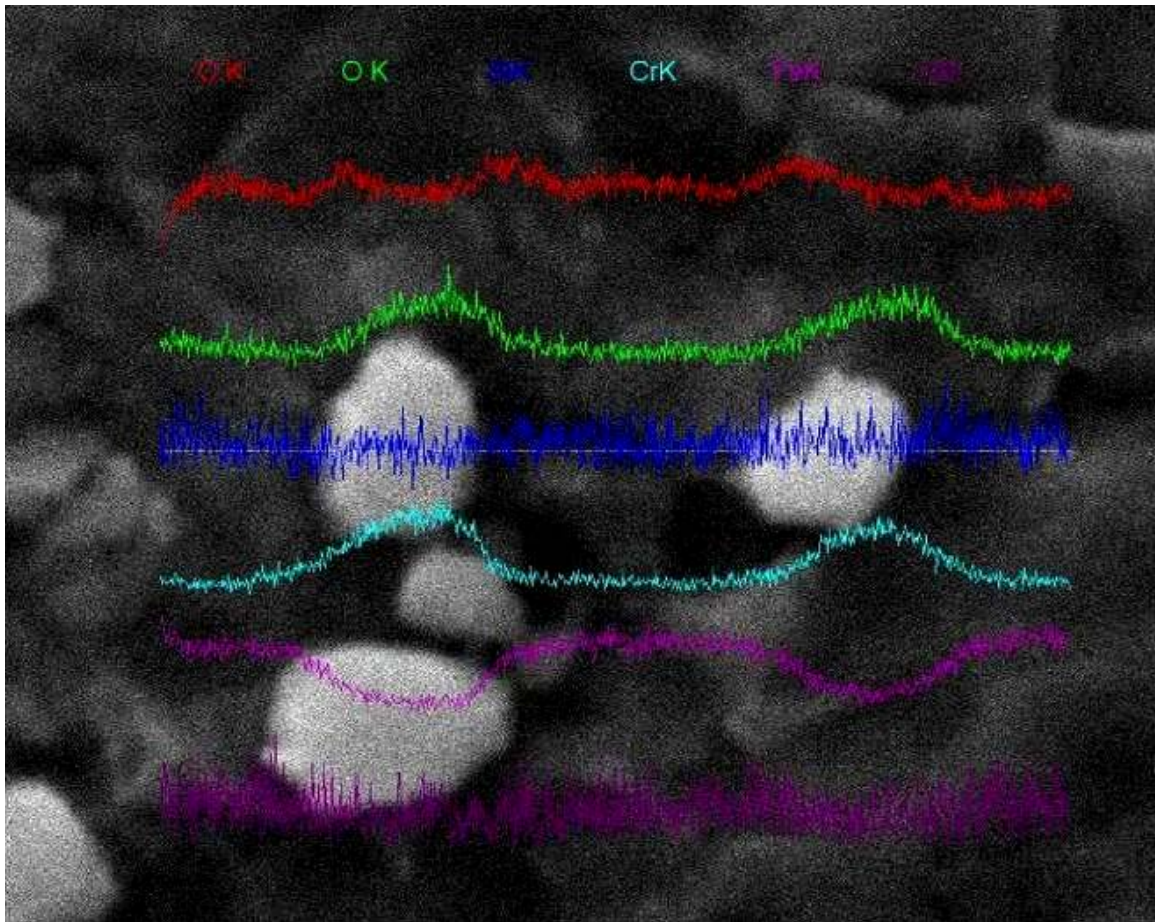


Figure 9.3 – Linear EDX analysis of chemical composition

The microstructure obtained after rolling on a screw mill before entering the workpiece into the matrix is characteristic of this type of deformation and confirms the data presented in [57, 64].

The study of samples after three passes at the combined installation "screw rolling – ECA-pressing" (figure 9.1 (a) and figure 9.1 (b) showed a change in the striped texture of the central bar zone to a more equiaxed structure with a grain size of about 3-6 microns. The peripheral part of the workpiece retained its former ultra-fine-grained character. A typical picture of the transition zone at a distance of 0.5 radius from the center of the bar is shown in figure 9.4.

The transition zone after the second pass still retains traces of the oriented "rolling" structure, although significantly changed. After the third pass, the transition region has a fine-grained structure with a grain size of about 1-1.5 microns. For the characteristic areas of each section, the average grain size was calculated by the method of secant (two intersecting sections diagonally each image) [119]. The values obtained are presented in the form of a graph in figure 9.5. The graph shows that the grain size decreases monotonically with each pass.

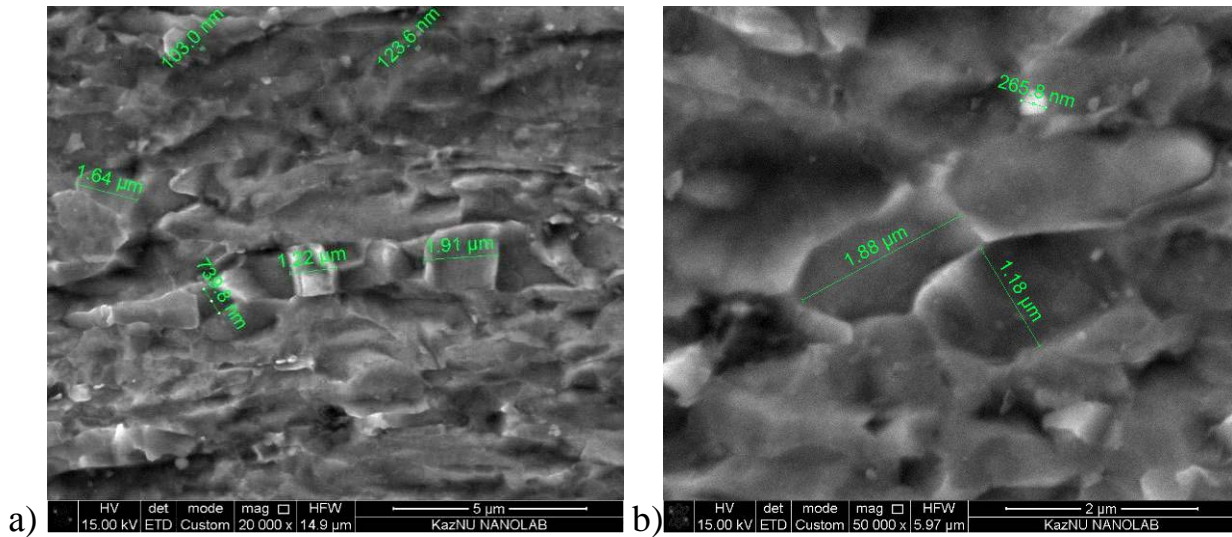


Figure 9.4 – Microstructure of the transition zone at a distance 1/2 of radius from the center of the rod after the second (a) and third passage (b)

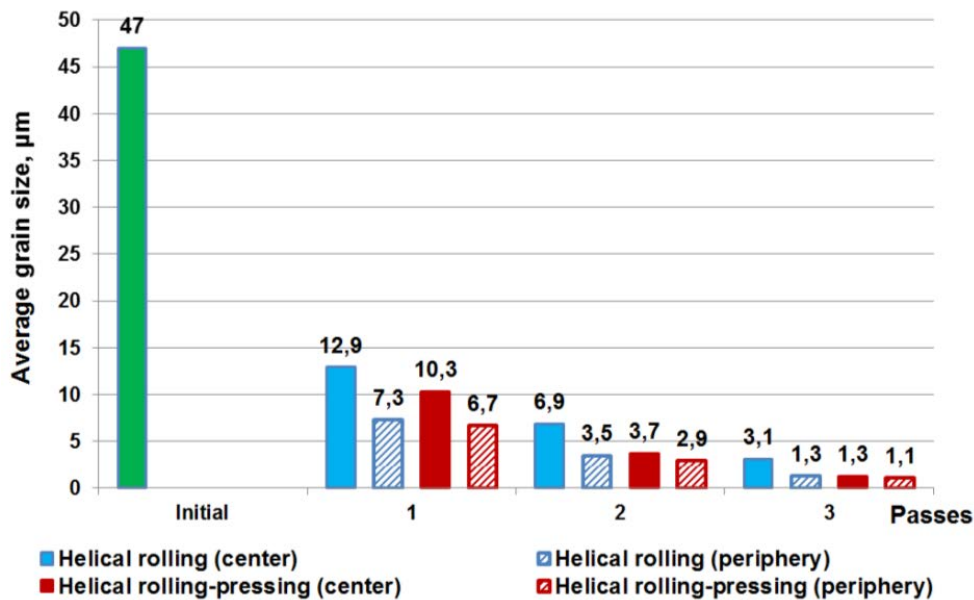


Figure 9.5 – Average grain size of steel AISI-5140 by passes

The results of measurements of the grain size of steel AISI 5140 show that the high intensity of shear deformation during helical rolling, and combined process "helical rolling-pressing", allows to greatly grind the structure. Moreover, the combined process refines the grain to a greater extent, allowing to receive the grain with a minimum average size up to 1 μm and maximum values of microhardness. At the same time, metallographic investigations showed the transformation of the oriented lamellar structure of central regions in a more equiaxed structure with a predominance of large-angle grain boundaries. This allows to increase the uniformity of distribution properties of the product, which is confirmed by measurements of microhardness.

Microhardness Vickers (HV) was measured by a semiautomatic method using hardness testing machine FM-800 under a load 10 N during 15 seconds. That

was enough to produce clear prints of the indenter. In each characteristic area were carried out 5 measurements at a distance of not less than 2.5 of diagonal of print from the previous injection. The microhardness of steel AISI 5140 after helical rolling from 30 mm to 19 mm was maximum up to 478-483 HV on the periphery and 400 HV in the center of the rod. Thus, the microhardness of the rod after helical rolling, compared to the initial state increased more than 2 times. However, between the peripheral and axial zones of the rod there is a difference of about 80 HV. The average microhardness values after 5 measurements in each point were 433 HV on the periphery and 363 HV in the center of the rod. This difference is due to the specific microstructure of these zones, as well as longer cooling of the center of the rod, where, due to increased temperature, more intensively proceeded static recrystallization and annihilation of defects in the lattice.

Comparison of the microhardness of the axial and peripheral zones of the rod after three passes of combined process shows a narrowing of the difference in the microhardness up to 40 HV, that is less than 10 %. It allows to speak about the effectiveness of a new combined process "helical rolling-pressing" to reduce the non-uniformity of properties after helical rolling. The average microhardness values show an increase of microhardness to values 438 HV on the periphery and 426 HV in the center of the rod with a gradual slowing of its dynamics (the decrease of the difference values). Measurement of average microhardness of steel AISI 5140 in the initial state and after each pass are presented in figure 9.6.

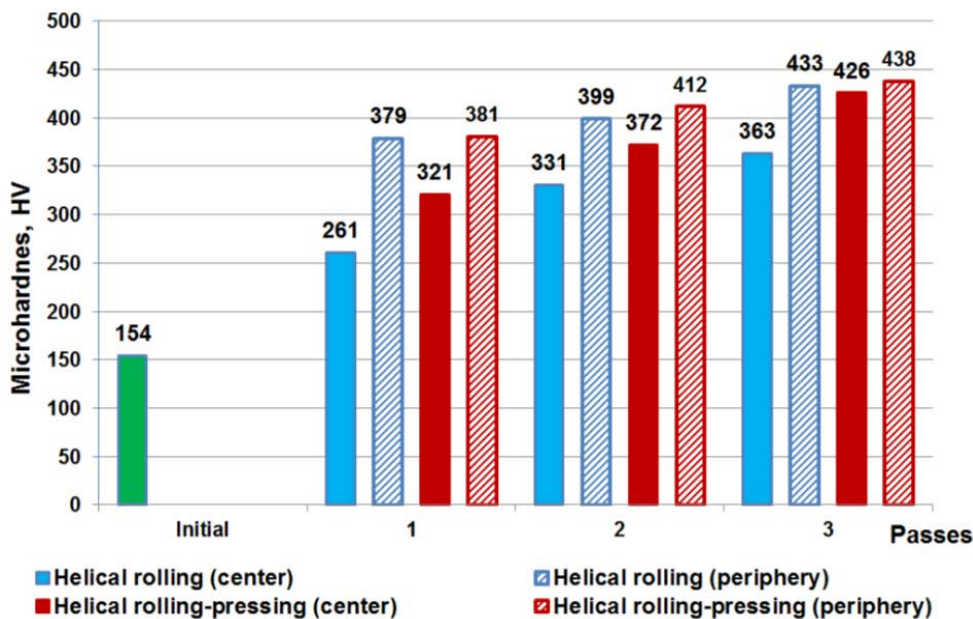


Figure 9.6 – Microhardness of steel AISI 5140

## 9.2 Microstructure evolution and mechanical properties changes of technical copper M1

Figures 9.7-9.8 show optical photos of the microstructure before and after deformation. Metallographic analysis of copper after helical rolling showed that

grain refinement occurs after each pass. It was discovered that the grain structure during deformation under a combined scheme of deformation "helical rolling-pressing" is processed more intensely. The minimum average grain size was revealed after the third pass of the combined process and it was equal to 4,1  $\mu\text{m}$  in the periphery and 5,9  $\mu\text{m}$  in the center of the rod. The minimum grain size was 3  $\mu\text{m}$ . The grain size is shown in figure 9.9 determined on the samples.

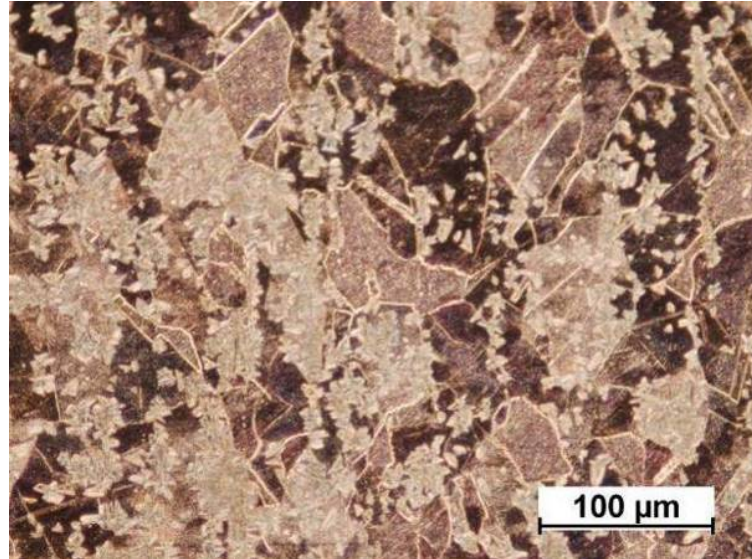
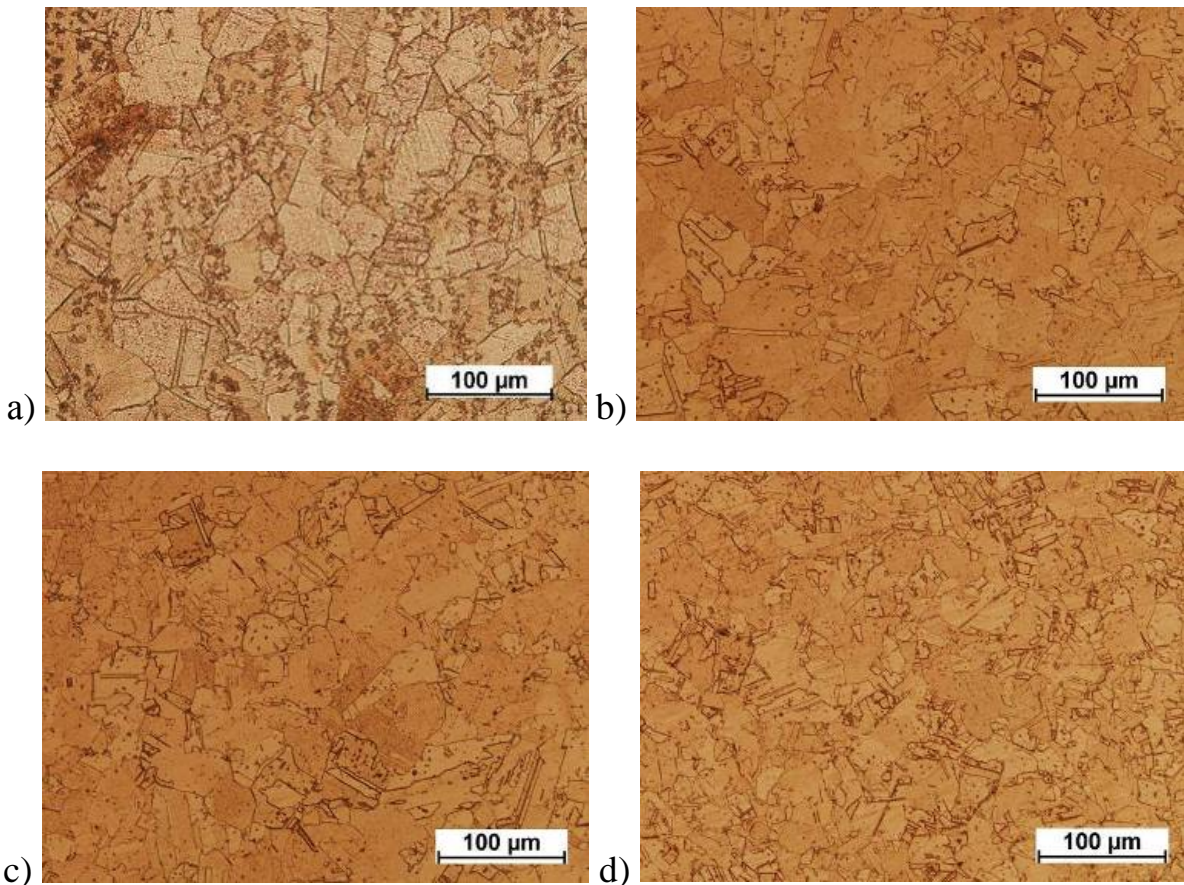
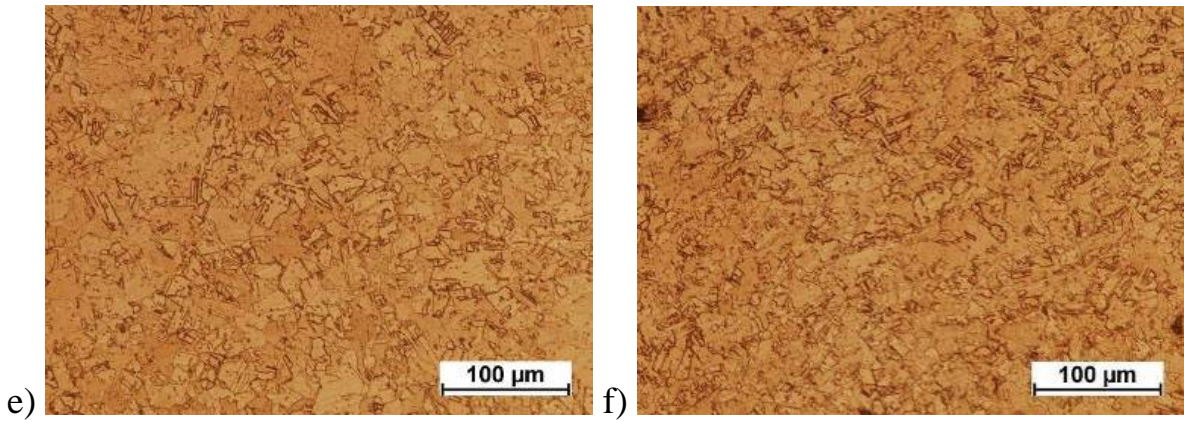


Figure 9.7 – Initial copper structure





a, c, e - the structure of copper subjected to deformation on the screw rolling mill to a diameter of 20, 18.5 and 17 mm, respectively;  
 b, d, f – the structure of copper subjected to deformation according to the combined scheme "screw rolling-pressing" to a diameter of 20, 18.5 and 17 mm, respectively

Figure 9.8 – Optical photos of the copper microstructure

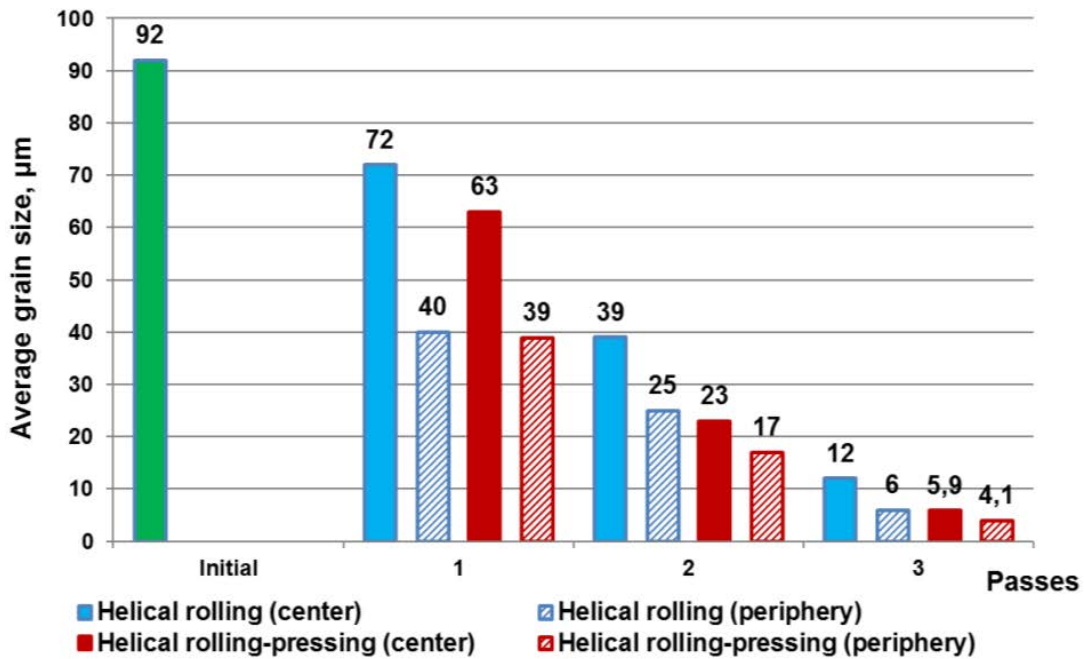


Figure 9.9 – Average copper grain size by passes

Samples were also investigated on Vickers microhardness (HV) by using the hardness testing machine AntonPaar embedded in the optical metallographic microscope "Leica-IRM". The load was 5 N during 10 seconds. Results of determining the microhardness and average grain size are represented in figure 9.10.

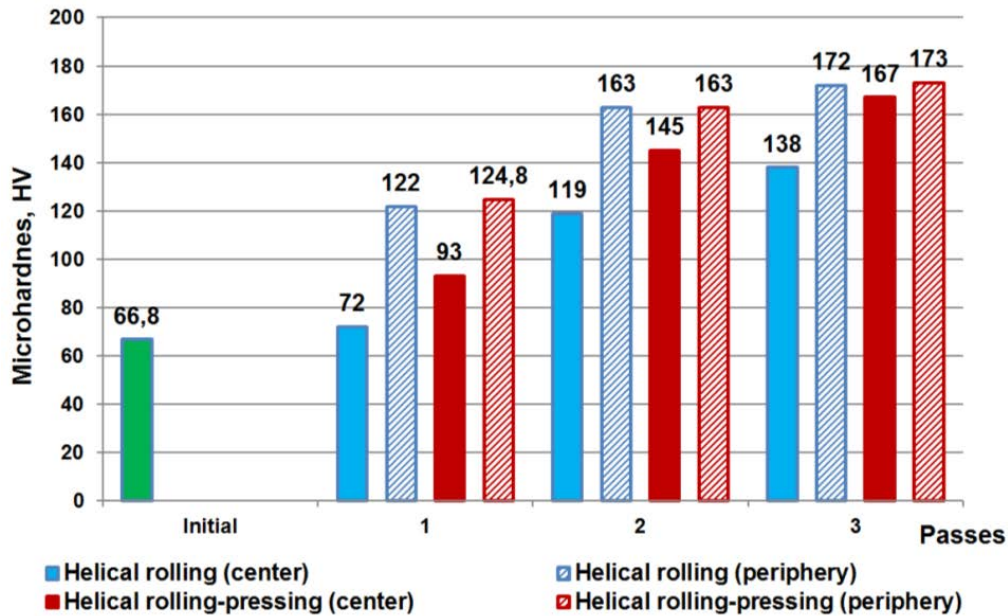


Figure 9.10 – Microhardness of copper

The measurements showed that the maximum microhardness value was obtained after 3 cycles of "helical rolling-pressing" and was 173 HV, which is 2.5 times more than the microhardness of the initial sample. Analyzing the change of the microhardness it can be concluded that the microhardness increases with the degree of accumulated strain. Based on the results of metallographic analysis and microhardness it was revealed that the greatest grain refinement with the maximum quality level can be obtained by combined process "helical rolling-pressing" after three passages.

### 9.3 Microstructure evolution and mechanical properties changes of complex alloyed stainless heat-resistant steel AISI-321

Selected samples were investigated on transmission electron microscope Jeol JEM-100CX. On high-precision cutting-off machine Struers AccuTom-5 in longitudinal section of the rod were cut out the plates of 0.3 mm thickness. Then, using special punch from each of them in the central and peripheral zones were cut 2 disks with a diameter of 3 mm. Prepared samples were investigated on the TEM under accelerating voltage of 100 kV.

The initial structure of the steel is austenitic structure with a grain size of about 20-35 microns is shown in figure 9.11. Photos of the peripheral and axial zones of the rod after screw rolling are shown in figure 9.12.

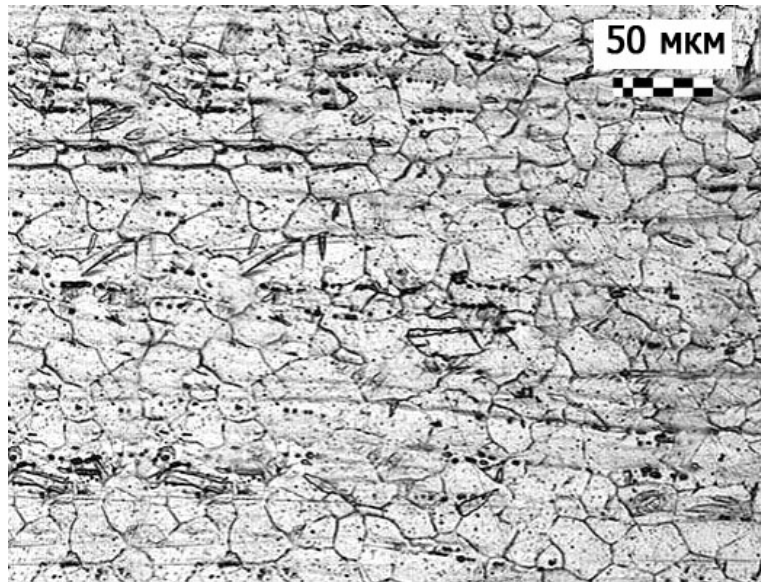


Figure 9.11 – Initial microstructure of steel AISI-321

In the peripheral part of the bar (figure 9.12 a), the structure is equiaxed grains with a predominance of large-angle boundaries. In the axial zone (figure 9.12 b) are clearly visible micro-shear bands, combining in some parts of the sample in bundles or methodology stretching for long distances. To an even greater extent, this phenomenon was developed in the axial zone of the rod deformed on the screw mill in work [116]. Also in many areas were marked by the so-called «knife boundaries», such as [120], are powerful extended straight or smoothly curved clear lines and oriented along the direction of the main axis of deformation. This structure is characterized by strong uniaxial deformation. Fragmented traces of the described structure are found in the axial zone after the second pass through the combined technology, which is clearly seen in figure 9.13 (typical knife boundaries are showed with green arrows).



a)

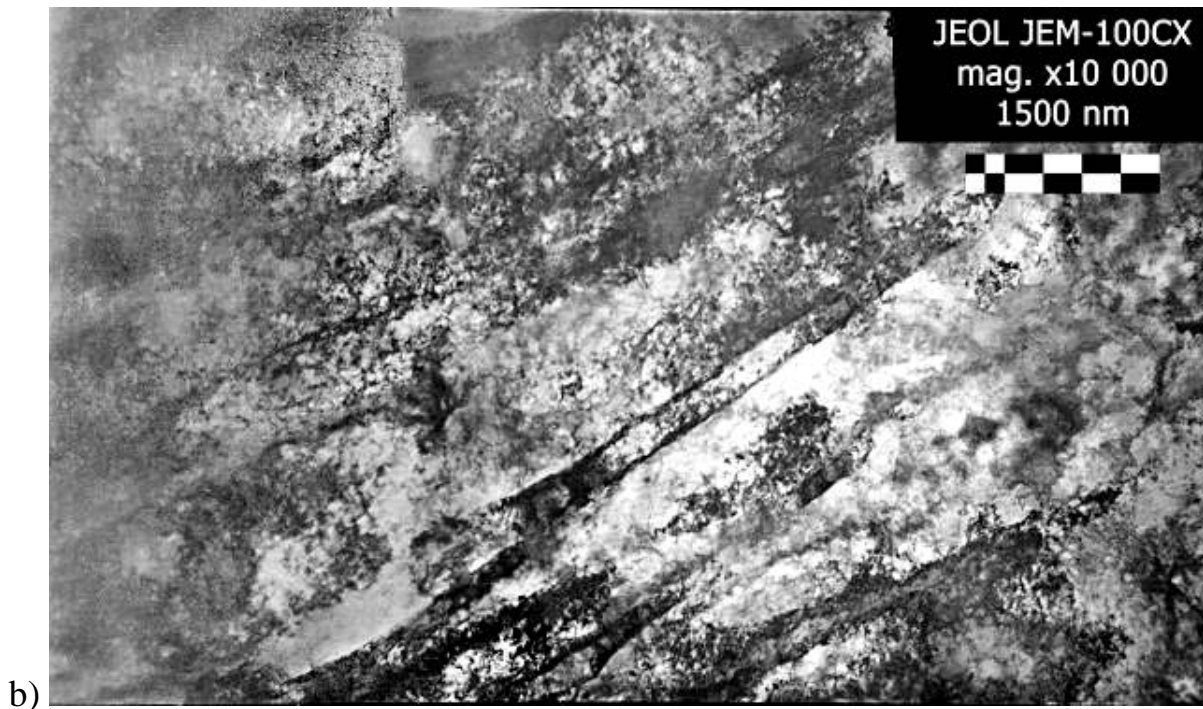
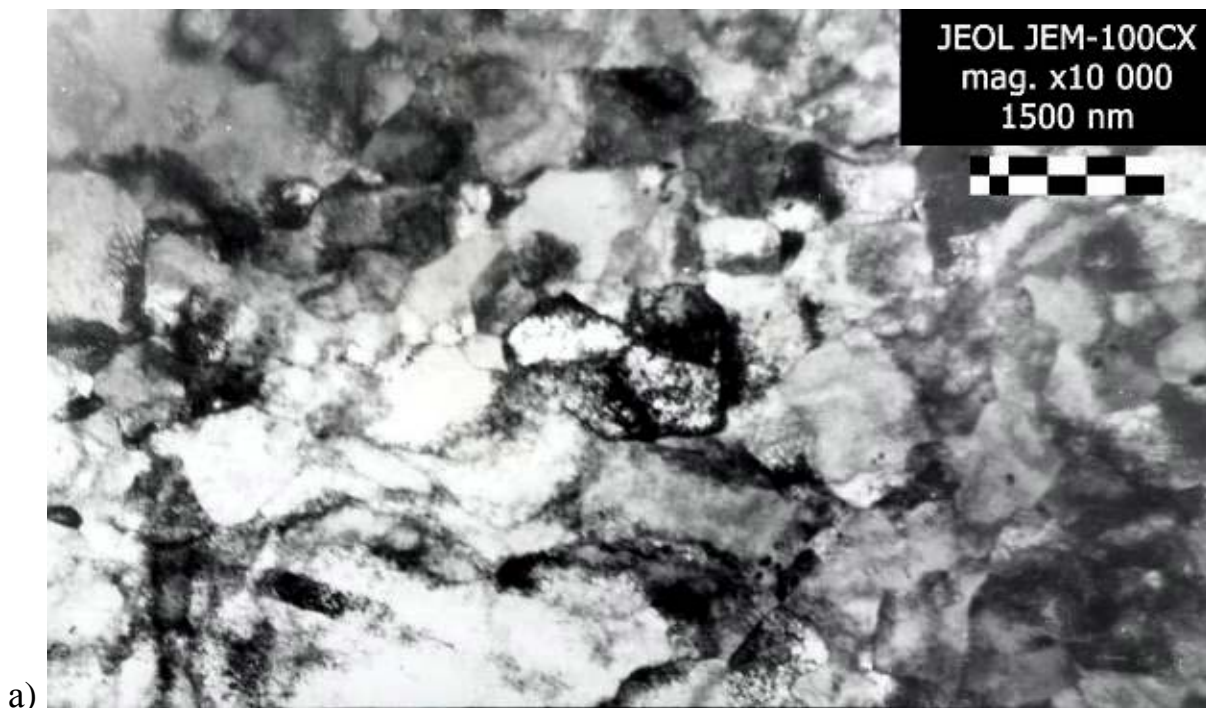
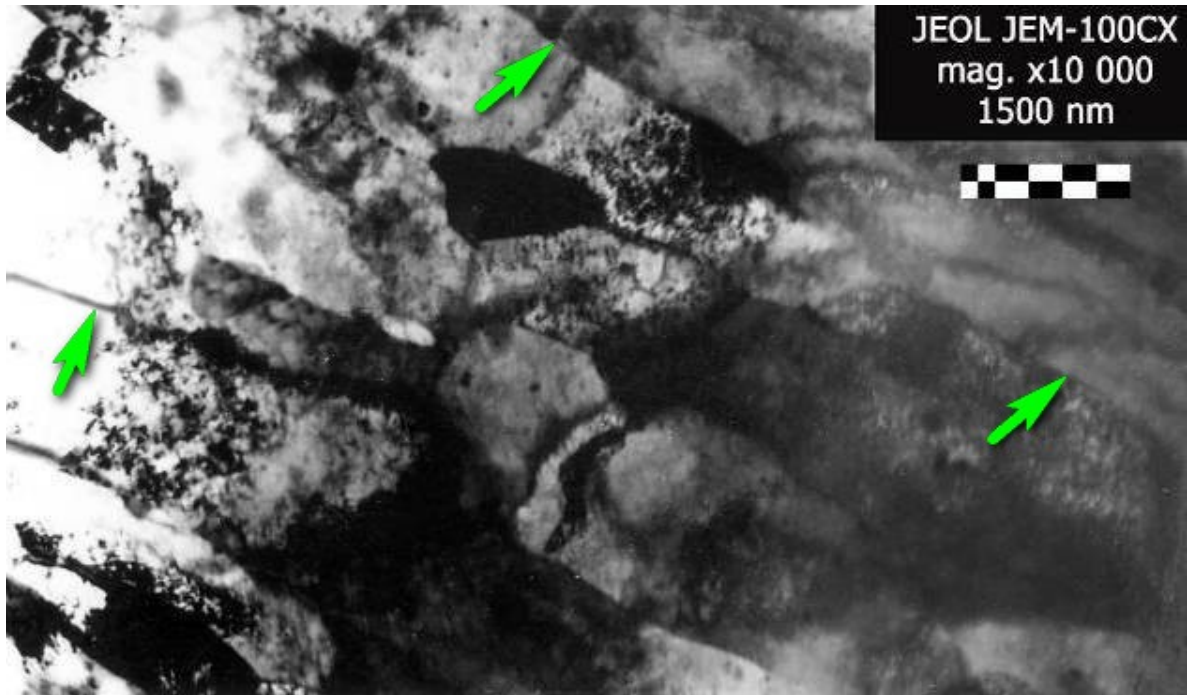


Figure 9.12 – The structure of the peripheral (a) and axial (b) zones of the rod after rolling of 30 mm to 19 mm

In the peripheral part of the rod (figure 9.13a) after two passes of combined technology, the structure is also represented by equiaxed grains with size less than 1 micron. Thus, in the axial zone (figure 9.13b) in spite of noticeable artifacts still oriented structure, the grains are less elongated compared to this area after rolling. This phenomenon is explained by the change of direction of shear deformation on the perpendicular in the axial zone of the rod during the realization of combined process "helical rolling-pressing".

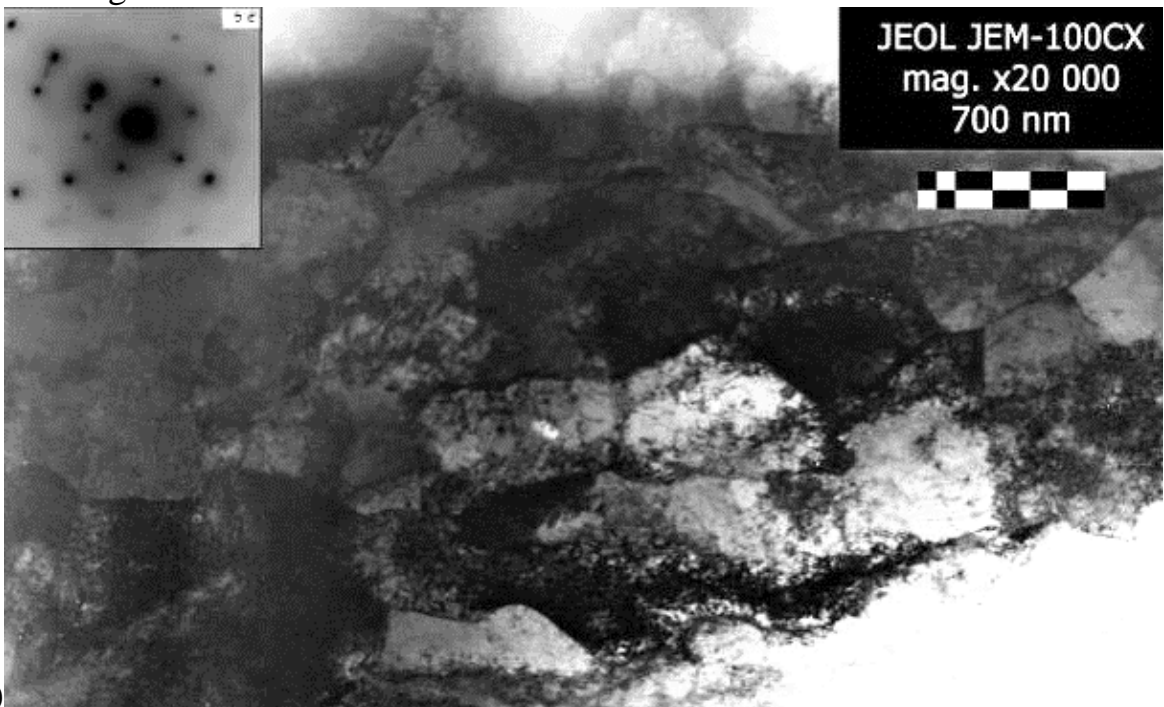




b)

Figure 9.13 – Structure of the peripheral (a) and axial (b) part of the rod after a second pass of combined process "helical rolling-pressing"

Fine structure of the axial and peripheral zones of the rod after the third is shown in figure 9.14.



a)

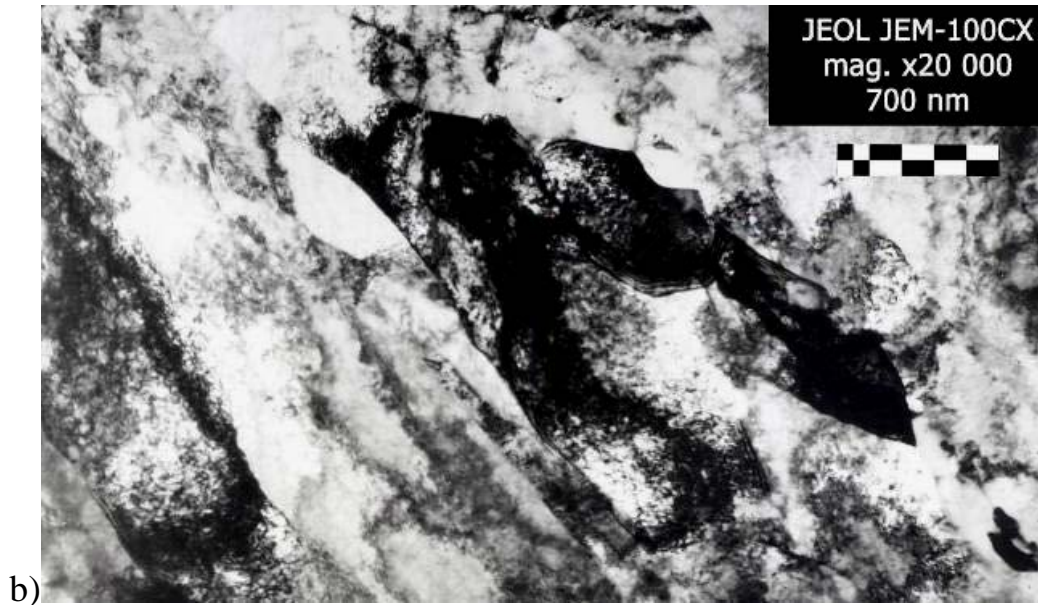


Figure 9.14 – Fine structure of the peripheral (a) and axial (b) zones of the rod after the third pass

Peripheral area shows the preservation of the equiaxed grain structure with predominantly large-angle boundaries and grain sizes of 500-800 nm. Dislocations are visible in the current contrast within the grains together in a cellular structure. Axial area still retains some traces of the former structure, however, the grain size and the nature of their mutual arrangement more resembles the peripheral region. Thus, it can be concluded that three passes of intense shear deformation by new combined process can significantly change the structure of the central regions of a deformable rod.

Also, at each stage of deformation, mechanical properties of the obtained bars were investigated. For this purpose, from each bar were cut at 3 cylindrical sample, which is then grind on a lathe to the required shape, after which, tests were carried out on a torsion-tensile testing machine MI-40KY. Graphs of mechanical properties, as well as a graph of changes in the average grain size along the passages are shown in figures 9.15 – 9.17.

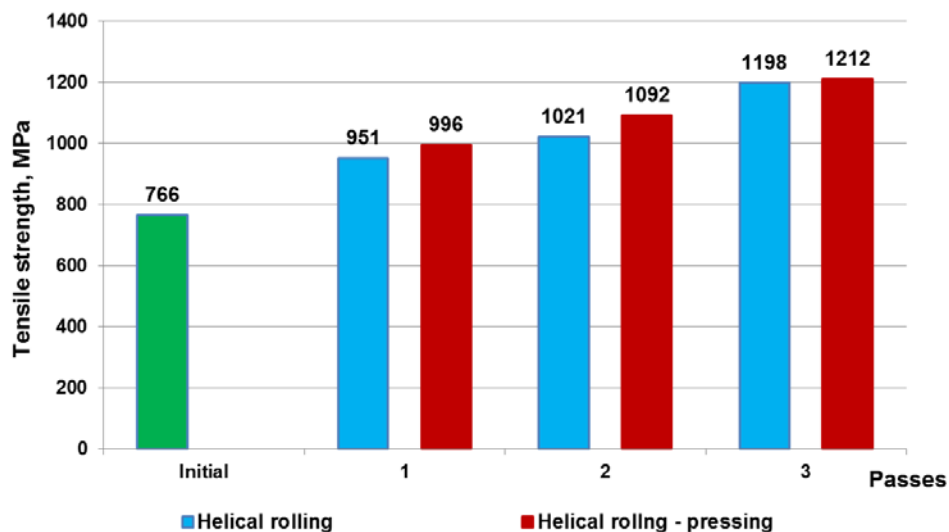


Figure 9.15 – Tensile strength of steel AISI-321 by passes

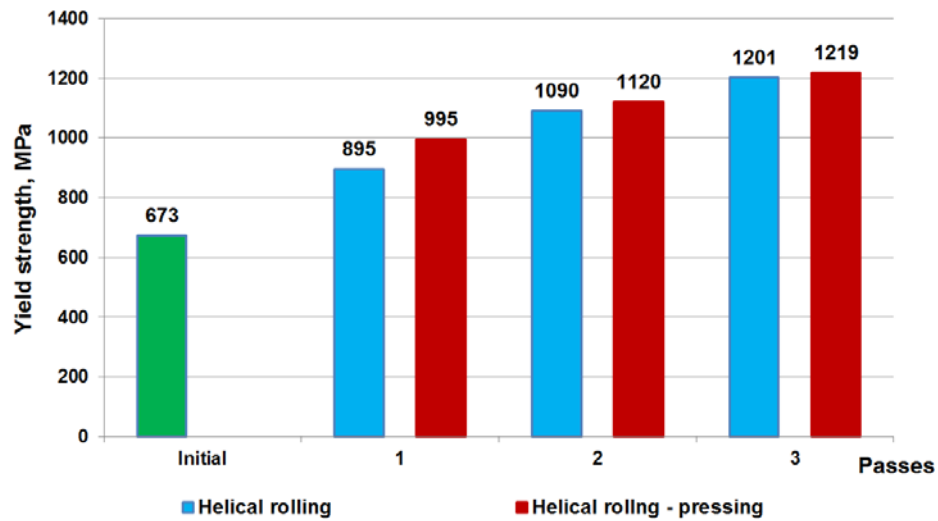


Figure 9.16 – Yield strength of steel AISI-321 by passes

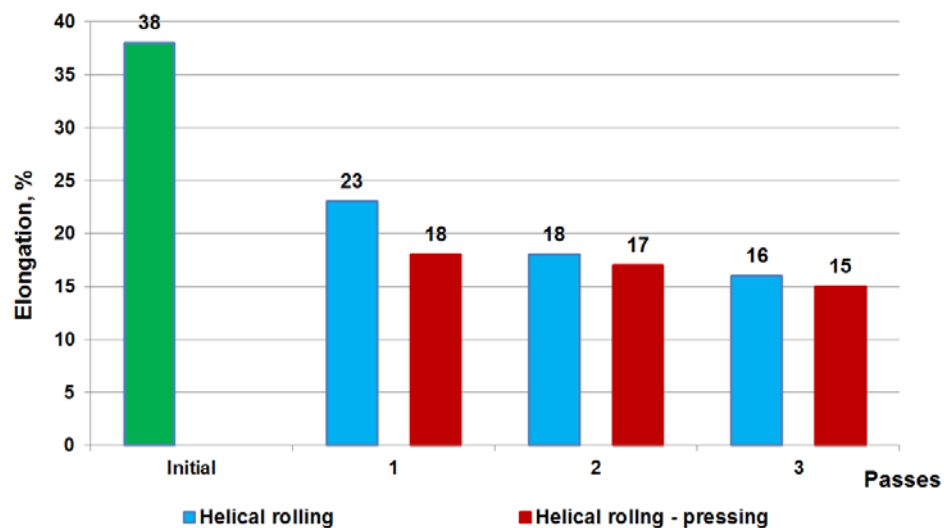


Figure 9.17 – Elongation of steel AISI-321 by passes

As it can be seen from figures 9.15 – 9.17, helical rolling, as well as helical rolling-pressing significantly increase the level of strength properties by grain refinement. This also contributes to the titanium content, which inhibits grain growth. Thus, the plastic properties in comparison with the decrease slowing, remaining at a good level for the deformed material, and even a little higher than the plastic properties of the steel processed by equal channel angular pressing at such temperatures, known from [118]. To increase the plastic characteristics is possible by low tempering. It is also worth noting that the deformation was conducted on the limiting hardware conditions, and an even greater reduction in deformation temperature in addition to the more grain refinement will lead to stopping the process or equipment damage. Therefore, the temperature of 800 °C can be considered as optimal for the deformation by such combined method.

## 10 QUALITATIVE ANALYSIS THE QUALITY OF THE PRODUCTS WITH ENERGY EFFICIENCY IN VIEW

As it is known, the features of the microstructure of metals and alloys determine their mechanical and operational properties. In domestic and foreign practice, for microstructure analysis and control the technologies based on the comparison of the observed structure with the standards, as well as various methods of quantitative metallographic analysis, such as the average grain size, the average grain area, the average quadratic deviations of these values, the specific surface of grain boundaries, determining the degree of grain inequality, the phase ratio, the proportion, type and nature of the distribution of non-metallic inclusions in steels and other indicators [105, 109], are used for the analysis and control of microstructure. It is important to note that these methods are not unambiguous and do not fully correspond to each other, which complicates the objective and accurate comprehensive assessment, justifying the relevance of the use of complex metallographic analysis based on the methods of qualimetry and mathematical statistics.

The basis of qualimetry is the principle of deriving a single numerical equivalent of quality (called a complex quality indicator,  $K_0$ ) from the hierarchical structure of the quality indicators of individual properties [121, 122-125]. Properties can be any number of many, as a rule, they are grouped into more common properties (mechanical, chemical, aesthetic, etc.). At the first stage, a property tree is always formed. The value of the contribution of each property (or group of properties) to the complex quality indicator is determined by the tree. Weight coefficients are assigned for each property. First, the group (tier) coefficients are determined, then, based on them, the weighting coefficients for each specific property. Herewith,

$$\sum \alpha'_i = \alpha'_g, \quad (10.1)$$

where  $\alpha'_i$  – weighting factor within a property group;  
 $\alpha'_g$  – group (tier) weighting factor.

At the same time, each tier must comply with the condition:

$$\sum \alpha_i = 1, \quad (10.2)$$

where  $\alpha_i$  – weight ratio:  $0 \leq \alpha_i < 1$ .

Then define the method of consolidating the assessments of individual properties to obtain a complex quality indicator  $K_0$ . The simplest and most common way is shown in the formula (10.3):

$$K_0 = \sum_1^n \alpha_i k_i, \quad (10.3)$$

where  $k_i$  – single quality indicator.

Also known option:

$$K_0 = \prod_1^m k_i^{\alpha_i}. \quad (10.4)$$

The feature of the second option is that the zero value of any quality indicator turns into zero the entire expression, whereas in the first, the zero value of one of the indicators only reduces the overall score.

There is a reasonable question that the simple distribution of numerical weighting coefficients is not sufficient to determine the contribution of each property to quality. For example, a product with an inappropriate content of some elements of the chemical composition, with satisfactory mechanical properties can be used, while the discrepancy of the geometry of the product to the system of the accepted tolerances and landings (especially the lower deviation for the shaft and the upper for the hole) is a clear defect with arbitrarily outstanding other properties.

In this regard, in addition to the accepted hierarchical distribution of properties in the hierarchy, it is also advisable to divide all single properties into dominant and compensating properties in parallel (in the terminology of G.S. Gun).

The objective function of information  $K_0$  must have special properties: the zero value of any of the dominant indicators causes a zero value of the complex indicator, the zero value of a single compensated indicator does not entail a reduction to zero of the complex indicator. These properties allow to take into account not only the quantitative difference in the significance of individual indicators, but also the qualitative or otherwise – the status of the dominant or compensated indicator. This division of quality parameters most fully reflects the specifics of the products of different industries [126].

The function is a so-called "convolution". For a single convolution of the estimated function can be used, grounded in the works of G.S. Gun [126-131]:

$$K_0 = \left[ \prod_i D_i^{\alpha_i} \cdot \sum_j \beta_j k_j \right]^{0,5}, \quad (10.5)$$

$$\sum_i \alpha_i = 1; \sum_j \beta_j = 1,$$

where  $\alpha_i$  and  $\beta_j$  – the parameters of the dominant and compensated weighting of indicators;

$D_i$  – quality assessment for the  $i$ -th dominant figure;

$k_j$  – assessment of the quality of  $j$ -th compensated indicator.

The above function is not without drawbacks. There are also other methods of convolution, but as a rule, they are highly complex, and often also represent some applied special cases. In this regard, it can be recommended, with a relatively small property tree and a small number of dominant properties, to use the formula (10.3) with a logical condition of zero reversal of the entire function, with a zero value of one of the dominant indicators. This makes it much easier to set the target function in many applications (such as MS Excel).

Now, we need to somehow assess the quality of individual properties, and thus derive a single (differentiated) quality indicator for each property. In fact, this is a rationing operation. It involves the following tasks:

1) all differentiated quality indicators of all properties (normalized values) should be in the same range, which corresponds to the range within which the complex quality indicator should change (usually [0;1]);

2) adequate rationing limits, that is, the boundaries of the area of natural values of the property relative to which the normalization is performed (often these values are set by standards, or are reference, otherwise set by the researcher);

3) adequate direction of the normalization function. Function can: increase; decrease; increase to a certain value, and then decrease; according to the principles of evaluation "the more the better", "the less the better", or on both sides tends to the reference value (also known as Z, S and a type of functions);

4) the form of the normalization function, the quality assessment can vary linear, or one of the nonlinear methods or a combination of them (exponentially, trigonometrically, etc.), this also includes such special cases of A-functions as asymmetry and trapezidity (fixed "area" of the highest value in the place of the maximum A-normalization function) and all their combinations;

5) each unit property is assigned individually the normalization boundaries, direction and form of the normalization function.

In accordance with this, we will analyze the methods of rationing. Typically, a function requires specifying the boundaries of the regulation. This is not difficult if there are established standards. If they do not satisfy the researcher, or none at all, they are assigned from the subjective representations of the researcher, or, use special methods of rationing that do not require predetermined strict boundaries and operating moments of distribution of higher orders (such as dispersion). Such methods are quite complex and cumbersome. Let's start with one of these techniques, also known as empirical [121].

Finding a differentiable quality index is reduced to the normalization of the natural values of this property, and subsequent processing according to the double exponential Harrington distribution law [132].

$$k_{ij} = \exp[-\exp\{-Y_{ij}[R_{ij}(r_{ij})]\}], \quad (10.6)$$

where  $r_{ij}$  – the natural value of the qualimetric assessment obtained from the measurements;

R and Y – normalized values.

The processing function, also known as the desirability function, serves to smooth the normalized value, and to clearly differentiate the estimates on the desirability scale (table 10.1). The function is shown in figure 10.1.

As you can see, in order to get a high score, the normalized values must be greater than 1 (score ~ 0.63). Moreover, the zero value of the normalized index gives ~ 0.37. Thus, the final score tends to 1 for any value greater than 2 (score 0.8) and tends to zero for any value less than -0.5 (score 0.2). This is convenient for unambiguous assessment of the obtained quality level.

Table 10.1 – Desirability scale

Dimensionless scale	Indicator $K_0$	Quality level
Very good	0,80 ... 1,00	Etalon
Good	0,63 ... 0,80	Premium grade
Satisfactory	0,37 ... 0,63	1 <sup>st</sup> grade
Bad	0,20 ... 0,37	2 <sup>nd</sup> grade
Very bad	0,00 ... 0,20	Defect

$$y = \exp(-\exp(-x))$$

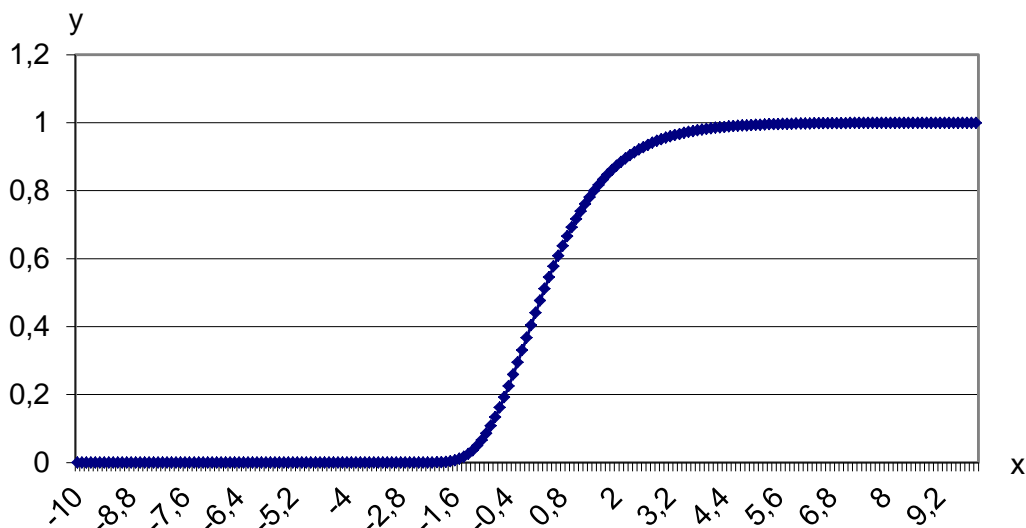


Figure 10.1 – Harrington desirability function

However, this requires a special normalization function that provides the desired range of values. This function does not depend on preset quality limits. The quality assessment is based solely on the characteristics of the distribution of the estimated value. The border quality is determined based on the average values, dispersion, distribution, and empirical coefficients. Set 6 boundaries (numerically equal to the constants  $A_1 \dots A_6$ ). Depending on the range in which the estimated value falls, the corresponding empirical normalization formula is applied [133-134]. All formulas correspond to the linear method of normalization of Z-type.

Constants  $A_1 \dots A_6$  are determined by empirical relations:

$$\left. \begin{aligned} A_1 &= \bar{r} + \alpha_1 \frac{S}{\sigma_N} ; & A_2 &= \bar{r} + \alpha_2 \frac{S}{\sigma_N} ; \\ A_3 &= \bar{r} - 2 \cdot S ; & A_4 &= \bar{r} + 2 \cdot S ; \\ A_5 &= \bar{r} - \alpha_2 \frac{S}{\sigma_N} ; & A_6 &= \bar{r} - \alpha_1 \frac{S}{\sigma_N} , \end{aligned} \right\} \quad (10.7)$$

where  $\bar{r}$  – arithmetic mean of the indicator  $r_i$ , obtained from a sample of N experimental values;

S – standard deviation;

$\alpha_1$  and  $\alpha_2$  – coefficients determined from equations (10.10);

$\sigma_N$  – parameter determined from equation (10.11).

Here to calculate the  $Y^*$  parameter at the condition  $A_j > A_{j+1}$ , the following relations are used (10.8):

$$\left. \begin{aligned} Y^* &= 0,48165 \frac{r_{ij} - A_1}{A_2 - A_1} - 0,47588, & r_i &\in [A_1, A_2) ; \\ Y^* &= 0,76634 \frac{r_{ij} - A_2}{A_3 - A_2} + 0,00577, & r_i &\in [A_2, A_3) ; \\ Y^* &= 0,72783 \frac{r_{ij} - A_3}{A_4 - A_3} + 0,77211, & r_i &\in [A_3, A_4] ; \\ Y^* &= 0,75043 \frac{r_{ij} - A_4}{A_5 - A_4} + 1,49994, & r_i &\in (A_4, A_5] ; \\ Y^* &= 2,348971 \frac{r_{ij} - A_5}{A_6 - A_5} + 2,25037, & r_i &\in (A_5, A_6] . \end{aligned} \right\} \quad (10.8)$$

For the case  $A_j < A_{j+1}$  it is necessary to use the relations (10.9):

$$\left. \begin{aligned} Y^* &= 0,48165 \frac{A_1 - r_{ij}}{A_1 - A_2} - 0,47588, & r_i &\in [A_1, A_2); \\ Y^* &= 2,348971 \frac{A_5 - r_{ij}}{A_5 - A_6} + 2,25037, & r_i &\in (A_5, A_6]. \end{aligned} \right\} \quad (10.9)$$

At the same time, for the intervals  $[A_2, A_3)$ ,  $[A_3, A_4]$ ,  $(A_4, A_5]$  for the dependencies (10.9), the relations (10.8) remain valid. The coefficients  $\alpha_1$  and  $\alpha_2$  are determined from the relations:

$$\alpha_1 = Y_N - 7,565 \frac{\sigma_N}{\sqrt{N}} - 2,97; \quad (10.10)$$

$$\alpha_2 = Y_N - 2,97,$$

where parameters  $Y_N$  and  $\sigma_N$  can be found from work [123] or determined by dependencies:

$$\begin{aligned} Y_N &= a + b \cdot \ln N; \\ \sigma_N &= c + d \cdot \ln N. \end{aligned} \quad (10.11)$$

Empirical coefficients  $a$ ,  $b$ ,  $c$  and  $d$  are obtained by mathematical processing of experimental data. The values of these coefficients for different sample sizes are presented in table 10.2.

For a more visual visualization of the method, two graphs were taken as an example from the work [140], devoted to the analysis of the quality of rolling rolls (figures 10.2 – 10.3). These are graphs of the dependence of the empirical normalized value of the real hardness distribution of the barrel of the cold rolling rolls on their natural value (figure 10.2) and the dependence of the differentiated quality index  $k_i$  on the natural values of the estimated parameter (figure 10.3).

Table 10.2 – Values of empirical coefficients

N	$a$	$b$	$c$	$d$
$0 < N \leq 40$	0,490	0,0144	0,725	0,1134
$40 < N \leq 80$	0,473	0,0192	0,862	0,0757
$80 < N \leq 150$	0,504	0,0121	0,923	0,0616

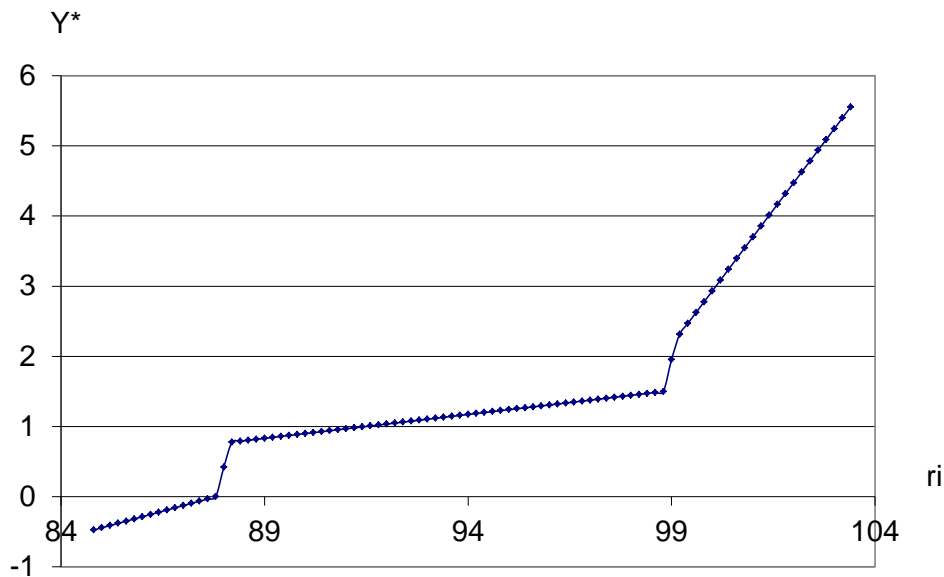


Figure 10.2 - Graph of dependence of the value of roll barrel hardness normalized by empirical method on their natural value

When plotting the graph, the boundary points  $A_1 \dots A_6$  for the original sample were fixed and the distribution of the natural value within  $(A_1; A_6)$  was constructed. According to the graph the sharp, almost discrete transitions are clearly visible

when using different formulas corresponding to the given ranges. The boundary points  $A_1 \dots A_6$  and the distribution characteristics used for this graph are respectively:  $r_i - 93,63$ ;  $S_i - 1,35$ ;  $A_1 - 84,79$ ;  $A_2 - 87,84$ ;  $A_3 - 88,14$ ;  $A_4 - 98,82$ ;  $A_5 - 99,12$ ;  $A_6 - 102,16$ .

The dependence of the differentiated quality index  $k_i$  on the natural values of the estimated parameter (figure 10.3) shows the smoothing of the significance growth with the increase of the natural value, as well as a particularly sharp transition in the range of  $k_i$  values (0.37; 0.62). This suggests that even small fluctuations in the natural value in the  $A_2$  boundary area lead to a significant change in the differentiated quality indicator.

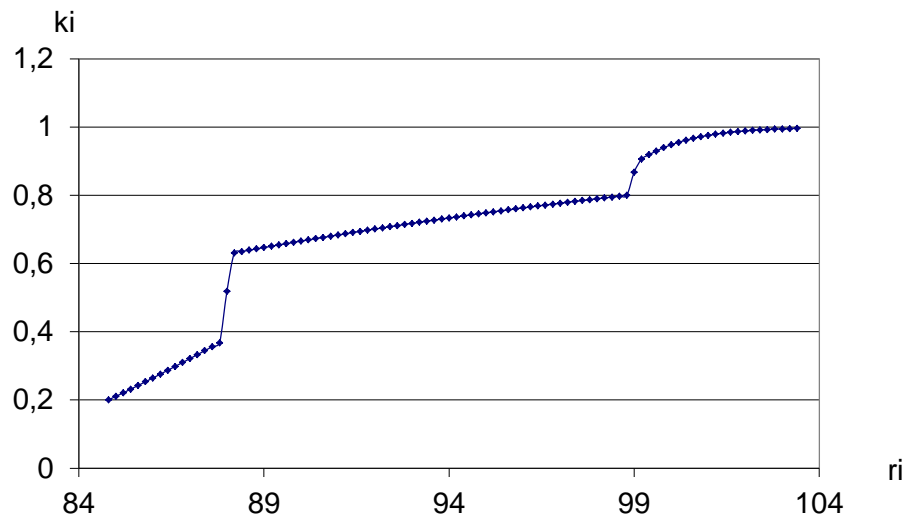


Figure 10.3 – The dependence of the differentiable quality indicator  $k_i$  from the natural values of the estimated parameters (the hardness of roll barrel)

The advantage of this method, as already mentioned, is the ability to work without pre-defined normalization boundaries. This is important when researching new materials and processes. Also, the method allows you to quickly, clearly and unambiguously evaluate and compare the resulting level of quality on a scale of desirability.

The following features limit the use of the technique, in any case, they need to pay attention to the choice and use of methods of rationing:

1) in principle, it is impossible to use this technique in the current edition to estimate quantities with rigidly specified quality limits (tolerances, chemical composition, etc.), since even the values outside the limits (defects) get high evaluation;

2) the increasing Z-shaped character of normalization makes incorrect the use of this technique in the current version to assess the quality of quantities on the principle of "the more, the worse" (S-type, for example, harmful impurities) or A-type (two-side border: for example, tolerance);

3) for almost any sample corresponding to the normal distribution, this method gives approximately the same estimates equal to 0.73. In other words,

"quality" means the minimum spread of values and its compliance with the normal distribution law;

4) in this regard, the possible incompatibility of simultaneous application with other methods of rationing, since, in fact, the main range of estimates is in the range (0.62 ÷ 0.82), which can cause incorrectness, in the derivation of a complex quality indicator, and actually violates the condition (10.1) of the common principles of rationing;

5) relatively low sensitivity of the method, for the possibility of real comparison of quality indicators, calculations must be made with an accuracy of 4, 5 or more decimal places;

6) it is possible to obtain more different estimates, it is necessary to calculate the variance and average (and, accordingly, the boundaries  $A_1...A_6$ ) for the general set, and then, separately compare the resulting quality indicators.

Restrictions (10.1) and (10.2) are bypassed by the introduction of a preliminary rationing operation by any suitable method (however, already require the definition of rationing boundaries). Then, the normalized value is normalized again according to the described method. Simplistically, this can be represented as a formula with preliminary rationing by the linear method:

$$k_i = \exp\{-\exp[-\langle\langle\text{empirical}\rangle\rangle(\langle\langle\text{linear}\rangle\rangle)]\}, \quad (10.12)$$

An example of the dependence of the differentiated quality index  $k_i$  on the natural values  $r_i$  (0.2; 0.66) by the formula (10.12) is shown in figure 10.4.

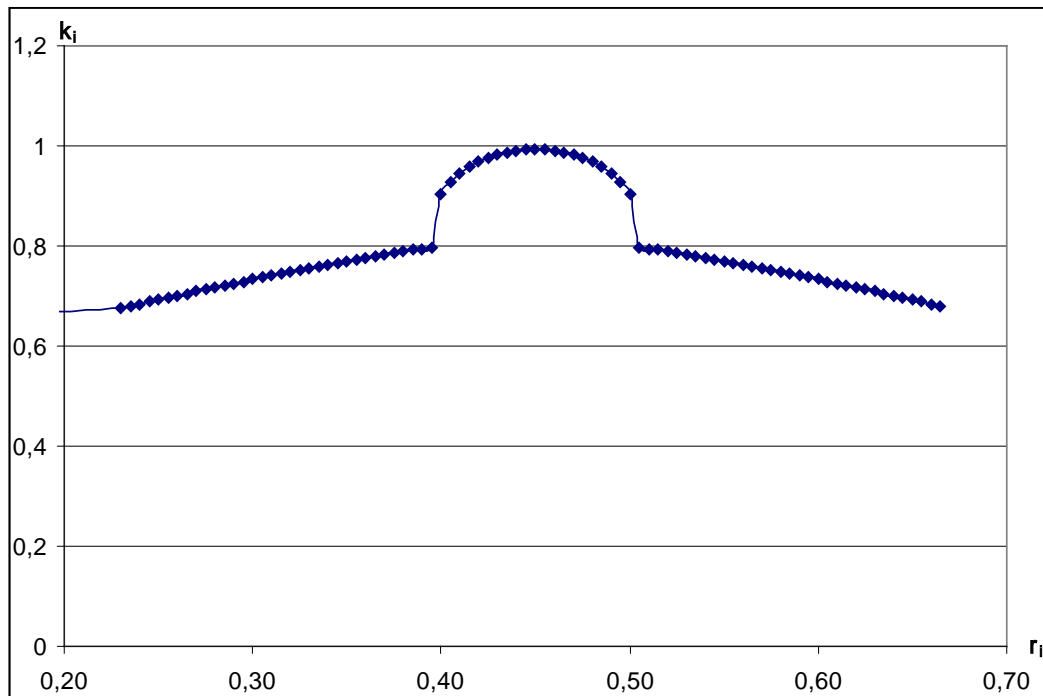


Figure 10.4 - Dependence of  $k_i$  on natural values of  $r_i$  by the formula (10.12)

In this method of calculation the differentiated quality index  $k_i$  behaves adequately, but:

1) the lower limit  $k_i$  starts at 0.647. According to the accepted linear normalization, all values of which are in the range (0;1), a lower estimate can not be obtained, therefore, for any normal distribution, the values of  $k_i$  will be in the range (0.6; 1). This is inconvenient and incorrect for comparison and work with indicators normalized in any other way;

2) in almost any nature of the distribution of the boundary values  $A_1 \dots A_6$  do not fit completely into the range (0; 1), and therefore, it may be advisable to take fixed values within (0; 1) for cases of work with already normalized in the range of data, or change the final formula, "pulling" the distribution of  $k_i$  in the desired range;

3) the already mentioned low sensitivity of the method becomes even lower, which, with an increase in the volume of calculations creates known problems.

The method was tested in works [135-136].

Now some known techniques for valuation with pre-sets the boundary values will be described. Such methods are simpler and usually include all 3 possible evaluation options (Z, S and A types). Let's start with the simplest and most common linear normalization technique [137].

Linear normalization function of Z and S types respectively (for responses limited on one side) (figure 10.5):

$$k_{ij} = \begin{cases} 0, & r < r_{\min}; \\ \frac{(r - r_{\min})}{(r_{\max} - r_{\min})}, & r \in [r_{\min}; r_{\max}]; \\ 1, & r > r_{\max}. \end{cases} \quad (10.13)$$

$$k_{ij} = \begin{cases} 0, & r < r_{\min}; \\ \frac{(r_{\max} - r)}{(r_{\max} - r_{\min})}, & r \in [r_{\min}; r_{\max}]; \\ 1, & r > r_{\max}. \end{cases} \quad (10.14)$$

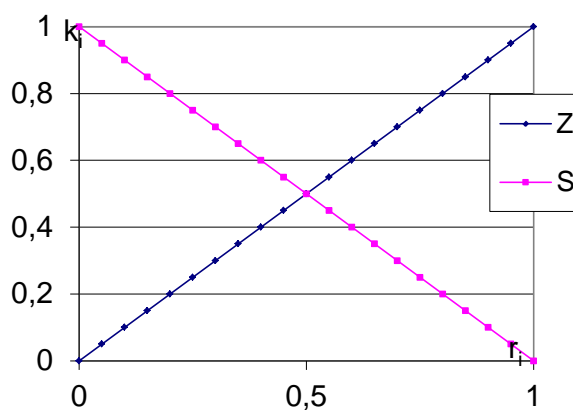


Figure 10.5 - Linear normalization functions of Z and S types

Linear function of A-type normalization (responses limited to two sides):

$$k_{ij} = \begin{cases} \frac{2(r - r_{\min})}{(r_{\max} - r_{\min})}, & r \in \left[ r_{\min}; \frac{r_{\min} + r_{\max}}{2} \right]; \\ \frac{2(r_{\max} - r)}{(r_{\max} - r_{\min})}, & r \in \left[ \frac{r_{\min} + r_{\max}}{2}; r_{\max} \right]; \\ 0, & r < r_{\min}, r > r_{\max}. \end{cases} \quad (10.15)$$

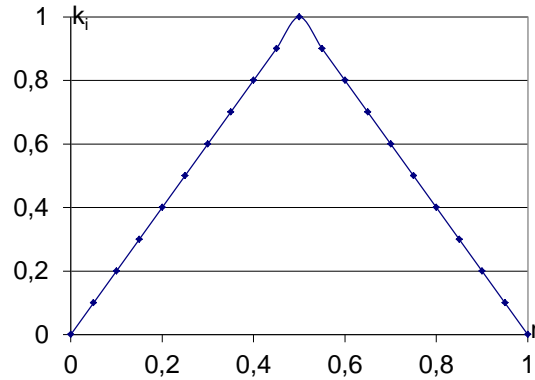


Figure 10.6 – Linear normalization function of A type

This technique is simple, reliable and clear, but the linear nature of the increase in the estimate may not satisfy everyone. Also, this method allows the construction of a trapezoidal function on the basis of A-type (10.13), by replacing the average value with two different values of the set range (for the left and right parts, respectively), the gap between which will form a "platform" at the top. In all other cases, the evaluation functions of a single quality indicator with a differentiated rate of change, that is, nonlinear, are used.

Let's consider trigonometric normalization functions of Z and S types respectively (figure 10.7) [137]:

$$k_{ij} = \begin{cases} 1, & r < r_{\min} \\ 0,5 + 0,5 \cos\left(\frac{(r - r_{\min})}{(r_{\max} - r_{\min})} \pi\right), & r \in [r_{\min}; r_{\max}]; \\ 0, & r > r_{\max}. \end{cases} \quad (10.16)$$

$$k_{ij} = \begin{cases} 0, & r < r_{\min} \\ 0,5 + 0,5 \cos\left(\frac{(r - r_{\max})}{(r_{\max} - r_{\min})} \pi\right), & r \in [r_{\min}; r_{\max}]. \\ 1, & r > r_{\max}. \end{cases} \quad (10.17)$$

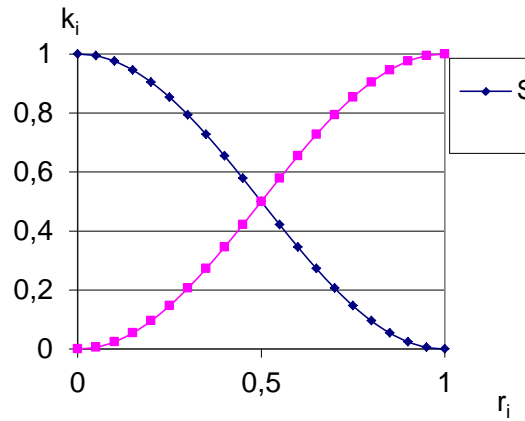


Figure 10.7 – Trigonometric normalization functions of Z and S types

By double compressing the X-axis and shifting the function (10.15) by  $\pi$  to the left along the ordinate axis, we derive the trigonometric A-type normalization function (figure 10.8):

$$k_{ij} = \begin{cases} 0, & r < r_{\min} \\ 0,5 + 0,5 \cos\left(\pi - \frac{2(r - r_{\max})}{(r_{\max} - r_{\min})} \pi\right), & r \in [r_{\min}; r_{\max}] \\ 0, & r > r_{\max} \end{cases} \quad (10.18)$$

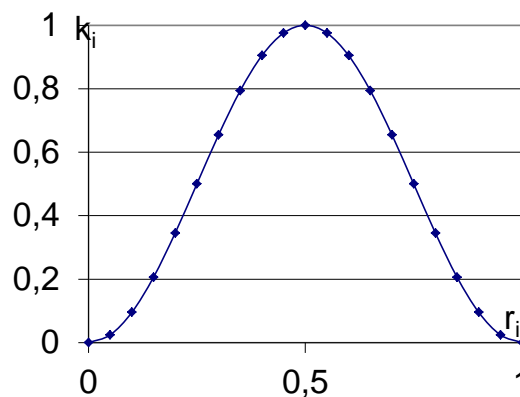


Figure 10.8 – Trigonometric normalization functions of A type

As it can be seen, functions are relatively simple to implement, and can replace linear functions of the corresponding types, where a smoother estimate near the boundary points is required. An important distinctive feature of the technique is the simultaneous smooth transition from the lowest to the highest assessment.

The following family of functions is based on the use of degree [134]. Most simply normalize the parabola, but this does not preclude the use of other degrees. Normalization can be carried out both on the concave and on the convex branch of the parabola. The functions of regulation Z and S types by concave branch are presented on figure 10.9 a:

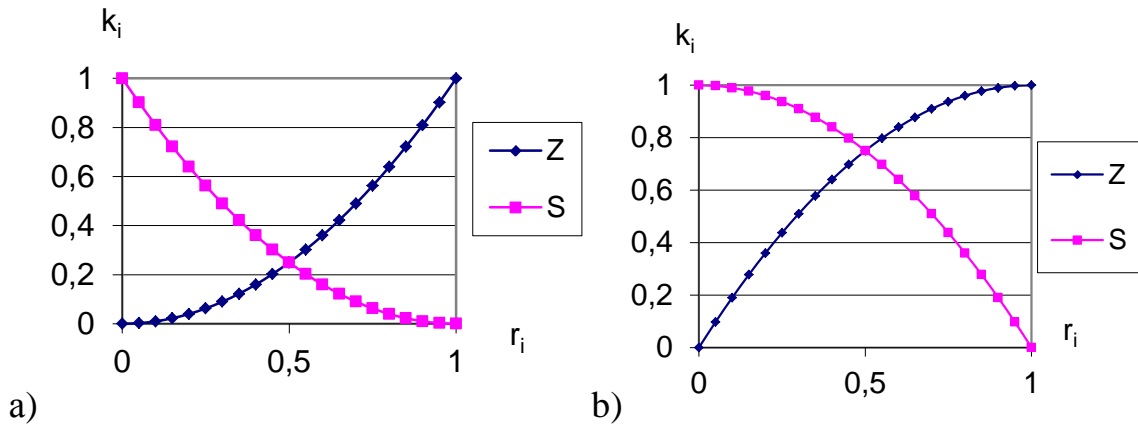
$$k_i = \frac{(R_i - R_{\min})^2}{(R_{\max} - R_{\min})^2}; \quad (10.19)$$

$$k_i = \frac{(R_i - R_{\max})^2}{(R_{\max} - R_{\min})^2}. \quad (10.20)$$

Normalization functions of Z and S types by convex branch are presented on figure 10.9 b):

$$K_i = 1 - \frac{(R_i^\sigma - R_{\max})^2}{(R_{\max} - R_{\min})^2}; \quad (10.21)$$

$$K_i = 1 - \frac{(R_i^\sigma - R_{\min})^2}{(R_{\max} - R_{\min})^2}. \quad (10.22)$$



a) – normalization on the parabola concave branch; b) – normalization on the parabola convex branch.

Figure 10.9 – Degree normalization functions of Z and S types

$$k_i = 1 - \frac{2^n \cdot \left( \left( \frac{r_{\min} + r_{\max}}{2} \right) - R_i \right)^n}{(R_{\max} - R_{\min})^n}. \quad (10.23)$$

Degree normalization function of A-type for different values of degree n is shown in figure 10.10.

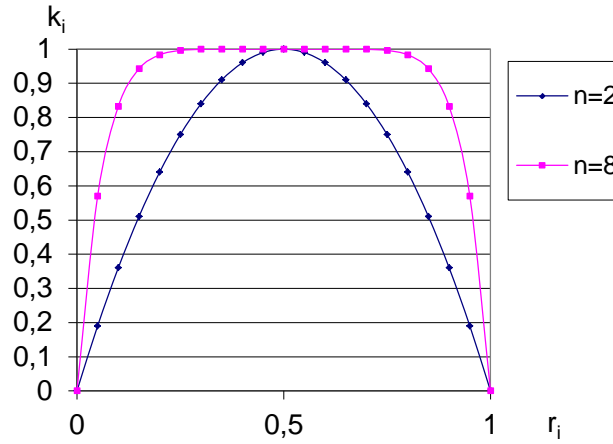


Figure 10.10 – Degree normalization function of A-type at n=2 and n=8

The degree method differs from the trigonometric one in that either the upper part of the function is smoothed at the sharp lower or the lower one at the upper sharp edge of the function (the first case also applies to the A-type). The last two methods (trigonometric and degree) have an important advantage in the fact that the functions of A-type of these methods are represented by only one relatively simple formula. This greatly simplifies the calculation, eliminating the many logical conditions in the normalization. Using the formula (10.21) allows you to build a "site" at the level of evaluation 1. This is achieved by increasing the degree, but occurs very abruptly.

Also, a number of restrictions on the ability to smoothly change the shape of the function, change the degree of convexity or concavity, especially in the case of A-type function. The use for concave and convex forms of degree normalization function of different types of formulas can also be attributed to the disadvantages.

From all these techniques, only linear method allows the use of asymmetric dependencies A-type, which can be useful if the desired optimum is not exactly in the middle between the boundary values, and offset.

The function proposed in our case is based on the well-known method [121] (formula 10.24), which initially provides only for the Z-type function. Since this technique has excellent characteristics (flexibility of changing the rate of increase of the estimate and the relative simplicity of calculation), it makes sense to derive the entire complex of normalization functions not only for the Z-type function.

The method of rationing in this technique is based on the exponential function. The linear normalization of the property occurs in the exponent, while the degree base serves as a measure of the steepness of the function. The s-type function is obtained by replacing the exponent numerator:

$$k_i = \begin{cases} 1 - \frac{1 - \Delta^Z}{1 - \Delta}, & Z = \frac{(r - r_{\min})}{(r_{\max} - r_{\min})}, r \in [r_{\min}; r_{\max}]; \\ 0, & r < r_{\min}, r > r_{\max}. \end{cases} \quad (10.24)$$

$$k_i = \begin{cases} 1 - \frac{1 - \Delta^Z}{1 - \Delta}, & Z = \frac{(r_{\max} - r)}{(r_{\max} - r_{\min})}, r \in [r_{\min}; r_{\max}] \\ 0, & r < r_{\min}, r > r_{\max}. \end{cases}, \quad (10.25)$$

where  $\Delta$  – degree base affecting the shape of the function.

Both types of functions are shown in figure 10.11, with a degree base value of 0.05.

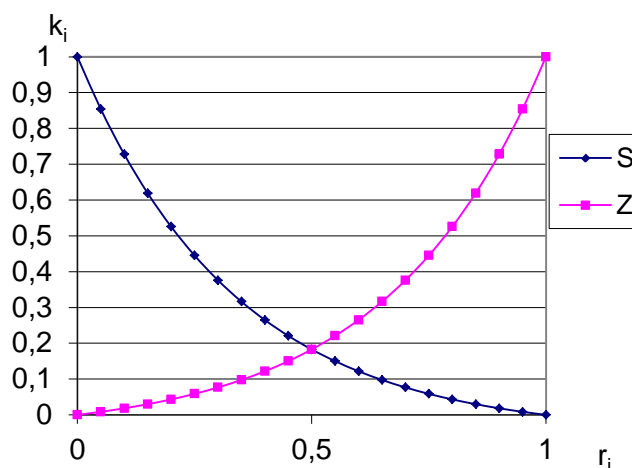


Figure 10.11 – Exponential normalization functions of Z and S types at  $\Delta=0,05$

The function is relevant for the estimation of quantities limited on the one side. Moreover, the significance of the value increases (or decreases) exponentially as it approaches the corresponding boundary. The basis of degree  $\Delta$  is crucial. By changing it, you can smoothly vary:

- concavity of the function, at  $\Delta < 1$  (optimal value 0.05);
- convexity of the function, at  $\Delta > 1$  (optimal value 10);
- zoom function to linear view at  $\Delta \rightarrow 1$ .

However,  $\Delta=1$  can not be used, since the denominator of the function turns to zero, but the use of  $\Delta=0.99$  gives a picture virtually indistinguishable from the linear. Different variants of changing the degree base  $\Delta$  are shown on the example of the S-type function in figure 10.12.

Now, we derive the A-type normalization function. The use of one formula, like (10.16) or (10.21) is impossible, because the exponential dependence has no inflection points, unlike parabola or periodic functions, so we divide the region in half between the boundary points, set the condition, and assign each of the resulting ranges its formula:

$$k_i = \begin{cases} 1 - \frac{1 - \Delta^{Z_1}}{1 - \Delta}, Z_1 = 1 + \frac{2 \cdot (r_{\min} - r)}{(r_{\max} - r_{\min})}, r \in \left[ r_{\min}; \frac{r_{\min} + r_{\max}}{2} \right]; \\ 1 - \frac{1 - \Delta^{Z_2}}{1 - \Delta}, Z_2 = 1 + \frac{2 \cdot (r - r_{\max})}{(r_{\max} - r_{\min})}, r \in \left[ \frac{r_{\min} + r_{\max}}{2}; r_{\max} \right]; \\ 0, \quad r < r_{\min}, r > r_{\max}. \end{cases} \quad (7.26)$$

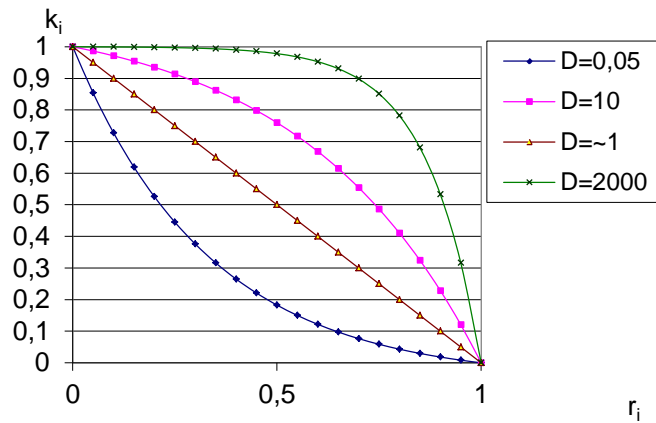


Figure 10.12 – The exponential normalization S-type function at different degree base ( $\Delta=0,05$ ;  $\Delta=10$ ;  $\Delta \rightarrow 1$ ;  $\Delta=2000$ )

Normalization A-type function for several versions of the degree base is shown in figure 10.13. Also, this technique allows to build A-type functions with asymmetry and trapezoidal (fixed "platform" of the highest value in the place of the maximum A-type normalization function), it is also possible to build functions with different types of steepness of branches and all sorts of combinations.

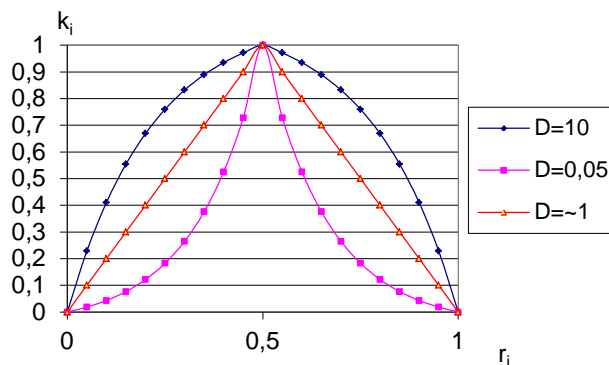


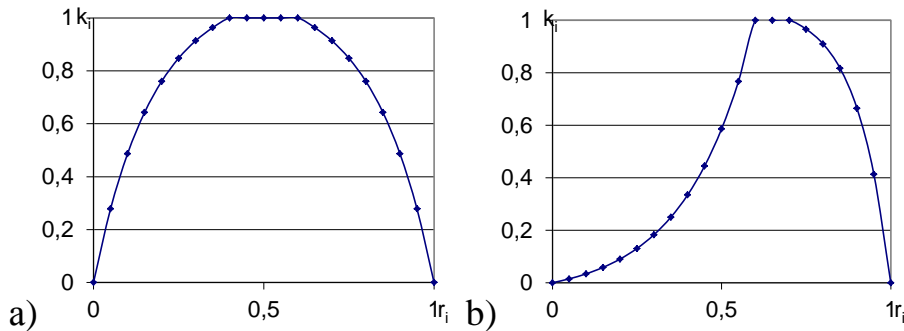
Figure 10.13 – The exponential normalization A-type function at different degree base ( $\Delta=10$ ;  $\Delta=0,05$ ;  $\Delta \rightarrow 1$ )

The proposed technique in the most common form will be as follows:

$$k_i = \begin{cases} 1 - \frac{1 - \Delta_1^{Z_1}}{1 - \Delta_2}, Z_1 = \frac{(c_1 - r_i)}{(c_1 - r_{\min})}, r \in [r_{\min}; c_1]; \\ 1 - \frac{1 - \Delta_2^{Z_2}}{1 - \Delta_2}, Z_2 = 1 - \frac{(r_{\max} - r_i)}{(r_{\max} - c_2)}, r \in [c_2; r_{\max}]; \\ 0, \quad r < r_{\min}, r > r_{\max}; \quad 1, \quad r \in [c_1; c_2]. \end{cases} \quad (10.27)$$

where  $c_1$  – start point of "platform »;  
 $c_2$  – end point of "platform »;  
 $\Delta_1$  – degree base of the left part of function (affects the shape);  
 $\Delta_2$  – degree base of the right part of function (affects the shape).

If  $c_1 = c_2 = r_{cp}$  and  $\Delta_1 = \Delta_2$ , then we obtain the formula (10.19), as a special case of a symmetric non-trapezoidal A-type function. If  $c_1 = c_2 = r_{\max}$  and  $\Delta_1 = \Delta_2$ , we get a Z-type function (10.22). Examples of different options are shown in figure 10.14.



a) symmetrical trapezoidal ( $c_1 = 0,4$ ;  $c_2 = 0,6$ ;  $\Delta_1 = \Delta_2 = 10$ );  
b) asymmetrical trapezoidal ( $c_1 = 0,6$ ;  $c_2 = 0,7$ ;  $\Delta_1 = 0,05$ ;  $\Delta_2 = 20$ );

Figure 10.14 – Different variants of the exponential normalization A-type function

Figure 10.14 shows that:

- the proposed function makes it possible to change the significance of the property in a very wide range, and to do it not discretely (in contrast to the power technique) but smoothly;

- this technique includes a linear, convex and concave functions, which is convenient, with a variety of estimated properties that require a special approach to the evaluation of each, also, it is especially convenient, with an automated method of calculation, since you can set one technique for the entire array, the form of the function is responsible for only one variable, and this is true for all three types of functions;

- the form of the normalization function is close to the normal distribution curve, which distinguishes it from other methods;

- also this technique is preferable to trigonometric, since it is often required (for example, in the assessment of harmful impurities) that the assessment, gradually increasing from the permissible limit, sharply increases the significance at the opposite border, this requirement is most met by the exhibitor;

- however, the function essentially excludes the simultaneous smooth transition from the lowest to the highest estimate, in contrast to the trigonometric technique, however, this limitation can also be circumvented by creating an additional condition and " splicing " of branches not by X, but by the Y axis, thus, in the most common form, the technique will be 4 functions, delimited by conditional quarters, which will allow to give the normalization at any form;

- A-type normalization allows the possibility of creating a "platform" of a given length at the level of the highest estimate by replacing the average value with two different values of the set range (for the left and right parts, respectively);

- A-type normalization allows for the asymmetry of the objective function, which allows you to set it with a variety of utility requirements when changing the criterion, is achieved by entering instead of the average value of the independent variable, and the corresponding adjustment of  $r_{\min}$  and  $r_{\max}$  for each of the ranges;

- also, it is possible to use functions with different variants of steepness of different branches of the A-type function.

These features allow to recommend a demonstration methodology for use as the common methodology for normalization of data.

AISI 321 steel subjected to deformation on the radial-shear rolling mill in three passes was selected for the qualimetric quality assessment.

For the qualimetric evaluation of the quality of the microstructure of steel AISI 321 as the base, such methods of quantitative metallographic analysis as determination of average grain size, the area of grains, the degree of grain inequality were used [105].

For the analysis of images of the structure the free software JMicroVision v1.2.7 from Nicolas Roduit was used. The program allows to automate the process of measuring the geometric characteristics of the grain. To do this, select the grain boundaries in automatic or manual mode. In this case, the manual mode was used, because grain boundaries were not enough contrast in all areas of all images for automatic recognition, which could lead to errors.

We will carry out the analysis on PEM-pictures after deformation. First, set the scale. To do this, open the image in the program, go to the tab Spatial Calibration and using a special tool measure the length of the scale mark in the photo, and then specify the length of the scale mark in nm. For these images, the scale was 5.6 pixels per 1 nm.

Then open the 2D Measurement tab, select the dimension of an arbitrary shape and trace the visible grain boundaries in turn. After manually marking the grain boundaries, the resulting shapes were automatically numbered (figure 10.15) and the above-mentioned geometric characteristics were calculated for them.

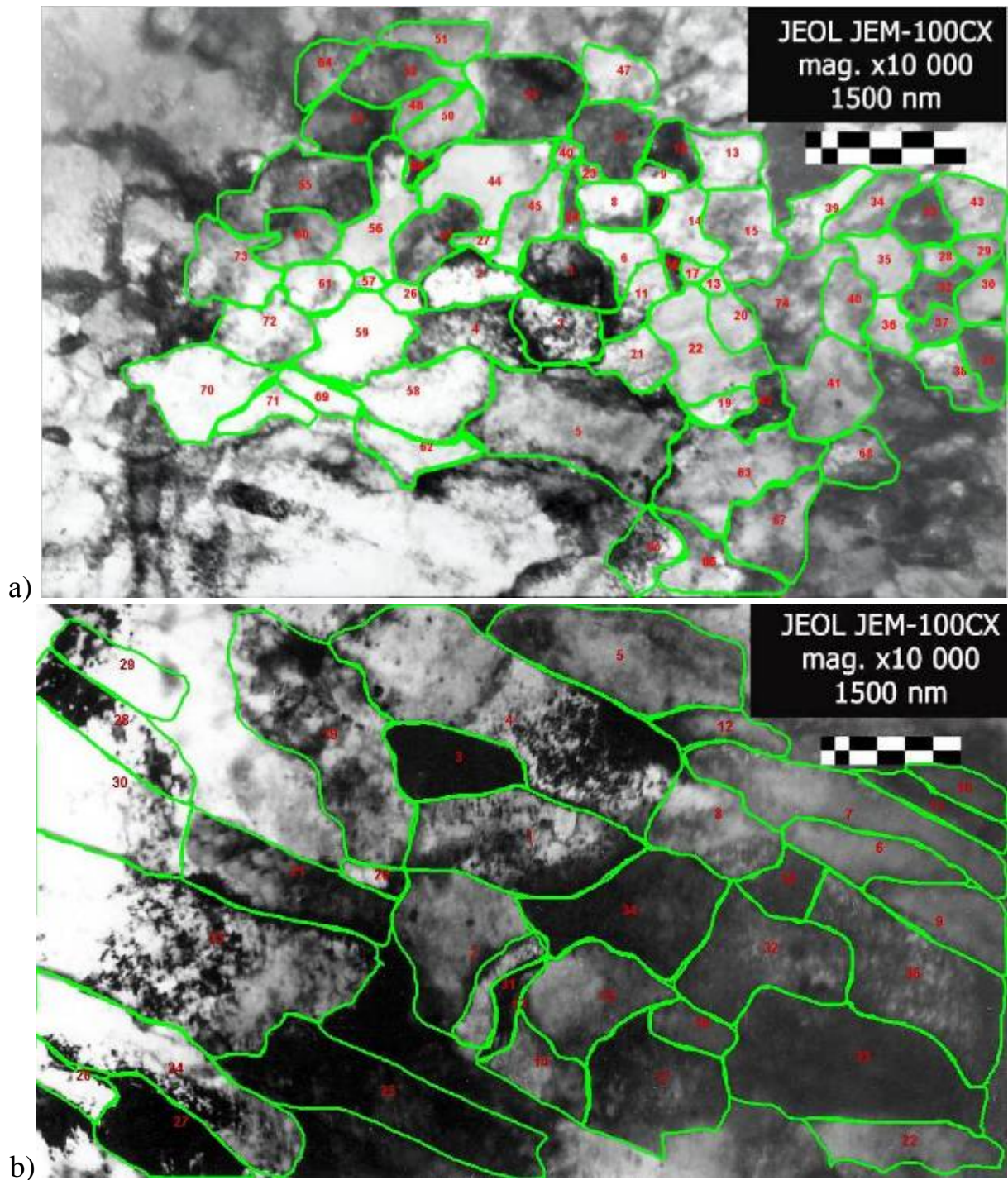


Figure 10.15 - Grain designations for images of the periphery (a) and the center (b) of the rod after deformation

If desired, the measured values can be visualized by selecting in Viewer tool - Label command and selecting the desired characteristic from the menu that appears. Thus, figure 10.16 shows the area values of some grains for the same pair of images of the structure after deformation.

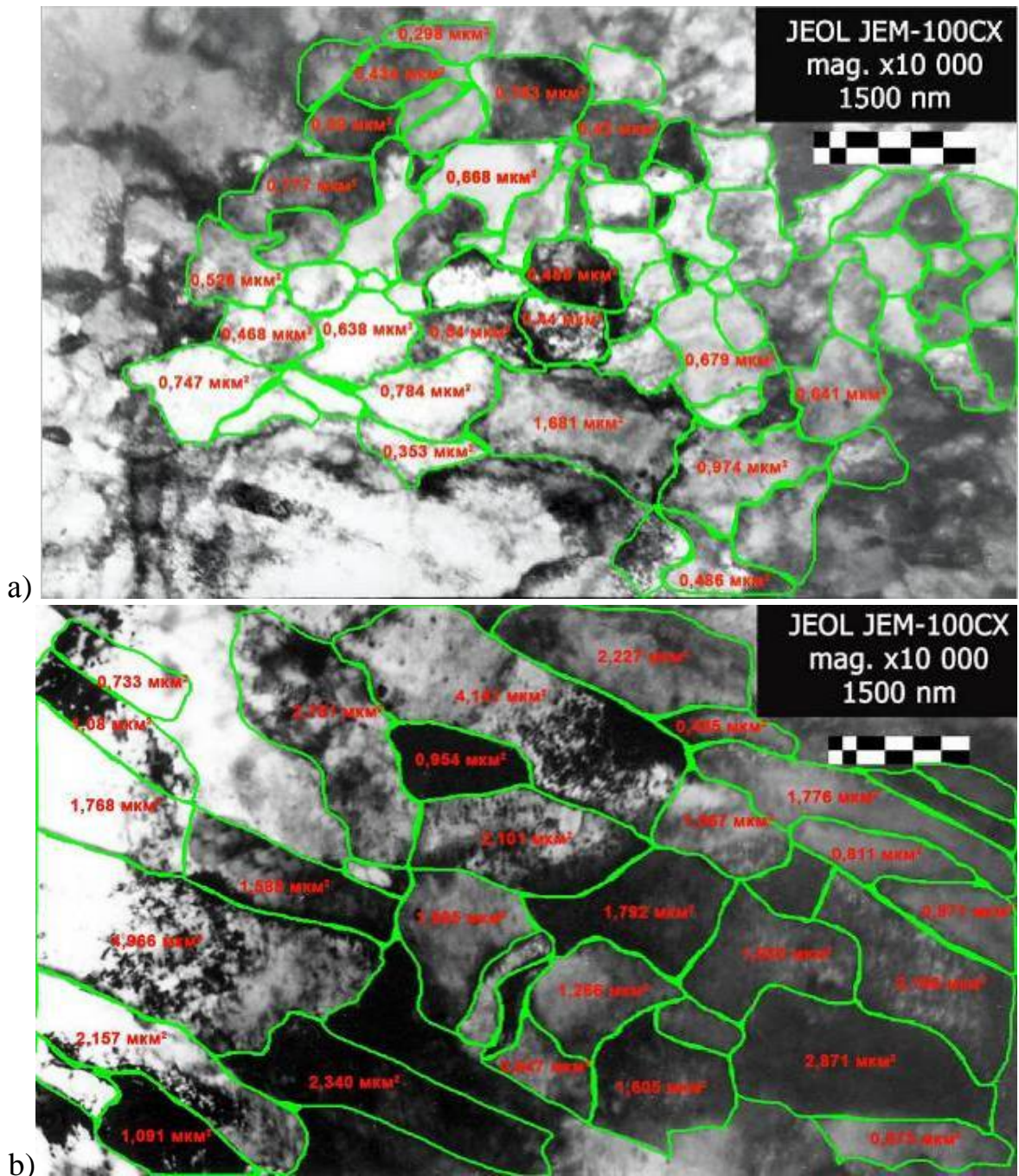


Figure 10.16 - Grain area of the periphery (a) and the center (b) of the rod after deformation

To work with geometric characteristics, open the Data Viewer tool, leave only the necessary characteristics in the table and copy them for further work in MS Excel. The program automatically determines the largest and smallest linear dimensions of the resulting shape, which are denoted as length and width. Figure 10.17 shows a screenshot of the Data Viewer tool window with a table of grain geometry characteristics.

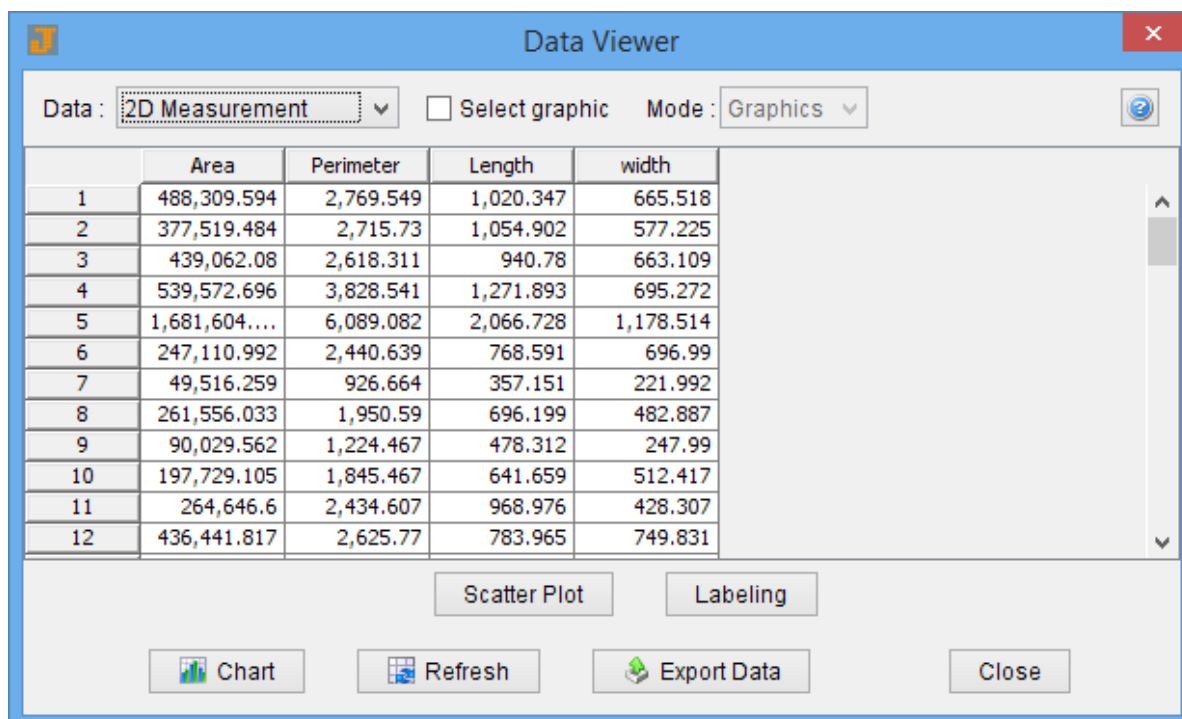


Figure 10.17 - Screenshot of the Data Viewer tool window with a table of grain geometric characteristics after the second pass

After importing the data into MS Excel, we calculate for each grain:

- average grain size, finding the arithmetic mean between length and width;
- the degree of grain inequality, as the ratio of length to width.

To calculate the complex quality index, we use the main geometric properties of the microstructure, which will make up the property tree and assign them the weighting coefficients. Then we define the boundaries of the normalization ranges. The lower bounds are assumed to be zero, and the upper ones will be rounded to the maximum value of the corresponding value of this property in the general set of all three passes. Then for each property we determine the type of the normalization function and its shape by selecting the parameter  $\Delta$ . To evaluate the quality and normalization of the selected properties, one-way boundaries and functions of Z and S types are best suited. Such properties as grain area and average grain size are rapidly gaining importance as the natural indicators of these properties decrease. The smaller the size and area of grain-the better. The degree of grain unevenness varies within [0;1]. The value 1 corresponds to the equiaxed grain, therefore, here we choose the Z-type function, the importance of which is growing rapidly as the natural value approaches 1. The form of normalization functions corresponds to the figure 10.11. The weighting coefficients are distributed equally and all the data are summarized in table 10.3.

Table 10.3 – Properties of the microstructure and coefficients of their ponderability

№	Property	Unit	Range		Function type	$\Delta$	Coefficient of ponderability
			min	max			
1	Grain area	nm <sup>2</sup>	0	3·10 <sup>6</sup>	S	0,05	0,33
2	Average grain size	nm	0	3000	S	0,05	0,33
3	Degree of grain inequality	-	0	1	Z	0,05	0,34

We show an example of calculating the complex quality index of the microstructure according to the second pass. Take the line of grain properties number 1 from table B1 of Appendix B, and using the formula (10.24) and the data of table 10.3 calculate the unit quality index by grain area:

$$k_i = \frac{1 - \Delta^{\frac{(r_i - r_{\min})}{(r_{\max} - r_{\min})}}}{1 - \Delta} = \frac{1 - 0,05^{\frac{(488310 - 0)}{(3000000 - 0)}}}{1 - 0,05} = 0,59.$$

Then we find, also according to the formula (10.24) a single indicator of quality for the average grain size:

$$k_i = \frac{1 - \Delta^{\frac{(r_i - r_{\min})}{(r_{\max} - r_{\min})}}}{1 - \Delta} = \frac{1 - 0,05^{\frac{(843 - 0)}{(3000 - 0)}}}{1 - 0,05} = 0,4.$$

After that, according to the formula (10.25) we find a single indicator of quality for the degree of inequality of grain:

$$k_i = \frac{1 - \Delta^{\frac{(r_{\max} - r_i)}{(r_{\max} - r_{\min})}}}{1 - \Delta} = \frac{1 - \Delta^{\frac{(0,65 - 0)}{(1 - 0)}}}{1 - \Delta} = 0,32.$$

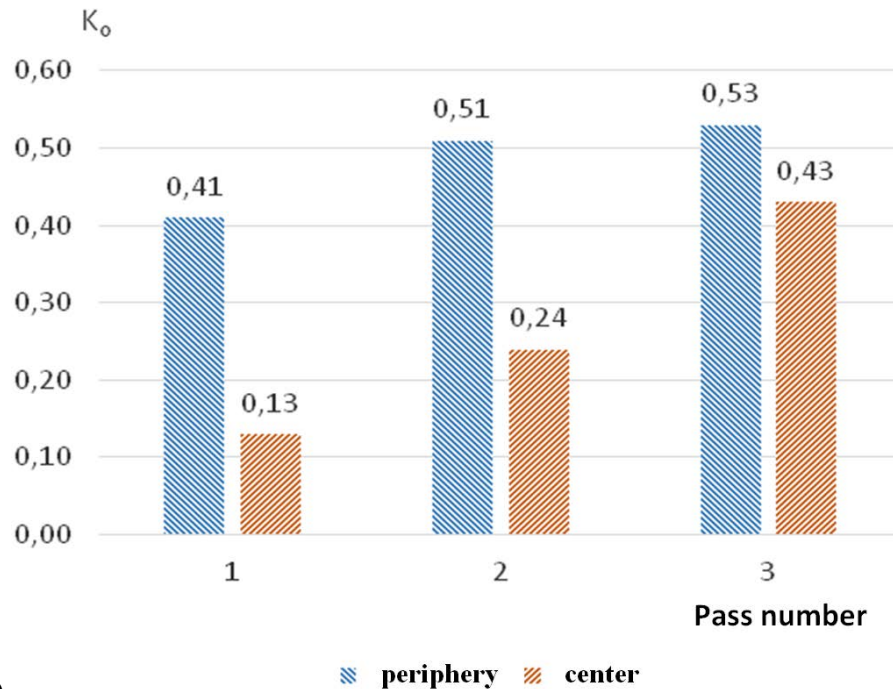
Now, according to the formula (10.3), we combine the calculated values into a complex quality index of grain no. 1:

$$K_0 = \sum_1^n \alpha_i k_i = 0,59 \cdot 0,33 + 0,4 \cdot 0,33 + 0,32 \cdot 0,34 = 0,44.$$

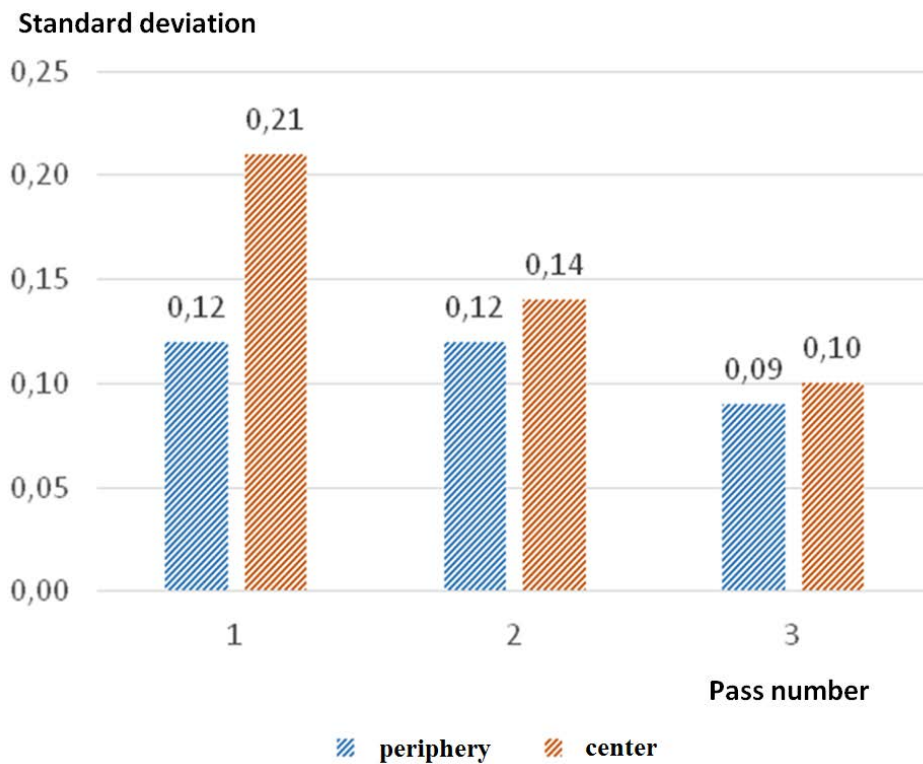
Similarly, find a comprehensive information for all detected grains. The result is summarized in a table. A fragment of the table of grain quality indicators of the periphery of the bar after the second pass is shown in Annex B-table B2.

Next, for the columns of quality indicators are average, minimum and maximum values, as well as the standard deviation, as a measure of the isotropy of

the microstructure. It is much more convenient to use the standard deviation for the complex quality index than for the areas of grain recommended in the classical work [105], because it becomes possible to compare the level of dispersion of structures of different sizes. The resulting values are grouped, for example, in our case by passes. After that, the results can be represented, for example, in the form of histograms (figure 10.18).



a)



b)

Figure 10.18 – Average values of complex quality index of the microstructure of steel AISI 321 for the passes (a) and its standard deviation (b)

In our case, the analysis of the complex quality index of steel AISI 321, subjected to 3 passes of deformation in the radial-shear rolling mill, shows that the greatest improvement in the experiences of the central area of the rod, from 0.13 to 0.43, that is more than 3 times. At the same time, the growth in the quality of the peripheral region is low (only 1.29 times) and tends to slow down. This is due to the fact that at a given temperature, with an increase in the degree of deformation, there is no further grinding of the structure, but only improves its shape, becoming more uniform, as also evidenced by the values of the standard deviation showing a minimum spread of values.

After the third pass, the quality of the microstructure of the central and peripheral parts is almost compared. The difference is 0.1, or 19 % compared to the difference of 0.28 (68 %) after the first pass. Grains become more equiaxed, but at the same time remain separate fragments of the former striped structure, as can be seen from figure 10.15 (b), whose irregular shape affects the assessment. At the same time, the number of such fragments gradually decreases, improving the structure.

## 11 RECOMMENDATIONS FOR THE IMPLEMENTATION OF A NEW COMBINED PROCESS "SCREW ROLLING – ECA-PRESSING" IN PRODUCTION

It is proposed to introduce into production a new technology for producing high-quality bars of ferrous and non-ferrous metals and alloys – the combined process "screw rolling – ECA-pressing". The developed technology will allow to obtain in industrial conditions a rod of ferrous and non-ferrous metals and alloys with ultra-fine-grained structure and an increased level of mechanical properties at lower energy and labor costs by reducing the number of passes rolling.

To implement the combined process "screw rolling – ECA-pressing" together with the screw rolling mill, it is necessary to use additional equipment – an equal-channel step matrix made in accordance with the developed drawing of this matrix (Annex A). Material for dies – stamp steel 5XB2C. The channel matrix needs to be polished.

The final heat treatment of the fabricated matrices after machining should be quenching and tempering. Heating of matrices assembled for quenching should be carried out in electric furnaces to a temperature of 880 °C. For a uniform distribution of temperature throughout the volume of the instrument should be carried out aging for 45 minutes at a temperature of tempering, after which it should be conducted by quenching in oil. The leave must be conducted at a temperature of 200 °C exposure time on release of 120 minutes (2 hours).

To increase the hardness and strength of the matrix should be subjected to heat treatment – quenching, at a temperature corresponding to the selected matrix for the manufacture of steel grade.

The diameter of the channel is selected according to the final diameter of the rod to be rolled. The channel lengths and the joint angle are selected in accordance with the drawing in Annex A, since the results of theoretical studies given in paragraph 7 show that the proposed channel joint angle and channel lengths provide the most favorable stress-strain state for obtaining an ultra-fine-grained structure and lower values of energy-power parameters.

To carry out the combined process "screw rolling – ECA-pressing" equal-channel step matrix must be placed directly behind the screw rolling mill, at a minimum distance from the working rolls.

Production of the rod according to the proposed technology for the combined the installation is the following:

The furnace is fed round billets with an initial diameter of 10-15% greater than the diameter of the matrix of the combined installation, to provide greater force due to compression in the rolls of the mill.

The matrix with the largest diameter of the channel is installed on the mill. The combined process is carried out. In this case, the subsequent blank pushes the previous one out of the matrix.

The last blank is extracted from the mill together with the matrix, and then extracted from the matrix.

The butt-end is straightened by rolling on the mill. Billets are put on heating. The current matrix is replaced by a smaller diameter matrix.

Preheated blanks are again processed by a combined process, but with a smaller diameter. In this case, the subsequent blank also pushes the previous one out of the matrix, and the last blank is extracted from the installation together with the matrix, and then from the matrix.

These operations are repeated several times, depending on the desired result and the characteristics of the equipment. At the same time, it is necessary to ensure that the butt-end of the last bar is always on the same side after all passes. This is necessary to reduce the consumption of metal in the trim. Once processing is complete, the butt-end is cut off.

This technology of metal forming can be used to produce high-quality bars of ferrous and non-ferrous metals and alloys. This method of deformation during its introduction into production does not require significant economic investments and can be implemented at industrial enterprises of the Republic of Kazakhstan for the production of metal bars as it does not require serious re-equipment of existing screw mills. Since for the implementation of this combined process, only the addition of a specially manufactured equal-channel step matrix intended for pressing the processed material through it is required in the design of the equipment.

Economic and energy efficiency of the technology of production of blanks on the proposed technology compared with the production technology of blanks produced by the traditional technology of multi-cycle equal-channel angular pressing is:

1) in reducing the number of deformation cycles necessary to obtain a uniform sub-structure-fine-grained structure from 6-8 with ECAP to 3 with a combined process "screw rolling – ECA-pressing", as evidenced by the comparison of ECAP steel research [12] with studies conducted in this work. This is possible due to the combination of severe deformation during screw rolling with severe deformation during ECAP in one process in one pass;

2) in a larger specific volume of material produced in one processing cycle by ensuring the continuity of the process. In ECAP, the length of one billet is usually limited to the value of about 10 of its diameters, while in the combined process of "screw rolling – ECA-pressing", the length of the billet can theoretically be arbitrarily large, but in practice it is likely to be tied to the industrial length of 6 m, or to the length of the working zone of the heating furnace, which in any case is disproportionately greater than the length of the billet in ECAP. It is also worth mentioning the time spent on changing the matrix in the combined installation and the supply of blanks to the press with traditional ECAP technology. Even if we take these costs equal to one cycle of processing the nominal length of the bar in 6 m, the production of combined installation of large batches, the gain in time will be obvious.

Thus, with comparable quality, productivity, and hence the efficiency of the combined installation "screw rolling – ECA-pressing" will be higher by at least 2 times.

## CONCLUSION

Thus, it can be concluded that the developed stand that implements the combined process "screw rolling – ECA-pressing" was tested for deformation by a new method of three different materials – technical copper M1, alloy structural steel AISI-5140 and complex alloyed stainless heat-resistant steel AISI-321. The deformation was carried out according to the same scheme for all three materials. The only difference was the temperature, approximately corresponding to the lower limit of the hot deformation temperature for the material, or slightly below it.

The conducted studies allow us to conclude that after a simple screw rolling in the rod, a two-layer structure with an equiaxed UFG surface and a striped oriented central zone is formed. These data are in good agreement with known research in this area.

Deformation on the combined technology for three passes allows to improve structure of the central zone of bars, having broken the focused striped structure. This is due to the non-monotonicity of deformation combined method. For steel AISI-5140, thus, it was possible to obtain a relatively uniform UFG structure with a predominance of large-angle intergranular boundaries and grain size of about 1  $\mu\text{m}$ . Also, this method of deformation leads to the release of chromium carbides of type  $\text{M}_3\text{C}$  in the structure of this steel with a size less than 1-0.2 microns. The greatest grain grinding up to 500-800 nm, achieved by deformation of steel AISI-321. This result is comparable with the results obtained on the same material by the traditional technology of equal-channel angular pressing for 6-8 cycles, which indicates a greater efficiency of the combined process compared to the traditional technology.

Mechanical properties in all cases increase uniformly, then somewhat slowing down its growth in the last passes, reaching a value of approximately 2-2.5 times from the original, which is comparable with the known results of studies of the influence of other SPD methods on the structure and properties of the materials under study.

A comprehensive quality assessment showed that the greatest improvement is experienced by the central bar area, from 0.13 to 0.43, that is, more than 3 times. At the same time, the quality growth of the peripheral region is low (only 1.29 times) and tends to slow down. This is due to the fact that at a given temperature, with an increase in the degree of deformation, there is no further refinement of the structure, but only improves its shape, becoming more uniform, as also evidenced by the values of standard deviation showing a minimum spread of values. The level of standard deviation in the central and peripheral zone is also almost compared after three passes.

Recommendations on application of the developed technology for production of a high-quality bar from ferrous and nonferrous metals and alloys were developed. This method of deformation during its introduction into production does not require significant economic investments and can be implemented at industrial enterprises of the Republic of Kazakhstan for the production of metal bars as it does not require serious re-equipment of existing screw mills.

Economic and energy efficiency of the proposed technology in comparison with the traditional technology of equal-channel angular pressing is to reduce the number of deformation cycles required to obtain a uniform sub-and ultra-fine-grained structure in 2 times and in a larger specific volume of material produced in one processing cycle by ensuring the continuity of the process.

Thus, with comparable quality, productivity, and hence the efficiency of the combined installation "screw rolling – ECA-pressing" will be higher by at least 2 times. All this indicates the prospects of using a new combined process "screw rolling – ECA-pressing" to produce long bars with sub-ultra - and ultra-fine-grained structure. Thus, it can be concluded that the proposed technology makes it possible to obtain long-length sub-and ultra-fine-grained materials with a structure and properties comparable to those obtained by other SPD methods, in particular ECAP. At the same time, the required set of properties is formed in fewer passes, and the developed installation has no restrictions on the length of the workpiece. This allows us to talk about the energy-saving advantages of the proposed technology and the prospects of its commercial application.

## REFERENCES

1. Валиев Р.З., Александров И.В. Объемные наноструктурные металлические материалы. Москва: Академкнига, 2007. - 398 с.
2. Структура и свойства нанокристаллических материалов / Ю.Р. Колобов, К.В. Иванов, Г.П. Грабовецкая, Р.К. Исламгалиев. - Екатеринбург: УрО РАН, 1999. -146 с.
3. Koch, C.C., Ovid'ko, I.A., Seal, S., Veprek, S. Structural nanocrystalline materials: Fundamentals and applications. Cambridge, England - Cambridge University Press, 2007. - 364 с.
4. Fabrication of bulk ultrafine-grained materials through intense plastic straining. Berbon, P.B., Tsenev, N.K., Valiev, R.Z., Furukawa, M., Horita, Z., Nemoto, M., Langdon, T.G. Metallurgical and Materials Transactions A: Physical Metallurgy and Materials Science Volume 29, Issue 9, 1998. – pp. 2237-2243.
5. R.Z. Valiev. Materials science: Nanomaterial advantage. Nature № 419 (6910) - pp. 887-889.
6. Пашинская Е.Г. Физико-механические основы измельчения структуры при комбинированной пластической деформации. Донецк: изд-во «Вебер», 2009. - 352 с.
7. Ефименко С.П. Современное состояние и перспективы развития теории обработки металлов давлением // Сталь. 2001. № 3. - С. 35-37.
8. Кайбышев О.А., Валиев Р.З. Границы зерен и свойства металлов. - Москва: Металлургия, 1987. - 214 с.
9. An investigation of grain boundaries in submicrometer-grained Al-Mg solid solution alloys using high-resolution electron microscopy. Horita, Z., Smith, D.J., Furukawa, M., Nemoto, M., Valiev, R.Z., Langdon, T.G. Journal of Materials Research. Volume 11, Issue 8, August 1996. – pp. 1880-1890.
10. Furukawa, M., Horita, Z., Nemoto, M., Langdon, T.G. The use of severe plastic deformation for microstructural control. Materials Science and Engineering. Volume 324, Issue 1-2, 15 February 2002. – pp. 82-89.
11. Terence G. Langdon. The characteristics of grain refinement in materials processed by severe plastic deformation // Rev. Adv. Mater. Sci. 2006. Vol. 13. - pp. 6-14.
- 12 The Hall-Petch relationship in nanocrystalline iron produced by ball milling. Jang, J.S.C., Koch, C.C. Scripta Metallurgica et Materiala. 24 (8), 1990. - pp. 1599-1604.
13. Koch, C.C. Synthesis of nanostructured materials by mechanical milling: Problems and opportunities. Nanostructured Materials Volume 9, Issue 1-8, 1997. – pp. 13-22.
14. Microstructures and properties of nanocomposites obtained through SPTS consolidation of powders. Alexandrov, I.V., Zhu, Y.T., Lowe, T.C., Islamgaliyev, R.K., Valiev, R.Z., Metallurgical and Materials Transactions A: Physical Metallurgy and Materials Science. Volume 29, Issue 9, 1998. – pp. 2253-2260.

15. Valiev, R.Z., Islamgaliev, R.K., Alexandrov, I.V. Bulk nanostructured materials from severe plastic deformation. *Progress in Materials Science*. Volume 45, Issue 2, 2000. – pp. 103-189.

16. Valiev, R.Z.. Superior strength in ultrafine-grained materials produced by SPD processing. *Materials Transactions*. Volume 55, Issue 1, 2014. - pp 13-18.

17. Zhilyaev, A.P., Langdon, T.G. Using high-pressure torsion for metal processing: Fundamentals and applications. *Progress in Materials Science* № 53 (6), 2008. - pp. 893-979.

18. The evolution of homogeneity in processing by high-pressure torsion. Xu, C., Horita, Z., Langdon, T.G. *Acta Materialia*. Volume 55, Issue 1, 2007. – pp. 203-212.

19. Alhamidi, A., Horita, Z. Grain refinement and high strain rate superplasticity in aluminum 2024 alloy processed by high-pressure torsion. *Materials Science and Engineering A*. Volume 622, 2015. – pp. 139-145.

20. S. Erbel, "Mechanical properties and structure of extremely strainhardened copper", *Met. Technol.* 12, 1979. – pp. 482–486.

21. Патент РФ № 2547984. Способ интенсивной пластической деформации кручением под высоким циклическим давлением (RU 2547984). Салимгареев Х. Ш., Валиев Р. З., Мурашкин М. Ю., Валиев Р. Р., Сабиров И. Н., Смирнов И. В. ФБГОУ "Санкт-Петербургский государственный университет" (СПбГУ). МПК С21J 6/04. опубл. 10.06.2012 г.

22. Патент РФ № 2391414, Способ обработки изделий из магнитно-мягких аморфных сплавов интенсивной пластической деформацией. Глезер А. М., Добаткин С. В., Перов Н. С., Плотникова М. Р., Шалимова А. В. ФГУП "ЦНИИчермет им. И.П. Бардина". МПК С21D 6/04. опубл. 10.06.2010 г.

23. Патент РФ № 2382687. Способ деформирования заготовки с обеспечением интенсивной пластической деформации и устройство для его осуществления. МПК В21J5/06, В21J13/02. Колмогоров Г. Л., Беляев А. Ю. ГОУ "Пермский государственный технический университет", опубл.: 27.02.2010.

24. Головин Ю.И. «Введение в нанотехнику». - М.: Машиностроение, 2007. – 240 с.

25. Капорович, Владимир Владимирович. Прессование профильного материала из стружки алюминиевых сплавов с наложением сдвиговых деформаций: дис. ... канд. техн. наук. – Ростов-на-Дону, 1985. – 232 с.

26. Патент России №98107870, МПК В21J5/00. Способ деформационной обработки заготовок / Утяшев Ф.З., Кайбышев О.А., Валитов В.А. - Заявл. 19.07.1999; Опубл. 20.05.2001

27. Segal, V.M. Materials processing by simple shear. *Materials Science and Engineering*. Volume 197, Issue 2, 1995. – pp. 157-164.

28. Сегал В.М. Патент СССР № 575892, 1977.

29. Ruslan Z. Valiev, Terence G. Langdon. Principles of equal-channel angular pressing as a processing tool for grain refinement. *Progress in Materials Science* 51 (2006). - pp. 881–981.

30. Патент РФ № 2181314. Устройство для обработки металлов давлением. Рааб Г.И., Кулясов Г.В., Полозовский В.А., Валиев Р.З., 2002.
31. Найзабеков А. Б., Ашкеев Ж. А., Лежнев С.Н., Толеуова А. Р. Исследование процесса деформирования заготовок в равноканальной ступенчатой матрице./ Изв. вузов. Черная металлургия.2005.№2.–С.16-18.
32. Патент РФ № 2240197. Способ комбинированной интенсивной пластической деформации заготовок. Валиев Р.З., Салимгареев Х.Ш., Рааб Г.И., Красильников Н.А., Амирханов Н.М. Уфимский государственный авиационный технический университет. В21J5/00, С22F1/18, В21С25/00. Оpubл.: 20.11.2004
33. Утяшев Ф.З., Еникеев Ф.У., Латыш В.В., Петров Е.Н., Валитов В.А. Термомеханическая обработка для формирования ультрамелкозернистой структуры путем интенсивной пластической деформации. Тезисы международной конференции "Investigation and Application of severe Plastic deformation" NATO Sc., 1999. - С. 73-77.
34. European Patent №EP1861211, В21С23/01; В21J5/00; В21С23/01; В21J5/00. Severe plastic deformation of metals / Rosochowski Andrzej. - 2007.12.05
35. L. Olejnik, A. Rosochowski. Methods of fabricating metals for nanotechnology. Bulletin of the Polish Academy of Sciences - Technical sciences Vol. 53, No. 4, 2005. - pp. 413-423.
36. Патент Украины №58015. Устройство для упрочнения давлением / Медведская Э.А., Матросов Н.И., Дугадко А.Б., Спусканюк В.З., Белошенко В.А., Шевченко Б.А. - Оpubл. 15.07.2003. Бюл. № 7.
37. Равноканальная угловая гидроэкструзия – эффективный метод формирования субмикроструктурного состояния материалов / В.З. Спусканюк, Т.Е. Константинова, А.А. Давиденко, И.М. Коваленко, Т.А. Закорецкая, Л.Ф. Сенникова, Н.Н. Белоусов, Л.В. Лоладзе, А.В. Завдоев // Удосконалення процесів і обладнання обробки тиском в металургії і машинобудуванні. Краматорськ, 2007. - С. 37-42.
38. Особенности равноканальной многоугловой экструзии / В.З. Спусканюк, А.Б. Дугадко, И.М. Коваленко, Н.И. Матросов, А.В. Спусканюк, Б.А. Шевченко // Физика и техника высоких давлений. - 2003. - Т. 13, № 3. - С. 85-96.
39. Влияние величины деформации равноканальным многоугловым прессованием на структуру и свойства сплава NbTi / Н.И. Матросов, В.П. Дьяконов, В.В. Чишко, Н.Г. Кисель, Е.А. Павловская, Л.Ф. Сенникова, Э.А. Медведская, О.Н. Миронова // Физика и техника высоких давлений. 2007. Т. 18, № 3. - С. 98-103.
40. Ashkeev Zh.A, Naizabekov A.B., Lezhnev S.N., Toleuova A.R. Billet deformation in uniform-channel stepped die (2005) Steel in Translation, 35 (2). - pp. 37-39.
41. Beygelzimer Y., Orlov D. and Varyukhin V. A new severe plastic deformation method: Twist Extrusion // Ultrafine Grained Materials II; Ed. By Y.T.

Zhu, T.G. Langdon, R.S. Mishra, S.L. Semiatin, M.J. Saran, T.C. Lowe. TMS (The Minerals, Metals & Materials Society). 2002.– pp.297–304.

42. Seung Chae Yoon, Young Seok Jang, Hyoung Seop Kim. Plastic Deformation of Metallic Materials during Twist Extrusion Processing // J. Kor. Inst. Met. & Mater. 2006. V. 44, № 7. – pp. 480-484.

43. Useful properties of twist extrusion / Y. Beygelzimer, V. Varyukhin, S. Synkov, D. Orlov // Materials Science and Engineering A. 2009. V. 503. – pp. 14-17.

44. В. Н. Варюхин, Я. Е. Бейгельзимер, С. Г. Сынков, А. В. Решетов, Р. Ю. Кулагин. Опытнo-промышленная установка винтовой экструзии для проведения маркетинговых исследований объемных наноматериалов. Металл и литье Украины №6 2010. – С. 17-21.

45. Я.Е. Бейгельзимер, В.Н. Варюхин, Д.В. Орлов, С.Г. Сынков. Винтовая экструзия – процесс накопления деформации.– Донецк: Фирма ТЕАН, 2003.– 87 с.

46. Microstructural evolution over a large strain range in aluminium deformed by cyclic-extrusion-compression. Richert, M., Liu, Q., Hansen, N. Materials Science and Engineering A №260 (1-2), 1999. - pp. 275-283.

47. Perspective of nanomaterials production, by cyclic extrusion compression method of exerting unconventional, large plastic deformations. Richert, M., Hawrytkiewicz, S., Richert, J., Zasadziński, J. Solid State Phenomena 101-102. 2005. - pp. 37-42.

48. Kwapisz, M., Knapinski, M., Dyja, H., Laber, K. Analysis of the effect of the tool shape on the stress and strain distribution in the alternate extrusion and multiaxial compression process. Archives of Metallurgy and Materials. Volume 56, Issue 2, 2011. – pp. 487-494.

49. Salishev G.A., Valiakhmetov O.R., Galejev R.M. Formation of submicrocrystalline structure in the titanium alloy VT8 and its influence on mechanical properties // J. Mater. Sci. 1993. V.28.– pp.2898–2904.

50. Найзабеков А. Б., Лежнев С. Н., Голумбовская С. Ю. Эволюция микроструктуры металла, деформируемого в бойках с упругими элементами // Тезисы докл. межд. конф. «Теория и технология процессов пластической деформации – 2004». Москва, 2004. – С. 105-107.

51. Найзабеков А. Б., Ногаев К. А. Исследование работы кузнечного инструмента, реализующего поперечный сдвиг заготовки. // Труды университета. 2005. №1. – С.43-45.

52. Найзабеков А. Б. Научные и технологические основы повышения эффективности процессовковки при знакопеременных деформациях. Алматы: издание РИК по учебной и методической литературе, 2000. - 336 с.

53. Логинов Ю.Н., Буркин С.П. Исследование процесса прессования через вращающуюся матрицу.// Изв. вузов. Черная металлургия. 1995, №4. – С. 33-38.

54. Пашинская Е.Г., Толпа А.А. Возможности интенсивной прокатки со сдвигом для формирования ультрамелкозернистой структуры на примере углеродистой эвтектоидной стали // Металлы. 2004. № 5. - С. 85-92.

55. Патент України №13768U, МПК В21В1/00. Спосіб отримання сортового прокату/ Пашинська О.Г., Кукуй Д.П., Маншилін О.Г., Феофілактов А.В. - Заявл. 24.10.05; Опубл. 17.04.06, Бюл. №4.

56. Найзабеков А. Б., Быхин М. Б., Ногаев К. А., Быхин Б. Б., Шапинов Е. С. Инновационная технология получения сортового проката. Казахстанской Магнитке 50 лет (сборник научных трудов) – Алматы, РИК по учебной и методической литературе, 2010. - 320 с.

57. Пат. № 2293619 Российская Федерация, МПК В21В 19/00. Способ винтовой прокатки / Галкин С. П.; заявитель и патентообладатель НИТУ МИСисунок – № 2006110612/02, заявл. 04.04.2006; опубл. 20.02.2007. Бюл. изобр., 2007, № 5.

58. Пат. № 2009737 Российская Федерация, МПК<sup>5</sup> В21В19/02. Трехвалковый стан винтовой прокатки и технологический инструмент стана винтовой прокатки. Романцев Б. А., Михайлов В. К., Галкин С. П., Дегтярев М. Г., Карпов Б. В., Чистова А. П.; – № 5031365/27; заявл. 13.01.1992, опубл. 30.03.1994.

59. Галкин С. П. Трехакторно-скоростные особенности радиально-сдвиговой и винтовой прокатки. «Современные проблемы металлургии», Днепрпетровск. "Системні технології" - 2008, том 11. - С. 26-33.

60. Galkin, S.P. Radial shear rolling as an optimal technology for lean production. Steel in Translation №44 (1), 2014. - pp. 61-64.

61. Галкин С.П. Теория и технология стационарной винтовой прокатки заготовок и прутков малопластичных сталей и сплавов. Диссертация на соискание степени доктора технических наук. Москва, 1998. - 401 с.

62. Галкин С.П., Михайлов В.К., Романцев Б.А. Технология и министан винтовой прокатки как технико-технологическая система.// Производство проката, №6, 1999.

63. Ю. Р. Колобов, М. Б. Иванов, Е. В. Голосов. Формирование наноструктурированных состояний и связанных с ними улучшенных свойств материалов медицинского и технического назначения Наносистемы, наноматериалы, нанотехнологии Nanosystems, Nanomaterials, Nanotechnologies 2011, т. 9, № 2. - С. 489-498.

64. Lopatin, N.V., Salishchev, G.A., Galkin, S.P. Mathematical modeling of radial-shear rolling of the VT6 titanium alloy under conditions of formation of a globular structure. Russian Journal of Non-Ferrous Metals №52 (5), 2011. - pp. 442-447.

65. Лопатин, Николай Валерьевич. Улучшение технологической деформируемости сталей 45 и У10А термомеханической обработкой с использованием радиально-сдвиговой прокатки: дис. ... канд. техн. наук. – Уфа, 2007. – 125 с.

66. Raab, G.J., Valiev, R.Z., Lowe, T.C., Zhu, Y.T. Continuous processing of ultrafine grained Al by ECAP-Conform. Materials Science and Engineering A Volume 382, Issue 1-2, 2004. - pp 30-34.

67. Semenova, I.P., Polyakov, A.V., Raab, G.I., Lowe, T.C., Valiev, R.Z. Enhanced fatigue properties of ultrafine-grained Ti rods processed by ECAP-

- Conform. Journal of Materials Science. Volume 47, Issue 22, 2012. – pp. 7777-7781.
68. Long-length ultrafine-grained titanium rods produced by ECAP-conform. Raab, G.I., Valiev, R.Z., Gunderov, D.V., Misra, A., Zhu, Y.T. Materials Science Forum 2008. v 584-586 PART 1. - pp. 80-85.
69. Development of ECAP-Conform to produce ultrafine-grained aluminum. Raab, G.I., Safin, F.F., Lowe, T.C., Zhu, Y.T., Valiev, R.Z. TMS Annual Meeting, 2006. - pp. 171-175.
70. M. Duchek, T. Kubina, J. Hodek, J. Dlouhy. Development of the production of Ultrafine-grained titanium with the Conform equipment. Materials and technology 47 (2013) 4. – pp. 515–518.
71. Zhu Y.T., Lowe T.C., Valiev R.Z., Stolyarov V.V., Latysh V.V., Raab G.I. // Ultrafine-grained titanium for medical implants. US Patent 6,399,215 of 2002.
72. Sidelnikov, S.B. Classification and fields of application of integrated and combined methods to process nonferrous metals and alloys. Izvestiya Vysshikh Uchebnykh Zavedenij. Tsvetnaya Metallurgiya (3) 2005. - pp. 45-49.
73. С.Б. Сидельников, Ю.В. Горохов, С.В. Беляев. Инновационные совмещенные технологии при обработке металлов. Journal of Siberian Federal University. Engineering & Technologies 2 (2015 8). – pp. 185-191.
74. Сидельников С.Б. Разработка совмещенных процессов литья-прокатки-прессования и программного обеспечения для их проектирования с целью повышения эффективности производства пресс-изделий из алюминия и его сплавов: дис. ... д-ра. техн. наук. – Красноярск, 2005. – 125 с.
75. Сидельников С.Б., Довженко Н.Н. Загиров Н.Н. Комбинированные и совмещенные методы обработки цветных металлов и сплавов: монография // М.: МАКС Пресс, 2005.- 344 с.
76. Галиев, Роман Илсурович. Разработка и исследование процесса совмещенной прокатки-прессования с целью повышения эффективности производства длинномерных пресс-изделий из алюминиевых сплавов: дис. ... канд. техн. наук. – Красноярск, 2004. – 193 с.
77. Пат. 2334574 РФ, МПК В22D 11/06, В21С 23/00. устройство для непрерывной прокатки и прессования профилей/ Беляев С.В., Довженко Н.Н., Сидельников С.Б., Соколов Р.Е., Пещанский А.С., Плетюхин С.А., Рудницкий Э.А. / Оpubл. 27.09.2008.
76. Пат. 111659 РФ, МПК В22D 11/06, В21С 23/00. Устройство для непрерывного литья и прессования металла методом конформ / Ю.В. Горохов, С.В. Беляев, В.Г. Шеркунов и др. / Оpubл. 27.08.2012, Бюл. № 24.
77. Пат. 2100136 РФ, МКП В 22 D 11/06, В 21 С 23/00. Установка для непрерывного литья и прессования / Сидельников С.Б., Довженко Н.Н., Ешкин А.В. / Оpubл. 27.12.1997, Бюл.№ 36.
78. Пат. 2200644 РФ, МПК В22D11/06, В21С23/08. Устройство для непрерывного литья и прессования полых профилей / Сидельников С.Б., Довженко Н.Н., Гришечкин А.И. и др. / Оpubл. 20.03.2003, Бюл. № 8.

79. Пат. 2064364 РФ, МПК В22D11/06, В21С23/08. Способ получения биметаллической полосы. Лехов О. С. Оpubл. 20.03.2003. 27.07.1996.

80. Лехов О. С., Туралаев В.В., Лисин И.В. Туев М.Ю. Исследование совмещенного процесса непрерывного литья и деформации для производства биметаллических полос. Вестник МГТУ 2012. – С. 69-73.

81. Пат. Республики Казахстан № 25863. МПК В21J 5/00. Устройство для непрерывного прессования металла. Найзабеков А. Б., Лежнев С. Н., Панин Е. А. 2013 заявитель и патентообладатель РГП КГИУ. – № 2011/0762.1, заявл. 02.07.2011; опубл. 15.02.2013. Бюл. изобр., 2013, № 7.

82. Theoretical studies of the joint "rolling-extrusion" process aimed at making sub-ultra-fine-grained structure metal. Lezhnev, S.N.; Naizabekov, A.B.; Panin, Ye. A. Proceedings paper of the 20th International Conference on Metallurgy and Materials (METAL) Pages: 272-277. Brno, Czech Republic, 2011.

83. Panin E.A., Naizabekov A.B., Lezhnev S.N. Simulation of the joint 'rolling-pressing' process using equal-channel step die./17-th International Conference on metallurgy and materials METAL-2008, Ostrava, Czech Republic, 2008.

84. Lezhnev, S., Panin, E., Volokitina, I. Research of combined process rolling-pressing influence on the microstructure and mechanical properties of aluminium. Advanced Materials Research. 2013. v. 814. - pp. 68-75.

85. Кузьминов И.И., Панин Е.А., Толкушкин А.О., Хасымхан Ж. Развитие и совершенствование технологий получения высококачественных длинномерных заготовок путем совмещения непрерывного литья и интенсивной пластической деформации. Труды международной конференции «Vědecký průmysl evropského kontinentu - 2014» 27 listopadu - 05 prosinců 2014 roku. Díl 20 Technické vědy. - С. 83-86.

86. Пат. 2349403 РФ, МПК В21С25. Устройство для обработки материалов давлением / Салимгареев Х. Ш., Валиев Р.Р, Гундеров Д. В., Исламгалиев Р.К. Капитонов В.М. / Оpubл. 27.09.2008.

87. Пат. 2184657 РФ, МПК В41В19/02. Способ совмещенной непрерывной винтовой и продольной прокатки/ / Закорко Н.П.; Сивак Б.А.; Зуев И.Г.; Жерновков С.П. Оpubл. 10.07.2002.

88. Патент РФ №2278747. МПК В21В19/02 Жерновков С. П. Способ совмещенной непрерывной винтовой и продольной прокатки. Оpubл. 27.06.2006.

89. Патент РФ №2347631 МПК В41В19/02. Способ получения заготовок с мелкозернистой структурой совмещенной винтовой и продольной прокаткой. Валиев Р.З., Салимгареев Х. Ш., Валиев Р.Р. опубл. 27.02.2009.

90. Найзабеков А.Б., Лежнев С.Н., Панин Е.А. Теоретические исследования совмещенного процесса «прокатка-прессование» с использованием равноканальной ступенчатой матрицы. Изв. вузов. Черная металлургия, Москва, 2008, №6. - С. 22-26.

91. Сорокин В.В. Марочник сталей и сплавов. 2003 – 492 с.

92. A. Naizabekov, V. Talmazan, A. Arbuz, T. Koinov, S. Lezhnev. Study of axial forces with the purpose to realize a combined process «helical rolling-

pressing». Journal of Chemical Technology and Metallurgy, 50, 2, 2015. - pp. 217-222.

93. Фастыковский А.Р. К вопросу о процессе прокатки-прессования // Известия вузов. Цветная металлургия, 2004, №2. - С.67-70.

94. [http://www.simufact.de/en/solutions/sol\\_form.html](http://www.simufact.de/en/solutions/sol_form.html) (simufact.forming manual).

95. Найзабеков А.Б., Лежнев С.Н., Панин Е.А., Jitai Niu. Влияние геометрических и технологических факторов на напряженное состояние металла при осуществлении совмещенного процесса прокатка-прессование с использованием равноканальной ступенчатой матрицы и калиброванных валков. Технология производства металлов и вторичных материалов. Темиртау, 2009, №1. – С. 163-176.

96. Найзабеков А.Б., Лежнев С.Н., Ногаев К.А., Панин Е.А. Исследование влияния геометрических факторов при равноканальном прессовании на энергосиловые параметры деформирования. Технология производства металлов и вторичных материалов. Темиртау, 2008, №2. – С. 52-59.

97. Найзабеков А.Б., Лежнев С.Н., Ногаев К.А., Панин Е.А. Анализ влияния технологических факторов на усилие прессования при деформировании заготовок в равноканальной ступенчатой матрице. Технология производства металлов и вторичных материалов. Темиртау, 2008, №2. – С. 59-64.

98. H. Yada, N. Matsuzu, K. Nakajima, K. Watanabe and H. Tokita: Trans. ISIJ 23 (1983). – pp. 100–109.

99. ГОСТ 5639-82. Стали и сплавы. Методы выявления и определения величины зерна.

100. Filho, A. Ferrante. Severe plastic deformation by equal channel angular pressing: product quality and operational details / A. Filho, É.F. Prados, G.T. de Valio, J.B. Rubert, V.L. Sordi; M. Ferrante // Materials Research. – 2011. – Vol. 14, № 3. – P. 335-339

101. Орлов, П.И. Основы конструирования. Справочно-методическое пособие в 3-х книгах. - 2-е изд., перераб. и доп. – М.: Машиностроение, 1977. – 574 с.

102. Дунаев, П.Ф., Леликов О.П. Конструирование узлов и деталей машин: учебное пособие для студ. техн. спец. вузов. - 8-е изд., перераб. и доп. - М.: Академия, 2004. – 496 с.

103. <http://kompas.ru/> Официальный сайт программного продукта Компас-3D, компании Аскон (дата обращения – 20.11.2015).

104. Галлагер, Р. Метод конечных элементов. Основы: пер. с англ. – М.: Мир, 1984. –156 с.

105. Новиков, И.И. Теория термической обработки металлов. Учебник для вузов. - 4-е изд., перераб. и доп. – М.: Металлургия, 1986. – 480 с.

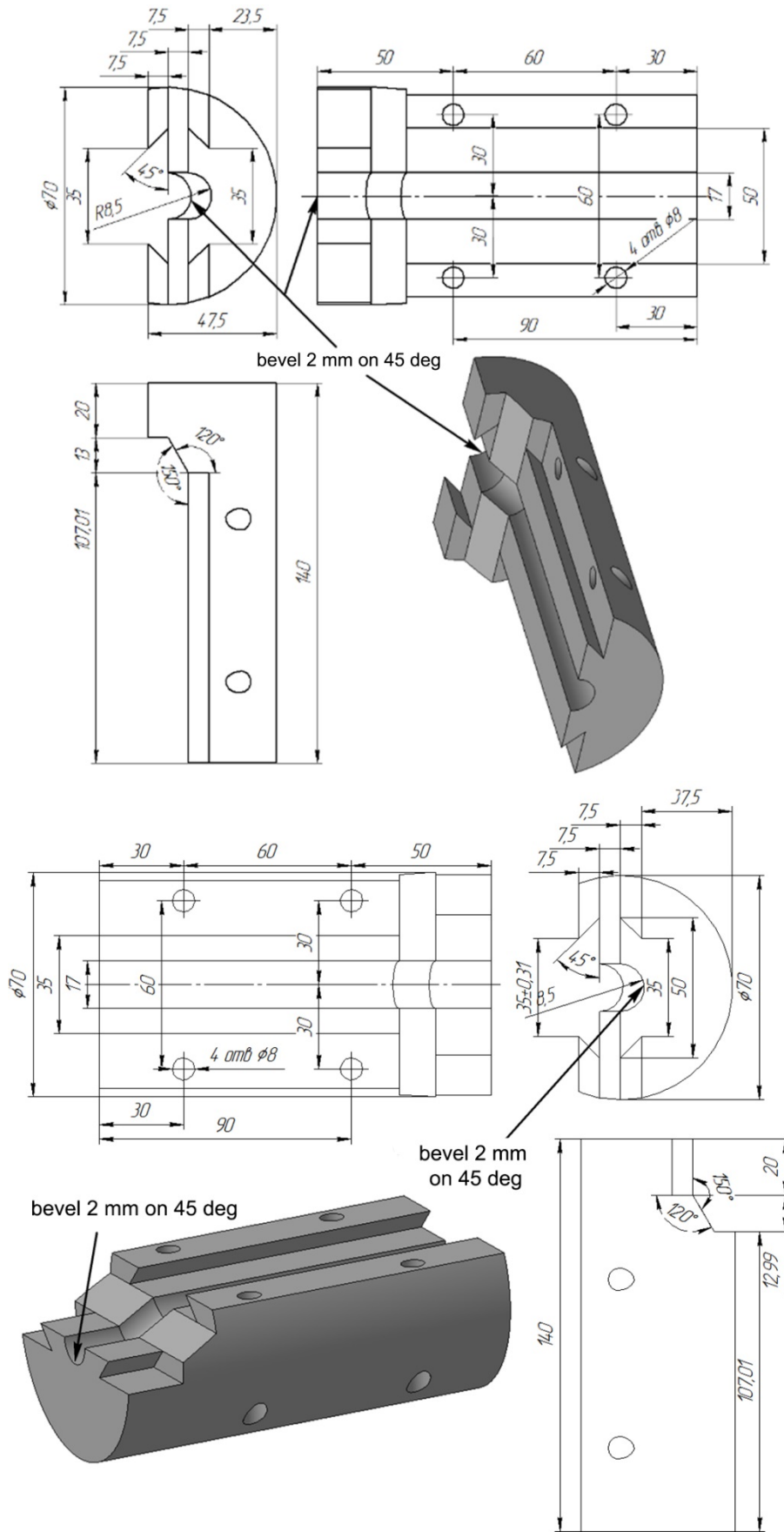
106. Характеристика электропривода. [Электронный ресурс] - Режим доступа: <http://www.krona-sm.com/kharakteristika-elektroprivoda.html>, свободный. Загл. с экрана. 12.05.2015

107. Тетерин, П.К. Теория поперечной и винтовой прокатки. – М.: Металлургия, 1983. – 270 с.
108. Потапов, И.Н., Технология винтовой прокатки / И.Н. Потапов, П.И. Полухин. – М.: Металлургия, 1990. – 344 с.
109. Романцев, Б.А. Трубное производство / Б.А. Романцев, А.В. Гончарук, Н.М. Вавилкин, С.В. Самусев. – М.: Изд. Дом МИСиС, 2011. – 970 с.
110. Ковалев, Д. А. Исследование и разработка технологии процесса поперечно-винтовой прокатки для повышения пластичности заэвтектических силуминовых сплавов: дисс. ... канд. техн. наук. – М., 2011. -140 с.
111. <http://www.zetlab.ru/> Официальный сайт НПО "Электронные технологии и метрологические системы" г. Москва (дата обращения – 20.11.2015).
112. Макаров Р. А., Ренский Л. В. Тензометрия в машиностроении. – М.: Машиностроение, 1975. – 356 с.
113. Львовский, Е.Н. Статистические методы построения эмпирических формул: Учеб пособие для ВТУЗов. – М.: Высшая школа, 1988. – 239 с.
114. Пат. №2379148 Российская Федерация, МПК В21J5/06, В21J13/02, С22F1/04 Способ прессования металлов и устройство для его осуществления / А.Ф. Шаяхметов, А.В. Боткин, Р.З. Валиев, Г.И. Рааб, Акбашев Р.Р., Уфимский государственный авиационный технический университет; заявл. 07.04.2008; опубл. 20.01.2010 - 2 с.
115. Найзабеков А.Б., Арбуз А.С. Влияние поперечно-винтовой прокатки на микроструктуру стали 40Х // Вестник КазНТУ. – 2015. – №5 (111). – С. 249-255.
116. Naizabekov A., Lezhnev S., Tsay K., Arbuz A. Effect of cross rolling on the microstructure of steel // Nanocon 2015, 7th International Conference on Nanomaterials - Research & Application. 14th - 16th Oct 2015, Brno, Czech Republic, EU.
117. Х. Дыя, Т. Байор, А.Б. Найзабеков, С.Н. Лежнев, А.С. Арбуз, А.С. Бужинский. Влияние поперечно-винтовой прокатки на микроструктуру меди // Сборник докладов VII Международного Конгресса «Цветные металлы и минералы». – Красноярск, 2015. – С. 1228-1232.
118. Рыбальченко О.В. Влияние интенсивной пластической деформации на структуру, механические и служебные свойства стали 08Х18Н10Т: дис. ... канд.техн.наук. - М., 2014. – 167 с.
119. ГОСТ 5639-82. Стали и сплавы. Методы выявления и определения величины зерна.
120. Сарафанов Г.Ф., Перевезенцев В.Н. Закономерности деформационного измельчения структуры металлов и сплавов. -Нижний Новгород, 2007. - 96 с.
121. Мигачев Б.А., Найзабеков А.Б. Элементы квалиметрии для технических приложений. – Алматы: РИК по УиМЛ, 2001. – 125 с.
122. Азгальдов Г.Г., Райхман Э.П. О квалиметрии. – М.: Изд-во стандартов, 1973. – 172 с.

123. Азгальдов Г.Г., Гличев А.В., Панов В.П. Что такое качество? - М.: Экономика, 1968. – 135с.
124. Азгальдов Г.Г. Разработка теоретических основ квалиметрии: автореф. дис. ... д-ра. экон. наук. – М., 1981. – 60 с.
125. Азгальдов Г.Г. Общие сведения о методологии квалиметрии. – М.: Стандарты и качество, 1994. – № 11.
126. Гун Г.С., Пудов Е.А. Комплексная оценка качества: методич. указ. – Магнитогорск: МГМИ, 1986. – 138 с.
127. Гун Г.С., Чукин М.В. Оптимизация процессов деформирования изделий с покрытиями в технологиях и машинах обработки давлением. – Магнитогорск: МГТУ им. Г.И. Носова, 2006. – 152с.
128. Гун Г.С., Пудов Е.А. Комплексная оценка качества: методич. указ. – Магнитогорск: МГМИ, 1986. – 138 с.
129. Гун Г.С. Управление качеством высокоточных профилей. – М.: Металлургия, 1984. – 151 с.
130. Г.С. Гун, Г.Ш. Рубин, Е.А. Пудов и др. Комплексная оценка стальной канатной проволоки // Сталь. – 1983. – №1. – С. 56-57.
131. Гун Г.С. Метод комплексной оценки качества металлопродукции // Известия вузов. Черная металлургия. – 1982. – №8. – С. 62-66.
132. Использование функции желательности Харрингтона при решении оптимизационных задач химической технологии, М.: РХТУ им. Д. И. Менделеева, 2003. – 51 с.
133. Закиров Д. М. Развитие теории оценки качества и практики производства метизов автомобильного назначения на основе разработки конкурентоспособных технологий: дис. ... докт. техн. наук. – Магнитогорск, 2008. – 270 с.
134. Чукин М.В. Развитие теории и оптимизация процессов технологического и эксплуатационного деформирования изделий с покрытиями: дис. ... докт. техн. наук. – Магнитогорск, 2001. – 398 с.
135. Naizabekov A., Samsonov D., Krivtsova O., Lezhnev S., Talmazan V. Arbuz A. Comparative evaluation of technologic lubricants // Metal 2013 - 22nd International Conference on Metallurgy and Materials, May 15th – 17th 2013, Brno, Czech Republic, EU.
136. Naizabekov A., Krivtsova O., Talmazan V. Arbuz A. Analysis of the quality of hot-rolled steel for side-members // Metal 2013 - 22nd International Conference on Metallurgy and Materials, May 15th – 17th 2013, Brno, Czech Republic, EU
137. Андреев А. В. Выбор и формирование результативной технологии производства шипов противоскольжения на основе аддитивной квалиметрической модели: дис. ... канд. техн. наук. – Магнитогорск, 2008. – 140 с.

# ANNEX A

## Drawings of ECA matrix for the combined process



## ANNEX B

### Chemical composition of the materials used

Table B1 – Chemical composition of steel 5HV2S

C	Si	Mn	Ni	Cr	Mo	W	V	Cu
0.45 - 0.55	0.8 - 1.1	0.15 - 0.45	till 0.35	0.9 - 1.2	till 0.3	1.8 - 2.3	till 0.3	till 0.3

Table B2 – Mechanical properties of steel 5HV2S after heat treatment

Yield stress, MPa	Ultimate stress, MPa	Elongation, %	Contraction, %	Impact strength, kJ /cm <sup>2</sup>
1960	1810	6	13	15

## ANNEX C

### Fragments of samples of intermediate calculations the integrated indicator of quality

Table C1 – A fragment of a sample of values of geometric parameters of grains from the image of the periphery of the bar after the second pass

№	Square, nm <sup>2</sup>	Perimeter, nm	Length, nm	Width, nm	Average size, nm	Degree of non-equivalence
1	488 310	2 770	1 020	666	843	1,53
2	377 519	2 716	1 055	577	816	1,83
3	439 062	2 618	941	663	802	1,42
4	539 573	3 829	1 272	695	984	1,83
5	1 681 604	6 089	2 067	1 179	1 623	1,75
6	247 111	2 441	769	697	733	1,10
7	49 516	927	357	222	290	1,61
8	261 556	1 951	696	483	590	1,44
9	90 030	1 224	478	248	363	1,93
10	197 729	1 845	642	512	577	1,25
11	264 647	2 435	969	428	699	2,26
12	436 442	2 626	784	750	767	1,05

Table C2 – A fragment of the sample of values of indicators of quality of grain from the image of the periphery of the rod after a second pass

№	Single quality indicators by properties $k_i$			Complex index $K_0$
	Square	Average size	Degree of non-equivalence	
1	0,59	0,40	0,32	0,44
2	0,67	0,41	0,22	0,43
3	0,63	0,42	0,38	0,48
4	0,56	0,34	0,22	0,37
5	0,14	0,16	0,24	0,18
6	0,77	0,45	0,74	0,66
7	0,95	0,74	0,29	0,65
8	0,76	0,53	0,37	0,55
9	0,91	0,68	0,20	0,59
10	0,81	0,54	0,52	0,62
11	0,76	0,47	0,15	0,45
12	0,63	0,44	0,87	0,65

**Naizabekov Abdrakhman Batyrbekovich, Lezhnev Sergey Nikolaevich,  
Arbuz Alexandr Sergeevich, Panin Evgeniy Alexandrovich**

**THEORETICAL AND TECHNOLOGICAL BASES OF OBTAINING  
SUB-ULTRA-FINE-GRAINED STRUCTURAL METALS AND ALLOYS  
BY THE NEW COMBINED PROCESS  
"SCREW ROLLING – ECA-PRESSING»**

*Monograph*

Signed for printing 29.04.2019 y. Format 60×84 1/16  
Volume 10,75 п.л. Pressrun 300 pcs. Order №56.